MICROPLASTICS IN MUNICIPAL DRINKING WATER, BOTTLED WATER AND BEVERAGES

Determination of their occurrence, sources, distribution, and modelling of their physical-chemical behaviours

A Report

to the Water Research Commission

by

Gibbon Ramaremisa, Michelle Ndlovu, Patricia Chauke, Rudolph M Erasmus, Luke Chimuka, Dalia Saad, and Hlanganani Tutu

School of Chemistry, University of the Witwatersrand, South Africa
School of Physics, Microscopy and Microanalysis Unit, University of the Witwatersrand, South Africa

WRC report no. 3220/1/25
ISBN 978-0-6392-0724-7

May 2025

This is the final report of WRC project no. C2022-2023-00813

EXECUTIVE SUMMARY

BACKGROUND

In the recent United Nations Intergovernmental Negotiating Committee on Plastic Pollution in Busan, South Korea, Inger Andersen (Executive Director of the UN Environmental Programme) concluded by saying, “The world’s commitment to ending plastic pollution is clear and undeniable. Here in Busan, talks have moved us closer to agreeing on a global legally binding treaty that will protect our health, our environment, and our future from the onslaught of plastic pollution”. This underpins the urgency with which plastic pollution, and microplastics (MPs), in particular, have to be dealt with due to their ubiquity and persistence in global ecosystems. Pollution by MPs is well documented, and there has been intensive research done to determine their physical-chemical properties in most American, European, and Asian countries. Most of this research has been dominated by a focus on marine environments, which act as the largest repositories and became the first areas to which attention was drawn to the seriousness of the problem.

MP research has since evolved to include freshwater bodies and biota, food, tea, groundwater, alcoholic, and non-alcoholic beverages. There have been calls from the international community for Africa to follow suit by providing estimates of MP pollution across the continent. However, a lack of funding and expertise has hindered Africa’s contribution to this important emerging research field. Microplastic pollution has been identified as a direct or indirect hindrance to achieving twelve of the seventeen Sustainable Development Goals (SDGs) set by the United Nations. These goals are a universal call to action made to safeguard our co-existence with nature and as a species by eradicating poverty, protecting the environment, and ensuring that everyone lives in peace and prosperity.

Groundwater makes up the largest proportion of freshwater sources in the world and billions of people depend on it for their daily needs; as such, it should be sustainably managed. In South Africa’s North West and Gauteng Provinces, groundwater is essential for socioeconomic development. However, contamination of this resource by MPs can be a deterrent to such development. Agricultural practices, such as plastic mulching, application of MP-coated fertiliser, and solid waste, are suspected to be a source of MP in soil, which eventually migrates into groundwater aquifers. Additionally, discarding MP-infested wastewater into rivers, which recharge groundwater aquifers, serves as another contamination source. Characterisation of the physical-chemical properties of MPs in groundwater is essential to determine their sources and the potential threats they pose to humans and aquatic organisms. A review of the literature revealed that research on MPs in groundwater on the continent is almost non-existent, yet this is the largest source of water in arid and semi-arid regions. Thus, the generation and collation of data on MPs in groundwater is essential for any management efforts to ensure sustainable use.

Microplastics are made up of different polymers, which behave differently in the environment. During manufacturing, different metals are added to polymers, which may later be desorbed and released into the environment. Moreover, metals released into the environment through various human activities, such as the previously desorbed metal, may adsorb to MPs. Sorption is a fundamental physical-chemical process involving fluid transfer to solids. Sorption occurs either through adsorption or absorption. During adsorption, dissolved substances (adsorbates) interact with solid MP surfaces (adsorbents) to form a solid-liquid interface. On the other hand, the adsorbates penetrate the adsorbent’s polymeric matrix. It is often impossible to delineate between the two processes and they can occur concurrently. Although the adsorption of various pollutants (i.e., metals, PCBs, PAHs, DDTs and antibiotics) onto MPs has been well documented in the literature, there exists limited knowledge in the development and use of numerical models that can accurately supplement experimental data. Drawing from all the above information, it is apparent that a comprehensive study and assessment of the footprint of MPs in aqueous systems such as fresh water (including surface and groundwater), processed water (e.g., bottled water) and beverages is important. Modelling of the physical-chemical processes prevailing in these systems is important to understand the behaviour of MPs in the context of other contaminants that occur alongside them. Other systems, such as soils and plants (through uptake) also remain important, and further studies should seek to integrate them into the general aqueous environments so as to achieve a complete overview of the distribution and cyclisation of MPs. It is on this basis that this study has been predicated.

AIM AND OBJECTIVES

This study aimed to conduct a comprehensive characterisation of MPs in river water, sediments, groundwater, drinking water (tap and bottled), tea, and beverages and model their potential physical-chemical behaviour in such systems. This would provide a benchmark on which future and advanced studies can hinge and provide insights into how these contaminants could be removed from water. To do this, the following objectives were pursued:

1. To monitor the occurrence and distribution of MPs in different aqueous environmental media.
2. To characterise the physical-chemical properties (i.e., shape, size, colour, polymer type, and additives) of different MPs and their additives using a stereomicroscope, FTIR, FEG-SEM, SEM-EDS, and micro-Raman spectroscopy to define their sources, pathways, and potential anthropogenic inputs.
3. To characterise MPs with respect to chemical constituents such as additives and their degradation products and potential release to media to which they are exposed.
4. To conduct geochemical modelling simulations by coupling PHREEQC and parameter estimation (PEST) to supplement experimental results and acquire a comprehension of the generalised surface complexation of MPs to account for release, and potential as micro-and nanovectors of other contaminants.

METHODOLOGY

Surface river water and sediments

Surface water and sediment samples were collected over approximately 50.4 km between the Eskom Lethabo weir and the Vaal River Barrage. Surface water samples were collected using a 55 µm plankton net towed along the river's surface. Global Positioning System (GPS) coordinates were taken at each sampling point to determine the distance sampled. Volume filtered through the net was calculated using a flowmeter. Surface water samples were subjected to wet peroxide digestion, modified from the National Oceanic and Atmospheric Administration method. Density separation was performed using saturated NaCl and NaI. Filter papers were allowed to air dry under the laminar flow cabinet and stored in covered glass Petri dishes until further analysis.

Microplastics in tea bags, tap water, bottled water, and non-alcoholic and alcoholic beverages

A literature review was done to evaluate different methods of sampling, sample extraction, and characterisation frequently used when analysing MPs in tea bags, tap water, bottled water, and non-alcoholic and alcoholic beverages. These methods were then applied, following some appropriate modifications where required, while ensuring quality assurance to avoid sample contamination. Tap water from Tembisa, Braamfontein, and Silver Lakes was allowed to run for one minute and samples were collected using glass jars. Different brands of tea bags, bottled water, non-alcoholic and alcoholic beverages samples were purchased from Makro, Shoprite, and other local supermarkets in Gauteng Province. Each sample was vacuum filtered through a Whatman® glass microfibre (GF/F) filter. To minimise the interference of organic matter during physical and chemical characterisation, each filter was subjected to modified wet peroxide using ferrous sulphate and hydrogen peroxide at room temperature. The biological dye, Rose Bengal solution, was applied to each filter paper, left to react at room temperature, and rinsed off. The filters were subsequently stored in glass Petri dishes until characterisation. Physical characterisation of MPs for shape and size identification was conducted using a stereomicroscope. In instances where the results were inconclusive, confirmations were conducted manually. This included simple tests such as the break test to distinguish between plastic and non-plastic particles. Raman micro-spectroscopy was used for chemical characterisation, which involved the identification of polymer types and additives based on functional groups present.

Microplastics in groundwater

Using glass jars, groundwater was collected from residential and communal taps and boreholes in the Gauteng and North West Provinces. Hydrochemical parameters (e.g., pH and electrical conductivity) were determined using a Hanna multiparameter HI98194 (Hanna Instruments Pty Ltd, Johannesburg, SA). Each sample was vacuum filtered through a Whatman® glass microfibre (GF/F) filter. Similar sample preparation and characterisation (physical and chemical) of MPs as described above were followed.

Modelling the physical-chemical behaviour of MPs

Characterisation of the physical-chemical properties of commercially sourced polyethylene (PE), polypropylene (PP), polystyrene (PS), and polyvinyl acetate (PVA) particles was conducted as they serve as surrogates for MPs in the environment. To acquire a close representation of environmentally present MPs, the above MPs were left exposed to ultraviolet light and other environmental factors to allow for their ageing for a year. This was to simulate the conditions that MPs can undergo once released into the environment. Characterisation of their physical-chemical properties was carried out with the use of a stereo microscope, FEG-SEM, SEM-EDS, and FTIR spectroscopy. Acid-base titration experiments were carried out to determine the MPs' point of zero charge (pHpzc). Batch experiments were conducted to determine the optimal conditions (pH, metal concentration, and adsorbent dosage) for adsorption. Inductively coupled plasma optical emission spectroscopy (ICP-OES) was used to determine the quantity of metals adsorbed by MPs. Lead (Pb) was used as a proxy adsorbing element. To validate and supplement experimental data, generalised surface complexation modelling simulations were conducted by coupling PHREEQC and parameter estimation (PEST) modelling codes. PEST was run in singular value decomposition (SVD) or least squares with QR-factorisation (LSQR) mode to ensure the attainment of a unique solution to the inverse problem. This is important in cases where there are many parameters than there are experimental data.

RESULTS AND DISCUSSION

Microplastics in water and sediments

Particles that satisfied the visual criteria set for the characterisation of particles as MPs were detected in all surface water and sediment samples. In surface waters, 848 MP particles were detected with an average of 38.5 particles/sample. Microplastic concentration ranged from 0.13 to 2.52 particles·m^{-3} (mean: 0.61 ± 0.57 particles·m^{-3}). In sediment samples, 1254 MP particles were identified with a mean of 50.2 per sample. MP abundances ranged from 29 to 11028.6 particles/(kg_dw) (mean: 463.3 ± 284.1 particles/(kg_dw)). Based on previous reports made on the Vaal River and other freshwater systems, urban centres, wastewater treatment plants, and tributaries were the most probable sources of MPs in the Vaal River. However, the MP abundance in sediments was the highest of all freshwater systems compared. Coloured fibres and fragments were the most abundant MP shapes and contributed more than 80% in both sample types. The majority of MPs in surface water (89%) and sediments (82.1%) were less than 2 mm in size. Coloured MPs were more abundant in surface waters (82.7%) and sediments (60.2%) than transparent MPs. The surfaces of MPs were degraded, weathered and contained different smaller materials. Degradation may enhance their potential to act as vectors for other substances in humans and biota. Eight different polymers were detected in both sample types. Polyethylene (PE) and Polypropylene (PP) were the most abundant MP polymers in surface waters (85.2%) and sediments (79.1%). The abundance of PP and PE is consistent with other studies and global demands.

C.I Pigment Black 7, C.I Pigment White 6, and C.I Pigment Yellow 83 are plastic additives and were detected in MPs.

Microplastics in tap water, bottled water, tea bags, and non-alcoholic and alcoholic beverages
Microplastics were detected in all tap water samples from Tembisa, Braamfontein, and Silver Lakes with an average size of 0.55 ± 0.49 mm, 0.49 ± 0.42 mm, and 0.63 ± 0.79 mm, respectively. There was a high abundance of fibrous MPs, with over 77% identified in all three sampling areas, 391 particles were identified as MPs in Tembisa tap water, with an average of 39.1 ± 4.92 particles per sample. Microplastic abundances ranged from 4.00 to 20.0 particles·ℓ^{-1}, with an average abundance of 12.6 ± 4.92 particles·ℓ^{-1}. A total of 527 particles in Braamfontein tap water were identified as MPs, with an average of 52.7 ± 18.7 particles per sample. The MP abundances in Braamfontein tap water samples ranged from 9.00 to 31.3 particles·ℓ^{-1}, with a mean abundance of 17.6 ± 6.24 particles·ℓ^{-1}. A total of 318 particles were detected in Silver Lakes tap water samples, with an average of 31.8 ± 12.0 particles/sample. Silver Lakes tap water MP abundances ranged from 4.70 to 15.7 particles·ℓ^{-1} with an average of 10.6 ± 4.02 particles·ℓ^{-1}.

In bottled water, 373 particles were detected with an average of 24.9 ± 17.0 particles/sample with a mean size of 0.61 ± 0.61 mm. Microplastic abundances in bottled water ranged from 6.00 to 18.0 particles·ℓ^{-1} with a mean of 10.4 ± 3.76 particles·ℓ^{-1}. Similar to tap water samples, there was a high abundance of fibres (83.3%) in bottled water samples. Microplastics were detected in all non-alcoholic and alcoholic beverages. In non-alcoholic beverages, 188 particles were detected with an average of 12.5 particles per sample, and abundances ranged from 2.00 to 13.3 particles·ℓ^{-1}, with a mean abundance of 7.22 ± 4.45 particles·ℓ^{-1}. There were 391 in alcoholic beverages with an average of 27.9 ± 15.5 particles/sample, and abundances ranged from 8.60 to 29.3 particles·ℓ^{-1}, with a mean abundance of 15.9 ± 7.71 particles·ℓ^{-1}. There was a high abundance of fibrous MPs in non-alcoholic (79.3%) and alcoholic beverages (58.1%). A total of 156 particles were detected from cut tea bags, with an average of 15.6 ± 5.83 particles per tea bag. Microplastic abundances in tea samples ranged from 4.39 to 10.49 particles/g (mean: 6.2 ± 2.0 particles·g^{-1}). The mean abundance for black and rooibos tea samples was 6.54 ± 2.56 and 5.78 ± 1.44 particles·g^{-1}, respectively. Fibres (58.1%) and fragments (38.7%) were the most abundant morphotypes in tea bags.

The surfaces of MPs were degraded, weathered and contained different smaller materials. Degradation may enhance their potential to act as micro-vectors for other substances in domestic animals and humans. Six different polymers were identified in tap water, bottled water, and alcoholic beverages namely: High-density polyethylene (HDPE), Polyester (PES), Polyurethane (PU), Polyamide (PA), Polyethylene terephthalate (PET), Poly(hexamethylene terephtalamide)/Nylon-6T, and Poly(acrylamide-co-acrylic acid) (Poly(AM-co-AA). Additionally, five additives or colourants, namely: C.I. Pigment Red 1, C.I. Solvent Yellow 4, Potassium indigotetrasulfonate, Perylene, C.I. Direct Yellow 62, and C.I. Pigment Black 7, were identified via Raman analysis in tap water, alcoholic beverages, and non-alcoholic beverages. A review of the literature revealed that these colourants have extensive applications in the synthetic polymer industry and with a variety of potentially toxic activities in the body; some were banned carcinogens and mutagens.

Microplastics in groundwater
Microplastics were detected in all twenty groundwater samples from unconfined and semi-confined karst aquifers in the North West and Gauteng Provinces. North West groundwater samples had an average MP concentration (12.5 ± 7.60 particles·ℓ^{-1}) higher than that of the Gauteng groundwater samples (6.99 ± 2.69 particles·ℓ^{-1}). Overall, MP concentrations ranged from 3.67 to 30.3 particles·ℓ^{-1} (mean: 11.1 ± 6.9

particles·ℓ^{-1}). In groundwater samples, 668 particles satisfied the requirements to be regarded as MPs, with a mean of 33.4 ± 21.2 particles/sample. Lower MP concentrations were recorded in groundwater samples collected from systems with filters. Comparison with other studies revealed relatively low contamination of South African groundwater. The estimated daily intake from groundwater ingestion in South African men, women, and children is 0.57, 0.40, and 0.93 particles/(kg·day), respectively. This is concerning since groundwater in rural areas in the North West is consumed without purification or filtration.

Fibrous MPs were the most abundant morphotype, accounting for 63.8% and 81.4% in Gauteng and the North West Province, respectively. Fibrous MPs represented at least 52% of all shapes in each groundwater sample. In Gauteng Province, there was a smaller portion of pellets (16.2%), fragments (14.3%) and films (5.71%) determined. On the other hand, there was an even smaller portion of fragments (11%), pellets (6.4%), and films (1.24%) in the North West Province groundwater. The high abundance of MP fibres is consistent with a majority of similar studies on groundwater around the world, which have identified fibres as the abundant type of MPs. Microplastics in groundwater samples were detected in all seven size classifications considered in this study. At least 66% of the particles in all samples were less than 1 mm. Microplastics in groundwater samples had an average size of 0.57 ± 0.57 mm.

Fibres ranged in size from 0.05–4.52 mm, with an average size of 0.70 ± 0.58 mm. Fragments had an average size of 0.15 ± 0.2 mm (range: 0.03–1.2 mm). Pellets ranged in diameter from 0.02–1.16 mm, with an average diameter of 0.08 ± 0.16 mm. Films had an average size of 0.21 ± 0.19 mm (range: 0.04–0.78 mm). Microplastic sizes in groundwater samples had the following trend: fibres > films > fragments > pellets. Three different polymers were identified, namely PU, PET, and Polybutylene terephthalate (PBT). Additionally, six colourants (C.I. Pigment Red 1, C.I Pigment White 6, C.I. Vat Blue 1, 4-(4-Nitrophenylazo)resorcinol, C.I.Direct Yellow 12, and C.I. Pigment Blue 15) were identified. These colourants, some of which are banned carcinogens and mutagens, have extensive applications in the synthetic polymer industry and display a variety of potentially toxic activities in the body.

Modelling the physical-chemical behaviour of MPs

For the MPs that were used for adsorption studies (following exposure to natural elements and ageing), stereomicroscopic analysis on them revealed that PE and PP had elliptical shapes, PS had a cylindrical appearance and PVA had a spherical shape. SEM analysis revealed that PE and PS appeared with a relatively smooth surface morphology compared to PP and PVA. Notably, the surfaces of PP and PVA exhibited rough and porous morphology. SEM-EDS revealed that there were no Pb additives before the adsorption process. Additionally, PE and PVA mainly contained carbon (C), aluminium (Al), and oxygen (O). PP contained C, O, Al, and Si. PS had C, O, Al, S, and Fe. Potential sources of these elements may include kaolin, mica, SiO2, CaCO3, wollastonite, $CaSO_4{\cdot}2H_2O$, Al2O3, Al(OH)3, and Fe2O3 compounds. These would usually occur in the synthesis process where additives and catalysts are used. FTIR analysis confirmed the presence of functional groups characteristic of PE, PP, PS, and PVA. The pHPZC of the different adsorbents was found to be pHPZC(PE) = 4.2, pHPZC(PP) = 6.7, pHPZC(PS) = 2.4, and pHPZC(PVA) = 3.3. Thus, the adsorbents were negatively charged beyond their respective pHPZC and positively charged below their pHPZC.

As predicted, the solution's initial pH was a significant factor in the adsorption process of Pb on MPs since the process is primarily mediated by favourable interactions between oppositely charged sorbents and sorbates. PP and PVA had relatively higher adsorption capacities than PS and PE, which could in part be due to the relatively rough and porous surfaces of the former as opposed to the smooth and slippery surfaces of the latter. Moreover, PS had an intense Fe peak, which may decrease the adsorption capacity of the PS adsorbent. Thus, the optimal pH values for PE, PP, PS, and PVA were 7, 7, 6, and 7, respectively. Experimental data was used to calibrate the PHREEQC model at pH 2-9 with 5 mg·ℓ^{-1} Pb(II) solution and adsorbent dosages of 16.5, 7.50, 17.3, and 20 g·ℓ^{-1} of PE, PP, PS, and PVA, respectively, at 25°C. PHREEQC-PEST numerical modelling was conducted in SVD mode for PP and LSQR mode for PE, PS, and PVA. There were no statistically significant differences between the experimental and modelled data for the adsorbents. Thus, PHREEQC was successfully calibrated using PEST to determine sorption constants and accurately represent experimental data. The adsorption capacity of Pb(II) generally increased with increasing adsorbent dosage until 16.5, 7.50, 40.5 and 20.0 g·ℓ^{-1} for PE, PP, PS, and PVA, respectively. PHREEQC-PEST modelled adsorption of Pb(II) as a function of pH at different adsorbent dosages, corroborated experimental data and the adsorption efficiency generally increased with adsorbent dosage beyond pH = 5. The effect of initial concentration on the adsorption of Pb(II) by the adsorbent at fixed pH and adsorbent dosage for PE, PP, PS, and PVA was evaluated in batch studies. The quantity of Pb(II) adsorbed increased with concentration due to the availability of active sites up to 15, 17.5, 11.8, and 22.4 mg·ℓ^{-1} for PE, PP, PS, and PVA, respectively, after which there was saturation of the adsorbent's active sites.

CONCLUSION

This study was successful in conducting a comprehensive characterisation of MPs in river water, sediments, groundwater, drinking water (tap and bottled), tea, and beverages and modelling the potential physical-chemical behaviour of MPs in such systems. This was done by determining the occurrence and distribution of MPs in the above-mentioned media. Characterisation of the physical-chemical properties (i.e., shape, size, colour, polymer type, and additives) of different MPs and their additives using a stereomicroscope, FTIR, FEG-SEM, SEM-EDS, and micro-Raman spectroscopy was accomplished. Fibres were found to be dominant, followed by films, fragments and pellets. Their colours varied from black, white, yellow and red as a result of colourants and additives in them. The physical-chemical properties were used to define the sources, pathways, and potential anthropogenic inputs of MPs in such systems, e.g., fibres usually point to synthetic textile sources in addition to common plastics. To gain insight into the behaviour of MPs in different media, batch experiments and ICP-OES were used to determine the optimal adsorption parameters of Pb(II), the proxy used for adsorbing metals, on MP adsorbents. The study was able to present, for the first time, the coupling of PHREEQC and PEST modelling codes to determine surface complexation parameters that provided the best fit for limited experimental data.

The estimated surface complexation constants were then used to execute various computational simulations on generalised surface complexation modelling of Pb(II) on PE, PP, PS, and PVA MPs under different conditions that had not been conducted in the laboratory. The achievement of generalisation of sorption by polymeric surfaces is useful in understanding the short and long-term implications of MPs in the environment. This further reveals the potential of MPs as contaminants and as potential micro- and nanovectors for other contaminants in the environment. These findings provide a context in which further studies can be framed, which can lead to better decision-making and policy formulation regarding MPs in fast-moving consumer goods and water systems.

PUBLICATIONS AND PRESENTATIONS ARISING FROM THIS STUDY

- Gibbon Ramaremisa, Michelle Ndlovu, and Dalia Saad. Comparative assessment of microplastics in surface waters and sediments of the Vaal River, South Africa: Abundance, composition, and sources. Journal of Environmental Toxicology and Chemistry, DOI: 10.1002/etc.5482.
- Gibbon Ramaremisa, Hlanganani Tutu, and Dalia Saad. Detection and characterisation of microplastics in tap water from Gauteng, South Africa, Chemosphere, DOI: 10.1016/j.chemosphere.2024.141903.
- Gibbon Ramaremisa, Rudolph M. Erasmus, Hlanganani Tutu, and Dalia Saad. Occurrence and characteristics of microplastics in South African beverages, Environmental Pollution, DOI: 10.1016/j.envpol.2024.125388
- Dalia Saad, Michelle Ndlovu, Gibbon Ramaremisa, and Hlanganani Tutu. Microplastics in freshwater environment: the first evaluation in sediment of the Vaal River, South Africa. Heyilon, DOI: 10.1016/j.heliyon.2022.e11118

PRESENTATIONS

- Gibbon Ramaremisa, Hlanganani Tutu, and Dalia Saad. Detection and characterisation of microplastics in tap water from Gauteng, South Africa, Analitika conference, 10-14 March 2024, Oral presentation.
- Ramaremisa Gibbon, Saad Dalia, and Chimuka Luke., An in-depth identification and characterisation of microplastics in the Vaal River, South Africa., South African Chemical Institute (SACI) Central Section Young Chemist's Symposium, 19 August 2022, Oral Presentation.
- Ramaremisa Gibbon, Saad Dalia, and Chimuka Luke., An in-depth identification and characterisation of microplastics in the Vaal River, South Africa., South African Chemical Institute (SACI) National Symposium, 3 October 2022, Poster Presentation.
- Dalia Saad, Gibbon Ramaremisa, Michelle Ndlovu, and Patricia Chauke, Microplastics profile in the Vaal River, South Africa, 11th Oppenheimer conference, Midrand, South Africa, 5–7 October 2022.
- Dalia Saad, Gibbon Ramaremisa, and Luke Chimuka, Microplastics abundance, characteristics, and sources in surface water of the Vaal River, South Africa, Baltic Conference, and Fellow Summit 2022, Stockholm, Sweden, 28–30 August 2022.
- Dalia Saad, Gibbon Ramaremisa, Michelle Ndlovu, and Patricia Chauke, Microplastic abundance, distribution, and composition in water, sediment, and fish of the Vaal River: A significant freshwater system in South Africa, ACS Spring 2023, Indianapolis, US, 26-30 March 2023.

ACKNOWLEDGEMENTS

Reference group member	**Affiliation**
Dr Nonhlanhla Kalebaila	Water Research Commission
Ms Charmaine Khanyile	Water Research Commission
Dr Buyisile Kholisa	Water Research Commission
Prof Lawrence Madikizela	University of South Africa
Prof Elvis Fosso-Kankeu	University of Johannesburg
Prof Jean Mulopo	University of the Witwatersrand
Prof Richard Greenfield	University of Johannesburg
Prof Vusumzi Pakade	University of South Africa
Prof Henk Bouwman	North-West University
Prof Nelson Odume	Rhodes University
Prof Beatrice Opeolu	Cape Peninsula University of Technology
Prof Titus Msagati	University of South Africa
Prof Vhahangwele Masindi	Magalies Water
Mr Peter Manyara	International Union for Conservation of Nature
Ms Pamela Nxumalo	Department of Environment, Forestry and Fisheries

CONTENTS

LIST OF FIGURES

LIST OF TABLES

ACRONYMS AND ABBREVIATIONS

AB	Alcoholic beverage
ANOVA	Analysis of variance
BW	Bottled water
CTC	Cut-tear-curl
DWTPs	Drinking water treatment plants
EDI	Estimated daily intake
EPA	Environmental Protection Agency
EPSs	Extracellular polymeric substances (EPSs)
ESG	Environmental, social, and governance
FCMs	Food contact materials
FEG-SEM	Field emission gun-scanning electron microscopy
FMCG	Fast-moving consumable goods
FTIR	Fourier transform infrared spectroscopy
HDPE	High-density polyethylene
HQI	Hit quality index
ICP-OES	Inductively coupled plasma optical emission spectroscopy
IVRS	Integrated Vaal River System
JHB	Johannesburg
LDPE	Low-density polyethylene
LSQR	Least squares with QR-factorisation
MERI	Marine and Environment Research Institute
MPs	Microplastics
MQW	Milli-Q water
NAB	Non-alcoholic beverages
NIAS	Non-intentionally added substances
PE	Polyethylene
PES	Polystyrene
PEST	Parameter estimation
pH	Potential of hydrogen
PHREEQC	pH redox equilibrium in C
PITS	Potassium indigotetrasulfonate
Poly(AM-co-AA)	Poly(acrylamide-co-acrylic acid)
POPs	Persistent organic pollutants
PP	Polypropylene
PS	Polystyrene
PU	Polyurethane
PVA	Polyvinyl acetate

PVC	Polyvinyl chloride
RMS	Raman microspectroscopy
RSA	The Republic of South Africa
RTBA	Ramotswa Transboundary Aquifer
SAHRC	South African Human Rights Commission
SANBWA	South African National Bottled Water Association (SANBWA).
SANS	The South African National Standard
SARC	South African Rooibos Council
SCM	Surface complexation model
SDGs	Sustainable Development Goals
SEM	Scanning electron microscopy
SEM-EDS	Scanning electron microscopy-Energy dispersive spectroscopy
SEM-XEDS	Scanning electron microscopy-Energy dispersive X-ray spectroscopy
SVD	Singular value decomposition
TED-GC-MS	Thermal extraction-desorption gas chromatography-mass
TS	Tembisa sample
UN	United Nations
WWTPs	Wastewater treatment plants
ZAR	South African Rand

1 INTRODUCTION

1.1 BACKGROUND

This chapter presents the background on microplastics (MPs) on which the study is predicated. This provides a context for the motivation and purpose of the study, which has been described for river water, sediments, tap water, bottled water, beverages, groundwater, and sorption processes. Furthermore, it gives context behind the study design and its aims.

Water is an essential nutrient and an essential multifunctional constituent of the body, serving as a thermoregulator, cell-building material, shock absorber, lubricant, solvent, and carrier of various compounds, nutrients, and waste products. An array of sensitive physiological mechanisms precisely regulates water balance and levels of hydration in response to changes in consumption and losses, and thus changes in plasma osmolarity. The main purpose of drinking water treatment plants (DWTPs) is to make freshwater drinkable in terms of colour, odour, and taste, as well as to remove pathogenic microorganisms and harmful substances from the water (Acarer, 2023; Jéquier & Constant, 2010; Popkin et al., 2010). The South African National Standards (SANS) 241 for potable drinking water provides the minimum requirements for potable water to be considered safe for human consumption. Although the strict legislation of the SANS governs water boards and utilities, there is a class of contaminants of emerging concern (CEC) known as MPs, which do not have a minimum physical or chemical requirement, according to SANS 241.

1.1.1 Plastics and microplastics

Plastics were commercialised in the 1950s, and by the 1970s, they became the most widely used materials in the world. Due to their low production cost, light weight, durability, and mechanical strength, plastics are widely used for different industrial and commercial purposes (Amaral-Zettler et al., 2020; Andrady, 2017; Fred-Ahmadu et al., 2020). Additionally, commercially produced polymers contain different types of additives, such as fillers/reinforcements, heat stabilisers, colourants, flame retardants, and plasticisers, which are added during manufacturing to enhance certain properties for desired performance and marketability. Fillers and reinforcements make up more than 50% of the additives in plastics (Fred-Ahmadu et al., 2020; Hahladakis et al., 2018). A list of some additives for different uses is provided in Table 1-1.

Table 1-1: Polymer additives and their purpose (Fred-Ahmadu et al., 2020; Hahladakis et al., 2018).

Type of additive	Examples	Uses and purpose
Fillers and reinforcements	Clay, glass composites, boron or carbon fibres	Improving the flexibility, durability, and flexibility of polymeric films
Colourants	Cobalt diacetate, titanium dioxide, Cadmium, chromium, and lead compounds	Add specific colours to polymers
UV resistance	Oxanilides, octylphenol benzophenones, and benzotriazoles	Slow down the oxidation of plastics exposed to sunlight
Heat resistance	Cadmium and lead compounds, nonylphenol, and Bisphenol-A (BPA)	Preventing thermal degradation of polymers
Flame retardants	Polybrominated diphenyl ethers (PBDEs), tetrabromobisphenol A (TBBPA)	Reduce flammability
Plasticizers	Phthalic esters (PAEs), aliphatic dibasic acid esters, and benzoate esters	Render plastics pliable, flexible, and processable

Due to their low production cost, light weight, durability, and mechanical strength, plastics are widely used for different industrial and commercial purposes (Andrady, 2017; Fred-Ahmadu et al., 2020). Plastic materials offer many benefits to society; however, their negative impacts on the environment have become of great concern. Despite significant advances in waste management strategies and recycling technology, only 18% of plastic waste is recycled, 24% is incinerated and the remaining 58% is released into the environment. Consequently, they were considered the biggest environmental threat until the discovery of MPs in the early 21st century (Chamas et al., 2020).

Macroscopically, plastic items can cause death by suffocation and entanglement of several aquatic biota. Microscopically, MPs are generally defined as plastic debris whose longest dimension is less than 5 mm. Although this definition is not comprehensive concerning the macro, micro, and nano size domains, it has generally been accepted by scientists as a pragmatic option. Microplastics have also been characterised as CECs, “extremely persistent in the environment”, and as potential anthropogenic markers of the Anthropocene epoch due to their ubiquity in global ecosystems. Depending on their source, MPs are classified into primary or secondary MPs. Primary MPs are plastic particles manufactured in a microscopic size. They are commonly used in personal care products (e.g., toothpaste, face wash, cosmetics), industries (e.g., drilling fluids, industrial abrasives, and 3D-printer particles), and domestic applications (e.g., cleaning reagents). Secondary MPs, on the other hand, are formed from the breakdown of large plastics as a result of mechanical, chemical, or biological degradation (Catarino et al., 2021; Hartmann et al., 2019; Onoja et al., 2022; Park & Park, 2021; Samandra et al., 2022). Microplastics are present in various shapes, *viz.* fragments, spheres, fibres, films, flakes, foams, beads, pellets (and nurdles), sheets, granules, and foils in aquatic systems (Koelmans et al., 2019).

Sources of secondary MPs in aquatic environments are numerous and diverse and include synthetic textiles (35%), vehicle tyres (28%), dust (24%), road markings (7%), marine coatings (3.7%), personal care products (2%) and plastic nurdles (0.3%). Microplastics have been detected in the hydrosphere, atmosphere, lithosphere, and biosphere (Wright & Kelly, 2017). Degradation alters the physical-chemical properties of these MPs, such as colour, surface morphology, crystallinity, particle size, density, reactivity, surface functionality, and hydrophobicity. Degradation results in surface heterogeneity through the formation of cracks, scratches, and pores, making MPs less hydrophobic and buoyant (Guo & Wang, 2019; Hoellein et al., 2014; Kumar et al., 2021; Wang et al., 2021). Microplastics have several potential pathways into the hydrosphere such as wastewater effluent, sewage sludge, wear and tear of tyres, atmospheric fallout and deposition, direct disposal from the public, beach littering, and runoff from agricultural, recreational, industrial, and urban areas (Bellasi et al., 2020; Boucher & Friot, 2017; Dris et al., 2015; Zubris & Richards, 2005).

Although it was once believed that human exposure to MPs was primarily through ingestion, recent evidence suggests that inhalation also plays a significant role. Around the world, there is a growing body of literature that has documented the direct retention of MPs in and beyond human airways. Inhalation is predicted to account for tens of thousands of MPs inhaled each day, representing about 50% of the total daily intake (Carlsten, 2024; Eberhard et al., 2024; Lu et al., 2023; Song et al., 2024). A study by Lu et al. (2023) revealed that smoking cigarettes may significantly exacerbate human exposure to MPs, with MP concentration in smokers (mean: 25.86 ± 23.97 particles$\cdot$g^{-1}) being almost twice as high as in non-smokers (mean: 13.37 ± 15.26 particles$\cdot$g^{-1}). Consequently, the widespread presence and pervasive nature of MPs have raised concerns about their sustainability.

1.1.2 Sustainable Development Goals and MPs

Seventeen Sustainable Development Goals (SDGs) were introduced by the United Nations (UN) in 2015, with the target year for achieving them being 2030. The UN SDGs serve as a global clarion call to action to eradicate poverty, safeguard the environment, and guarantee that everyone lives in peace and prosperity. The 169 targets of the 17 SDGs are evaluated using 247 unique indicators. The issue of MPs (which has largely been biased towards the marine environment) has been recognised in the UN SDGs under Goal 14, which is to conserve and sustainably use the oceans, seas, and marine resources for sustainable development. Specifically, target 14.1: By 2025, prevent and significantly reduce marine pollution of all kinds from land-based activities, including marine debris and nutrient pollution. This will be measured by indicator 14.1.1: Index of coastal eutrophication and floating plastic debris (Walker, 2021). However, Walker (2021) identified 15 SDGs that are directly or indirectly impacted by MP pollution, as indicated in Table 1-2.

Table 1-2: United Nations Sustainable Development Goals directly impacted by MPs (Walker, 2021)

UN SDG goal	**Challenges posed by MPs to implementing the goal**
Goal 1. End poverty in all its forms everywhere	Without comprehensive plastic waste monitoring and reduction, the implementation of Goal 1 would be difficult due to its negative impacts on ecosystems and economic impacts on communities.
Goal 2. End hunger, achieve food security and improved nutrition, and promote sustainable agriculture	The consumption of MPs could be hazardous to human health because they are present in food packaging, agricultural soils, fruits, vegetables, fish, and shellfish.
Goal 3. Ensure healthy lives and promote well-being for all at all ages	The presence of MPs in humans (placenta, reproductive organs, skeletal tissues, blood, and faecal matter) is via ingestion, inhalation, and dermal exposure of MPs in packed food products, foodstuff, and air.
Goal 6. Ensure the availability and sustainable management of water and sanitation for all	Microplastics are present in treated wastewater effluent and drinking water.
Goal 7. Ensure access to affordable, reliable, sustainable, and modern energy for all	The burning of MPs in waste-to-energy systems increases greenhouse gas emissions, which pollute the atmosphere.
Goal 9. Build resilient infrastructure, promote inclusive and sustainable industrialisation, and foster innovation	Innovation is required for sustainable bio-based alternatives to fossil fuel–based plastics to contribute to a circular economy.
Goal 10. Reduce inequality within and among countries	The growing increase in plastic waste exports from developed to developing countries has led to widening inequalities.
Goal 11. Make cities inclusive, safe, resilient, and sustainable	Indiscriminate disposal of plastics in countries with inadequate waste management systems is choking critical urban infrastructure, such as drains and sewers, leading to widespread and unsustainable plastic pollution in urban areas.
Goal 12. Ensure sustainable consumption and production patterns	Mismanagement of plastic waste and unsustainable global plastic production.
Goal 13. Take urgent action to combat climate change and its impacts	Greenhouse gases are released at every stage of a plastic's life cycle.
Goal 15. Protect, restore, and promote sustainable use of terrestrial ecosystems, sustainably manage forests, combat desertification, and halt and reverse land degradation and halt biodiversity loss	Landfills, urban and rural locations, protected areas, and agricultural soils are all affected by improper MP waste management.

1.1.3 Scientific evidence and public risk perception

Globally, MPs have been detected in groundwater (Mintenig et al., 2019; Samandra et al., 2022); tap water (Kosuth et al., 2018; Mintenig et al., 2019; Pivokonsky et al., 2018); bottled water samples (Mason et al., 2018; Oßmann et al., 2018; Schymanski et al., 2018; Weisser et al., 2021; Zuccarello et al., 2019); soft and energy drinks (Shruti et al., 2020); white wine (Prata et al., 2020); beer (Diaz-Basantes et al., 2020, 2020; Kosuth et al., 2018); milk (Diaz-Basantes et al., 2020; Kutralam-Muniasamy et al., 2020); salt (Fadare et al., 2021; Karami et al., 2017; Kosuth et al., 2018); sugar and honey (Liebezeit & Liebezeit, 2013); and teabags (Hernandez et al., 2019; Shruti et al., 2020). As evidenced above, there has been significant progress made in the field of MP research since 1972, when Carpenter and Smith reported the first evidence of MP particles in the Sargasso Sea. However, there is still a lot more to be learned about the presence of nano-and MPs in South African freshwater sources and beverages (Carpenter & Smith, 1972; Mortensen et al., 2021; Ramaremisa et al., 2024).

In an emerging field of study, studies on MPs have sparked societal, political, and scientific interest, which has resulted in novel techniques for their characterisation as well as political and legal actions. This has resulted in the adoption of legislation aimed at MPs. For instance, the Microbead-Free Waters Act of 2015 and the European Commission 2018 Directive 2019/904 have been adopted by the United States of America (U.S.A.) and the European Union (EU), respectively. Furthermore, the presence of MPs in various environmental media (i.e., soil, atmosphere, freshwater, and marine water), commercially sold goods, fauna, and biota has raised concerns about their toxicity in academia and media. Although MPs can act as vectors for other contaminants such as metals, pharmaceuticals, and pesticides, many people perceive MPs as being less harmful than these contaminants. Thus, there is a need for increased risk communication to the public by the government, scientific community, print, and online media. Surveys conducted have also indicated that members of the public who are aware of MPs generally associate them with being more of a threat to the environment than to humans. In light of this, there have been calls made by members of the public for governments and the scientific community to provide solutions for the mitigation and/or eradication of MPs. Nevertheless, this noble endeavour faces several challenges, such as the belief by fellow scientists and the public that there is sensationalised reporting on the toxicity of MPs by scientists and the media. Additionally, there is a lack of automated analytical capability, standardisation of sampling, sample extraction and reporting, quality control and assurance, and characterisation protocols. Furthermore, the heterogeneity of MPs themselves makes it difficult to assess toxicity and to model their physical, chemical, and biological behaviour (Catarino et al., 2021; Völker et al., 2020).

1.2 PROJECT AIMS

This study aimed to conduct a comprehensive characterisation of MPs in river water, sediments, groundwater, drinking water (tap and bottled), tea, and beverages and model their potential physical-chemical behaviour in such systems. This would provide a benchmark on which future and advanced studies can hinge and provide insights into how these contaminants could be removed from water. To do this, the following objectives were pursued:

1. To monitor the occurrence and distribution of MPs in different aqueous environmental media.
2. To characterise the physical-chemical properties (i.e., shape, size, colour, polymer type, and additives) of different MPs and their additives using a stereomicroscope, FTIR, FEG-SEM, SEM-EDS, and micro-Raman spectroscopy to define their sources, pathways, and potential anthropogenic inputs.
3. To characterise MPs with respect to chemical constituents such as additives and their degradation products and potential release to media to which they are exposed.
4. To conduct geochemical modelling simulations by coupling PHREEQC and parameter estimation (PEST) to supplement experimental results and acquire a comprehension of the generalised surface complexation of MPs to account for release, and potential as micro-and nanovectors of other contaminants.

2 LITERATURE REVIEW

2.1 INTRODUCTION

This chapter provides an overview of the general literature on microplastics (MPs) and their pollution footprint in different aqueous media globally and locally. Contamination by MPs has also been described in their context as potential carriers of other contaminants prevalent in the aqueous systems in which they occur. Traditional modelling approaches that are commonly used have been described. A brief overview of theoretical methods for the characterisation of MPs has also been presented.

2.2 MICROPLASTICS IN FRESHWATER ENVIRONMENTS

2.2.1 Surface water – a case of the Integrated Vaal River System

The Republic of South Africa (RSA) is on an upward development trajectory; however, safe and clean water is increasingly becoming a resource in short supply. It is estimated that there will be water pollution and scarcity in two-thirds of the world by 2050. Currently, in RSA, there is little over 1200 m^3/person/year of freshwater to a population officially close to 60.6 million, making the country be classified as a water-stressed nation (Iloms et al., 2020; Mainardi-Remis et al., 2021; Statistics South Africa (StatsSA), 2023). A key component of the supply of this limited resource is the Integrated Vaal River System (IVRS). The IVRS is a complex interconnected system of water transfers from rivers, dams, canals, and pipelines. The IVRS supports approximately 50% of South Africa’s gross domestic product (GDP) (Matlakala et al., 2019; Muller et al., 2019). Rand Water is Africa's largest potable water utility and one of the largest in the world. According to the National Treasury, 98% of raw water used by Rand Water is extracted from the IVRS, treated, and supplied to at least 952 in Gauteng, Free State, North West, and Mpumalanga Provinces. The diverse industries include iron and steel, petroleum, paper and pulp treatment plants, plastic and building material manufacturers, power stations, and mining industries (Iloms et al., 2020; Muller et al., 2019; SAHRC, 2021; Weideman et al., 2020).

In addition to being an essential water source for industries, the IVRS, via Rand Water, has served as potable water to South Africans for more than 119 years. The raw water is extracted from the IVRS and treated at the Vereeniging and Zuikerbosch purification and pumping stations. It is then pumped to four main pumping stations (Zwartkopjes, Palmiet, Eikenhof, and Mapleton) situated on the southern outskirts of Johannesburg. Eventually making its way to 60 reservoirs located at central points and then supplied to over 16 million customers (Rand Water, 2022; SAHRC, 2021). MPs in drinking water sources are removed with varying degrees of efficiency in treatment units. However, DWTPs cannot remove all MP particles, and these eventually are consumed from tap water. The possibility of oral exposure of MPs to humans has placed research on MPs in tap water at the forefront in the past few years (Acarer, 2023; Feld et al., 2021; Shruti et al., 2021).

The IVRS has been under threat of pollution by domestic and industrial effluents, acid mine drainage, agricultural runoff, and litter (Saad et al., 2022; Tempelhoff et al., 2007; Wepener et al., 2011). Several water quality issues have been identified, including an increase in salinity, sulphates, nitrates, phosphates, microbial pollutants, dissolved solids, and MPs. Wastewater treatment plants around the IVRS have a history of operating beyond design capacity, breaking down, and having dilapidated infrastructure. An audit of 68 WWTPs in South Africa found that only six were compliant with effluent quality. Consequently, wastewater is rarely treated to acceptable standards, thereby polluting receiving surface water sources. Municipalities around the IVRS have been identified as being in contravention of the National Water Act (Madikizela et al., 2022; Verster & Bouwman, 2020; Vilakati et al., 2021; Wepener et al., 2011). Iloms et al. (2020) found a correlation, though it may not necessarily infer causation, between effluent from industries within the Sedibeng District Municipality and outflow from the Leeuwkuil WWTP into the Vaal River.

A report by the South African Human Rights Commission (SAHRC) on the Vaal River deemed the level of pollution as being “beyond acceptable levels”, impacting the natural ecosystem, endangering the fish and people’s health, and violating constitutional rights (SAHRC, 2021). Of interest to this particular study is that there is evidence of widespread MP pollution in the IVRS, which is the main water source. Considering its national importance and the risks posed to its water quality, it is essential to investigate the abundance of the physical and chemical characteristics of MPs in the Vaal River’s surface waters and sediments. Furthermore, it is imperative to study the extent of pollution in tap water and other consumable liquid products.

2.2.2 Microplastics in groundwater

2.2.2.1 Groundwater as an important source of water

An aquifer is defined as “A geological formation which has structures or textures that hold water or permit appreciable water movement through them” (Figure 2-1) (Nel, 2017). Karst aquifers make up a quarter of the global drinking water sources and are formed through the process of karstification. Karstification is the natural process whereby soluble rocks, like dolomite and limestone, dissolve when acidic rainwater seeps through them. When rainwater interacts with carbon dioxide, it forms the weak acid, carbonic acid (H_2CO_3). When carbonic acid percolates through dolomitic rock ($MgCa(CO_3)_2$), it causes the dissolution of the carbonate minerals. This leads to the formation of a heterogeneous conduit network of primary and secondary rock minerals, and the chemical process is expressed by Equation 1. Karstification results in the formation of cracks, fractures, cavities, and sinkholes, which provide a means of groundwater circulation and recharge. Karst aquifers constitute about a quarter of the world’s drinking water sources and play an essential role in sustaining the regional ecosystem and human health (An et al., 2022; Atangana & Noutchie, 2014; Panno et al., 2019). Approximately 97.4% of the Earth’s water is saline water found in oceans, seas, and saline lakes; only 2.5% is freshwater. Of the available freshwater, approximately 68.7% is contained in glaciers and ice caps, 30.1% is groundwater, and 1.2% is surface water in rivers, streams, and non-saline lakes. Of the 30.1% of groundwater, approximately 25% is from karst aquifers (Figure 2-2). Globally, at least two billion people on the planet depend on groundwater for their freshwater needs, which include drinking, farming, home, and industrial uses (Nel, 2017; Panno et al., 2019; Samandra et al., 2022). Although groundwater is an essential part of human existence, it is not exempted from invasive and ubiquitous MP pollutants.

$$CaMg(CO_3)_2 + 2H_2CO_3 \rightarrow Ca(HCO_3)_2 + Mg(HCO_3)_2 \qquad (1)$$

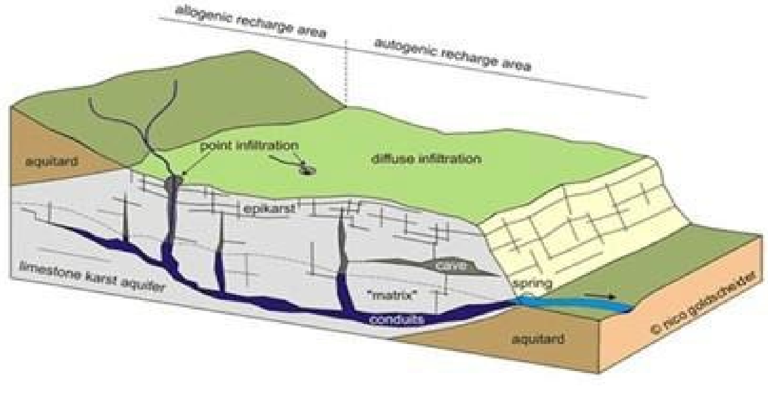

Figure 2-1: Conceptual model illustrating the duality of groundwater recharge, infiltration, and flow in a karst system (Atangana & Noutchie, 2014).

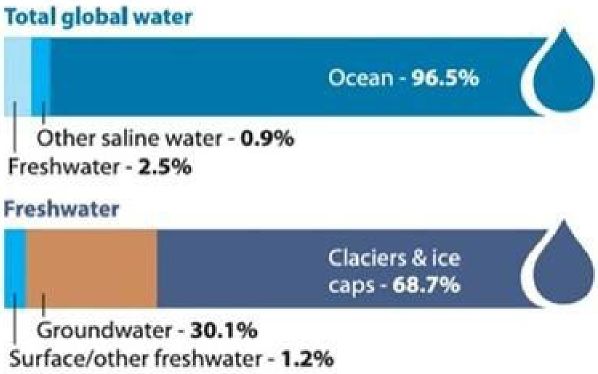

Figure 2-2: The Earth's freshwater source apportionment (Nel, 2017).

In Africa, it is estimated that more than 75% of people depend on groundwater for their daily needs. In South Africa, groundwater is a key source of freshwater. Global warming has contributed to high temperatures, reduced atmospheric moisture, and low rainfall, and as such, there has been an increased dependence on groundwater (Leketa et al., 2019; Nel, 2017). South Africa's Gauteng and North West Provinces rely on groundwater for socioeconomic development. These provinces have some of the country's significant karst dolomite aquifers. The karst dolomite aquifers form part of the Malmani Subgroup of the Chuniespoort Group, part of the Transvaal/Bushveld Supergroup. The Ramotswa Transboundary Aquifer (RTA) is an unconfined to semi-confined aquifer and forms part of the Ngotwane sub-catchment in the Upper Limpopo River Basin (Altchenko et al., 2017; Cobbing, 2018; Gemmell et al., 2021). The RTA dolomite aquifer covers an area between Botswana and South Africa in the Limpopo River Basin (Figure 2-3). Groundwater in the aquifer is found in the dolomite's karstified region, which is characterised by subterranean drainage systems consisting of sinkholes, fracks, and caverns (Altchenko et al., 2017). The aquifer is intruded by three vertical dikes, which create compartments with high transmissivity and storage capacity (Modisha, 2017).

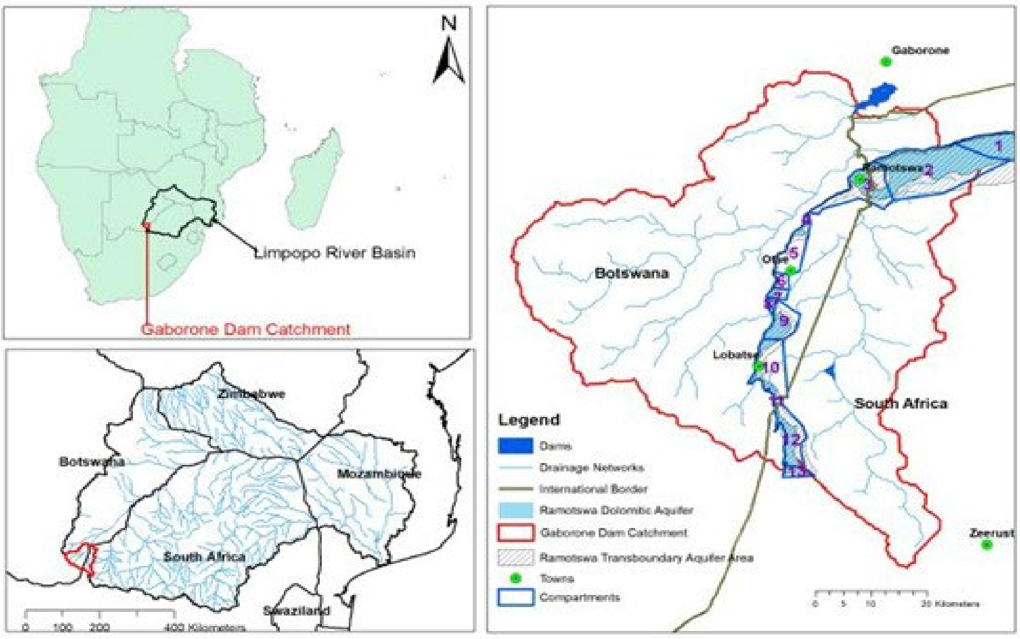

Figure 2-3: Location of the Ramotswa transboundary aquifer area (International Water Management Institute, 2025).

A combination of direct infiltration and diffused rainwater infiltration are the primary methods by which groundwater is recharged. The Ngotwane and Marico Rivers (Klein Marico and Groot Marico) are the RTA's main rivers. The Ngotwane River flows northward to the Limpopo River and serves as the boundary between Botswana and South Africa and recharges groundwater during the rainy season (Altchenko et al., 2017; Gaffoor et al., 2022; Gemmell et al., 2021; Martin, 2020; McGill et al., 2019).

The North West Province (NWP) is a rurally oriented spatial system with approximately 2480 rural settlements and thus can be classified as being made up of scattered urban nodes spread across a substantial rural backdrop. The NWP is divided into four district municipalities (i.e., Southern, Bojanala, Bophirima, and Ngaka Modiri Molema) comprising twenty-one local municipalities. Within the NWP, fractured dolomite aquifer compartments provide vast subsurface water storage on which over 80% of the rural population depends for their water requirements. Additionally, karst dolomite aquifers of the RTA have an ecologically significant role in supplying springs that feed major rivers. The South African population is currently estimated to be over 60.6 million, and as such, there has been a demand for an increase in agricultural produce, which has led to the expansion of irrigated agriculture into semi-arid areas. This expansion has resulted in the over-abstraction of groundwater and declining groundwater levels, which raise the costs of water provision and threaten sustainable development (Altchenko et al., 2017; Bierkens & Wada, 2019; Cobbing, 2018; Martin, 2020). Figure 2-4 shows dried-up boreholes, which serve as signs of over-abstraction and declining groundwater availability for residents in the Ramotshere Moiloa Local Municipality.

Figure 2-4: Dried-up boreholes in the North West Province.

Within the municipality, there are approximately 3238 boreholes but only 15.5% have specified uses including agriculture (n = 178), domestic (n = 143), stock water (n = 130), irrigation (n = 41), public (n = 3), gardening (n = 3), and mining (n = 1). Various towns and villages which depend on groundwater include Itsoseng, Lichtenburg, Mahikeng, Ottoshoop, Ventersdorp, Zeerust, Braklaagte, Driefontein, Dinokana, Groot Marico, Gopane, Swartfontein, Kwa-Ntsweng, Lekgophung, and Supingstad (Altchenko et al., 2017; Martin, 2020). Groundwater in Gauteng Province (GP) and North West Province (NWP) is affected by various pollution sources. In Gauteng, there have been reports of groundwater contamination in the Malmani dolomite aquifer by acid mine drainage (AMD) from old gold mines. Additionally, the discharge of partially treated wastewater into surface waters, such as the Vaal River, has contributed to groundwater contamination during recharge. Microplastics were previously reported in the Vaal River's surface water and sediments (Leketa et al., 2019; Ramaremisa et al., 2022; Weideman et al., 2020).

An assessment of groundwater near the Vaal River is essential to determining whether MPa are present in groundwater, surface water and sediment as this would suggest that they can undergo vertical migration from surface water to sediments and eventually groundwater. Due to the high groundwater table and fractured rock soil, pit latrines in the RTA have been directly linked to nitrate pollution in groundwater through wastewater infiltration. Wastewater treatment plants (WWTPs) were introduced in urban areas such as Gaborone, Lobatse, Ramotswa and Zeerust, and yet these have failed to effectively deal with waste produced due to an increase in the population in these urban areas. Consequently, discharge from WWTPs and spillages from the sewer network have negatively affected groundwater quality. Approximately 50% of the RTA is reported to be highly vulnerable to sanitation pollution (Martin, 2020; McGill et al., 2019). Thus, wastewater is a potential source of MPs in groundwater as a result of seepage of recharge by river water contaminated by wastewater.

The sustainable management of the groundwater resources of the RTA is impeded by several issues that member nations must confront. In addition to challenges such as over-abstraction, sanitation pollution, climate change and variability, and institutional mismanagement, there is a lack of data on contaminants of emerging concern (CECs) such as hormones, flame retardants, pesticides, endocrine disruptors and MPs (Shehu et al., 2022). To the best of our knowledge, there have been no studies that have examined the presence, concentration, or environmental drivers of MPs in South African karst groundwater systems. Data on the MP concentration in South African groundwater is essential for risk communication and comparison of physical-chemical properties of MPs from different aquifers, karst and alluvial aquifers to better understand the processes involved in groundwater contamination. Such data can be used to understand the relationship between physical-chemical (shape, size, and polymer type) properties of the MPs, soil type, prevailing environmental conditions and groundwater chemistry. Additionally, this data is essential for any groundwater management efforts to ensure that groundwater is used sustainably.

2.2.2.2 Research on MPs in Groundwater

The widespread use of agricultural plastic mulch, MP-coated fertiliser, solid waste application (e.g., sewage sludge and landfill), atmospheric deposition, and other sources, including surface water runoff, are thought to be some of the main sinks of MPs. Various studies conducted worldwide have consistently emphasised the detrimental impact of MPs in soil systems and reached a consensus that MPs may also be crucial for the migration of metals and toxic organic chemicals (Mu et al., 2022; Wan et al., 2022). The high concentrations of MPs detected in soils have fuelled concerns about their vertical migration from soil to groundwater, as shown in Figure 2-5. The vertical migration of MPs is further exacerbated by reports that soil invertebrates, such as the Anecic earthworm *Lumbricus terrestris*, may assist in the transmission of MPs through the soil profile into groundwater when they burrow (Huerta Lwanga et al., 2017; Mu et al., 2022; Re, 2019).

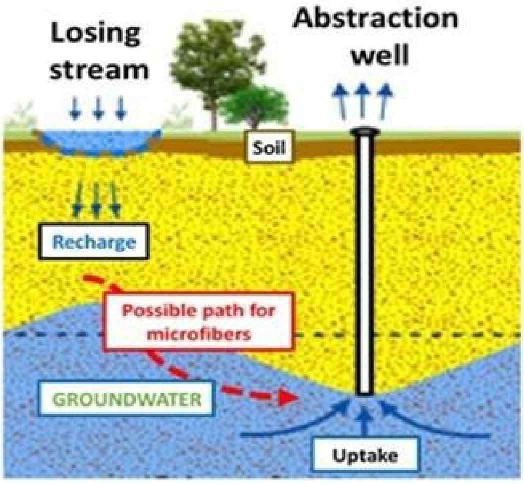

Figure 2-5: Schematic representation of possible MP pathway into groundwater (Re, 2019).

Concerns regarding the vertical migration of MPs have led to the initiation of studies which have focused on determining the physical-chemical properties of MPs in groundwater. Globally, there are fewer studies on MPs in groundwater than for freshwater bodies such as rivers and streams, mainly due to difficulties in sampling groundwater. As shown in Figure 2-6, only 201 papers have been published since 2017 on MPs in groundwater. The majority of studies were conducted in China (n = 91), the Republic of Korea (n = 37), the United States (n = 28), India (n = 21), and Australia (n = 20). There is a clear lack of such studies in Africa, which is a significant knowledge gap that this study aimed to address and provide a foundation on which further studies can be based. Additionally, there is limited research on the effect of hydrochemical parameters on MP abundance, with less than 50% of the studies recording on-site groundwater quality parameters. The majority of studies employed wet peroxide oxidation using Fenton's reagents during sample processing, a third employed density separation and only three studies used a dye to stain synthetic or non-synthetic polymers. As highlighted previously, as is the case with MP research in general, there is a lack of standard procedures for MP sampling in groundwater (Kim et al., 2023; Lee et al., 2024; Mu et al., 2022; Sangkham et al., 2023). However, the International Organisation for Standardisation and other organisations are currently working on developing standard procedures, but one major obstacle is the shortage of research and investigations that are readily available for use as references (Cha et al., 2024).

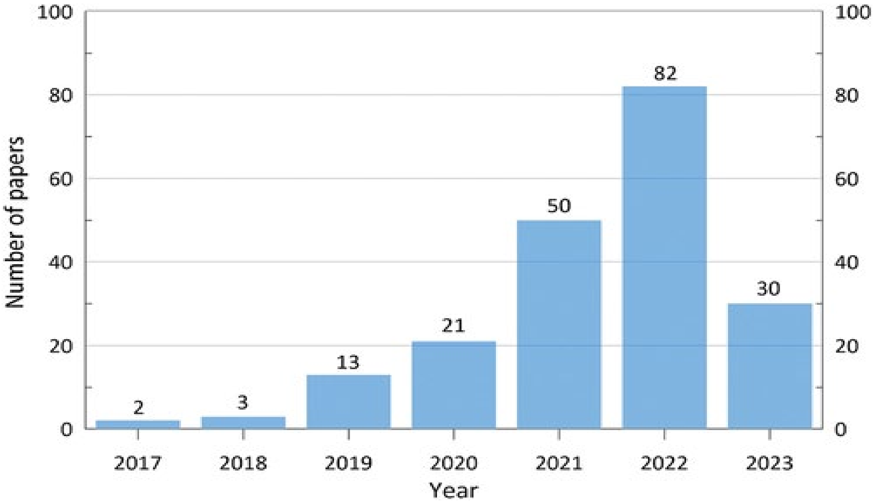

Figure 2-6: Peer-reviewed MP articles on groundwater (Lee et al., 2024).

2.3 MICROPLASTIC CONTAMINATION IN COMMERCIAL BEVERAGES

2.3.1 Microplastics occurrence in bottled water

The global bottled water industry is estimated to be worth over ZAR 4 trillion and produces more than 350 billion litres yearly (Bouhlel et al., 2023). The RSA bottled water industry is estimated to be worth ZAR1.5 billion, generated from about 100 bottled water companies. Multinational bottled water companies and corporations have an hourly output of about 20,000 litres. The global rise in the popularity of bottled water has been in large part due to its association with healthy living and a growing distrust in tap water quality. Additionally, it has been preferred over tap water due to its taste and comfort (Insight Survey, 2021; Mainardi-Remis et al., 2021; SANBWA, 2023; Zhou et al., 2021).

In 1997, presentations were made to the Department of Health to draft and implement legislation specifically aimed at regulating bottled water by the South African National Bottled Water Association (SANBWA). This led to the adoption of legislation R718, based on the Codex Alimentarius for all South African packaged water sales to the populous. In addition to R718, bottled water manufacturers are required to adhere to legislation that pertains to hygiene, food safety, quality, packaging, and environmental legislation (Foodstuffs Cosmetics and Disinfectant Act, National Water Act, etc). Per the legislation, R718, bottled water (or packaged water) is regarded as a food product and is thus governed by the Department of Health. According to Legislation R718, natural water, water defined by origin, and prepared water are the three types of bottled water products in RSA (SANBWA, 2021). Natural Water (natural mineral water or natural spring water) accounts for the largest portion (~70%) of bottled water and is water sourced from a natural or drilled underground source. Water defined by origin (spring and mineral water) is the second largest portion (~20%) and is defined as water sourced from a specific environmental source (spring or subterranean water-bearing strata). If the water has passed through antimicrobial treatment, it cannot be regarded as “natural” water. Prepared water (~20%) is sourced from an underground or municipal source and then subjected to either antimicrobial treatment, reverse osmosis, or ozonation, altering its physical-chemical properties (SANBWA, 2023). Legislation and regulations for bottled water by the Department of Health do not specifically consider the level of MPs present.

According to Bouhle & Smakhtin (2023), bottled water companies are exempted from strict standards and regulations applied to tap water, and only a few chemical parameters are deemed adequate for the sale of bottled water. The global bottled water industry is expected to double during the current decade; thus, governments must strengthen legislation on the industry and water quality standards. Legislation should provide improvements to bottled water quality control, prevent groundwater and land exploitation, and reduce plastic waste in the environment due to PET and HDPE bottles and MPs within bottled water (Bouhlel & Smakhtin., 2023).

2.3.2 Microplastics in alcoholic and non-alcoholic beverages

The large range of goods that make up beverages meant for human consumption can be classified into alcoholic and non-alcoholic beverages. Beers, wines, and spirits are common alcoholic beverages, while tea, coffee (hot and cold), soft drinks, milk, and carbonated and noncarbonated sweetened beverages are non-alcoholic options (Shruti et al., 2020). In 2021, South Africa was ranked tenth in the world and first in Africa in terms of beer consumption. South African Breweries (SAB) is South Africa’s biggest alcoholic beverage producer. South African Breweries brews about 3.1 billion litres of alcoholic beverages per year. SAB houses local and international brands such as Castle, Brutal Fruit, Redd’s, Stella Artois Lager, Coronita Extra, Newlands Spring, Beck’s, Lion Lager, Flying Fish, Hansa Pilsener, Budweiser, and Carling Black Label (Verlag W. Sachon. 2020; SAB. 2020).

The current total urban household expenditure on beer (2.21%) accounts for more than non-alcoholic (hot and cold) beverages (1.84%), footwear (1.01%), tobacco (1.97%), vegetables (1.27%), sweets and desserts (0.58%) and fruit (0.33%). With three main types of alcoholic beverages: beer, wine (red wine, white wine, and spirit coolers), and spirits (brandy, whiskey, liqueur, and vodka) it is estimated that 51.5% of households purchases of alcoholic beverages were devoted beer, followed by Wine (26.6%), and then spirits (21.9%) (StatsSA., 2023). In terms of consumption, alcoholic and non-alcoholic beverages are the third most purchased products (6.13%) behind processed (8.57%) and unprocessed food (6.73%) (StatsSA, 2023). An analysis of MPs in beverages is essential to estimate the extent to which consumers are exposed to these pollutants. The beverage industry is an attractive prospect for MPs' research due to various reasons. Freshwater is the biggest ingredient in bottled water (mineral, spring, and general potable) water and beverages (alcoholic and non-alcoholic). Bottled water and beverage industries consume copious quantities of freshwater during production and cleaning. For every 1ℓ of bottled water produced, approximately 3ℓ of regular freshwater is used. Moreover, other ingredients in beverages, such as sugar, oranges, wheat, barley, or tea, are produced by the agricultural sector, which is one of the largest consumers of water (Mainardi-Remis et al., 2021).

Given the prevalence of MPs in the Vaal River's freshwater systems, water may be the first source of MPs in bottled water and beverages. It has been reported that there is a release of non-intentionally added substances (NIAS) into bottled water exposed to moderate temperatures (40-60 ℃). The authors reported a release of compounds such as 2,4-di-tert-butylphenol and bis(2-hydroxyethyl)terephthalate, which are degradation products from phenolic antioxidants and PET monomers. Additionally, Bach et al. (2014) and Aigotti et al., (2022); reported the release of NIAS (formaldehyde, bisphenols (A and S), acetaldehyde, Antimony (Sb), Octocrylene, and 4- cumyl phenol) from PET bottles (Aigotti et al., 2022; Bach et al., 2013). It has also been widely reported that exposing plastic containers to Ultraviolet (UV) radiation and oxygen leads to the formation of free radicals, chain scission, crosslinking, and secondary oxidative reactions. It has also been observed that as time passes, plastics become brittle and yellow, thus eventually leading to more MP formation (Sewwandi et al., 2023). Taking this into consideration, it is therefore important to investigate the effect of storage conditions on the MP concentration in South African bottled water and beverages.

Research on MPs in bottled water and beverages has potential far-reaching implications for the fast-moving consumable goods (FMCG) industry, considering the latest international expectation of organisations to conduct business within acceptable environmental, social, and governance (ESG) precepts and ethos. Thus, providing evidence of pollution by MPs is an important foundation for conducting a socio-economic assessment that addresses the social, economic, and environmental costs of such pollution. ESG aspects have become very pronounced and will impact investment in industries quite significantly going into the future. For instance, financial institutions are no longer offering investment finance for coal exploration and mining as a result of carbonisation strategies.

2.3.3 Tea bags as a source of microplastics tea beverages

The most popular teas (black, green, white, and oolong tea) across the world are natural beverages from an evergreen bush of the genus *Camellia Sinensis*, with over 80 known species. Tea bags were developed by Thomas Sullivan in 1908 to provide packaging for tea leaves. Tea bags were initially made of gauze and have grown in popularity since their commercialisation in the 1920s (Yurtsever, 2021). Recent iterations of tea bags either contain or are made up of different polymer-based food contact materials. Black tea is traditionally produced by harvesting tea leaves and allowing them to wither in cool, dry air. The tea leaves are then crushed, subjected to oxidation, and dried in a furnace to stop the oxidation and dehydrate them. After these processes, the leaves are ready for storage and consumption. Popular varieties of black tea include Darjeeling, Assam, Turkish, and Ceylon teas. Commercial producers may also use the cut-tear-curl (CTC) to store tea leaves in tea bags. The CTC method entails crushing, tearing, and curling withered leaves to produce fine tea leaves. Green tea differs from black tea because withered leaves do not undergo the oxidation process. The world's tea production (~85%) is dominated by multinational companies such as Unilever, Associated British Foods, Tata Tetley, and Van Rees (Khumalo, 2012). Tea is one of the world's most widely consumed beverages, and its RSA market was estimated to be worth ZAR 1.1 trillion in 2021 and is predicted to rise to ZAR 1.4 trillion by 2027. A large market share is dominated by Black tea, with Green tea expected to increase in market share in the next decade and may eventually overtake Black tea. The rise in tea sales is driven by its perceived health benefits, especially among millennials, over other beverages (Insight Survey, 2022).

Rooibos is South Africa's caffeine-free alternative to traditional tea varieties. Rooibos tea was discovered by Dutch settlers in the 1700s who were looking for a cheaper alternative to black tea. Rooibos is made from the indigenous *Aspalathus linearis* bushy herb grown in the Western Cape's Cederberg Mountains. Other tea varieties generally come from *Camellia sinensis* plants. Rooibos tea is considered a food by the European Union. It is reported that more than half (31 million) of South Africans prefer Rooibos tea over other alternatives. Approximately 14,000 tons are produced annually, with half of this being exported to more than 30 countries around the world (Areo et al., 2022; Joubert & De Beer, 2011; South African Rooibos Council, 2023). Studies by Yurtsever (2021) and Hernandez (2019), reported that nearly 13,000 and 11.6 billion MPs were released from tea bags. Yurtsever (2021) and Ali (2023) further recommended that tea consumers consider switching to loose tea instead of using tea bags. Tea is the second most-consumed beverage after water in South Africa; thus, it's imperative to determine the level of MP pollution in tea. A review of the literature revealed that there were no previous studies to investigate MPs in Rooibos tea in South Africa. This is a major research gap that this study aims to address.

2.4 PHYSICO-CHEMICAL BEHAVIOUR OF MICROPLASTICS

2.4.1 Sorption

Sorption is a fundamental physical-chemical process that involves the transfer of fluids (liquids and gases) to solids. Sorption can occur through chemical, physical, and ionic processes (Figure 2-7). Adsorption predicts the quantity of elements that can be sorbed to an adsorbent surface. The process of chemical partitioning between two phases is constantly changing, and a state of equilibrium is reached when the concentrations in both phases remain constant (Wang & Guo, 2020). Sorption processes play a vital role in numerous fields, including earth science, environmental chemistry, and both chemical and civil engineering. In the environment, adsorption regulates the movement and reduction of harmful contaminants in surface and groundwater, such as naturally occurring Arsenic (As), Lead (Pb), and Uranium (U), as well as anthropogenic pollutants chromium from tanning and electroplating industries, or agricultural runoff containing pesticides, phosphate, and nitrate fertilizers. Sorption by plants is beneficial for the retention of micronutrients, such as Zn, Fe, Ni, Cu, and Mn (Bullen et al., 2024; Fred-Ahmadu et al., 2020; Fu et al., 2021).

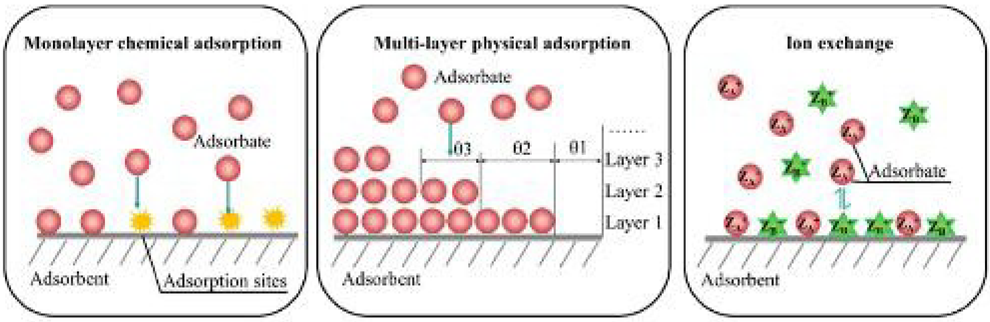

Figure 2-7: Different adsorption mechanisms (Wang & Guo, 2020)

Metals are commonly incorporated into polymers during production to act as inorganic pigments, flame retardants, heat stabilisers, and catalysts (Murphy, 2001). MPs in the environment sorb metals due to their larger specific surface area, porosity, and hydrophobicity or release metals from their surfaces as they are degraded. Alternatively, environmental processes such as photo-oxidation, mechanical abrasion, and biofilm development can alter the physical-chemical properties of MP particles, which may cause them to have an electric charge and allow them to adsorb metal ions to maintain charge balance. Microbes produce biofilms by generating a matrix of extracellular polymeric substances (EPSs). Extracellular polymeric substances can provide a bridge for the attachment of MPs to metals through the formation of bonds through chemical groups such as amide, carbonyl, carboxyl, phosphoric, phenolic, and hydroxyl (Amaral-Zettler et al., 2020; Wang et al., 2019b).

The adsorption of various pollutants onto MPs has been studied, including heavy metals, polychlorinated biphenyls (PCBs), polycyclic aromatic hydrocarbons (PAHs), dichloro-diphenyl-trichloroethane (DDTs), and antibiotics (Guo et al., 2019; Turner & Holmes, 2015). A study by Liu et al. (2022) determined metal concentration in suspended matter, plankton, and MPs from water samples in Hong Kong. The authors reported high concentrations of Cd (676 mg/kg), Pb (1,742 mg/kg), and Zn (1,712 mg/kg). Furthermore, different MP polymers contained different metals, which suggested there was selective adsorption of metals based on polymer composition. Metals such as Sb, As, Cd, Mn, and Pb were detected in higher concentrations in PE MPs, while PS MPs had higher concentrations of Be, Ni, V, Co, Cr, and Zn. In an earlier study by Turner & Holmes (2015), the authors noted that the difference in ion concentration between the sorbate and adsorbate is crucial to adsorption. Cations in the liquid phase may compete with other ions for cationic exchange sites on MPs, thus, adsorption affinity may decrease under high ionic strength (Turner & Holmes, 2015).

2.4.2 Effects of the surrounding media

2.4.2.1 Effect of pH

The sorption processes on MPs are influenced by hydrophobic and electrostatic interactions. The surrounding media's pH significantly affects the adsorption behaviour of pollutants. Puckowski et al. (2021) reported greater adsorption of pharmaceuticals at opposite extremes of the pH scale (pH = 2 and 12). This remains an important aspect to explore since charges on these molecules tend to change at particular pH values. This change should also be considered in the context of the surface charge of the adsorbent. An aspect will be explored later when discussing a substance's point of zero charge (pzc). For metals, their precipitation may occur simultaneously with adsorption. Precipitation increases in high pH (pH > 7) environments; moreover, metals will form complexes with carbonate, sulphur or phosphate species (Figure 2-8) (National Academies of Sciences, Engineering, and Medicine, 2017; Oliveira et al., 2019; Powell et al., 2009).

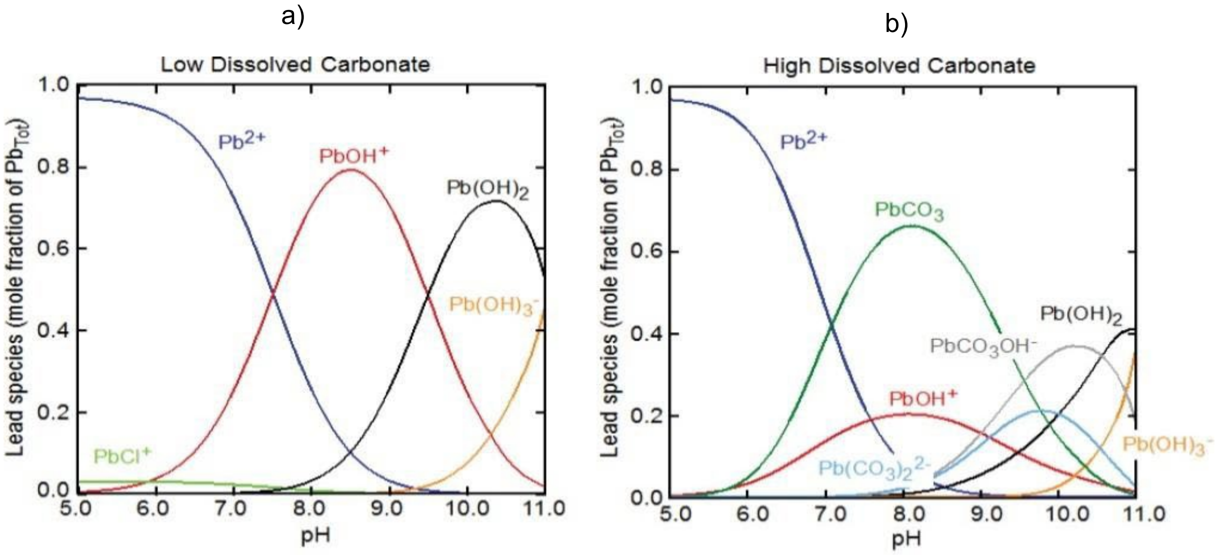

Figure 2-8: The concentration of Pb species as a function of pH for (a) low and (b) high dissolved carbonate concentrations calculated with PHREEQC (National Academies of Sciences, Engineering, and Medicine, 2017).

2.4.2.2 Effect of dissolved organic matter

Organic matter may lower the ability of organic contaminants to bind to MPs by attracting and retaining them (Wu et al., 2019). However, the opposite may be true for inorganic pollutants. Godoy et al. (2019), used batch series to assess the adsorption of metals by five distinct types of MPs under varying conditions in aquatic environments. They discovered higher metal adsorption in waters with substantial biological and chemical oxygen demands, such as urban effluent and agricultural water, consistent with other studies (Richard et al., 2019; Wijesekara et al., 2018). As indicated erstwhile, aquatic environments in South Africa present interesting scenarios such as the mixing of acid mine drainage with sewage or high pH water draining through dolomitic media. This is where hydro/geochemical modelling becomes an important tool to predict associated changes in the water chemistry and implications on sorption processes.

2.4.3 Effects of the adsorbent

The ability of plastic to absorb water is contingent upon the intermolecular interactions that occur between the polymer and the contaminants. Van der Waals forces, hydrogen bonding, and cavity creation are the three types of interactions that are most important for the sorption of compounds in water. As a result, each polymer has a unique physical-chemical structure, and this affects the adsorption capacity as well as potential interactions between the polymer and the water (Godoy et al., 2019). A key chemical component in adsorption is polymer functional groups and additives. As shown in Figure 2-9, calcite is the most widely used filler and in some instances a whitening pigment in the world. Additives may enhance or attenuate adsorption by polymers.

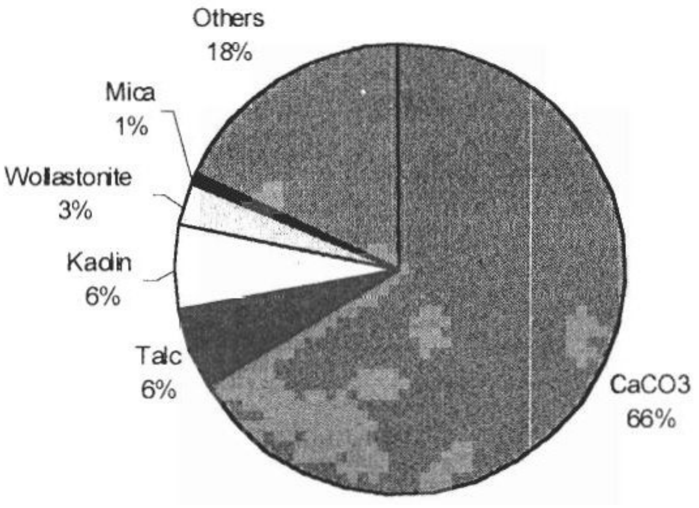

Figure 2-9: A graph of the world's plastic filler consumption in 2001 (Houssa, 2003).

Degradation of MPs in the environment increases surface heterogeneity through cracks, scratches, and the formation of pores. Hence, decreasing particle size will result in increased surface area and sorption sites (Kumar et al., 2021; Wang et al., 2019a). As would be expected, the sorption capacity of nanoplastics was reported to be 1 to 2 orders of magnitude greater than that of MPs (Velzeboer et al., 2014). While MPs are highly attracted to hydrophobic organic contaminants, weathering and degradation of MPs lead to the formation of oxygen-containing functional groups and thus greater affinity for hydrophilic pollutants (Luo et al., 2020). The degradation processes discussed here also require further study concerning the release of constituent components of MPs such as additives, plasticisers and colourants.

The point of zero charge (pzc) gives information on the attraction and repulsion involving an absorbent and a sorbate. It is classified as the pH value when the charge on both positively and negatively charged sites is equal. Additionally, it allows us to confirm that one of the processes involved in metal sorption is electrostatic force. The pzc can be determined through the potentiometric titration technique, mass titration technique and immersion technique. Each technique has some inherent shortcomings; for instance, mass titrations often require the use of large quantities of the adsorbent, and the polymerization of some particles makes it conduct. The immersion technique can achieve low accuracy (±1 pH unit) (Fiol & Villaescusa, 2009; Vakros et al., 2002).

2.4.4 Adsorption models

The adsorption mechanisms have previously been explored by modelling adsorption equilibrium data, characterizing the adsorbent both before and after adsorption, conducting molecular dynamics simulations, and performing density functional theory (DFT) calculations (Fred-Ahmadu et al., 2020; Tourinho et al., 2019; Wang & Guo, 2020).

2.4.4.1 Empirical adsorption isotherms

Elements can adhere to surfaces via monolayer or multilayer adsorption processes. At equilibrium, isotherms can be utilised for understanding the connection between equilibrium analyte concentrations in the sorbate solution and the adsorbent. These are empirical formulas that have been effectively used to analyze the adsorption data of various chemicals onto surfaces, including MPs (Fred-Ahmadu et al., 2020; Tourinho et al., 2019).

2.4.4.2 Linear isotherm

The linear isotherm describes the distribution of adsorbates in the solid and liquid phases. Van der Waals forces, hydrophobic interactions, and electrostatic forces all contribute to partitioning processes. The linear model in Equation 2, which was developed from the Langmuir model, assumes a low adsorption site coverage (Figure 2-10). The Langmuir model approximates Henry's law in low-pressure gas adsorption on materials (Wang & Guo, 2020). The linear model has the following form:

$$q_e = KC_e \qquad (2)$$

With q_e ($mg \cdot g^{-1}$) = adsorbed amount at equilibrium, Ce ($mg \cdot g^{-1}$) = adsorbate concentrations at equilibrium, K ($\ell \cdot g^{-1}$) = partition coefficient.

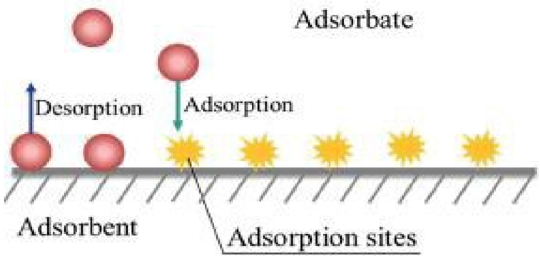

Figure 2-10: Adsorption mechanism assumed by the linear model (Wang & Guo, 2020).

2.4.4.3 The Freundlich isotherm

Equations 3 and 4 define the Freundlich isotherm for heterogeneous surfaces with non-ideal and reversible adsorption phenomena utilised for adsorption on the heterogeneous surface with adsorbate interaction. The variability might be attributed to distinct functional groups on the adsorbate and varying adsorbent-adsorbate interactions.

$$q_e = K_F C_e^{\frac{1}{n}} \qquad (3)$$

$$\log q_e = \log K_F + \frac{1}{n} \log C_e \qquad (4)$$

Where qe (mg·g^{-1}) = adsorbed amount at equilibrium, K_F [(mg·g^{-1})·(mg·ℓ$^{-1}$)$^{-1/n}$] = Freundlich constant, Ce (mg·ℓ$^{-1}$) = the equilibrium concentration of the adsorbate, n (dimensionless) = measure of the adsorption intensity or surface heterogeneity.

2.4.4.4 Temkin isotherm

The Temkin isotherm suggests that a linear reduction in the heat of adsorption occurs with coverage and a uniform distribution of adsorption energy due to interactions between the adsorbent and adsorbate. Neglect is given to adsorbate concentration values that are both extremely high and low in the liquid phase (Wang & Guo, 2020). Temkin isotherm model is represented by Equations 5 and 6.

$$q_e = \frac{RT}{b_T}\ln A_T C_e \tag{5}$$

$$q_e = \frac{RT}{b_T}\ln A_T + \frac{RT}{b_T}C_e \tag{6}$$

Where K_T (ℓ·mol^{-1}) = Temkin isotherm constant related to the heat of adsorption, Ce (mg·ℓ$^{-1}$) = the equilibrium concentration of the adsorbate, R (8.314 J·K^{-1}·mol^{-1}) = Universal gas constant, and T (K) is the absolute temperature.

2.4.5 Polanyi's potential theory-based models

Polanyi's potential theory is a framework for describing adsorption processes, particularly those involving gases and solid surfaces. It implies that the adsorption potential varies with distance from the adsorbent surface, and molecules are adsorbed when the adsorbent's potential energy is low enough to attract the adsorbate. This theory contributes to understanding the distribution of adsorbates about the adsorbent's energy, emphasizing how adsorptive forces vary with distance from the surface (Wang & Guo, 2020).

2.4.5.1 Dubinin-Radushkevich (D-R) isotherm

The Dubinin-Radushkevich (D-R) isotherm model, adopted from the Polanyi potential theory of adsorption, does not make any assumptions about surface homogeneity or constant adsorption potential. The model describes the adsorption of metals onto a heterogeneous adsorbent whose distribution of adsorption sites follows a Gaussian energy distribution. The model is employed to assess the type of sorption process as well as its mean energy (Abdelnaeim et al., 2016). The D-R model is represented by equation 7.

$$q_e = q_{mD-R}e^{-K_{D-R}\varepsilon^2} \tag{7}$$

Where q_{mD-R} (mg·g^{-1}) is the maximum amount of adsorbate adsorbed, K_{D-R} (mol^2·KJ^{-2}) is the Dubinin-Radushkevich constant related to the mean free energy of adsorption, ε (kJ·mol^{-1}) is the Polanyi potential, which is equivalent to RTln(C_s/C_e), C_s (mg·ℓ$^{-1}$) is the solubility of adsorbates.

2.4.5.2 Dubinin-Astakhov (D-A) model

The D-A is a more generalised semi-empirical version of the D-R model, which can be used when investigating the micropore structures of the adsorbent (Cheng & Hu, 2016). The D-A model is represented by Equations 8 and 9.

$$\theta_e = e^{\left[\left(\frac{\varepsilon}{E_{D-A}}\right)^{n_{D-A}}\right]} \tag{8}$$

$$q_e = q_{mD-A}e^{\left[\left(\frac{\varepsilon}{E_{D-A}}\right)^{n_{D-A}}\right]} \tag{9}$$

Where $q_{mD\text{-}A}$ ($mg \cdot g^{-1}$) is the maximum amount of adsorbate adsorbed, ε ($kJ \cdot mol^{-1}$) is the Polanyi potential which is equivalent to RTln(Cs/Ce), $E_{D\text{-}A}$ ($kJ \cdot mol^{-1}$) is the characteristics energy, $n_{D\text{-}A}$ is a constant related to the per cent of pore-filling.

2.4.6 Chemical adsorption models

Chemical adsorption models, also known as chemisorption models, explain the chemical interaction of adsorbate molecules with an adsorbent's surface. Chemisorption is the development of strong chemical bonds between the adsorbate and the adsorbent, which typically results in major modifications to the adsorbate's electronic structure. Chemisorption has numerous key aspects. Strong Interaction, for example, is characterised by greater contacts than physical adsorption (physisorption), often mediated by covalent, ionic, or metallic connections. Because each adsorption site may normally connect with just one molecule, monolayer formation usually results in a monolayer of adsorbate on the adsorbent surface. Irreversibility is owing to strong bonding; chemisorption is frequently irreversible or needs significant energy to reverse. The process is specific to the chemical constitution of both the absorbent and the adsorbate, which means that not all molecules will chemisorb on the same surface.

2.4.6.1 Langmuir isotherm

Irving Langmuir provided a mathematical explanation of the monolayer adsorption between adsorbates and homogeneous flat adsorbent surfaces. The non-linear and linear forms of the Langmuir isotherm are presented by Equations 10 and 11. The Langmuir isotherm assumes equal amounts of adsorbed and desorbed molecules on the surface per unit of time at equilibrium (Figure 2.11) (Langmuir, 1916).

$$q_e = \frac{q_m K_L c_e}{1 + K_L c_e} \qquad (10)$$

$$\frac{1}{q_e} = \frac{1}{q_m} + \frac{1}{q_m K_L c_e} \qquad (11)$$

Where q_m = maximum monolayer coverage capacity ($mg \cdot g^{-1}$) and K_L ($\ell \cdot mg^{-1}$) = the Langmuir constant.

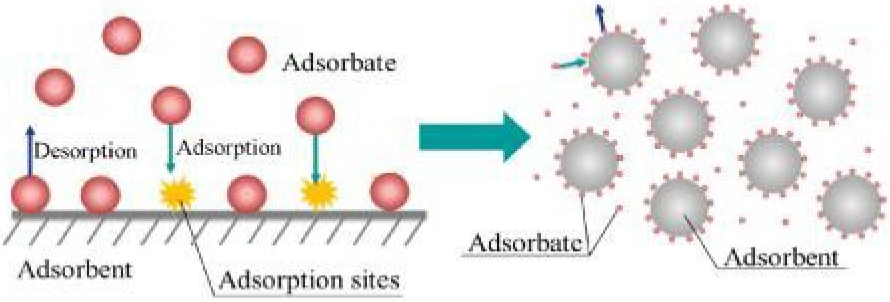

Figure 2-11: The adsorption mechanisms according to the Langmuir isotherm model (Wang & Guo, 2020).

2.4.6.2 Volmer isotherm model

Similar to the Langmuir isotherm model, the Volmer model is a monolayer adsorption model. The model implies adsorbate molecules can move on the adsorbents' surfaces, and interactions between adsorbates are insignificant (Volmer, 1925). The Volmer model is represented by Equation 12.

$$b_v C_e = \frac{\theta_e}{1-\theta_e} e^{\frac{\theta_e}{1-\theta_e}} \qquad (12)$$

Where b_v ($\ell \cdot mg^{-1}$) is the affinity constant, $\theta_e = q_e/q_{mV}$ (q_{mV} ($mg \cdot \ell^{-1}$) is the maximum adsorbed amount estimated by the Volmer model and qe ($mg \cdot g^{-1}$) is the adsorbed amount at equilibrium (Volmer, 1925).

2.4.7 Physical adsorption models

The multi-layer adsorption process is modelled using theoretical physical adsorption isotherm models. Driving the physical adsorption is primarily the Van Der Waals force (Wang & Guo, 2020).

2.4.7.1 Brunauer-Emmett-Teller (BET) isotherm model

The adsorption of gas to multimolecular layers is modelled by the BET isotherm model. The theoretical multi-layer physical adsorption model, as expressed by Equation 13, has been utilised to compute the pore size distribution and specific surface areas of the porous material. As depicted in Figure 2-12, the BET isotherm assumes there is multi-layer homogeneous adsorption and that the adsorption energies are different across different layers; the adsorption rate equals the desorption rate (Brunauer et al., 1938; Wang & Guo, 2020).

$$q_e = \frac{q_{mBET} C_{BET} C_e}{(C_S - C_e)\left[1 + (C_{BET} - 1)\frac{C_S}{C_e}\right]} \qquad (13)$$

Where qe ($mg \cdot g^{-1}$) is the adsorbed amount at equilibrium, C_{BET} is the constant, and C_s ($mg \cdot L^{-1}$) is the solubility of the adsorbate. C_s can be calculated as an adjustable parameter or treated as a constant taken from solubility data.

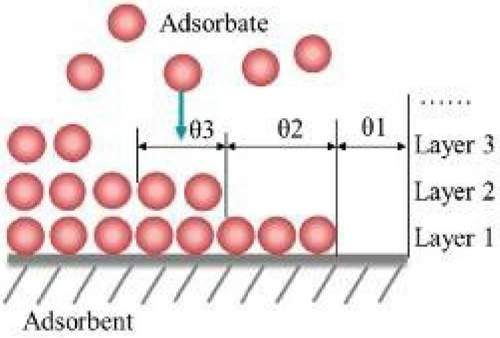

Figure 2-12: The adsorption mechanisms according to the BET model (Wang & Guo, 2020).

2.4.7.2 Aranovich model

The Aranovich isotherm is a two-parameter model used to simulate adsorption across a wider range of adsorbate concentrations. The model may be applied to calculate the surface area of porous adsorbents. Furthermore, it assumes the adsorbent's surface is uniform and homogenous, there is only a "nearest neighbour" interaction, and the desorption energy is contingent on the number of layers. The model is represented by Equation 14 (Aranovich, 1992).

$$q_e = \frac{q_{mA} C_A \frac{C_e}{C_{SA}}}{\sqrt{\left(1 - \frac{C_e}{C_{SA}}\right)\left(1 + C_A \frac{C_e}{C_{SA}}\right)}} \qquad (14)$$

Where q_{mA} ($mg \cdot g^{-1}$) is the adsorbed amount at equilibrium, C_A is the Aranovich constant, and C_{sA} ($mg \cdot L^{-1}$) is the adsorbates monolayer saturation concentration (Aranovich, 1992). This model will change to Henry's law at low C_0.

2.4.8 Kinetic models

Adsorption kinetic models are commonly used to predict pollutant adsorption's effectiveness and rate-limiting processes onto MPs. Adsorption kinetics are divided into four steps: (a) bulk transport, (b) external mass transfer (film diffusion), (c) intra-particle diffusion, and (d) chemisorption. Lagergren's pseudo-first-order, Ho's pseudo-second-order, Elovich equation, intraparticle diffusion, and film diffusion models are the most commonly used adsorption kinetic models for characterising the adsorption of sorbates onto surfaces (Table 2-1). Pseudo-first-order and pseudo-second-order models assess the entire adsorption process, whereas the intraparticle diffusion and liquid film diffusion models focus on the rate-limiting steps of adsorption (Fred-Ahmadu et al., 2020; Guo et al., 2019; Zhang et al., 2018). The pseudo-second-order model is predicated on the premise that chemisorption, which involves valency forces through the sharing or exchange of electrons between sorbent and sorbate, might be the rate-limiting phase. The Elovich equation is generally applicable to chemisorption kinetics for heterogeneous adsorbents (Cheung et al., 2000). The physical distribution in a solid-liquid system influences the adsorption process when it follows the pseudo-first-order model. If the pseudo-second-order model appropriately represents the adsorption kinetics, the sorbent's adsorption process is often chemisorption. The intraparticle diffusion model states that adsorbates diffuse within the adsorbent's pores. The liquid film diffusion theory is driven by physical-chemical interactions, including hydrophobic interactions and covalent forces (Gong et al., 2019; Zhang et al., 2018).

Table 2-1: Kinetic models.

Kinetic model	Equations	References
Pseudo-first-order	$q_t = q_e(1 - e^{-k_1 t})$	Fred-Ahmadu et al. (2020)
Pseudo-second-order	$q_t = \frac{k_2 q_{e,2}^2 t}{1 + K_2 q_{e,2} t}$	Ho & McKay, (1999)
Elovich	$q_t = a + b\ln(t)$	Cheung et al. (2000)
Film diffusion	$\ln(1 - \frac{C_t}{C_0}) = -k_3 t$	Wang & Guo, (2020)
Intraparticle diffusion	$q_t = k_p t^{0.5} + S$	Guo et al. (2019)

q_t (mg·g^{-1}) = adsorbed amount at time t, $q_{e,1}$ (mg·g^{-1}g) = adsorption capacity of the pseudo-first-order equation, $q_{e,2}$ (mg·g^{-1}) = adsorption capacity of the pseudo-second-order equation, a (mg·g^{-1}) = parameter in the Elovich equation, b (mg/g·min) = Elovich equation parameter, C_t (mg·ℓ$^{-1}$) = adsorbate concentration at time t, C_0 (mg·ℓ$^{-1}$) = initial adsorbate concentration, C_e (mg·ℓ$^{-1}$) = adsorbate concentration, k_1 (h^{-1}) = the rate of adsorption of the pseudo-first-order equation, k_2 [g·mg^{-1}·h] = the rate of adsorption of the pseudo-second-order equation, k_3 (h^{-1}) = film diffusion model constant, k_p [mg/g·h$^{0.5}$] = intraparticle diffusion model constant, S (mg·g^{-1}) = intraparticle diffusion model constant

2.4.9 Thermodynamics

Thermodynamics studies are essential for assessing the reaction's spontaneity, endothermic or exothermic nature, and the possibility of adsorption. To this end, thermodynamic parameters such as the standard Gibbs free energy (ΔG^0), change in enthalpy (ΔH^0), and entropy change (ΔS^0) need to be determined. This can be done using Equations 15-17.

$$K_d = \frac{C_o - C_e}{C_e} \qquad (15)$$

$$\Delta G^0 = -RT\ln K_C \qquad (16)$$

Van't Hoff's equation:

$$\ln K_d = \frac{\Delta S}{R} - \frac{\Delta H}{RT} \qquad (17)$$

Where R (8.314 $J \cdot mol^{-1} \cdot K^{-1}$) = the ideal gas constant, T (K) = temperature, K_d ($\ell \cdot mol^{-1}$) = equilibrium constant, C_e ($mg \cdot \ell^{-1}$) = concentration of the adsorbate at equilibrium, C_O ($mg \cdot \ell^{-1}$) = initial concentration of the adsorbate.

2.4.10 Geochemical modelling

Although the adsorption models mentioned above do well at explaining the adsorption process, there are drawbacks, such as the models being valid for a limited set of experimental conditions and being unable to respond to changes in pH, ionic strength, or competing adsorbates. Laboratory and field experiments include inherent flaws and uncertainties, such as the absolute pH of solutions and the equilibrium constants. These drawbacks can be overcome by using Surface complexation models (SCMs) that can adjust to variations in experimental conditions and accurately simulate the system's chemistry (Bullen et al., 2024; Zavarin et al., 2022). Surface complexation models contain databases with equilibrium reaction constants (log K) for adsorption, aqueous phases, gas phases, and precipitation reactions to provide sensitivity to changes to the adsorbate and adsorbent (i.e., pH, ionic strength, redox potential, concentration, surface area, and surface site density). SCMs are run on geochemical modelling software (e.g., PHREEQC, MODFLOW, FITEQL, PHAST, HYTEC GeoSurf, Visual MINTEQ, and Geochemist's Workbench).

The final model may consist of numerous nonlinear equations that are collectively solved by applying the Newton-Raphson approach (Bullen et al., 2024; Li & Zarzycki, 2022).

2.4.10.1 Geochemical modelling with pH-Redox-Equilibrium in C (PHREEQC)

The United States Geological Survey (USGS) created PHREEQC, an open-source modelling software for low-temperature hydrogeochemistry, in the C/C++ programming languages. PHREEQC is available in compiled form or as source code. PHREEQC has several advantages, such as being able to perform various geochemical calculations, including the speciation in different environments, reaction pathways, and one- one-dimensional reactive transport and is also compatible with numerous databases (e.g., *phreeqc.dat, sit.dat, wateq4f.dat, pitzer.dat, llnl.dat, tipping_hurley.dat, and minteq.v4.dat*). The modeller can select a database based on their need since the different databases do not contain the same parameters. Additionally, the databases can be paired with application programming interfaces (APIs), Artificial Intelligence (AI), and machine learning (ML) models (e.g., Python, Stacking Ensemble ML regressor, and MATLAB), and model-independent parameter estimation software (e.g., PEST and hydro-particle swarm optimisation (hydroPSO)). These can be to estimate sorption/surface complexation constants and site density parameters from experimental data (Abdelaziz et al., 2019; Chang et al., 2023; Hasrod et al., 2024; Lu et al., 2022; Parkhurst & Appelo, 2013; Vega-Garcia et al., 2021). Although SCMs have been successful in modelling adsorbate-sorbate interactions, advances in AI and ML may lead to the replacement of some SCMs and fitting algorithms with AI-based surrogates when databases become well-developed (Hasrod et al., 2024; C. Li & Zarzycki, 2022).

2.4.10.2 Parameter estimation software (PEST)

PEST software can be run in five main modes depending on the problem the modeller faces. The different PEST modes include parameter estimation, predictive analysis, regularisation, pareto, and another mode. Parameter estimation mode estimates parameters for a well-posed inverse problem. Predictive analysis minimises/maximises the value of a prediction while maintaining the calibration objective function below a certain value, regularisation estimates parameters for an ill-posed inverse problem. Pareto mode can be used for direct predictive hypothesis-testing or balancing measurement-to-measurement fit against regularisation (Doherty et al., 1994; Zavarin et al., 2022). When PEST software is coupled with PHREEQC, there are four files required, namely: template file (*.tpl), instruction file (*.ins), control file (*.pst) and batch file (*.bat) (Figure 2-13). The template file reflects the model input file, except that the parameter to be estimated in the input file of PHREEQC (*.pqi) is substituted with a series of characters, whereas an instruction file provides PEST with instructions on how to retrieve experimental data so that the simulated parameters from PHREEQC's output file (*.pqo) will be close to the experimental data.

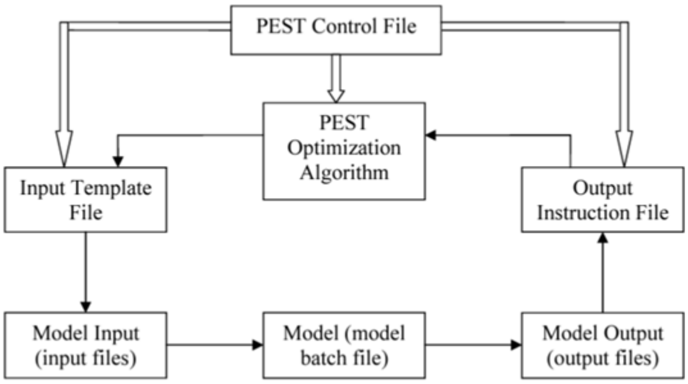

Figure 2-13: Schematic diagram of coupling PEST with geochemical modelling software (Lin, 2010).

The control file contains information on the model program to be run, experimental observations, the number of parameters to be estimated, parameter groupings, boundary conditions of model parameters, the number of instructions, template and control files. The batch file executes PHREEQC and PEST. PEST files can be prepared using general-purpose text editors (e.g., Notepad++, Notepad and Visual Studio Code) (Abdelaziz et al., 2019; Bachmaf & Merkel, 2011; Bullen et al., 2024; Mosai et al., 2024). PEST is supported by five main utility software programs (TEMPCHEK, INSCHEK, PESTCHEK, PESTGEN, and PARREP), which aid with PEST input file generation. TEMPCHEK, INSCHEK, and PESTCHEK are used to ensure the accuracy and compatibility of the input datasets in template, instruction, and control files before executing PEST. The PESTGEN utility software generates a PEST control file with standard values for most PEST input variables. PARREP generates a new PEST control file using an existing PEST control file and a set of values from a parameter value file (Doherty et al., 1994).

2.4.11 Modelling physical-chemical behaviour

Lead (Pb) is an element naturally found in low concentrations throughout the Earth's crust, including rocks, soils, sediments, and water. Natural Pb enrichment can occur through several geologic processes, leading to the formation of ore deposits. Lead may be distributed in the environment both naturally and by deliberate transfer. Lead has extensive applications in electroplating, steel, electrical, and explosives industries. Water is the main mode of natural transportation (Figure 2-14). Pb concentrations in water may be lower than other dissolved species, yet it can still be transferred by colloidal or suspended particles such as MPs (National Academies of Sciences, Engineering, and Medicine, 2017; Oliveira et al., 2019; Tang et al., 2020). Lead is a toxic metal, even in trace quantities and exposure can endanger aquatic organisms and affect human health. Due to its ability to accumulate in biological systems, it can cause a variety of ailments and even death. Among trace metals, Pb has been proven to have a high affinity for plastic surfaces in field and laboratory experiments (Godoy et al., 2019; Liu et al., 2022; Oliveira et al., 2019). However, most metal-MP interactions have been studied mostly in terms of concentrations and adsorption-desorption processes (Godoy et al., 2019; Qi et al., 2021). To date, there have been no studies that have used numerical models to validate the experimental data or simulate conditions that were not experimented with in the laboratory. This study aimed at exploring that knowledge gap by determining the sorption capacities of Pb (as a surrogate for other metals) onto different polymeric surfaces of MPs and under varying conditions, typically those encountered in the environment(s) in which MPs are generally exposed to. The approach using PHREEQC and PEST presents opportunities to understand the sorption of metals onto heterogeneous and non-conventional surfaces. The predictions also allow for the determination of sorption at conditions outside the general experimental scope.

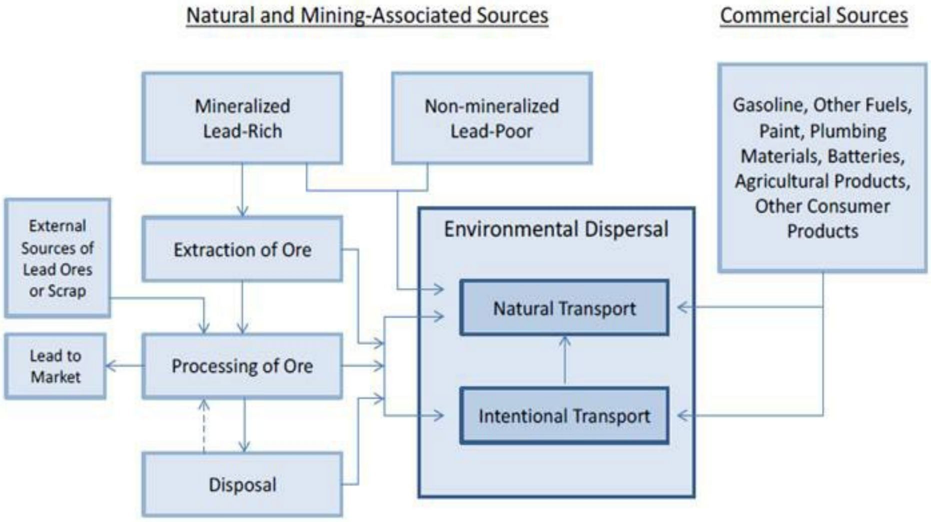

Figure 2-14: Source of lead in the environment (National Academies of Sciences, Engineering, and Medicine, 2017).

South Africa lacks a comprehensive characterisation and modelling of the physical-chemical behaviour of MPs in water systems (surface water, groundwater, tap, and bottled water) and bottled beverages. Consequently, there is limited data on the characterisation of MPs with respect to their chemical constituents, additives, degradation products, and potential release to the media to which they are exposed. The sorption processes of MPs in water systems have not been extensively explored worldwide (Godoy et al., 2019). South Africa is primed well for such work by the interesting mix of environments it presents for study. An understanding of the sorption chemistry of contaminants stands to improve our knowledge of the potential role of MPs as micro- and nano-vectors of other contaminants, exogenous or endogenous to them, and their transformation to other chemical substances. This can be used to understand and address the socio-economic ramifications of their pollution through evidence-based recommendations, decision-making support, policy formulation, comprehensive risk assessment, and management.

2.5 MICROPLASTIC CHARACTERISATION TECHNIQUES

2.5.1 Scanning electron microscope (SEM) and energy dispersive spectroscopy (EDS)

A scanning electron microscope (SEM) provides information regarding a sample's surface morphology, crystallinity, elemental composition, and electrostatic behaviour to a depth of 1 µm. A schematic diagram of an SEM system is shown in Figure 2-15. SEM is similar to the design of a stereomicroscope, with the main difference being the type of lenses used, with electromagnetic/electrostatic lenses used in SEM and glass lenses used in a stereomicroscope. An SEM consists of an electron gun or source (i.e., Tungsten (W) filament, Lanthanum hexaboride (LaB_6), and field emission gun (FEG) that generates electrons that are accelerated with voltages in the range of 0.2 to 40 kV. SEM is operated in high vacuum environments (10^{-6} to 10^{-10} Torr).

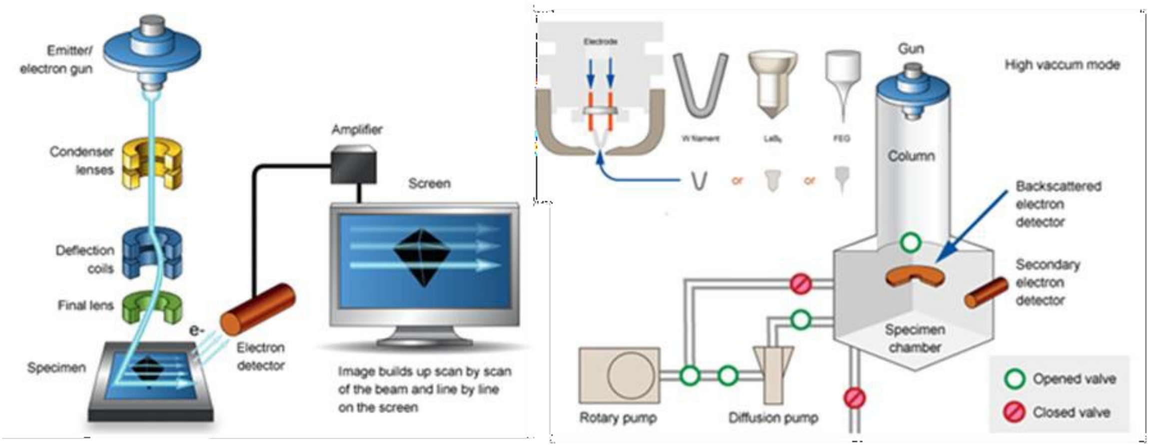

Figure 2-15: Schematic diagram of a SEM system.

The SEM column provides a pathway for electrons through two or three electromagnetic lenses (i.e., condenser and final lenses). The electron deflection system consists of deflection coils, which aid in focusing the electron beam into a fine probe that passes through the objective to the sample. The beam is scanned over the surface of the sample, and X-rays, Auger, backscattered, and secondary electrons are emitted. Information on the sample is provided by an electron detector from the sample's backscattered and secondary electrons. The surface morphology builds up per scan and is then viewed on and can be viewed on a screen. FEG SEMs are operated at higher vacuum pressure, which makes them more expensive; however, they provide better sample resolution (1 nm) than W filament and LaB_6 SEMs (Mohammed & Abdullah, 2018; Vernon-Parry, 2000). X-rays occur when an electron is emitted, a K-shell electron is dislodged by the electron beam, and another electron fills the hole or vacancy in the K-shell. The electronic transitions are unique to a particular element; thus, SEM can be coupled with EDS to determine elements present in polymers. The application of SEM-EDS in MP research has gained notoriety in the past decade as a key tool for determining elemental composition (Girão et al., 2017; Vernon-Parry, 2000).

2.5.2 Inductively coupled plasma optical emission spectroscopy (ICP-OES)

ICP-OES is based on the principle of the spontaneous emission of photons generated from excited ions or atoms excited by a radio frequency. Plasma is a superheated, electrically neutral matter made up of ions, electrons, and neutral particles. ICP typically comprises three concentric quartz tubes, specifically outer, intermediate, and inner tubes. The top of the quartz tube or torch is surrounded by a water-cooled induction coil coupled to a radiofrequency generator. The argon gas is introduced into the torch and a radio frequency field is operated at 4 to 50 MHz and a forward power of 1000 to 5000 W is applied. This causes a magnetic field surrounding the coil and an ignition from a Tesla coil that generates electrons and ions. The generated current moves in a closed circular circuit, heating the argon gas to produce an ion beam at 7,000 to 10,000°C. The argon gas further serves as a coolant as it flows in the outer tubes. A nebulizer transforms an aqueous sample into an aerosol mist, which is then delivered into the inner tube of the ICP. When heated by the plasma, atoms become excited and emit light when they return to a lower energy state. The atomic emissions are separated into their components by a diffraction grating to allow light intensity measurement by a photomultiplier tube (PMT) (Figure 2-16). The PMT monitors the intensity of emission signals at certain wavelengths. The intensity of the emission signal is going to be proportional to the element's concentration in the plasma (Khan et al., 2022; Sneddon & Vincent, 2008).

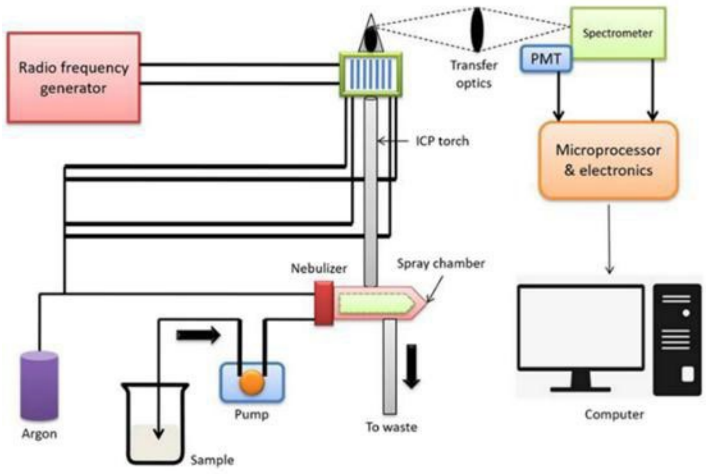

Figure 2-16: Schematic of a typical ICP-OES system (Khan et al., 2022).

2.5.3 Fourier-transform infrared spectroscopy (FTIR)

Spectroscopy involves examining how electromagnetic radiation interacts with various materials. The techniques used in spectroscopy can rely on phenomena such as emission, absorption, and fluorescence scattering. FTIR is used for determining chemical properties based on molecular vibrations and rotations. Atoms form chemical bonds and functional groups which constantly vibrate (Bumbrah & Sharma, 2016; Hou et al., 2018). The device's centrepiece is a Michaelson interferometer (Figure 2-17), which includes an infrared source, a beam splitter, two mirrors, and a detector. In this setup, the beam splitter directs some of the infrared radiation (IR) to two mirrors, one of which remains still while the other moves continuously to collect data. The IR beams reflected by the mirrors are then recombined at the beam splitter before passing through the sample to the detector, which captures all wavelengths. The beam splitter recombines the two beams, and interference arises due to the variable path lengths provided by the moving mirror. The detector's recorded data is a Fourier transform of the transmitted IR light for a given sample, which is convolved into an IR spectrum. FTIR includes two test methodologies (transmission mode and reflection mode) based on whether or not an infrared radiation (IR) beam passes through the sample (Hou et al., 2018; Tintor et al., 2024).

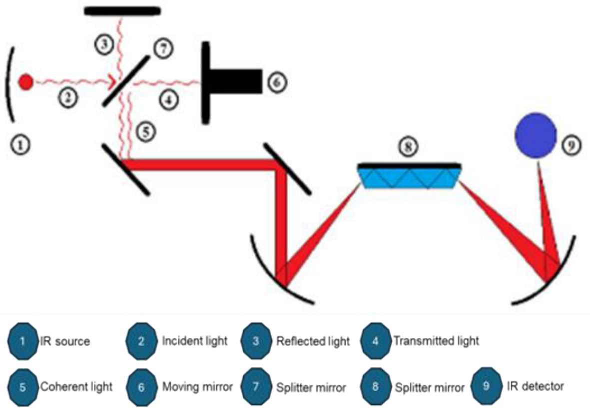

Figure 2-17: Architectural design of an FTIR (Hou et al., 2018).

2.5.4 Raman spectroscopy

Raman spectroscopy (RMS) is a scattering technique (i.e., the Raman Effect) (Figure 2-18). When monochromatic radiation interacts with matter, it gets scattered, and the majority of the scattered radiation will have the same frequency (i.e., Rayleigh scattering) as the incident radiation and a small fraction will have a different frequency (i.e., Raman scattering). RMS is based on determining the difference in the frequency of the Raman scattered radiation and the incident monochromatic radiation. If the frequency of the incident radiation is higher than that of the scattered radiation, Stokes lines appear in the Raman spectrum. If the incident radiation's frequency is lower, anti-Stokes lines are present. Raman spectrophotometers can be dispersive, using prisms or gratings, or non-dispersive, utilizing interferometers like the Michelson interferometer in FTIR. Initially, spectrophotometers used a Mercury arc lamp as a light source until the development of laser sources such as Argon ion, Krypton ion, Helium-Neon, Near Infrared (IR) diode lasers, Neodymium–Yttrium Aluminum Garnet, and Neodymium–Yttrium Ortho-Vanadate. In the early development of Raman spectrophotometers, thermoelectrically cooled photomultiplier tubes and photodiode array detectors were employed. Subsequent technological advancements facilitated the transition to more sensitive charge transfer devices (CTDs), including charge-coupled devices (CCDs) and charge-injection devices (CIDs) (Baker et al., 2016; Bumbrah & Sharma, 2016).

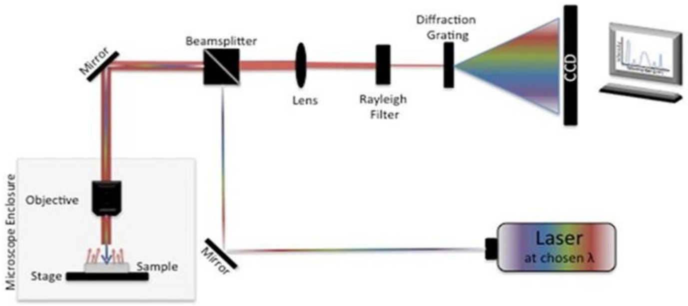

Figure 2-18: Architectural design of a Raman spectrometer (Baker et al., 2016).

3 MATERIALS AND METHODS

3.1 INTRODUCTION

This chapter presents the experimental protocols followed to achieve the study objectives. It covers the procedures for quality control and assurance during experiments and the methodology used to achieve the results. Aspects related to risk assessment and data treatment have been included.

3.2 QUALITY CONTROL MEASURES

Adequate measures were adopted to avoid/reduce cross-contamination, sample loss from leakages during filtration, and interference during analysis. Only metal and glass apparatuses and containers were used during sampling. In the laboratory, all experimental equipment and containers were washed with filtered Milli-Q® Type 1 Ultrapure water and rinsed with ethanol, and all work was conducted under a laminar flow cabinet. Cotton laboratory coats and powder-free nitrile gloves were worn during all experiments. The use of plastic apparatus was minimised throughout the experiments. To mitigate against the potential contamination of samples by MPs in chemicals, all solutions were filtered through a Whatman® GF/F glass microfibre filter (Cytiva Danaher Group, Buckinghamshire, United Kingdom) before use. In addition, adequate blank experiments were conducted to account for contamination from atmospheric deposition. Furthermore, there was daily instrumental calibration, triplicate samples, the use of internal and check standards, and statistical analysis to validate experimental data (Ramaremisa et al., 2022, 2024).

3.3 CHEMICALS AND MATERIALS

All chemicals and materials used were obtained from Sigma Aldrich (Merck KGaA, Darmstadt, Germany) and De Bruyn Spectroscopic Solutions (Johannesburg, South Africa). All chemicals were used without further purification: ethanol 96% AR reagent, 50% (v/v) hydrogen peroxide, lead(II) nitrate (≥99.0%), sodium chloride (99%), sodium hydroxide (98.5%), nitric acid (55%), Rose Bengal ≥80% dye content, Scott Duran® glass bottles (100 mℓ), certified multi-element aqueous certified reference material (CRM), and Scandium (Sc) certified single element aqueous CRM (99.999%), and iron (II) sulphate heptahydrate ACS reagent ≥99.5%. PE, PP, PS, and PVA MPs were modified to enhance their adsorption potential. Microplastic adsorbents were subjected to environmental weathering by placing them in glass Petri dishes and leaving them on the roof of the Humphrey Raikes building at the University of the Witwatersrand for a year (July 2023-2024).

3.4 SAMPLING

3.4.1 Surface water and sediments

Surface water and sediment samples were collected over approximately 50.4 km between the Lethabo weir (Panfontein) and the Vaal River Barrage (Windsor on Vaal AH) (Figure 3-1). This region of the Vaal River has water flowing in from tributaries such as the Suikerbosrand, Klip, Wilge, Mooi, Waterval, Taaibosspruit, Leeuspruit, and Rietspruit Rivers. Surface water samples were collected using a 55 µm plankton net (0.25 m in diameter, 0.5 m in length) (Hydro-bios, Germany). To avoid contamination and ensure undisturbed sampling conditions, the plankton net was positioned outside the wake of the boat. The plankton net was towed along the river’s surface for 15 to 30 minutes; between each tow, the sample was retrieved from the cod end, and the net was rinsed with the river water. Samples were then stored in pre-cleaned glass jars. Global Positioning System (GPS) coordinates were taken at each sampling point to determine the distance sampled.

Figure 3-1: The Vaal River sampling area (Google Earth Pro, Alphabet Inc., California, U.S.A).

Volume filtered through the net was calculated using a flowmeter (General Oceanics model 2030R) attached to the inside of the net frame (Egessa et al., 2020; Frias et al., 2019; Weideman et al., 2020) (Figure 3-2). For sediments, twenty-five samples were collected at 3 km intervals from the top 10 cm of the riverbed using a 500 mℓ Van Veen grab sampler (Eijkelkamp, Netherlands). A rope was tied to the hanger of the Van Veen and slowly lowered into the river from the side of the boat. Once it reached the bottom, the Van Veen closed and was pulled out with a sediment sample. At each sampling site, three replicates were collected and mixed in a 2ℓ borosilicate glass using a stainless-steel spoon to establish sample representativeness. The composite sample was then placed into a pre-cleaned glass jar (Figure 3-3).

Figure 3-2: Surface water sampling procedure.

Figure 3-3: Sediment sampling procedure.

3.4.2 Groundwater sampling

Twenty groundwater samples were collected from five borehole-connected taps in suburbs in Gauteng (Braamfontein, Vereeniging, and North Riding), and fifteen borehole-connected taps in villages and towns in the North West (Zeerust, Supingstad, Lekubu, Kwa-Ntsweng, Mokgola, and Braklaagte). The taps are connected to plastic storage containers through plastic tubing. Pumps pump water from the borehole into storage tanks and then taps (Figure 3-4). At each sampling point, a sample was collected into 3ℓ pre-washed glass jars, stored in cooler boxes and taken to the laboratory for further processing. Sample location, field chemical parameters, and adjacent land use conditions were recorded (Ramaremisa et al., 2024). Field chemical parameters: pH, oxidation-reduction potential (ORP), electrical conductivity (EC), absolute conductivity, resistivity, total dissolved solids (TDS) and salinity were recorded using a calibrated Hanna multiparameter HI98194 (Hanna Instruments Pty Ltd, Johannesburg, SA).

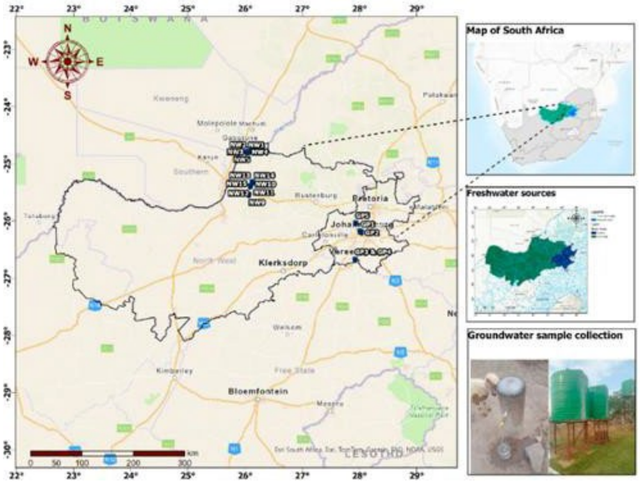

Figure 3-4: Study areas and groundwater sampling (ArcGIS Pro, ESRI Inc., Redlands, CA, USA).

3.4.3 Tap water sampling

Samples were collected between March and July 2023 from conventional taps in the Gauteng Province. Samples were collected from Tembisa and Braamfontein in Johannesburg and Silver Lakes in Pretoria. Before collection, tap water was allowed to run for one minute, followed by collection into 3ℓ pre-washed glass jars, stored in cooler boxes and taken to the laboratory for further processing (Chu et al., 2022). The pH of all tap water samples was determined using an InsMark M-log pH meter (InsMark lab instrument supplier, Shanghai, China). Their values were found to meet the minimum specifications set by SANS 241 of 5 ≤ pH ≤ 9.7.

3.4.4 Tea and commercial beverages sampling

Samples of assorted brands of teas, bottled water (still, sparkling, and flavoured), alcoholic and non-alcoholic beverages were purchased between May and September 2023 from supermarkets in South Africa. The brands' names will be omitted for ethical reasons. From each brand, three teabags were selected at random, and their mass was recorded. Beverages from the same brand packaged in different packaging materials were purchased to determine the effect of packaging material on MPs' physical-chemical properties. Non-alcoholic and alcoholic beverage brands are abbreviated as NABB and ABB, respectively. Non-alcoholic beverages with PET and Aluminium packaging are referred to as NAB (PET) and NAB (Aluminium). Alcoholic beverages in glass and aluminium packaging are referred to as AB (Glass) and AB (Aluminium) (Appendix A).

3.5 SAMPLE EXTRACTION

3.5.1 Surface water

Under an ESCO laminar flow cabinet (ESCO Micro Pte. Ltd., Singapore) at the Analytical MP laboratory at the University of the Witwatersrand. Surface water samples were subjected to wet peroxide digestion, modified from the National Oceanic and Atmospheric Administration method (Masura et al., 2015). To each water sample, 30 mℓ of 0.07 M $FeSO_4 \cdot 7H_2O$ and 30 mℓ of 30% (v/v) H_2O_2 were added. Samples were allowed to achieve complete digestion for 24-48 hours at room temperature (Hurley et al., 2018; Tagg et al., 2015). Density separation was performed using the two-step density separation protocol developed by Nuelle et al. (2014). Forty-five mℓ of saturated NaCl (1.2 g/mℓ) was initially added to the sample, allowed to density separate, and filtered through a Whatman® GF/A glass microfibre filter; subsequently, 45 mℓ of NaI (1.8 g/mℓ) was added, and the sample was allowed to settle before filtration. Filter papers were allowed to air dry for 24 h under the laminar flow cabinet and stored in covered glass Petri dishes until further analysis (Figure 3-5).

Figure 3-5: Surface water extraction procedure.

3.5.2 Sediment samples

Sediment samples were oven-dried at 40°C for 10 days, after which the dry masses obtained were weighed. The samples will be sieved through a 5 mm metal sieve (Qiu et al., 2015, 2016). Under an ESCO laminar flow cabinet, 10% (w/v) KOH solution was added to the dry sediments at a ratio of 1:3 (w/v), the mixtures were stirred for 5 min, covered with aluminium foil, and heated at 40°C for 24 h. Once digested, NaI solution (1.8 g/mℓ) was added at a ratio of 1:3 (v/v), stirred for 5 minutes, and left to stand for 24 hours. NaI salt was recycled and reused to limit its environmental impacts and to reduce costs. Following density separation, supernatants from sediment and surface water samples were filtered through a Whatman® GF/A glass microfibre filter (Figure 3-6). Filter papers were allowed to air dry for 24 h under the laminar flow cabinet and stored in covered glass Petri dishes until further analysis.

Figure 3-6: Sediment sample extraction procedure.

3.5.3 Tap water, beverages, and groundwater samples

Samples were vacuum filtered through Whatman® GF/F glass microfibre filters (Ø = 47 mm, 0.42 mm = thickness, and pore size = 0.7 µm) (Cytiva Danaher Group, Buckinghamshire, United Kingdom). The filters were subjected to wet peroxide oxidation using 5 mℓ of 0.07 M $FeSO_4{\cdot}7H_2O$ and 5 mℓ of 30% (v/v) H_2O_2. After digestion, 5 mℓ of 0.2 mg/mℓ Rose Bengal (4,5,6,7-tetrachloro-2′,4′,5′,7′-tetraiodofluorescein) solution was applied to each filter residue, allowed to stain natural and non-plastic particles such as natural fibres like cotton, which are optically similar to plastic fibres, and then washed off with Milli-Q Type 1 Ultrapure water. The Rose Bengal staining method to further reduce the overestimation of the suspected MPs. The filter was allowed to dry and stored in glass Petri dishes until analysis (Figure 3-7) (Aldrich Essentials, Merck KGaA, Darmstadt, Germany) (Alarcon et al., 2017; Gbogbo et al., 2020; Lam et al., 2020; Ramaremisa et al., 2024).

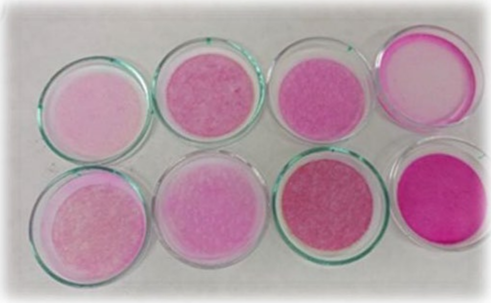

Figure 3-7: Rose Bengal dye-stained samples.

3.5.4 Tea samples

The teabags were cut open, and the contents were brewed for five minutes in 200 mℓ of Milli-Q® Type 1 Ultrapure water at 95°C. Filtered Milli-Q® Type 1 Ultrapure water was used to ensure that the MPs detected were from the teabags and not tap water. After brewing, the tea samples were stored in 325 mℓ clean glass jars. To each sample, 30 mℓ of 0.07 M $FeSO_4{\cdot}7H_2O$ and 30 mℓ of 30% (v/v) H_2O_2 were added and allowed to digest the organics present for 24 h (Figure 3-8) (Ramaremisa et al., 2022; Saad et al., 2024). After digestion, the supernatant was filtered through a Whatman® GF/F glass microfibre filter and subsequently stored in glass Petri dishes. The bottom layer was initially filtered through a 5 mm stainless-steel sieve and then filtered through a Whatman® GF/F glass microfibre filter. After filtration, 5 mℓ of 0.2 mg/mℓ Rose Bengal solution was applied to each filter and allowed non-plastic particles. The filter was allowed to dry and stored in glass Petri dishes until analysis (Alarcon et al., 2017; Gbogbo et al., 2020; Ziajahromi et al., 2017).

Figure 3-8: Tea samples brewed from teabags.

3.6 CHARACTERISATION

3.6.1 Physical characterisation

3.6.1.1 Stereomicroscope

Physical identification of particles was conducted using a Nikon stereomicroscope (Nikon MET SMZ745T) (Nikon Instruments Inc, New York, U.S.A.) with 6.7-50x magnification, equipped with the imaging source (TIS) camera USB 3.0 (The Imaging Source Europe GmbH, Germany). To ensure that the physical properties of all particles present on the filter paper were recorded, it was divided into four numbered quadrants, and each quadrant was meticulously analysed twice. All particles that were not stained by Rose Bengal were not counted as MP particles. Particle size, shape, and colour were determined and recorded with the aid of NIS Elements-D imaging software Version 5.30 (Nikon Instruments Inc, New York, U.S.A.). To mitigate against misidentification and subjectivity, the "break test" was used. Tweezers were used to probe individual particles. Plastic particles are flexible and do not break; instead, they bounce or spring when prodded. Particles that broke when touched were excluded (Egessa et al., 2020; Ramaremisa et al., 2022, 2024). To further mitigate against misidentification and subjectivity, visual criteria proposed in the literature were adopted to identify MPs in this study.

For particles to be considered MPs, they had to meet the following criteria (Marine and Environment Research Institute, 2015).

- The longest dimension of the particle should be less than 5 mm.
- Cellular or biological structures were not present on the particle. However, MPs may have organic material on their surface due to biofouling. Care was taken to note if it were entirely organic or were present in only a portion of the particle.
- The thickness of fibres should be constant along their whole length. However, sometimes splitting or fraying can occur, and particles were subjected to the break test to confirm their identification.
- Particles should exhibit a clear and homogeneous colour throughout. However, care was taken as particles may have patterns and stripes due to being biofouled or bleached.

Microplastic particles were classified according to different colour categories: blue, black, brown, yellow, red, green, grey, white, purple, red, and transparent. All MPs which were lighter or darker shades of a “primary/dominant ” colour were classified according to the “primary/dominant colour”. Hence, any particle that was either light blue or dark blue was classified as a blue particle. MPs were also categorised according to their shapes: fragments, pellets, fibres, and films (Frias et al., 2019; Ramaremisa et al., 2022; Su et al., 2016). Fragment particles were plastic particles from degraded hard plastic materials. Films were soft and thin sheet-like pieces of plastic from plastic carry bags and wrappers. Fibres were slender and elongated plastic pieces, with one dimension significantly longer than the other two. Pellets were round plastic particles with little or no signs of fragmentation. Particles were classified as fragments when they couldn’t be classified as fibre, pellet, or film. MPs were classified into different size ranges. The size of the pellets was defined as their diameter because of their spherical nature. However, the size of fibres, fragments, and films was defined as the separation between a particle's two most distant points (Egessa et al., 2020; Pivokonsky et al., 2018; Rodrigues et al., 2018; Tong et al., 2020). Characterising the physical properties of MPs will be used to identify potential sources, initially, in terms of MPs being from primary or secondary sources. Additionally, certain shapes may refer to specific sources and pathways.

3.6.1.2 FEG-SEM and SEM-EDS

The particles were affixed to double-sided adhesive carbon tape and then covered with a single layer of gold-palladium and carbon using sputter coating, which included a silver bridge. The TESCAN Vega 3 (TESCAN GROUP, Brno-Kohoutovice, Czech Republic) FEG-SEM and SEM-EDS operated in secondary electron and backscattered mode to examine MPs' surface structure and elemental composition (Mosai, 2021; Ramaremisa et al., 2024).

3.6.2 Chemical characterisation

3.6.2.1 Micro-Raman Spectroscopy

Chemical characterization was performed using the Horiba LabRAM HR Raman spectrometer (Horiba Jobin Yvon, Japan), equipped with gratings ruled at 600 lines per mm and a liquid nitrogen-cooled charge-coupled device detector. Wavelength calibration was performed each day of analysis by focusing on a silicon wafer and analysing the first phonon band of silicon at 517.89 cm^{-1}. The 514.52 nm radiation of an argon ion laser, ultra-long working distance (LWD) 50x, and 100× objective of an Olympus BX41 microscope (NA = 0.80) were used for spectra acquisition. The confocal pinhole was set at 100 µm. Raman spectra were recorded in the wavenumber range of 100-3350 cm^{-1}. The laser power was between 0.04 and 0.4 mW, the spot size varied between 0.1-0.3 µm. Due to high background fluorescence in some MPs, particles were subjected to photobleaching for 5-60 s before acquisition, depending on the intensity of the background fluorescence. The incident laser power, accumulation, and duration of exposures were varied between particles to avoid polymer degradation due to laser-induced heating and to acquire a better response signal. The Raman system was operated using LabSpec 6 software (Latcheman et al., 2024; Ramaremisa et al., 2022).

After spectra acquisition, polynomial baseline correction was performed on the raw Raman spectrum to reduce noise and enhance spectrum quality using LabSpec version 6 software (Horiba Scientific, Japan). In cases where the spectra could not be assigned to a polymer at the set threshold, a two or three-component search was done on KnowItAll® Informatics system software to identify the polymer and additives present. The chemical composition of polymers was identified by comparison with reference spectra in the SLOPP Library of MPs and polymer databases of KnowItAll software (John Wiley & Sons, Inc., Hoboken, New Jersey, United States), at a threshold or hit quality index (HQI) of 70% similarity between the sample and reference spectra (Ramaremisa et al., 2022).

3.6.2.2 FTIR Spectroscopy

MP adsorbents were characterised with Fourier Transform Infrared (FTIR) spectroscopy (Alpha, Bruker, Germany) in the 4000–500 cm^{-1} range to determine functional groups present.

3.7 ADSORPTION EXPERIMENTS

A Pb(II) stock solution was prepared by dissolving an appropriate amount of nitrate salt in deionized water and diluting it to the 100 mℓ mark in a volumetric flask to achieve a 1000 $mg \cdot \ell^{-1}$ concentration. The solutions were preserved with nitric acid and kept in the refrigerator at 4°C. On the day of the experiments, the working solutions were made from the stock solutions. To adjust the pH of the solutions, 0.01 $mol \cdot \ell^{-1}$ solutions of NaOH and HNO_3 were used along with the Hanna multiparameter HI98194 (Hanna Instruments Pty Ltd, Johannesburg, SA). Batch sorption experiments were conducted using acid-cleaned and Milli-Q rinsed 100 mℓ Scott Duran® laboratory bottles on a Labcon platform shaker (Labcon, South Africa) and a Biobase thermostatic shaker (Biobase Group, Shandong, China) (Figure 3-9a-b).

Experiments were conducted in triplicate (n = 3). To validate analytical precision, the percentage relative standard deviation (%RSD) was utilised. The Pb(II) concentrations were determined using ICP-OES with operating parameters in Table 3-1. The samples were spiked with a Scandium (Sc) internal standard before analysis using Spectro Genesis ICP- OES (Spectro Analytical Instruments Pty Ltd, Johannesburg, South Africa) (Mosai, 2021).

Figure 3-9: a) Labcon platform shaker and b) Biobase thermostatic shaker.

Table 3-1: ICP-OES operating parameters.

Parameter	**Parameter value**
Optic temperature	29-31°C
Coolant flow	4.9-14.0 Imps·s^{-1}
Auxiliary flow	1 mℓ·min^{-1}
Nebulizer flow	1 mℓ·min^{-1}
Nebulizer pressure	2–4 bar
Hvps voltage	3650 V
Hvps current	605 mA
Plasma power	1400 W
Pump speed	2 rpm
Argon pressure	6–7 bar

The adsorption capacities, q_e (mg·g^{-1}) of Pb(II) were determined using Equation (17). The adsorption efficiency (%) was calculated using Equation (18).

$$q_e = \frac{(C_i - C_e) \times V}{m} \tag{17}$$

$$\text{Adsorption efficiency} = \frac{(C_i - C_e)}{C_i} \times 100 \tag{18}$$

Where C_i is the initial concentration of the metal (mg·ℓ$^{-1}$) and C_e is the equilibrium concentration (mg·ℓ$^{-1}$), V (ℓ) is the volume of the solutions and m (g) is the mass of the adsorbent used.

3.8 MODELLING ADSORPTION PROCESSES

Due to the complexity that MPs could pose as sorption surfaces e.g., heterogeneity and imprecisely defined adsorption sites PHREEQC coupled with PEST was used to model the sorption process (surface complexation) of MPs using input data from experiments and characterisation techniques (e.g. pH, temperature, functional groups, surface area, and concentrations). A detailed description of how to download and couple PHREEQC and PEST can be inferred from Bachmaf & Merkel, (2011).

3.8.1 PHREEQC model construction

To simulate the adsorption of Pb(II) on MP adsorbents at different conditions, PHREEQC's interactive geochemical modelling code version 3.73-15968 was used on a Dell Inspiron 16 5620 laptop equipped with a 12th Gen Intel® Core™ i7-1255U @1.70 GHz. Further details on the keywords and their functions can be inferred from the PHREEQC manual (Parkhurst & Appelo, 2013). Figure 3-10 shows a PHREEQC input script for Pb adsorption on PE. Surf_CH represents methine sites on the surface of PE. Generalised methine surface groups were used since they were responsible for the surface complexation with Pb. To determine the major species of Pb, PHREEQC was used to simulate SOLUTION 1. The major species were provided under the "Distribution of species" header in the PHREEQC output script. Furthermore, the experimental conditions were specified, including the number of moles of the methine groups, concentration of adsorbate, specific surface area, adsorbent dosage/mass, temperature, etc. All simulations were the minteq.v4 database all necessary thermodynamic parameters for the major Pb species.

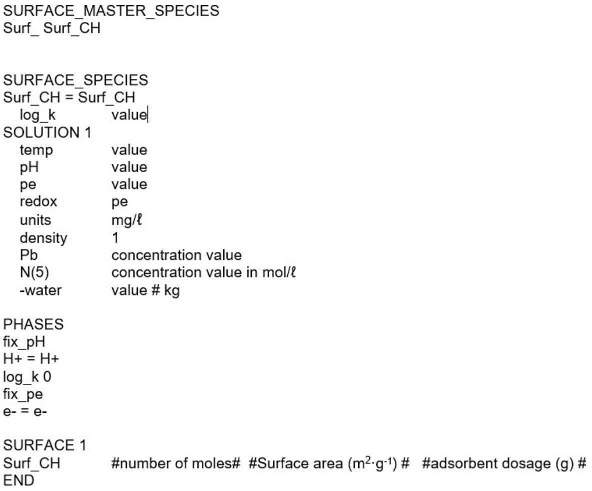

```
SURFACE_MASTER_SPECIES
Surf_ Surf_CH


SURFACE_SPECIES
Surf_CH = Surf_CH
   log_k          value
SOLUTION 1
   temp           value
   pH             value
   pe             value
   redox          pe
   units          mg/ℓ
   density        1
   Pb             concentration value
   N(5)           concentration value in mol/ℓ
   -water         value # kg

PHASES
fix_pH
H+ = H+
log_k 0
fix_pe
e- = e-

SURFACE 1
Surf_CH           #number of moles#  #Surface area (m2·g-1) #   #adsorbent dosage (g) #
END
```

Figure 3-10: PHREEQC input script for PE.

3.8.2 Parameter estimation

PEST version 18.21 was used on the Dell laptop described above to precisely determine the thermodynamic equilibrium constants (log k) for the sorption of Pb by polymeric adsorbents (Doherty et al., 1994; Mosai, 2021). Before running PEST, its utility programs TEMPCHEK, INSCHEK, and PESTCHEK are used to ensure the accuracy and compatibility of the template, instruction, and control files, respectively (Figure 3-11). The model to be run and experiment observations and parameters to be estimated were provided in the control file, as shown in Figure 3-12. The updated model parameter values are subsequently entered into the PHREEQC input file using a predefined template file. This approach guarantees that all essential parameters, modified based on experimental data and numerical simulations, are correctly formatted for compatibility with the PHREEQC (Figure 3-13). A definition of how model-generated output was to be processed to extract experimental observations for comparison with modelled data was provided in the instruction file (Figure 3-14a). The number of experiment observations was provided in the instruction file, and the execution of PHREEQC and PEST was conducted using the batch file (Figure 3-14b). PEST calibrates PHREEQC input parameters by employing the Gauss-Marquardt-Levenberg non-linear regression approach to minimise the objective function (ϕ) of the weighted least squares differences between experimental and model-simulated parameters as shown in Equation 19 (Doherty et al., 1994).

$$\Phi = \sum (c_i w_i - c_{0i} w_i)^2 \qquad (19)$$

where c_i and c_{0i} are the measured and simulated aqueous concentrations for the i_{th} observation and w_i is the weight associated with the i_{th} observation. If the disparity between simulated and observed values is significant, PEST will attempt to reduce the disparity by running numerical iterations until the difference is minimal and it stops (Doherty et al., 1994; Zavarin et al., 2022).

PEST was run in regularisation mode, which generates two objective functions: a “measurement objective function’’ where the “measurements or experimental results” are the preferred value of parameters or their preferred homogeneity, and a “regularisation objective function”. The aim of calibration in this case is to minimise both of these objective functions while paying attention to the relative importance that one plays over the other. Regularisation ensures numerical stability and the attainment of a unique solution to an ill-posed inverse modelling problem. PEST was run in singular value decomposition (SVD) or least squares with QR-factorisation (LSQR) regularisation modes. As shown in Figure 3-15, PEST in SVD mode transformed the parameter space into two orthogonal subspaces (i.e., solution and null subspaces). The solution space contains a combination of parameters (i.e., vectors) that can be uniquely estimated from the parameter space. When calibrating a model, only parameter combinations in the solution subspace are modified. LSQR mode also separates the parameter space into the solution and null subspace, parameter estimation is only computed using linear combinations of parameters in the solution subspace. Thus, the LSQR mode bears many similarities to the SVD mode, although the former has the advantage of being able to solve a larger parameter space (i.e., 100-1000) in a fraction of the time. Moreover, LSQR cannot guarantee the achievement of a solution with a minimum error variance (Doherty et al., 1994; Paige & Saunders, 1982). The PEST mode, which provided the highest correlation coefficient (R) between experimental and estimated SCM parameters, was chosen to model Pb adsorption on MPs. The correlation coefficient R is essentially a weighted Pearson correlation coefficient, and the weighting helps account for uncertainties in the observations, making it robust in evaluating models, especially in cases where measurements have different levels of uncertainty.

$$R = \frac{\sum(c_i w_i - m)(c_{0i} w_i - m_0)}{\sqrt{\sum(c_i w_i{}^2 - m)\sum(c_{0i} w_i{}^2 - m_0)}} \qquad (20)$$

Where c_i and c_{0i} are the measured and simulated aqueous concentrations for the i_{th} observation, w_i is the weight associated with the i_{th} observation, m and m_0 are the mean-weighted aqueous concentration and the mean-weighted simulated aqueous concentration, respectively (Doherty et al., 1994; Zavarin et al., 2022).

To determine SCM parameters, PEST computes the Jacobian matrix and uses it to develop and update the parameter set, improving the ability to acquire a higher objective function. PEST makes model calls during the iterations and updates its parameters based on a new Marquardt lambda value. PEST will gradually decrease the objective function until it reaches a minimum and stops. The modified model parameters (log_k) are subsequently written to PHREEQC input files via the template file. The procedure entails removing the previous set of model input files and creating a new set from the template files. To allow PEST to optimise parameters, the parameters provided were less than or equal to the number of experimental observations. PEST has the advantage of being able to avoid non-convergence problems experienced by other models while fitting multiple model parameters (Abdelaziz et al., 2019; Bullen et al., 2024; Doherty et al., 1994). After completion, PEST generated various PEST output files, including the run record file, which lists the mode PEST was running on, the number of iterations and the estimated parameters during each iteration (Figure 3-16).

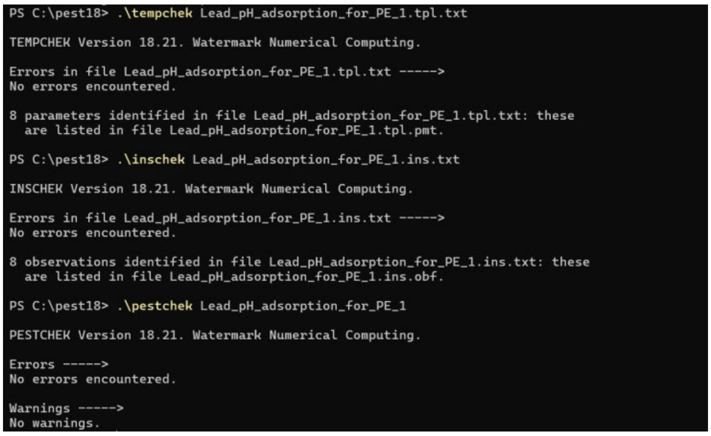

```
PS C:\pest18> .\tempchek Lead_pH_adsorption_for_PE_1.tpl.txt

TEMPCHEK Version 18.21. Watermark Numerical Computing.

Errors in file Lead_pH_adsorption_for_PE_1.tpl.txt ----->
No errors encountered.

8 parameters identified in file Lead_pH_adsorption_for_PE_1.tpl.txt: these
  are listed in file Lead_pH_adsorption_for_PE_1.tpl.pmt.

PS C:\pest18> .\inschek Lead_pH_adsorption_for_PE_1.ins.txt

INSCHEK Version 18.21. Watermark Numerical Computing.

Errors in file Lead_pH_adsorption_for_PE_1.ins.txt ----->
No errors encountered.

8 observations identified in file Lead_pH_adsorption_for_PE_1.ins.txt: these
  are listed in file Lead_pH_adsorption_for_PE_1.ins.obf.

PS C:\pest18> .\pestchek Lead_pH_adsorption_for_PE_1

PESTCHEK Version 18.21. Watermark Numerical Computing.

Errors ----->
No errors encountered.

Warnings ----->
No warnings.
```

Figure 3-11: Execution commands for TEMPCHEK, INSCHEK, PESTCHEK, and PEST.

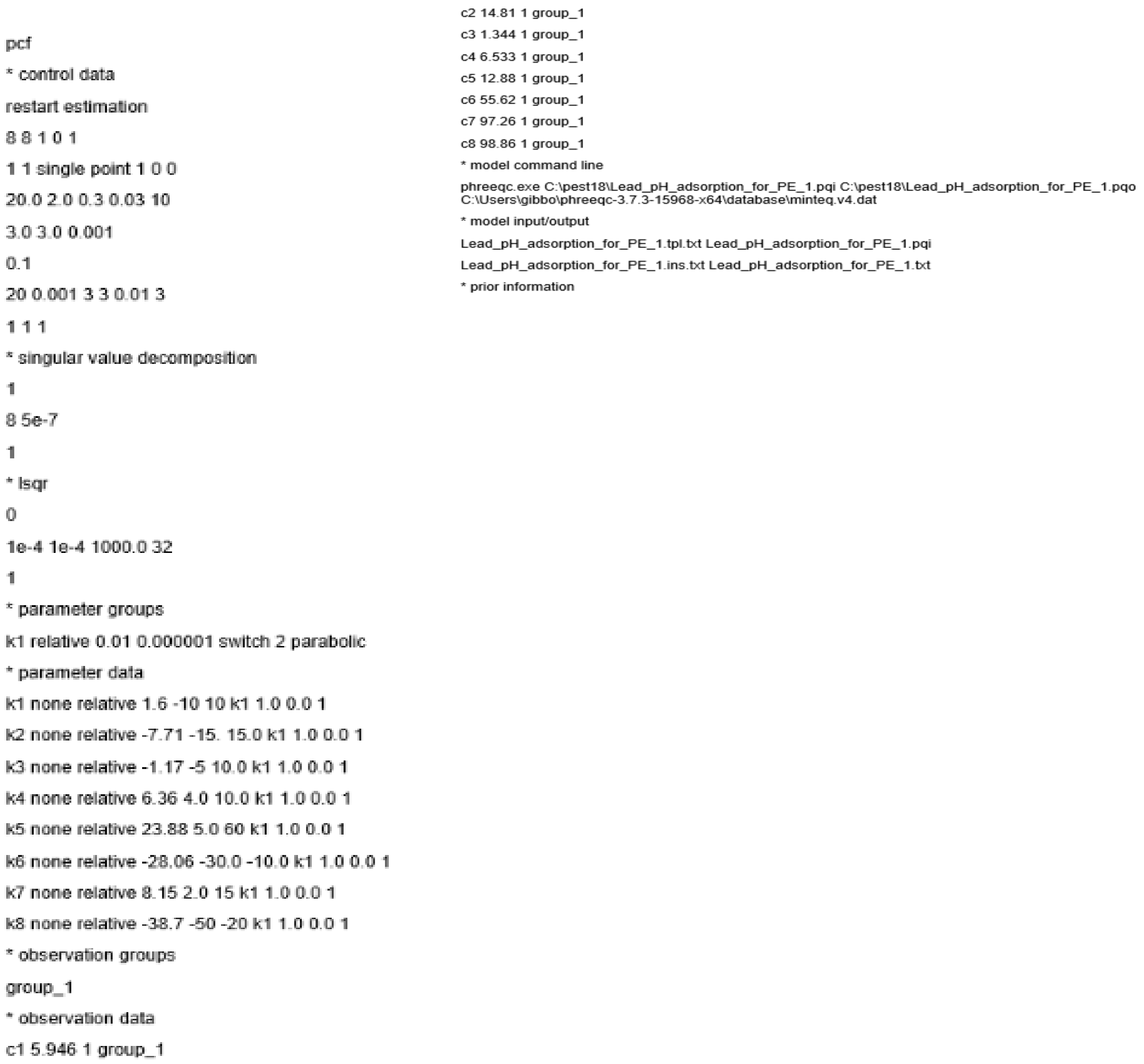

```
pcf
* control data
restart estimation
8 8 1 0 1
1 1 single point 1 0 0
20.0 2.0 0.3 0.03 10
3.0 3.0 0.001
0.1
20 0.001 3 3 0.01 3
1 1 1
* singular value decomposition
1
8 5e-7
1
* lsqr
0
1e-4 1e-4 1000.0 32
1
* parameter groups
k1 relative 0.01 0.000001 switch 2 parabolic
* parameter data
k1 none relative 1.6 -10 10 k1 1.0 0.0 1
k2 none relative -7.71 -15. 15.0 k1 1.0 0.0 1
k3 none relative -1.17 -5 10.0 k1 1.0 0.0 1
k4 none relative 6.36 4.0 10.0 k1 1.0 0.0 1
k5 none relative 23.88 5.0 60 k1 1.0 0.0 1
k6 none relative -28.06 -30.0 -10.0 k1 1.0 0.0 1
k7 none relative 8.15 2.0 15 k1 1.0 0.0 1
k8 none relative -38.7 -50 -20 k1 1.0 0.0 1
* observation groups
group_1
* observation data
c1 5.946 1 group_1
c2 14.81 1 group_1
c3 1.344 1 group_1
c4 6.533 1 group_1
c5 12.88 1 group_1
c6 55.62 1 group_1
c7 97.26 1 group_1
c8 98.86 1 group_1
* model command line
phreeqc.exe C:\pest18\Lead_pH_adsorption_for_PE_1.pqi C:\pest18\Lead_pH_adsorption_for_PE_1.pqo
C:\Users\gibbo\phreeqc-3.7.3-15968-x64\database\minteq.v4.dat
* model input/output
Lead_pH_adsorption_for_PE_1.tpl.txt Lead_pH_adsorption_for_PE_1.pqi
Lead_pH_adsorption_for_PE_1.ins.txt Lead_pH_adsorption_for_PE_1.txt
* prior information
```

Figure 3-12: PEST control file.

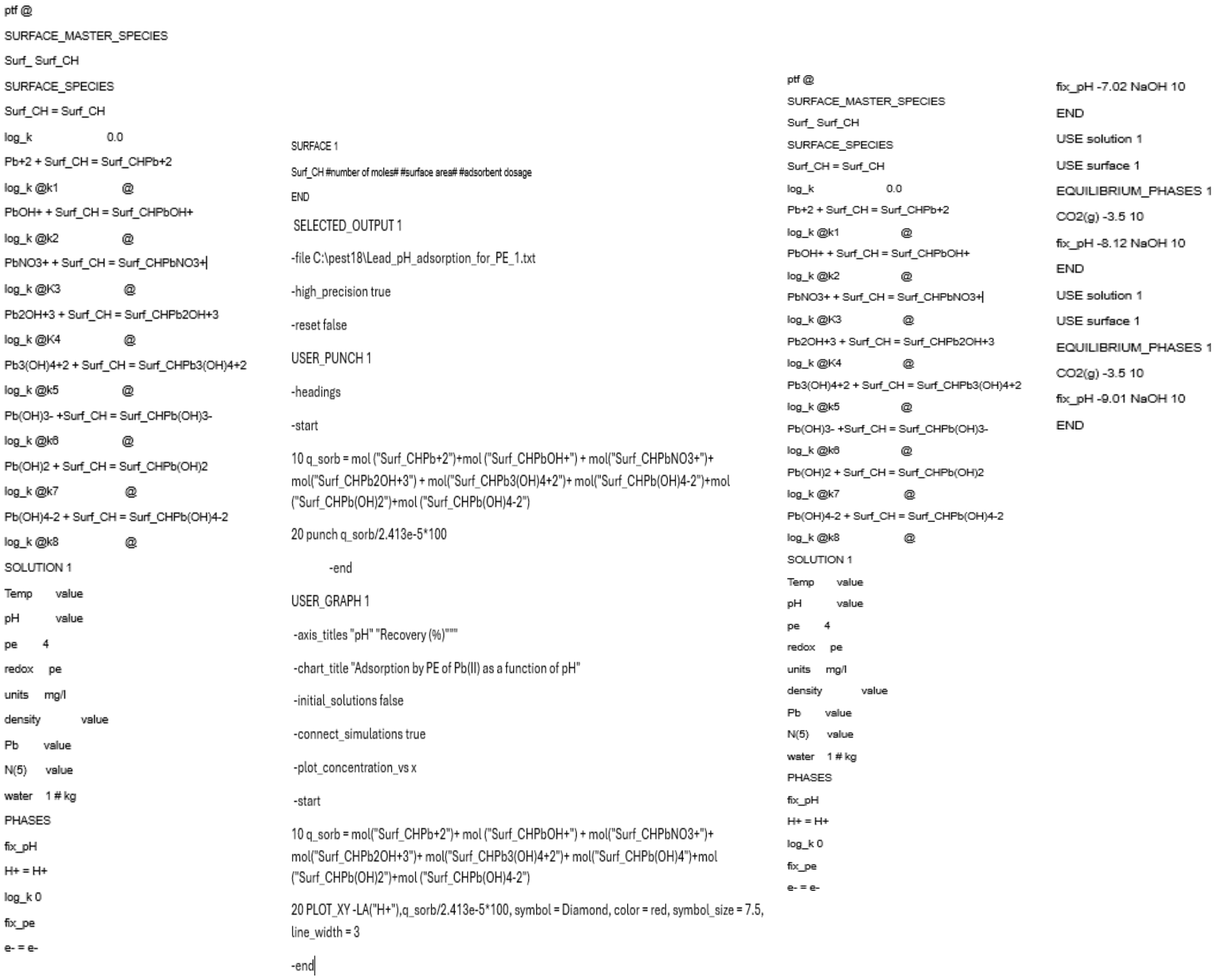

```
ptf @
SURFACE_MASTER_SPECIES
Surf_ Surf_CH
SURFACE_SPECIES
Surf_CH = Surf_CH
log_k                    0.0
Pb+2 + Surf_CH = Surf_CHPb+2
log_k @k1                @
PbOH+ + Surf_CH = Surf_CHPbOH+
log_k @k2                @
PbNO3+ + Surf_CH = Surf_CHPbNO3+|
log_k @K3                @
Pb2OH+3 + Surf_CH = Surf_CHPb2OH+3
log_k @K4                @
Pb3(OH)4+2 + Surf_CH = Surf_CHPb3(OH)4+2
log_k @k5                @
Pb(OH)3- +Surf_CH = Surf_CHPb(OH)3-
log_k @k6                @
Pb(OH)2 + Surf_CH = Surf_CHPb(OH)2
log_k @k7                @
Pb(OH)4-2 + Surf_CH = Surf_CHPb(OH)4-2
log_k @k8                @
SOLUTION 1
Temp      value
pH        value
pe      4
redox    pe
units    mg/l
density          value
Pb       value
N(5)     value
water    1 # kg
PHASES
fix_pH
H+ = H+
log_k 0
fix_pe
e- = e-
```

```
SURFACE 1
Surf_CH #number of moles# #surface area# #adsorbent dosage
END
 SELECTED_OUTPUT 1
-file C:\pest18\Lead_pH_adsorption_for_PE_1.txt
-high_precision true
-reset false
USER_PUNCH 1
-headings
-start
10 q_sorb = mol ("Surf_CHPb+2")+mol ("Surf_CHPbOH+") + mol("Surf_CHPbNO3+")+
mol("Surf_CHPb2OH+3") + mol("Surf_CHPb3(OH)4+2")+ mol("Surf_CHPb(OH)4-2")+mol
("Surf_CHPb(OH)2")+mol ("Surf_CHPb(OH)4-2")
20 punch q_sorb/2.413e-5*100
          -end
USER_GRAPH 1
 -axis_titles "pH" "Recovery (%)"""
 -chart_title "Adsorption by PE of Pb(II) as a function of pH"
 -initial_solutions false
 -connect_simulations true
 -plot_concentration_vs x
 -start
10 q_sorb = mol("Surf_CHPb+2")+ mol ("Surf_CHPbOH+") + mol("Surf_CHPbNO3+")+
mol("Surf_CHPb2OH+3")+ mol("Surf_CHPb3(OH)4+2")+ mol("Surf_CHPb(OH)4")+mol
("Surf_CHPb(OH)2")+mol ("Surf_CHPb(OH)4-2")
20 PLOT_XY -LA("H+"),q_sorb/2.413e-5*100, symbol = Diamond, color = red, symbol_size = 7.5,
line_width = 3
-end|
```

```
ptf @
SURFACE_MASTER_SPECIES
Surf_ Surf_CH
SURFACE_SPECIES
Surf_CH = Surf_CH
log_k                    0.0
Pb+2 + Surf_CH = Surf_CHPb+2
log_k @k1                @
PbOH+ + Surf_CH = Surf_CHPbOH+
log_k @k2                @
PbNO3+ + Surf_CH = Surf_CHPbNO3+|
log_k @K3                @
Pb2OH+3 + Surf_CH = Surf_CHPb2OH+3
log_k @K4                @
Pb3(OH)4+2 + Surf_CH = Surf_CHPb3(OH)4+2
log_k @k5                @
Pb(OH)3- +Surf_CH = Surf_CHPb(OH)3-
log_k @k6                @
Pb(OH)2 + Surf_CH = Surf_CHPb(OH)2
log_k @k7                @
Pb(OH)4-2 + Surf_CH = Surf_CHPb(OH)4-2
log_k @k8                @
SOLUTION 1
Temp      value
pH        value
pe      4
redox    pe
units    mg/l
density          value
Pb       value
N(5)     value
water    1 # kg
PHASES
fix_pH
H+ = H+
log_k 0
fix_pe
e- = e-
```

```
fix_pH -7.02 NaOH 10
END
USE solution 1
USE surface 1
EQUILIBRIUM_PHASES 1
CO2(g) -3.5 10
fix_pH -8.12 NaOH 10
END
USE solution 1
USE surface 1
EQUILIBRIUM_PHASES 1
CO2(g) -3.5 10
fix_pH -9.01 NaOH 10
END
```

Figure 3-13: PEST template file.

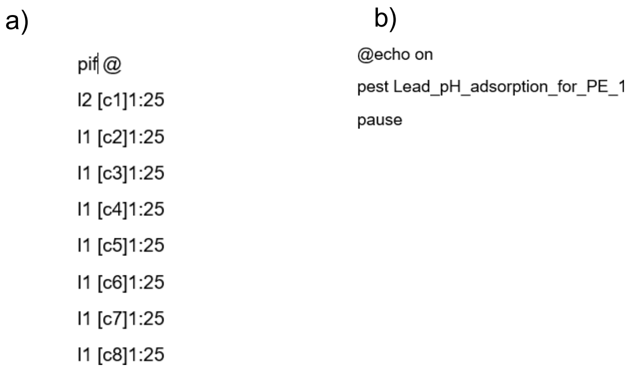

a)

```
pif| @
l2 [c1]1:25
l1 [c2]1:25
l1 [c3]1:25
l1 [c4]1:25
l1 [c5]1:25
l1 [c6]1:25
l1 [c7]1:25
l1 [c8]1:25
```

b)

```
@echo on
pest Lead_pH_adsorption_for_PE_1
pause
```

Figure 3-14: PEST a) instruction file and b) batch file.

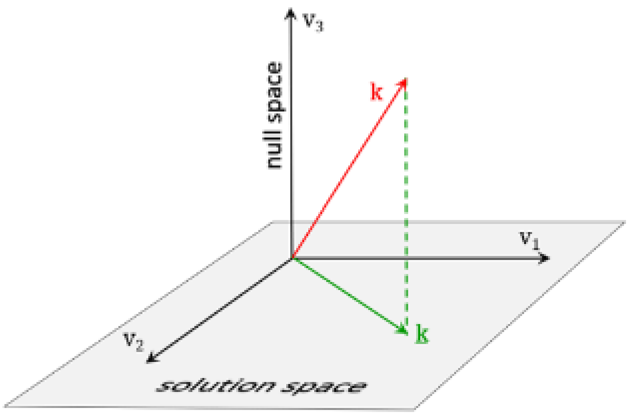

Figure 3-15: Orthogonal null and solution subspaces and their corresponding vectors.

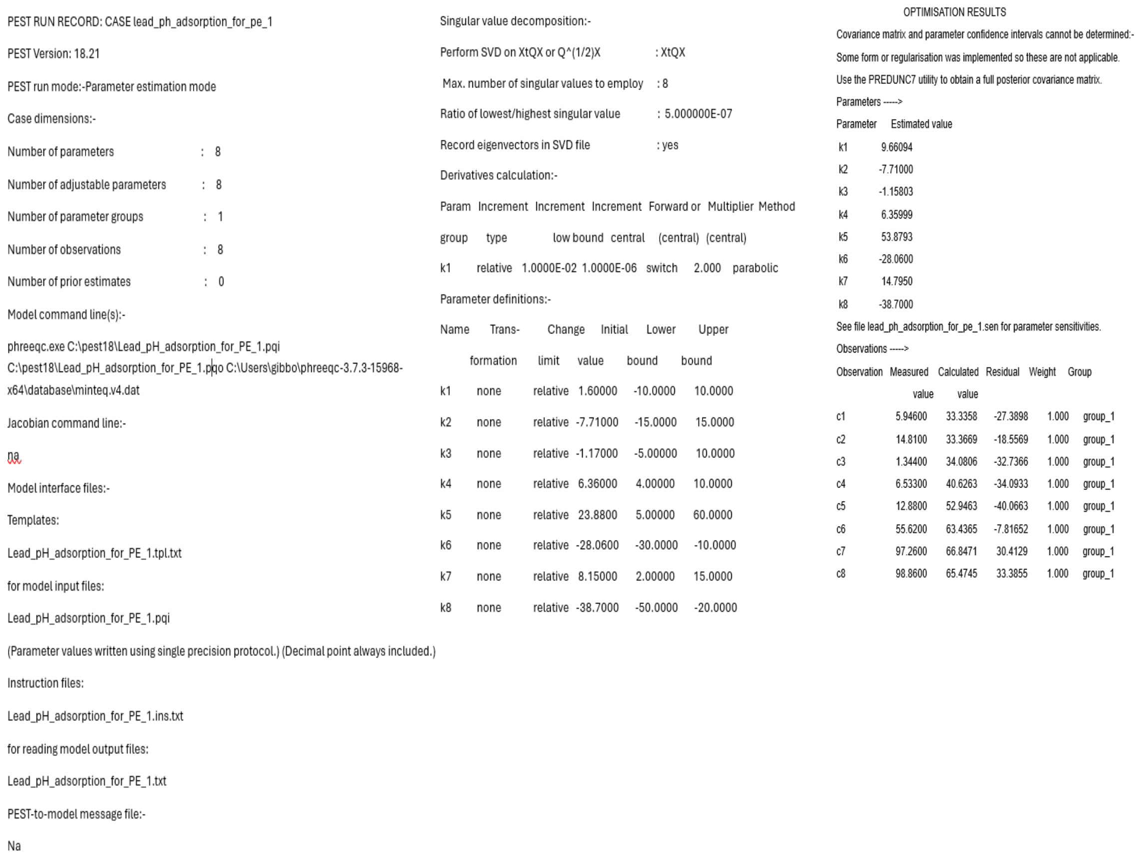

```
PEST RUN RECORD: CASE lead_ph_adsorption_for_pe_1

PEST Version: 18.21

PEST run mode:-Parameter estimation mode

Case dimensions:-

Number of parameters                  :   8

Number of adjustable parameters       :   8

Number of parameter groups            :   1

Number of observations                :   8

Number of prior estimates             :   0

Model command line(s):-

phreeqc.exe C:\pest18\Lead_pH_adsorption_for_PE_1.pqi
C:\pest18\Lead_pH_adsorption_for_PE_1.pqo C:\Users\gibbo\phreeqc-3.7.3-15968-
x64\database\minteq.v4.dat

Jacobian command line:-

na

Model interface files:-

Templates:

Lead_pH_adsorption_for_PE_1.tpl.txt

for model input files:

Lead_pH_adsorption_for_PE_1.pqi

(Parameter values written using single precision protocol.) (Decimal point always included.)

Instruction files:

Lead_pH_adsorption_for_PE_1.ins.txt

for reading model output files:

Lead_pH_adsorption_for_PE_1.txt

PEST-to-model message file:-

Na
```

```
Singular value decomposition:-

Perform SVD on XtQX or Q^(1/2)X              : XtQX

 Max. number of singular values to employ    : 8

Ratio of lowest/highest singular value       :  5.000000E-07

Record eigenvectors in SVD file              : yes

Derivatives calculation:-

Param  Increment  Increment  Increment  Forward or  Multiplier  Method

group     type           low bound  central    (central)  (central)

k1      relative  1.0000E-02  1.0000E-06  switch    2.000   parabolic

Parameter definitions:-

Name      Trans-       Change     Initial     Lower      Upper

          formation      limit      value      bound      bound

k1      none        relative   1.60000    -10.0000    10.0000

k2      none        relative  -7.71000    -15.0000    15.0000

k3      none        relative  -1.17000    -5.00000    10.0000

k4      none        relative   6.36000     4.00000    10.0000

k5      none        relative   23.8800     5.00000    60.0000

k6      none        relative  -28.0600    -30.0000   -10.0000

k7      none        relative   8.15000     2.00000    15.0000

k8      none        relative  -38.7000    -50.0000   -20.0000
```

```
                    OPTIMISATION RESULTS
Covariance matrix and parameter confidence intervals cannot be determined:-
Some form or regularisation was implemented so these are not applicable.
Use the PREDUNC7 utility to obtain a full posterior covariance matrix.
Parameters ----->
Parameter     Estimated value
 k1             9.66094
 k2            -7.71000
 k3            -1.15803
 k4             6.35999
 k5             53.8793
 k6            -28.0600
 k7             14.7950
 k8            -38.7000
See file lead_ph_adsorption_for_pe_1.sen for parameter sensitivities.
Observations ----->
Observation  Measured   Calculated  Residual   Weight    Group
                 value       value
c1             5.94600     33.3358    -27.3898    1.000    group_1
c2             14.8100     33.3669    -18.5569    1.000    group_1
c3             1.34400     34.0806    -32.7366    1.000    group_1
c4             6.53300     40.6263    -34.0933    1.000    group_1
c5             12.8800     52.9463    -40.0663    1.000    group_1
c6             55.6200     63.4365    -7.81652    1.000    group_1
c7             97.2600     66.8471     30.4129    1.000    group_1
c8             98.8600     65.4745     33.3855    1.000    group_1
```

Figure 3-16: PEST run record file.

3.9 RISK ASSESSMENT

3.9.1 Estimated daily intake (EDI)

An empirical approach was adopted to estimate the daily intake (EDI) of MPs from ingestion of tap water and groundwater using Equation 21, where C is the MP concentration (particles·ℓ^{-1}), IR is the recommended dietary ingestion rate, and BW is the estimated mean body weight (Altunışık, 2023).

$$\mathrm{EDI} = \frac{\mathrm{C} \times \mathrm{IR}}{\mathrm{BW}} \qquad (21)$$

According to South African dietary guidelines, the recommended IRs are 1.7 $\ell \cdot \mathrm{day}^{-1}$ for children (4–8 years), 2.7 $\ell \cdot \mathrm{day}^{-1}$ for women, and 3.7 $\ell \cdot \mathrm{day}^{-1}$ for men. The estimated mean body weights (BW) were 20.3 kg, 74.1 kg, and 71.9 kg for children, women, and men, respectively (Bourne et al., 2007; Wenhold & Faber, 2009).

3.9.2 MPCF and MPLI

Microplastic concentrations in this study were correlated with background literature values using the MP Contamination Factor (MPCF) analysis. Equations 22 and 23 were used to determine the MPCF and MP pollution load index (MPLI) in groundwater, respectively. In equation 22, MP_a is the MP concentration in sample a, and MP_m is the lowest mean MP concentration from the literature. The $MPCF_m$ value is 0.48 particles·ℓ^{-1} as adopted from Esfandiari et al. (2022). The MPCF were divided into four groups: low contamination (MPCF<1), moderate contamination (MPCF range: 1–3), considerable contamination (MPCF range: 3–6), and very high contamination (MPCF>6) (Altunışık, 2023; Esfandiari et al., 2022; Kabir et al., 2021). Microplastic pollution load index were classified as follows: ecological risk level 1 (MPLI <10), risk level 2 (MPLI range: 10-20), risk level 3 (MPLI range: 20-30), and danger level 4 (MPLI >30) (Khan et al., 2023; Li et al., 2023).

$$\mathrm{MPCF} = \frac{\mathrm{MP_a}}{\mathrm{MP_m}} \qquad (22)$$

$$\mathrm{MPLI_{sample\ type}} = \sqrt[n]{\mathrm{MPCF_1} \times \mathrm{MPCF_2} \times \mathrm{MPCF_3} \ldots \ldots \ldots \mathrm{MPCF_n}} \qquad (23)$$

3.10 STATISTICAL ANALYSIS

Statistical analysis was conducted on all data obtained to extract latent scientific data and relationships between data sets. All data were stored in Microsoft Excel 2016 (Microsoft Corporation, Redmond, Washington, United States), and all statistical tests were executed using IBM's SPSS Statistics version 27 (SPSS, Chicago, Illinois, USA). The Shapiro-Wilk test for normality and Levene's test of homogeneity of variances were applied as pre-tests to all data. Depending on the results, the data were then statistically analysed using parametric Independent samples T-test (n = 2) and One-way Analysis of variance (ANOVA) (n ≥ 3) or the non-parametric alternatives, Mann-Whitney U test (n = 2) and Kruskal-Wallis H Test (n ≥ 3). The tests were generally followed by an appropriate *post-hoc* analysis for pairwise comparisons. Differences between or within samples were considered statistically significant if the *p*-value was less than 0.05, and all tests were performed at a 95% confidence level. Numerical data are expressed as the average or mean ± SD unless specified otherwise. Figures were plotted using Microsoft Excel 2016 and OriginPro 2024b (OriginLab, Northampton, Massachusetts, USA) (Adu-Boahene et al., 2023; Ramaremisa et al., 2024).

4 MICROPLASTICS IN SURFACE WATERS AND SEDIMENTS

4.1 INTRODUCTION

This chapter provides and examines the findings on the occurrence and characterisation of MPs in surface water and sediments. Surface water and sediment samples were collected over approximately 50.4 km between the Lethabo weir (Panfontein) and the Vaal River Barrage (Windsor on Vaal AH).

4.2 MICROPLASTIC ABUNDANCES

Microplastics were detected in all surface water and sediment samples. A total of 848 particles in surface water were identified as MPs, with an average of 38.5 ± 35.5 particles/sample. Microplastic abundances in surface waters ranged from 0.13 to 2.52 particles·m^{-3} (Table 4-1), with a mean abundance of 0.61 ± 0.57 particles·m^{-3} (mean value ± SD). Abundance was determined as particles per kg of the sediments' dried weight (dw). A total of 1254 particles in sediments were identified as MPs, with an average of 50.2 ± 31.2 per sample. The average abundance of MPs in the sediments was 463.3 ± 284.1 particles/(kg_dw) (mean value ± SD) with a range from 29 to 11028.6 particles/(kg_dw) (Table 4-2).

Table 4-1: Microplastic abundance in surface water

Sample code	Volume sampled (m^3)	Number of particles	MP abundance (particles·m^{-3})
L1	88.5	17	0.27
L2	3.2	24	0.38
L3	2.4	8	0.13
L4	2.4	24	0.38
L5	1.1	46	0.73
L6	39.6	74	1.17
L7	81.7	159	2.52
L8	103.6	47	0.75
L9	40.0	103	1.63
L10	81.4	84	1.33
L11	76.9	26	0.41
L12	88.2	26	0.41
L13	58.2	17	0.27
L14	95.4	23	0.36
L15	97.7	11	0.17
L16	79.8	26	0.41
L17	78.1	18	0.29
L18	58.4	29	0.46
L19	50.1	13	0.21
L20	44.6	26	0.41
L21	90.4	27	0.43
L22	127.2	20	0.32

Table 4-2: Microplastic abundance in sediments

Sample code	Dry mass (kg)	Number of particles per sample	MP abundance (particles/(kg_dw))
S1	0.25	68	270
S2	0.08	75	937.5
S3	0.13	115	884
S4	0.14	82	585.7
S5	0.12	83	691.6
S6	0.14	79	564.2
S7	0.09	47	522.2
S8	0.18	44	244.4
S9	0.11	76	690.9
S10	0.18	86	477.78
S11	0.37	28	75.68
S12	0.03	12	400
S13	0.05	4	80
S14	0.41	23	56.1
S15	0.27	8	29.63
S16	0.09	55	611.11
S17	0.14	98	700
S18	0.07	25	357.14
S19	0.08	19	237.5
S20	0.06	24	400
S21	0.34	28	82.35
S22	0.04	19	475
S23	0.06	44	733.33
S24	0.07	72	1028.57
S25	0.10	40	400

4.3 SOURCES OF MPS IN THE VAAL RIVER

4.3.1 Urban centres

Samples were collected in a portion of the Vaal River where the urban areas of Vereeniging and Vanderbijlpark extend into the river. Both areas are well-developed and have high population densities. Local sources of MPs include industries, WWTPs, stormwater runoff, informal and formal settlements, and recreational activities (Wepener et al., 2011). Storm drainage and urban runoff may carry MPs from landfill sites, road paint, and tyre wear from vehicles into the Vaal River (Boucher & Friot, 2017). In sediments and surface water, MP abundance generally decreased with distance from urban centres, which suggests there was a short-distance transport of plastic debris from these urban centres into the river. Previously, the proximity of a freshwater body to urban areas with highly intensive anthropogenic activities is positively correlated with an increased number of MPs (Cable et al., 2017, 2017; Egessa et al., 2020; Meijer et al., 2021). For instance, lower MP abundances were detected further away from the Wuhan City Centre in China (Wang et al., 2017). The Vaal River has a vibrant tourism industry, and there are various tourist attractions such as Emerald Resort Animal World, Aquadrome, boat clubs, Lodgings, and Spas, which are potential sources of macroplastics that eventually degrade into MPs due to various processes in the Vaal River.

4.3.2 Wastewater treatment plants

Considering the bad state of the wastewater systems in the Sedibeng District Municipality, WWTPs could very much be a potential source of MPs. The Leeuwkuil, Sebokeng, Midvaal, and Rietspruit WWTPs are characterised by a history of breakdown, outdated equipment, operating beyond design capacity, and rarely treating wastewater to acceptable standards (Wepener et al., 2011; Iloms et al., 2020; SAHRC, 2021). In 2016, a feasibility study indicated that several of the biofilters and anaerobic digesters at the Leeuwkuil and Rietspruit WWTPs were not working. Additionally, only four of approximately eleven biofilters at the Rietspruit WWTPs were operational. This led to the irreparable collapse of the Emfuleni waste treatment system in 2018. In 2020, there were reports that the Sebokeng and Leeuwkuil WWTPs were operating above their hydraulic capacity. The breakdown of wastewater treatment infrastructure in the Sedibeng District Municipality caused sewage to flow into the Vaal River, which led to the death of thousands of fish (Ash., 2022; Evans., 2021; SAHRC., 2021). Sewage was observed flowing into the Vaal River near L5/S6 and L6/S7 during sampling. According to the SAHRC, wastewater and sewage spillages into the Vaal occur regularly as a result of a lack of maintenance, vandalism, and dilapidated infrastructure (SAHRC, 2021).

Assuming that WWTPs in Sedibeng can extract all MPs and concentrate them in wastewater sludge. Microplastics may eventually be released into the environment through wastewater. Rand Water’s Panfontein sludge disposal site, less than 3 km from the Vaal River, could be another potential source of MPs. Approximately 1300 tons of wastewater sludge are produced daily and are pumped to the sludge disposal site in the Midvaal Local Municipality. A portion of the wastewater sludge is stored in a drying paddock, while some are sprayed onto the land using irrigation equipment. Microplastics in the paddock-dried sludge may be resuspended, become airborne and end up in the Vaal River. The land around the Vaal Triangle is predominantly used for agricultural purposes. Microplastics in the sludge used for agricultural beneficiation may potentially become remobilized during flash flooding, resulting in the contamination of the Vaal River (Dris et al., 2015; Mokonyama et al., 2017).

4.3.3 The Vaal River’s tributaries

The Vaal Barrage catchment receives copious amounts of wastewater effluent through the Rietspruit, Taaiboschspruit, Leeuspruit, Kip, and Suikerbosrand Rivers. These tributaries carry stormwater and wastewater from southern Gauteng and northern parts of the Free State. Burst sewerage pipes were detected on the banks of the Rietspruit River, resulting in raw sewage flowing into the Rietspruit River (SAHRC, 2021; Tempelhoff et al., 2007). Tributaries have been observed to be a major source of MPs in the Qiantang River in China (Zhao et al., 2020), the Yangtze River in China (Zhang et al., 2015), and the Braamfontein Spruit in South Africa (Dahms et al., 2020). Fischer et al. (2016), investigated MP abundances in two freshwater Lakes in Italy. Although Lake Chiusi has a smaller catchment area than Lake Bolsena, a greater MP abundance was reported in Lake Chiusi. Lake Chiusi had an MP abundance of 2.7 to 3.7 particles·m^{-3}, and Lake Bolsena had 0.82 to 4.4 particles·m^{-3}. Two tributaries feed Lake Chiusi, while Lake Bolsena has no tributaries (Fischer et al., 2016).

4.3.4 Comparison to other studies

MP abundance in this study was only compared with studies that used the same units of abundance. MP abundances were generally lower in artificially and naturally regulated freshwater systems such as Lake Michigan, Lake Hövsgöl, Lijiang River, Feilaixia Reservoir (Beijiang River), and Laurentian Great Lakes. In the above-mentioned freshwater systems, sampling apparatus with higher mesh sizes were used, which could also account for their lower abundance (Feng et al., 2021). This was supported by studies by Dris et al. (2015) and Song (2015), both of which reported an increase in MP concentrations when using smaller 80 µm mesh nets than bigger 330 µm mesh nets. Similar abundances were reported when a 75 µm plankton net was used in the Lijiang River in China. Greater abundances were reported in freshwater systems from China, the USA, South Korea, South Africa, and Uganda. An important factor to consider in the Qiantang River, the Braamfontein Spruit, Nyl and Mogalakwena Rivers is that bulk sampling was employed. Generally, bulk sampling leads to smaller sample volumes, which causes a higher estimation of MPs (Dahms & Greenfield, 2025; Dahms et al., 2020; Liu et al., 2020b; Zhao et al., 2020; Zhang et al., 2021b).

The mean volume sampled in this study was 63.1 m^3 (6.3×10^4 ℓ), which is at least three orders of magnitude higher than the volumes sampled in the other studies. Higher MP abundances were also reported in the Lijiang River, a 12-V DC Teflon pump with a 25 µm sieve was used to collect samples. Studies have reported that the MP abundances reported for pump samples can be several orders of magnitude greater than net or trawl samples (Liu et al., 2020b; Zhang et al., 2021b). Similar to bulk sampling, pump-based water sampling generally results in small volumes filtered and may not accurately reflect the characteristics of MPs in the surface water. Trawl or net-based volume-reduced sampling filters larger volumes of water (several hundred m^3), which may be used to estimate the large-scale distribution of MPs. Discrepancies brought about the use of different sampling methods to highlight the need for a unified sampling method.

It should be noted that other factors may also influence MP abundances, such as population densities and human activities. For instance, higher abundances were reported in the Great Lakes tributaries, Haihe River, the Han River, Lake Victoria, and Yangtze River (Table 4-3), although volume-reduced sampling was employed with bigger mesh sizes (Egessa et al., 2020; Wang et al., 2017; Zhao et al., 2020). Lake Victoria is the second-largest freshwater lake in the world and is exposed to greater sources of anthropogenic waste as it is shared by Kenya, Uganda, and Tanzania. The fishery at Lake Victoria is the world's largest inland fishery, with over 200,000 people engaged in direct fishing (Egessa et al., 2020; Nyamweya et al., 2016). Similar arguments can be made for the Yangtze River, the longest river in Asia. China is the world's largest producer and consumer of plastic materials. Thus, the Yangtze River is expected to have a higher total amount of MP pollution (Feng et al., 2021; Xiong et al., 2018). On the other hand, in the Vaal River, only a handful of fishermen engage in recreational fishing activity.

Table 4-3: Microplastic abundances in surface water of different freshwater bodies

Study area	**Sampling apparatus**	**Abundance (particles·m^{-3})**	**Reference**
Lijiang River, China	300 µm plankton net	0.15 ± 0.15	Zhang et al. (2021b)
Beijiang River, China	112 µm plankton net	0.56 ± 0.45	Tan et al. (2019)
Lijiang River, China	75 µm plankton net	0.67 ± 0.41	Zhang et al. (2021b)
The Great Lakes tributaries, USA	333 µm neuston net	4.2	Baldwin et al. (2016)
Haihe River, China	333 µm manta trawl	14.2 ± 14.6	Liu et al. (2020b)
Lijiang River, China	12-V DC Teflon pump (25 µm sieve)	67.5 ± 65.6	Zhang et al. (2021)
The Han River, South Korea	100 µm manta trawl	7.0 ± 12.9	Park et al. (2020)
Qiantang River, China	20ℓ container	1183 ± 269	Zhao et al. (2020)
Braamfontein Spruit, RSA	25ℓ container	705	Dahms et al. (2020)
Nyl and Mogalakwena Rivers, RSA	20ℓ steel bucket	160 ± 197	Dahms & Greenfield, (2025)
The Vaal River, RSA	**55 µm plankton net**	**0.61 ± 0.57**	**This study**

N/A = Not available

While some freshwater studies have revealed similar findings, others have reported significantly different concentrations of MPs (Table 4-4). For instance, a Lake Taihu, China study reported similar MP pollution levels with a mean abundance of 893.48 to 245.74 particles/(kg_dw) (Zhang et al., 2021c). Similarly, Ding et al. (2019) reported comparable findings in the Wei River, China, with abundance values ranging from 360 to 1320 particles/(kg_dw). In both studies, the authors attributed the high abundance of MPs to discharges from industrial, agricultural, and other anthropogenic activities, which explains the similarity with the pollution status in the Vaal River. Globally, higher MP abundance in rivers is frequently reported in those within populous urban areas, as exemplified by the Vaal River. Freshwater bodies reported to have much lower MP contamination include the Qinghai-Tibet Plateau River in Tibet and eighteen streams in Auckland, New Zealand (Dikareva & Simon, 2019; Feng et al., 2021). A varying abundance of 4-1347.5 particles/(kg_dw) in sediment samples from the Braamfontein Spruit in Johannesburg, South Africa, was reported by Dahms et al. (2020).

Table 4-4: Microplastic abundances in sediments of different freshwater bodies.

Study area	Sampling apparatus	Abundance (particles/(kg_dw))	Reference
Qinghai-Tibet Rivers, Tibet	Spatula	41.5 ± 22.3	Feng et al. (2021)
Auckland, New Zealand	Bucket	80	Dikareva & Simon, (2019)
Taihu Lake, China	Peterson grab	893.5 ± 245.7	Zhang et al. (2021c)
Wei River, China	Sludge sampler	360–1320	Ding et al. (2019)
Lake Ziway, Ethiopia	Ekman grab	0.05–36.2	Merga et al. (2020)
Oxbow Lake, Nigeria	Grab sampler	347–4031 & 507–7593	Oni et al. (2020)
Bloukrans River, RSA	N/A	160.1	Nel et al. (2018)
The Braamfontein Spruit, RSA	N/A	166.8	Dahms et al. (2020)
Nyl and Mogalakwena, RSA	Steel spade	53.3 ± 23, 20 ± 16.3, and 13.3 ± 24.2	Dahms & Greenfield, (2025)
Macadamia orchard and Communal reservoirs, RSA	Steel spade	25.3–140.6	Mutshekwa et al. (2023)
The Vaal River, RSA	**Van Veen grab**	**463.3 ± 284.1**	**This study**

N/A = Not available

4.4 PHYSICAL PROPERTIES OF MPS

4.4.1 Microplastic shapes

Typical MP shapes observed are shown in microscopic images in the Figure. 4-1a-d.The major shapes observed in water samples were fibres (41.2%) and fragments (39.9%), with films and pellets seldom observed (10.9% and 7.7%, respectively). On the other hand, fragments were the most dominant shape in sediment samples, accounting for 63%, followed by fibres (34.7%). No films were present in sediment samples, and pellets were found to be less prevalent, accounting for only 2.3% of the total detected MPs (Figure 4-2a).

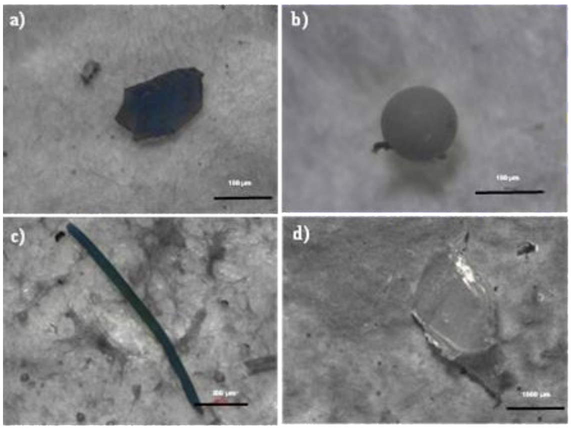

Figure 4-1: Microplastic shapes: a) fragment, b) pellet, c) fibre, and d) film

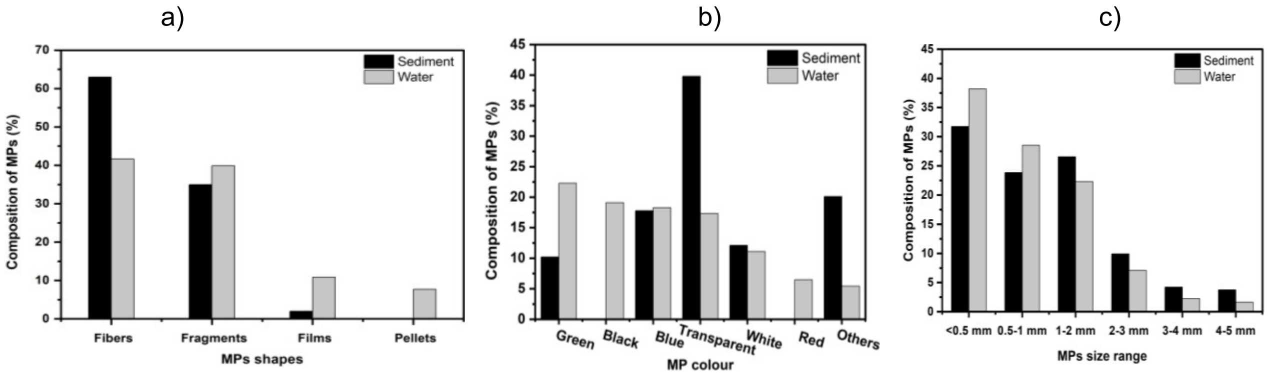

Figure 4-2: Distribution of MP a) shapes b) colours and c) sizes in water and sediment samples.

In surface water samples, MPs were found in a variety of colours, with green (22.3%), black (19.1%), and blue (18.3%) dominating the colour scheme. White (11.1%), red (6.5%), and other colours (pink, purple, yellow, and brown (5.4%) were less prevalent. Transparent MPs contributed the remaining 17.3%. Similarly, coloured MPs were most abundant in sediments, contributing 60.2% of the total MPs, of which blue (17.8%), white (12.1%), and green (10.2%) were most dominant. Other colours (brown, pink, black, yellow, and grey) were observed in small portions, 20.1% altogether. Transparent MPs contributed to the remaining 39.8% (Figure 4-2b). Size distribution was quite similar in water and sediment samples, showing a decreased abundance with size increase. In surface water, MPs smaller than 0.5 mm represented 38.2%, followed by 0.5–1 mm (28.5%), 1–2 mm (22.3%), 2–3 mm (7.1%), 3–4 mm (2.2%), and 4–5 mm (1.7%). Microplastics smaller than 0.5 mm accounted for 31.7%, 0.5–1 mm (23.8%), 1–2 mm (26.6%), 2–3 mm (9.9%), 3–4 mm (4.2%), and 4–5 mm (3.8%) in sediment samples. The size distribution of MPs in water and sediment samples is given in Figure 4-2c. The Spearman correlation test was run to determine the relationship between MP sizes and abundance in water and sediment. Correlation coefficients and p values, in both water ($r = 0.12$; $p = 0.60$) and sediment ($r = 0.43$; $p = 0.03$), indicate weak/insignificant correlation.

4.4.2 Surface morphology

The surface texture of selected MPs of various shapes was examined, and Figure 4.3(a–d) shows the SEM images. The images showed that the surfaces of MPs are rough, cracked, porous and contain smaller particles pitted on the surfaces. In the Vaal River, plastics/MPs are exposed to different weathering and degradation processes, which increase the surface area of MPs, resulting in an increased adsorption capacity. This enhances their potential to act as vectors for chemicals and microorganisms (Liu et al., 2020b; Mao et al., 2020; Sekudewicz et al., 2021). Degraded MPs are of great concern due to their higher adsorption capacity of co-existing pollutants. Although MPs have a high affinity toward hydrophobic organic pollutants, weathering/degradation of MPs introduces oxygen-containing functional groups, which increase their polarity and affinity towards hydrophilic pollutants. Thus, they may act as vectors for organic and inorganic pollutants.

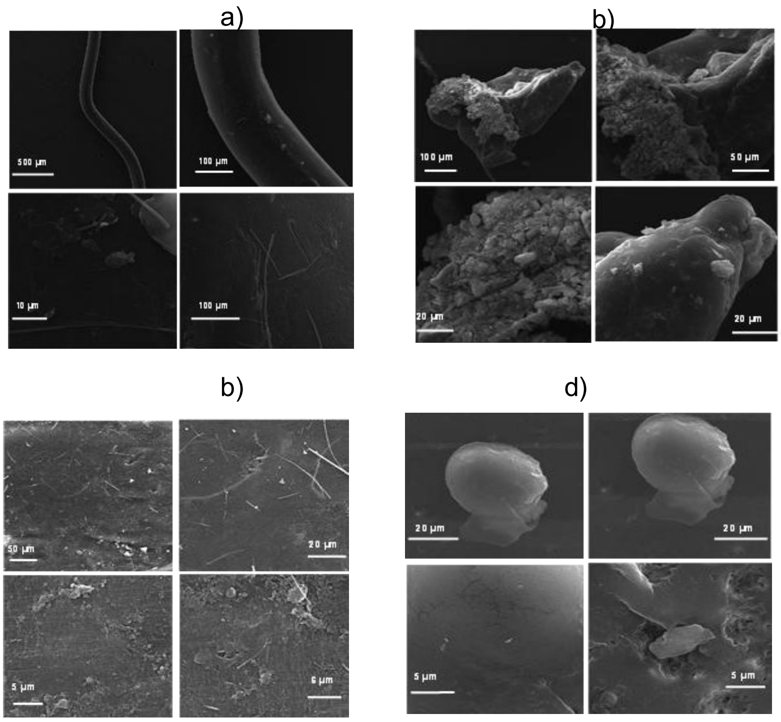

Figure 4-3: SEM micrographs of a) fibre b) fragment c) film, and d) pellet.

4.4.3 Ecotoxicological implications

More than 50% of MPs in surface water and sediments were less than 1 mm. It has been reported that the size of MPs affects their transport, distribution, and fate in water columns by affecting the magnitude of buoyant, gravitational, and drag forces. The higher surface-to-volume ratio enables small MP particles to have a lower relaxation time and lower settling velocity. This accounts for the high abundance of small MPs in surface water. However, small MPs may have faster sinking rates when bio-fouled, which could increase sedimentation rates and thus their abundance in sediments (Hoellein et al., 2014; Kowalski et al., 2016; Kumar et al., 2021; Lestari et al., 2020).

Plastic particles less than 1 mm pose the greatest threat to aquatic organisms. For instance, the adsorption capacity of nanoplastics has been reported to be at least two orders of magnitude greater than that of MPs. The desorption or leaching of toxic plastic additives has been reported to increase with a decrease in the sizes of MPs and has been reported to be more pronounced in MPs less than 1 mm (Koelmans et al., 2019; Luo et al., 2020; Velzeboer et al., 2014). Liu et al. (2020a) investigated the effect of MP sizes on the leaching of cadmium pigments into water under simulated sunlight. The authors reported that there was greater leaching of cadmium pigments in MPs less than 0.85 mm than in those with sizes above 0.85 mm. Consequently, there is great potential for a majority of MPs in the Vaal River to act as vectors for sorbed contaminants and enhance the bioavailability of plastic-derived toxicants along food chains (Bakir et al., 2012; Vethaak & Leslie, 2016).

A combination of MP shape and size may influence MPs' toxicity due to the differences in retention time, accumulation, and extent of physical damage. MP fibres, which were the most abundant shapes in surface water and second most in sediments, have been reported to have longer intestinal residence time and higher mortality in freshwater amphipods (*Hyalella Azteca*) than other shapes (Au et al., 2015). Gray & Weinstein. (2017) reported that fibres had a higher residence time and stronger acute toxicity than beads/pellets and fragments in grass shrimp (*Palaemonetes pugio*) (Gray & Weinstein, 2017). Similar observations were made by Qiao et al. (2019) in the guts of zebrafish *(Danio rerio*), where fibres had greater residence times and microbeads/pellets and fragments. The greater propensity of fibres to be retained in biota was also corroborated by an investigation of MPs in human colon tissue. MPs were detected in all colon tissue samples, with 96.1% of particles detected being fibres (Ibrahim et al., 2021; Qiao et al., 2019; Schwabl et al., 2019).

4.5 CHEMICAL COMPOSITION OF MPS

4.5.1 Polymer types

For reliable identification of MPs, chemical analysis is essential to support the preceding physical characterisation. Chemical characterisation was performed using Raman spectroscopy to identify polymer types. Eight polymers were identified in both surface waters and sediments, namely: Polyethylene (PE) (both Low-density polyethylene (LDPE) and High-density polyethylene (HDPE)), Polypropylene (PP), Poly(ethylene-co-vinyl acetate) (PEVA), Poly(ethylene-co-acrylic acid) (PEAA), Polyester (PES), Polyurethane (PU), Polyethylene/hexene-1-copolymer (PEH) and Polystyrene (PS). PE and PP were the most frequent polymers identified in both surface water and sediment samples and accounted for 85.2% and 79.1%, respectively (Figure 4-4a&b). A minor proportion of Poly(ethylene-co-vinyl acetate) (PEVA) (7.4%), Poly(ethylene-co-acrylic acid) PEAA (5.6%), and Polystyrene (PS) (1.9%) were detected in water samples. In sediment samples, there were low numbers of PEVA (14%), Polyethylene/hexene-1-copolymer (PEH) (2.3%), Polyester (PES) (2.3%), and Polyurethane (PU) (2.3%). The polymer type that makes up MPs is another essential part of determining the sources of MPs. The relatively high abundance of PE and PP in surface waters and sediments is consistent with global demands and observations made by previous studies (Feng et al., 2021; Lestari et al., 2020; Mao et al., 2020). In South Africa, Sasol Polymers and Safripol polymerise the ethylene and propylene into polyolefins (PE or PP). Polyolefins are the most ubiquitous synthetic commercial polymers, accounting for 50% of the total global plastic demand in 2021 (PlasticsEurope, 2021; Sadan and De Kock, 2020).

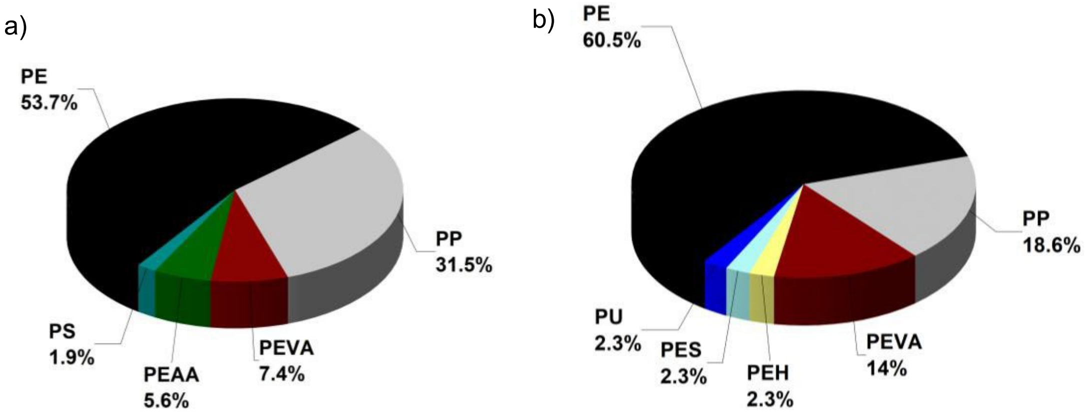

Figure 4-4: Composition of MP polymers in a) surface water and b) sediments.

4.5.1.1 Polyethylene

PE is the world's most produced polymer, PEs are divided according to their density, melting point, and molecular structure as either LDPE or HDPE. LDPE is a product of a non-catalysed high-pressure polymerization and is characterized by its highly branched chain structure. As a result of this, their density and crystallinity is reduced while flexibility increases. Applications for LDPE include packaging, bottles, plastic bags, clothes, water tanks, plastic furniture, and films. HDPE is a highly crystalline polymer produced from a low-pressure polymerization using Ziegler–Natta catalysts. HDPE has a linear polymeric chain, high density, and high melting point. Applications for HDPE include large containers, drums, fuel tanks, bottles, pipes, crates, and wrapping film (Novotna et al., 2019; Zohuri, 2012). Although PE is the most inert of the polyolefins, however, it can slowly degrade in the environment. The C−C backbone does not readily undergo hydrolysis and photo-oxidation due to the lack of UV-visible chromophores. However, impurities or structural defects can act as chromophores. This can cause PE to be readily oxidized by tropospheric radicals to unstable hydroperoxides, which are then converted to more stable UV-absorbing carbonyl groups. An increased rate of photo-oxidation has been reported for LDPE, relative to HDPE, due to the higher frequency of reactive branch points in LDPE (Chamas et al., 2020). A lack of reactive groups on the saturated organic backbone limits the applications of PE and PP polymers due to their limited compatibility with other polymers and other materials. Polymer blending is an economically effective way of developing polymers with distinct properties from those of each constituent. Modifications to PE and PP can be made by changing catalysts and incorporating linear α-olefin comonomers and/or blending with other polymers. The incorporation of block or grafting copolymers increases the compatibility and adhesion of polyolefins to other materials (Borsig, 1999; Park et al., 2005; Tham et al., 2015).

4.5.1.2 Polyethylene copolymers

PE copolymers detected in surface water and sediments include PEVA, PEH, and PEAA. PEVA is a copolymer of ethylene and vinyl acetate and PEH is an ethylene and hexene copolymer. PEVA is synthesised through free radical polymerisation with different acetate contents. The polar vinyl acetate group increases the plastic’s flexibility, filler compatibility, and fracture toughness. PEVA is used in applications such as agriculture films, footwear, flexible packaging, and electronic and electrical insulation (Bidsorkhi et al., 2014; Tham et al., 2015; Wang & Deng, 2019). PEH is synthesized when hexene is added to PE to produce a low-density plastomer with desired specifications, for example, mechanical and thermal properties (Hanifpour et al., 2019). As a result, its presence in the Vaal would be due to anthropogenic activities and repair jobs performed on the river's boats and houses. PEAA is a PE and co-acrylic acid copolymer typically synthesized through high-pressure free radical polymerisation. Increasing the acrylic acid content increases sealing properties and adhesion to polar substrates, aluminium, steel, and glass. PEAA plastics have a wide range of applications in flexible packaging material, compatibiliser in multi-layer films, sports equipment, electronic and electrical cables, and cosmetic bottles (Baughman et al., 2007; Wiggins & Bielawski, 2013).

4.5.1.3 Polyester

Polyester polymers contain the ester functional group in every repeat unit of their main chain. Polyethylene terephthalate (PET) is the most common thermoplastic polyester polymer. About two-thirds of PET is used for textiles, a quarter is used to manufacture PET bottles and the remaining quantity is used for films and special items. PES is used for packaging, picnic blankets, disposable face masks, fishing gear such as nets, and insulators, and as an alternative to glass. PES is nonbuoyant; however, adsorption of matter onto its surface and biofouling impact its transport and sedimentation (Gong et al., 2018; Rajendran et al., 2020).

4.5.1.4 Polystyrene

Polystyrene is an amorphous thermoplastic polymer used in various applications. Polystyrene is made of phenyl rings attached to every other carbon atom on the polymer chain. Polystyrene comes in two forms: either expanded PS (EPS) or high-impact PS (HIPS). Commercial HIPS generally contains fractions of polybutadiene (3–10%) and rubber (10–40%) to facilitate greater flexibility and durability. Applications include disposable cutlery, compact disk cases, meat trays, disposable plates, small household appliances, computers, and toys (Grigorescu et al., 2019). The presence of polystyrene particles is concerning to aquatic biota and, by extension humans due to their potential to inhibit cell viability, and gene expression, induce pro-inflammatory, alter mitochondrial depolarization and Adenosine triphosphate synthesis when ingested (Forte et al., 2016; Wu et al., 2019).

4.5.1.5 Polyurethane

Polyurethane is widely used in medical applications such as catheters and industrial products, particularly as foams. Polyurethane foams, commonly used in pharmaceutical and cosmetic industries, eventually end up as waste in the water cycle. Additionally, it is widely used in tyres, sponges, insulation, coats, paints, adhesives, and fibres (Islam et al., 2019; Matías, 2022; Sharma & Chatterjee, 2017).

4.5.2 Additives in surface water and sediments

C.I. Pigment White 6, C.I. Pigment Black 7, and C.I. Pigment Yellow 83 were identified via Raman analysis in surface water and sediment samples.

4.5.2.1 C.I. Pigment White 6

The sample Raman spectrum in Figure 4.5 was superimposable to reference spectra of Titanium dioxide (C.I. Pigment White 6), which is the most widely used plastic colourant in the world. TiO_2 exists in three crystalline structures: two tetragonal phases (anatase and rutile), and an orthorhombic phase (brookite) (Christie, 1994; Ramos-Corella et al., 2019). TiO_2 and Ti mixed-phase oxide compounds are widely used as a pigment and optical agent, particularly in PVC, PE, and alkyd resins. TiO_2 is extensively used in white carrier bags, window profiles, and others (Kemp & McIntyre, 2001; Lim et al., 2018). Colourants can affect the photostability of the polymer matrix. Generally, most colourants are added to increase photostability in addition to the primary function of imparting colour. However, polymer degradation and prolonged exposure to sunlight lead to the generation of reactive oxygen species, which degrade the polymer matrix. The two tetragonal phases of TiO_2 have opposite photoactivity when incorporated into polymers. When incorporated into polyolefins, rutile is relatively inactive. However, anatase has photocatalytic behaviour and leads to polymer degradation (Allen, 1994; Christie, 1994; Kemp & McIntyre, 2001).

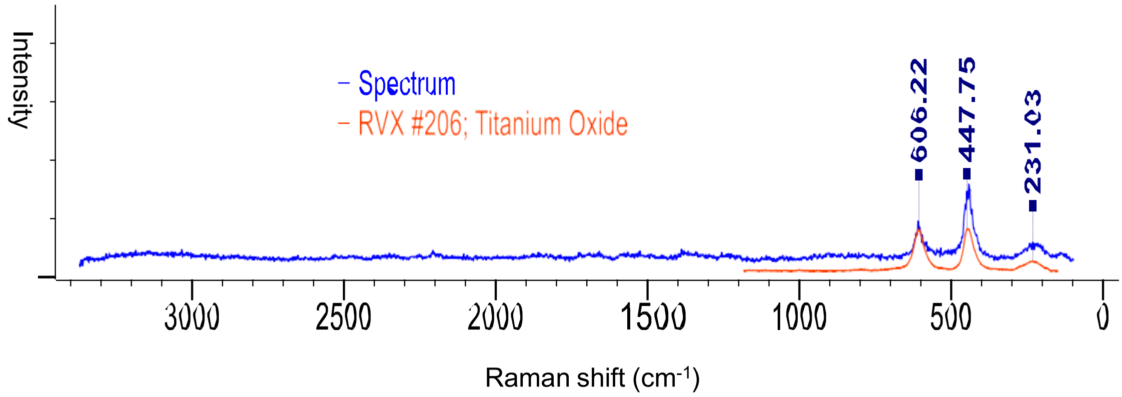

Figure 4-5: Sample and reference Raman spectra of TiO_2.

4.5.2.2 C.I Pigment Black 7

The sample Raman spectrum in Figure 4.6 was superimposable to reference spectra of Ivory Black (C.I Pigment Black 7). These pigments are commonly referred to as Carbon blacks. Carbon blacks are carbon-based pigments and reinforcing agents used in polymers and polymer blends. In terms of the volume of all pigments used by the plastics industry, carbon blacks are the second most widely used colourant in plastics (Coccato et al., 2015; Scherrer et al., 2009; Tomasini et al., 2012). Black particles generally contain carbon blacks as colourants, which exhibit carbon-like Raman spectra and their polymer types are sparsely confirmed via micro-Raman spectroscopy (Coccato et al., 2015; Käppler et al., 2016; Lenz et al., 2015; Scherrer et al., 2009; Tomasini et al., 2012). In most of its applications, carbon black is incorporated into a polymer matrix. However, according to Bott et al. (2014), carbon black particles generally do not leach from plastics into food. Consequently, carbon blacks are not considered a direct genotoxicant or reproductive toxicant (Bott et al., 2014; Chaudhuri et al., 2018).

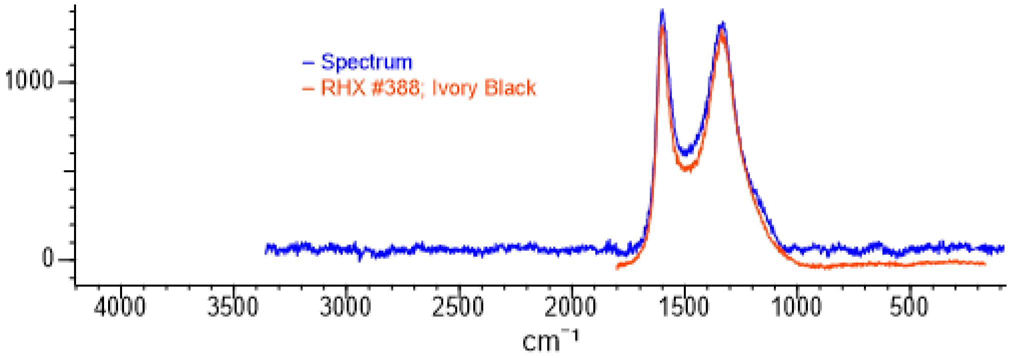

Figure 4-6: Sample and reference Raman spectra of Pigment Black 7.

4.5.2.3 *C.I. Pigment Yellow 83*

The sample Raman spectrum in Figure 4-7 was superimposable to reference spectra of (C.I. Pigment Yellow 83). C.I. Pigment Yellow 83 is part of a group of yellow classical organic pigments known as Diarylide yellows. Diarylide yellows are important yellow azo pigments used in polyethylene, polypropylene, flexible polyvinyl chloride, printing inks, and industrial coatings (Barrow et al., 2003; Christie, 1994). Pigment Yellow 83 has previously been detected in MP samples from Lake Gard (Imhof et al., 2013). Pigment Yellow 83 is insoluble in the body and in phagolysosomal solution *in vitro*, which simulates the lung environment. Pigment Yellow 83 is classified as carcinogenic (Hartwig & Commission, 2021). Thus, MPs containing the pigment yellow 83 could pose a threat to a wide variety of freshwater biota in the Vaal River and people that ingest them as a food source.

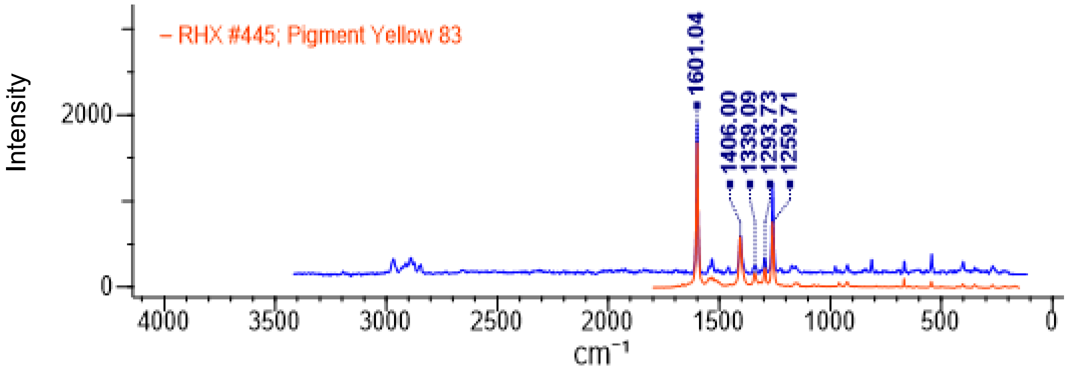

Figure 4-7: Sample and reference Raman spectra of Pigment Yellow 83.

4.5.2.4 *C.I. Pigment Yellow 6*

The sample Raman spectrum in Figure 4-8 was superimposable to reference spectra of Saffron (C.I. Pigment Yellow 6). According to evidence, Saffron was the first dyestuff known to humanity. It contains a water-soluble dye derived from *Crocus sativus L*. dried flower stamen. Crocetin and crocetin glycosyl esters are the primary chromophores in saffron (crocins) (Quintero Balbas et al., 2022). Saffron is a yellow pigment used in inks, paint, and coatings. This suggests that the pigment may have leached from paint chips that may have made their way to the Vaal River. Saffron is also used as a spice. The kitchens from the nearby resorts and hotels may incorporate spices in their meal preparations.

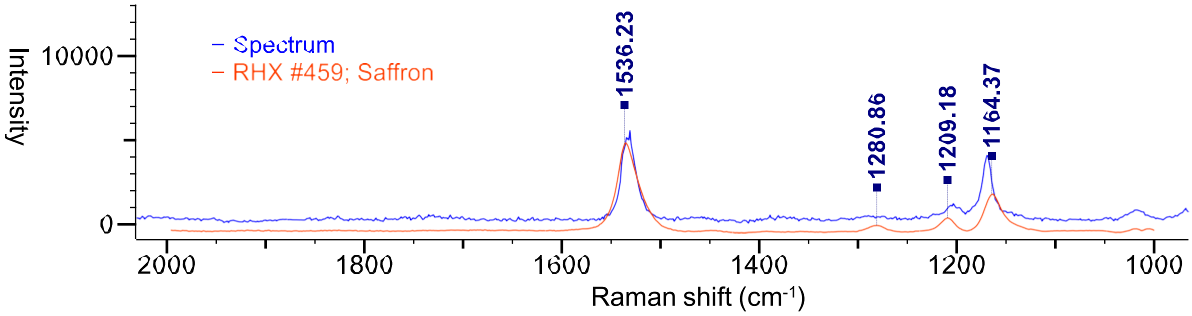

Figure 4-8: Sample and reference Raman spectra of Pigment Yellow 83.

4.6 SUMMARY

Microplastics (MPs) were detected in all surface water and sediment samples collected during the study, highlighting their widespread occurrence. The higher concentrations of microplastics in sediment samples suggest that sediments act as a significant sink for microplastic pollution. The consistently higher MP concentrations in sediments compared to surface waters may also reflect the tendency of plastic particles, particularly those with higher densities, to settle and accumulate over time. This trend is consistent with findings from similar freshwater and marine studies, where sediments often serve as repositories for historical and ongoing plastic pollution.

With regards to sources, the presence of microplastics in all surface water and sediment samples suggests multiple and diffuse sources of pollution. Likely contributors include urban runoff, wastewater effluents, stormwater discharges, and improper waste disposal in surrounding areas. The higher concentrations observed in sediments indicate long-term accumulation, possibly linked to persistent inputs from nearby residential, industrial, or recreational activities. The wide variability in microplastic abundance across samples also points to localized sources, such as plastic litter hotspots or discharge points, which may be intensifying contamination in specific areas.

More than half of the microplastics detected in both surface water and sediments were smaller than 1 mm, a size range known to significantly influence their environmental behaviour and biological impacts, and pose heightened ecological and health risks. They can release more plastic additives, absorb contaminants and are more likely to be ingested by aquatic organisms. Shape also plays a critical role in toxicity. Fibres, which were found to be dominant in surface waters and common in sediments, are more persistent in organisms' digestive tracts and have been linked to greater physical harm and mortality in both aquatic species and humans. Studies have shown fibres are the most retained form in aquatic animals and human colon tissue, suggesting long-term exposure and bioaccumulation risks.

5 MICROPLASTICS IN GROUNDWATER

5.1 INTRODUCTION

This chapter provides and examines the findings on the characterisation of MPs in groundwater. Samples were collected from five borehole-connected taps in suburbs in Gauteng (Braamfontein, Vereeniging, and North Riding), as well as borehole-connected taps in villages and towns in the North West (Zeerust, Supingstad, Lekubu, Kwa-Ntsweng, Mokgola, and Braklaagte).

5.2 HYDROCHEMICAL DATA

The sample location and hydrochemical parameters of groundwater (GW) samples collected in the North West Province (NWP) and Gauteng Province (GP) are shown in Table 5-1, respectively. Analysis of groundwater chemistry is essential for classifying and assessing water quality, as this allows possible changes in quality to be monitored over time. The quality assessment of groundwater depends primarily on the nature and concentration of its various chemical constituents, which are mostly derived from the geology of the particular region (Patterson et al., 2023). The mean value pH (mvpH), pH, oxidation-reduction potential (ORP), conductivity, absolute conductivity, resistivity, total dissolved solids (TDS), and salinity values of the groundwater ranged from -86.2–69.1, 6.79–8.48, 189.1–261.6 ORP (mV), 0.308–0.768 mS/cm, 295–980 µS/cm, 0.0032–0.0111 MΩ.cm, 375–431 ppm, and 0.15–0.42 practical salinity unit (PSU), respectively.

The ORP of groundwater samples suggested that they were primarily transiting to an oxic environment, determined mainly by the pump-and-store process involved. Conductivity is an indirect measure of dissolved constituents in water. In the groundwater samples, conductivity values were within the expected normal ranges, with some variation between individual sampling points. Relatively high conductivity values were recorded for most samples from areas with only dolomite–water interactions and no mixing of groundwater and rainwater. However, the conductivity values were relatively low in areas in which there is a mixing of groundwater, rainwater, and river water at particular sampling points, such as those in Mokgola and Braklaagte.

TDS is the total amount of all solid inorganic and organic substances (mineral salts, cations, metals, and anions) dissolved in water. The relatively high TDS values recorded for groundwater samples from Supingstad reflect the interaction of water with dolomite formations. Relatively low TDS values were recorded from Mokgola and Braklaagte, which is consistent with the mixed water system used in this area. The World Health Organisation (WHO) does not set guidelines for pH, TDS, and conductivity; however, it does list generally accepted values based on different guidelines set by the majority of countries around the world (WHO, 2022). The hydrochemical parameters were all within the limits set by the South African National Standards (SANS) 241 minimum requirements for safe potable drinking water and the WHO generally accepted values for safe drinking water.

Table 5-1: Hydrochemical parameters of groundwater samples.

Sample Code	Sample description	pH (mV)	pH	ORP (mV)	Conductivity (mS/cm)	Absolute Conductivity (µS/cm)	Resistivity (MΩ.cm)	TDS (ppm)	Salinity (psu)
GP1	Wits	-40.4	7.17	204.7	0.456	615	0.0018	231	0.25
GP2	Auckland Park	-35.9	7.26	221.4	0.531	703	0.0021	189	0.17
GP3	Vereniging BT	-41.3	7.36	189.8	0.613	813	0.0020	352	0.21
GP4	Vereniging AT	-58.7	7.68	207.2	0.620	765	0.0017	165	0.27
GP5	North Riding	-40.1	7.53	195.6	0.703	803	0.0015	208	0.23
NW1	Mokgojoa, Secondary School, Kwa-Ntsweng	-27.3	7.45	204.5	0.372	412	0.0027	178	0.17
NW2	Supingstad Clinic	-25.5	7.30	191.8	0.670	980	0.0110	431	0.42
NW3	Community tap 1, Supingstad	-31.9	7.42	200.5	0.762	843	0.0013	379	0.37
NW4	Matthews Mangope High School, Supingstad	-37.5	7.54	200.3	0.763	845	0.0013	381	0.37
NW5	Community tap 2, Supingstad	-31.8	7.42	207.7	0.768	837	0.0013	384	0.37
NW6	Community tap 3, Supingstad	30.1	7.38	189.1	0.767	836	0.0013	384	0.37
NW7	Community tap 4, Supingstad	-31.3	7.41	194.6	0.749	811	0.0013	375	0.36
NW8	Wonderboom Gate, Madikwe	-49.4	7.73	215.1	0.767	737	0.0026	384	0.38
NW9	Kingfisher Guesthouse, Zeerust	-22.4	7.17	221.5	0.486	508	0.0021	242	0.23
NW10	Islam General Dealer, Lekubu	-86.2	8.48	213.4	0.607	578	0.0016	304	0.29
NW11	Masengatsene Carwash and Grill	69.1	8.12	230.6	0.368	356	0.0027	184	0.18
NW12	Farmplot, Braklaagte	-53.0	6.79	261.6	0.319	309	0.0031	160	0.15
NW13	Mokgola Carwash	-83.7	8.43	236.5	0.308	295	0.0032	154	0.15
NW14	Mokgola Clinic	50.1	7.75	236.5	0.389	376	0.0026	195	0.19
NW15	Tsepo Café, (Elsenburg Turn), Mokgola Village	66.0	8.03	240.1	0.452	436	0.0022	226	0.22

5.3 MICROPLASTICS IN GROUNDWATER

5.3.1 MP concentrations in groundwater

Microplastics were detected in all groundwater from an unconfined and semi-confined karst aquifer from the North West and Gauteng Provinces (Figure 5-1a). Overall, MP concentrations had a mean concentration of 11 ± 6.9 particles·ℓ^{-1} (range: 3.7–30 particles·ℓ^{-1}). North West groundwater had a mean concentration of 13 ± 7.6 particles·ℓ^{-1} (range: 3.7–30 particles·ℓ^{-1}). On the other hand, Gauteng groundwater had a mean of 7.0 ± 2.7 particles·ℓ^{-1} (range: 4.3–11 particles·ℓ^{-1}). The highest MP concentration was from groundwater collected from NWP9 (Guesthouse in Zeerust). However, it should be noted that in Zeerust, the water used combines groundwater and dam water, which could account for the higher concentration of MPs. High MP concentrations were also observed in NWP1 and NWP3 from a secondary school in Kwa-Ntsweng and a community tap in Supingstad. Groundwater collected from a secondary school in Supingstad (NWP4) had the lowest MP concentration with 3.7 particles·ℓ^{-1}. Groundwater at this sampling point passed through filters and was also mixed with rainwater, which may account for the low concentrations. The Shapiro-Wilk Test revealed a statistically significant departure from normality, W(20) = 0.839, p = < 0.05. Thus, the requirements for the non-parametric Mann-Whitney U Test were satisfied. There were no statistically significant differences in MP concentrations from Gauteng and North West (Mann-Whitney U Test: U = 18, p = 0.098 > 0.05) (Figure 5-1b).

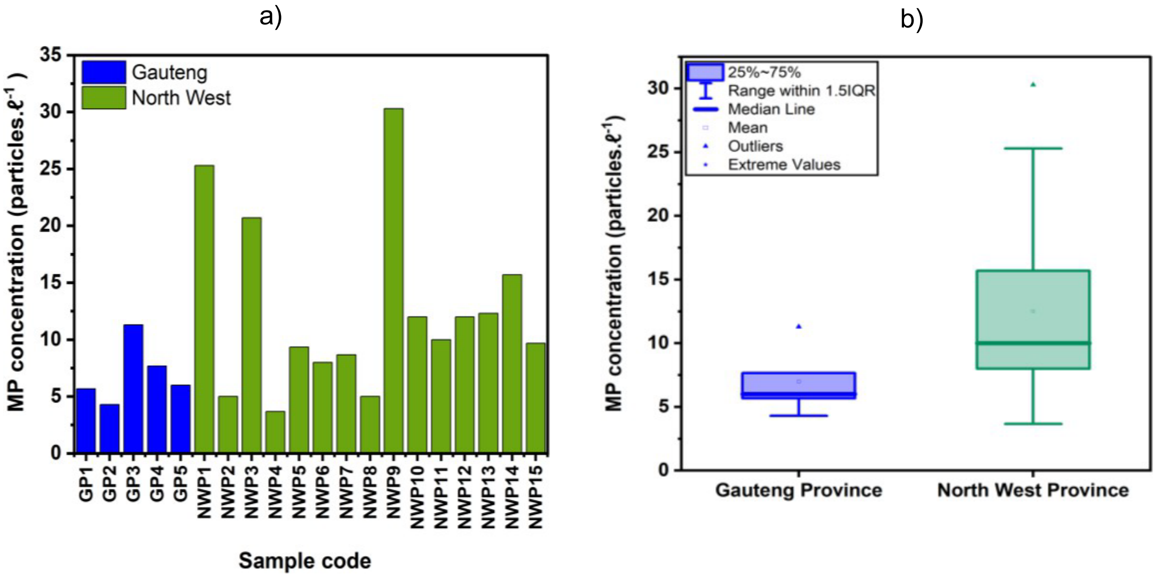

Figure 5-1: a) Microplastic concentrations and box plots of MPs in groundwater samples.

As shown in Figure 5-2 (a-f), there is a low to moderate negative correlation between MP concentration, pH (r = -0.0694), TDS (r = -0.2374), and absolute conductivity (r = -.42319). It has been reported that an increase in groundwater pH enhances the surface potential of MPs, thereby increasing their migration capacity (Gong et al., 2023; Jódar-Reyes et al., 2006). Similar observations were made by Kim et al. (2023) and Gong et al. (2023) from groundwater samples from Jeju Island, Korea and Dawanshan Island, China, respectively. It has been reported that high TDS can cause the aggregation of negatively charged MPs in water environments, leading to a high MP concentration (Cai et al., 2020). However, in this study, high TDS values in groundwater were correlated to a low MP concentration. This is consistent with a study by An et al. (2022), who reported a weak correlation between the MP concentration and TDS from a karst aquifer in Anshun, Guizhou Province, China (An et al., 2022).

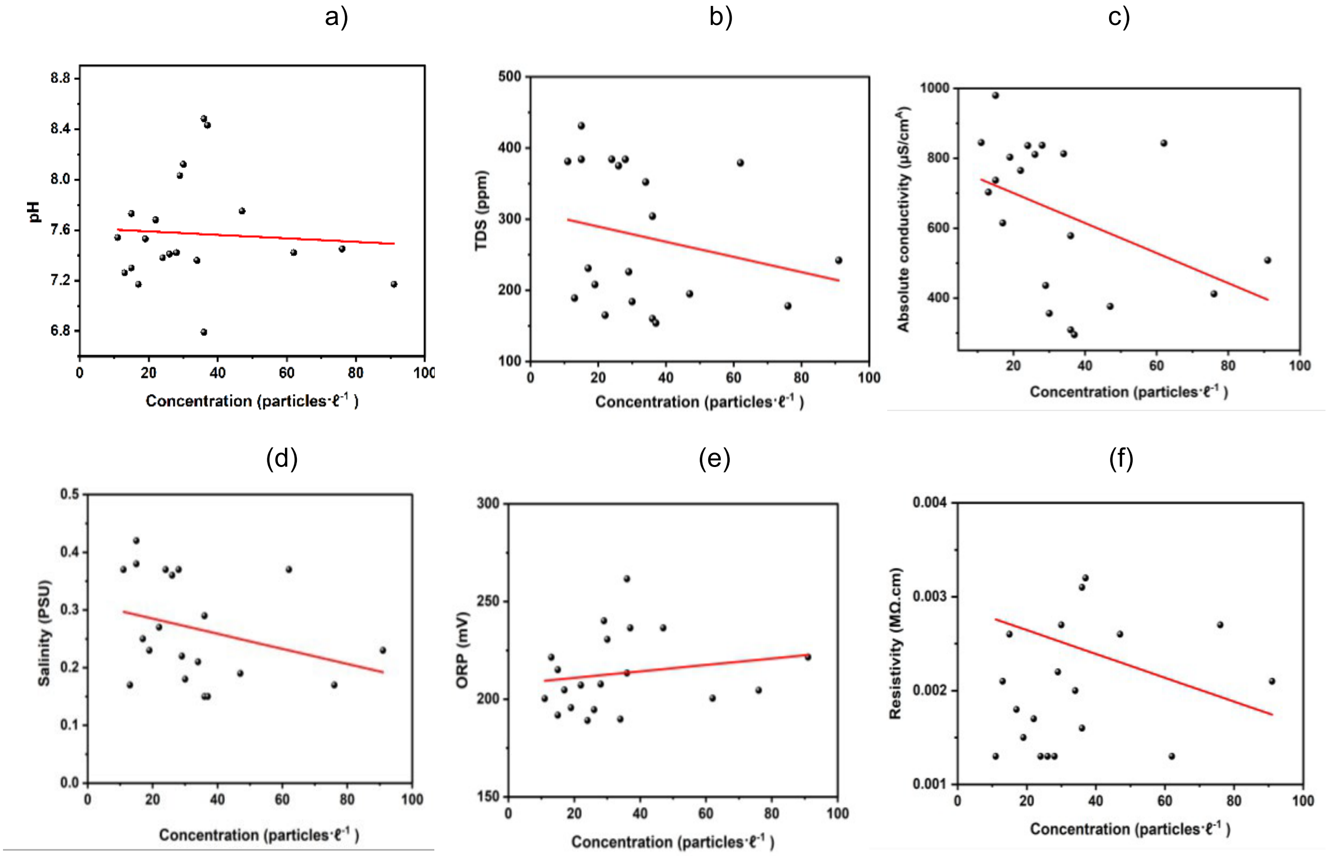

Figure 5-2: Plots of MP concentration against a) pH, b)TDS, c) absolute conductivity, d) salinity, (e) ORP and f) resistivity.

5.3.2 Physical characteristics of MPs in groundwater

The major shapes observed in all groundwater samples were fibres and fragments, accounting for 78.6% and 11.5%, respectively (Figure 5-3a). Films and pellets were present in smaller quantities and accounted for 7.93% and 1.95%, respectively. Fibres represented at least 52% of all shapes in each groundwater sample. Gauteng Province groundwater samples had a high proportion of fibres (63.8%), pellets (16.2%), and fragments (14.3%). Films accounted for the smallest proportion (5.71%). Groundwater from the NWP had a high abundance of fibres (81.4%) and fragments (11%). Pellets and films accounted for the smallest proportions, with 6.40% and 1.24%, respectively (Figure 5-3b). The majority (16.6%) of all fibres were from NWP9. Black (34.3%), blue (31.4%), and transparent (20.1%) were the most abundant MPs. The majority of fibres were blue (36%), black (32%), and transparent (21%). Similarly, fragments were mainly black (45.5%), blue (19.5%), and transparent (14.3%).

However, most of the pellets were black (45.3%), white (35.9%), and transparent (11.3%). The majority of films were transparent (53.8%) and white (23.1%), with minor proportions of black (15.4%) and red (7.70%) films detected (Figure 4.32c). Microplastics were detected in all seven size classifications. At least 66% of the particles in all samples were less than 1 mm, and MPs had a mean size of 0.57 ± 0.57 mm (Figure 5-3b). Fibres ranged from 0.05-4.52 mm (mean size: 0.70 ± 0.58 mm). Fragments had a mean size of 0.15 ± 0.2 mm (size range: 0.03–1.2 mm). Pellets had a size range of 0.02-1.16 mm (mean size: 0.08 ± 0.16 mm). Films had a mean size of 0.21 ± 0.19 mm (size range: 0.04-0.78 mm). Thus, the following trend was observed: fibres>films>fragments>pellets. As shown in Figure 5-3c, MPs in groundwater samples were distributed as follows: 0.1-0.5 mm (41.8%) > 0.5-1 mm (26.1%) > 0.02-0.1 mm (15.7%)>1-2 mm (13%)>2-3 mm (2.54%)>4-

5 mm (0.3%)>3-4 mm (0.15%). Groundwater from Gauteng had no particles greater than 3 mm. This could be due to the wide use of semi-permeable filter membranes, which may exclude particles >90 µm in diameter.

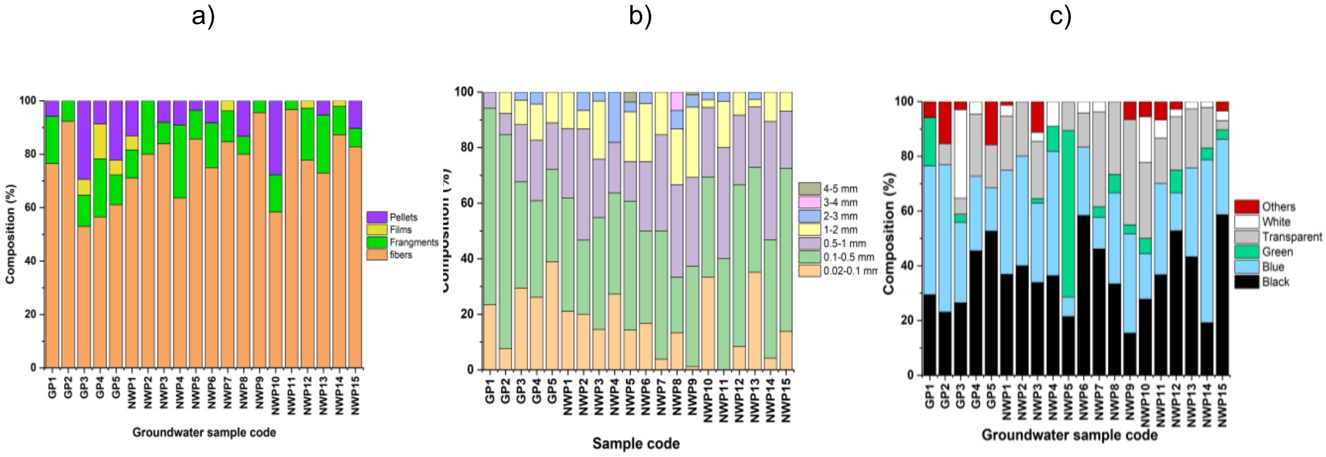

Figure 5-3: Composition of MP a) shapes b) size ranges and c) colours in groundwater samples.

5.3.3 Evaluation of potential risks associated with exposure to groundwater

The EDIs from groundwater in South African men, women, and children were 0.57, 0.40, and 0.93 particles/(kg.day), respectively. According to these estimates, more MPs are ingested by children than adults from groundwater. Paray et al. (2024) reported relatively high EDIs of 1.85 particles per person per day. Groundwater in rural areas in the North West is ingested without purification or filtration; thus, it can be inferred that at least 13 MPs could be ingested per litre of groundwater consumed. In comparison to the literature background mean MP concentration, all groundwater had very high contamination (MPCF > 6) and was categorised as danger level 4 (MPLI >30).

5.3.4 Chemical characterisation – polymer types

Characterisation was performed using micro-Raman spectroscopy to determine polymer types. In Figures 5-5 to 5-6, the reference spectra are in red, and the sample spectra are in blue or black. The names of the databases are abbreviated; for instance, the Raman-Forensic-Horiba database is abbreviated as RAX and WSARX for the Raman-Sigma-Aldrich Library of Raman Spectra-Wiley database. The polymer identity number (ID) and name of the reference polymer (i.e., RHX #531) in the database are also given. Six polymers were identified in the groundwater samples, namely Polybutylene terephthalate (PBT), Polyurethane (PU), and Polyethylene terephthalate (PET).

5.3.4.1 Polybutylene terephthalate

The Raman spectrum of the fibre in Figure 5-5 was superimposable to reference spectra of Polybutylene terephthalate (PBT). The spectra shared main peaks at 633.18 (C-O out-of-plane bending), 707.34 cm^{-1} (Benzene ring C-C stretch); 856.50–884.83 (C-H out-of-plane bending and C-C breathing mode of the benzene ring), 997.20 cm^{-1} (O-CH$_2$ stretch), 1130.9 cm^{-1} (C-C stretch); 1278.97– 1341.12 cm^{-1} (C=O-O stretch), 1614.78 cm^{-1} (C=C aromatic ring stretch), and 1716.44 cm^{-1} (C=O stretching) all assigned to PBT (Mak et al., 1998; Peñalver et al., 2023). Polyethylene terephthalate (PET) is the most common thermoplastic polyester polymer. Polyester polymers contain the ester moiety in every repeating unit. The ester functional group provides good adhesion to metals and metal oxides. PES is used for packaging, picnic blankets, disposable face masks, fishing gear such as nets and insulators, and as an alternative to glass (Gong et al., 2018; Klein et al., 2015; McClure, 2007).

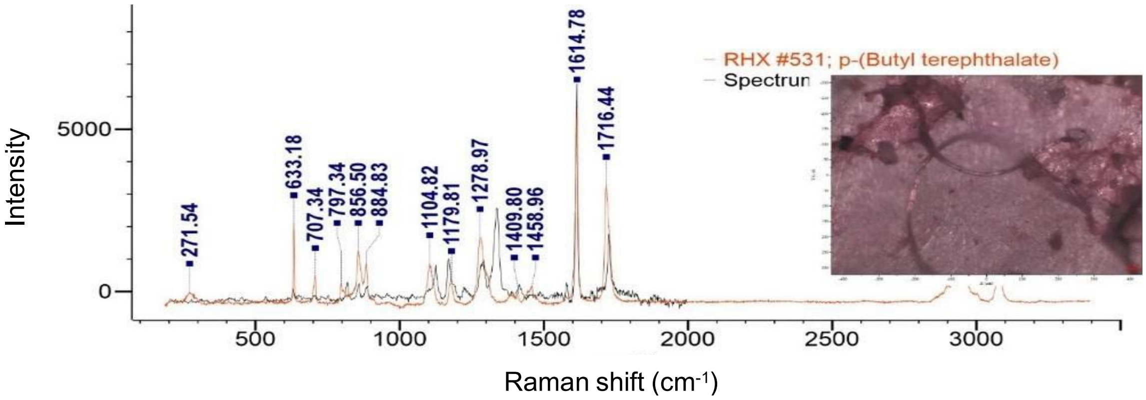

Figure 5-4: Raman micrograph, sample, and reference Raman spectra of PBT.

5.3.4.2 Polyethylene terephthalate

A transparent fibre had Raman spectra which were superimposable to the reference spectra of PET. The spectra shared main peaks at 630.8 cm^{-1} (C-H out-of-plane bending), 703.83 cm^{-1} (Benzene ring C-C stretch), 795.43 cm^{-1} (C-H out-of-plane bending), 858.11 cm^{-1} (C-H out-of-plane bending and C-C breathing mode of the benzene ring), 1119.42 cm^{-1} (C-O-C stretching), 1288.16 cm^{-1} (CH_2 twist), 1454.98 (CH_2 bending),1615.04 cm^{-1} (C=C aromatic ring stretch), and 1725.93 cm^{-1} (C=O stretch) all assigned to PET (Figure 5-6) (Chakraborty et al., 2022; Peñalver et al., 2023; Puchowicz & Cieslak, 2022). PET is the second most produced polymer resin, only to PP; about two-thirds of PET polymers are manufactured for the textiles industry and a quarter for the bottled water industry. The rest are used for films and special items. Polyethylene terephthalate is extensively used as a food-contact material. PET film's extraordinary blend of physical-chemical, thermal, and electrical properties has led to its extensive use in various markets, including the electrical and electronic industries, labels, and packaging (McClure, 2007).

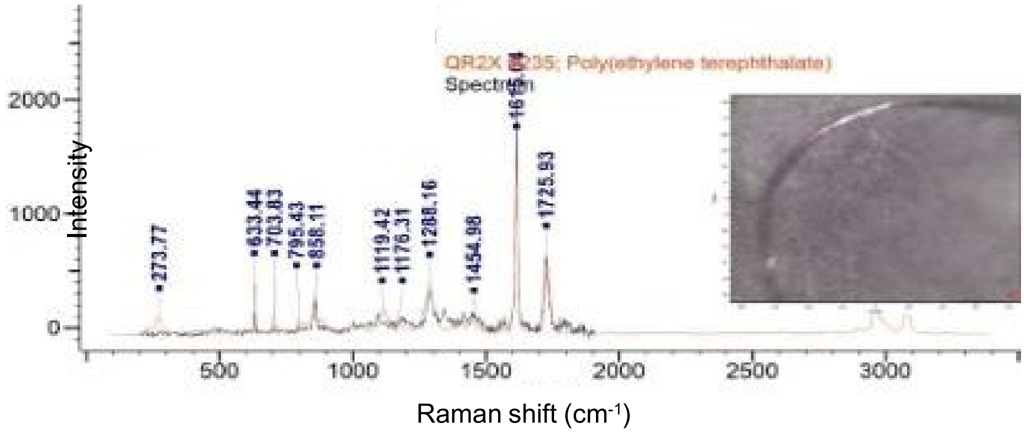

Figure 5-5: Raman micrograph, sample, and reference Raman spectra of PET.

5.3.4.3 Polyurethane

The Raman spectrum of the transparent fibre in Figure 5-7 was superimposable with reference spectra of PU. The sample and reference spectra shared main peaks at 1183.33 cm^{-1} (C-O-C symmetric stretch in urethane and C-H bending in the aromatic ring), 1337.2 cm^{-1}(CH_2 bending), 1454.32 cm^{-1} (N=C=O symmetric stretch and CH_2 bending), 1570.4 cm^{-1} (N-H bending and C-N stretch), 1614.42 cm^{-1} (C=C aromatic ring stretch), 1724.0 cm^{-1} (ester C=O stretch and urethane amide I C=O stretch) (Parnell et al., 2003; Weakley et al., 2012).

Polyurethanes are one of the most varied classes of polymers, with properties that can be tailored for a wide range of uses. They can be rigid and hard, flexible and soft, thermosetting, or thermoplastic. Polyurethanes are synthesised at room temperature through an addition reaction between polyisocyanates and polyols, resulting in carbamate (urethane) linkages in the polymer backbone. When the reaction is carried out in the presence of a blowing agent, PU foam is formed. Polyurethane is used in a wide range of products, including flexible and rigid foams (insulations for tanks, pipes, water heaters, refrigerators, and freezers), solid elastomers, extrusion and injection- moulded parts, coatings, sealants, and adhesives (De Souza et al., 2021; Islam et al., 2019; Sharma & Chatterjee, 2017).

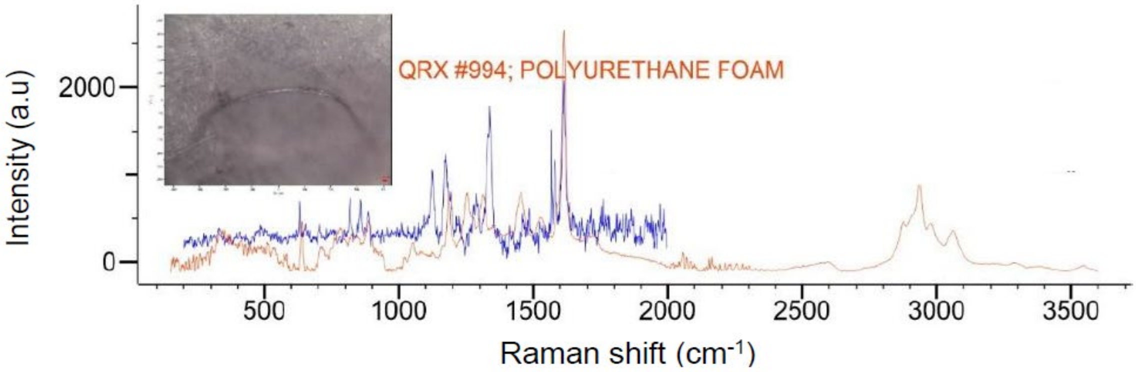

Figure 5-6: Raman micrograph, sample, and reference Raman spectra of PU.

The presence of PBT, PET, and PU is consistent with other studies which have recorded their high abundance in groundwater from the Jiaodong Peninsula, China (Mu et al., 2022). Additionally, PBT, PET, and PU have relatively higher densities (1.2–38 g/mℓ) than other consumer plastics such as PE, PP, PVA, and PS, which range from 0.89–1.09 g/mℓ. Thus, their higher density causes higher vertical migration capability through soils into groundwater, increasing their abundance (Mu et al., 2022; O'Connor et al., 2019).

5.3.5 Chemical characterisation – additives

Conjugated rings present in colourants are highly polarisable, and their Raman signals can completely overlay those of the polymeric matrix. Micro-Raman spectroscopy can be sensitive to both colourants and polymers (Imhof et al., 2016; Käppler et al., 2016). However, this high sensitivity leads to the general drawback of Raman micro-spectroscopy where high fluorescence from additives in MPs hinders the chemical identification of some particles (Käppler et al., 2016; Piyawardhana et al., 2022). During analysis, six colourants (C.I. Pigment Red 1, C.I Pigment White 6, C.I. Vat Blue 1, 4-(4- Nitrophenylazo)resorcinol, C.I.Direct Yellow 12, and C.I. Pigment Blue 15) were identified via Raman analysis in groundwater. In the text below, in addition to a colourant's name, its Colour index (C.I) generic name is also provided.

5.3.5.1 C.I Pigment White 6

The white fragment in Figure 5-7 has a Raman spectra which was superimposable to the reference spectra of C.I Pigment White 6 (TiO_2). The spectra shared characteristic peaks at 231.03 cm^{-1} (multiple phonon scattering processes), 447.75 cm^{-1} (E_g vibrational mode), and 606.22 cm^{-1} (A_{1g} vibrational mode) assigned to TiO_2 (Balachandran and Eror, 1982; Lim et al., 2018). C.I. Pigment White 6 is the world's most widely used plastic colourant, and its production is estimated to exceed 2 million metric tons by 2025 (Azizi & Daneshjou, 2024; Christie, 1994). TiO_2 exists in three crystalline structures: two tetragonal phases (anatase and rutile), and an orthorhombic phase (brookite) (Ramos-Corella et al., 2019). TiO_2 and Ti mixed-phase oxides are extensively used in the paint and polymer industry. TiO_2 is used as a pigment and optical agent, particularly in PVC, PE, and alkyd resins (Kemp & McIntyre, 2001; Lim et al., 2018; Schubert et al., 2019).

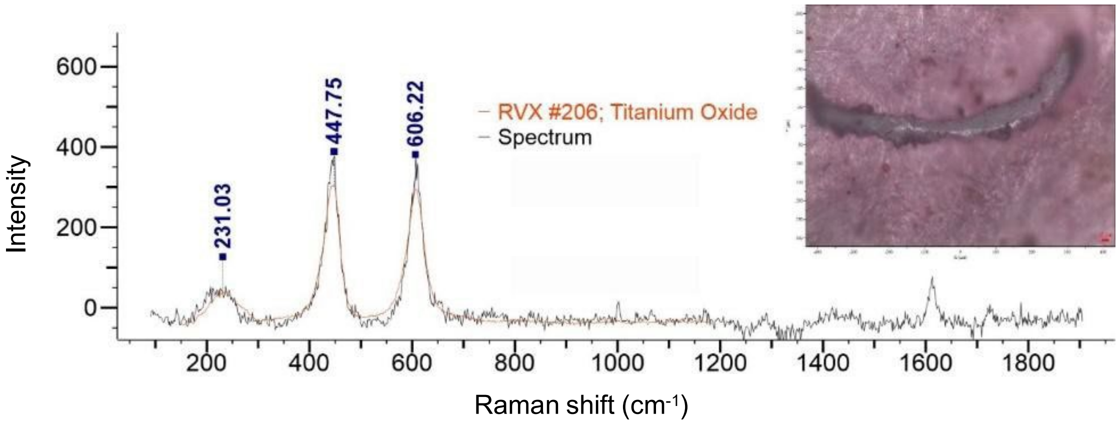

Figure 5-7: Raman micrograph, sample, and reference Raman spectra of C.I Pigment White 6.

5.3.5.2 C.I. Vat Blue 1

The white fragment in Figure 5-8 had Raman spectra which were superimposable to the reference spectra of C.I. Vat Blue 1. The spectra shared main peaks at 546.8 cm^{-1} (C-H and N-H bend), 599.0 (C=C stretch), 765.5 (C=C ring stretch and C-H bend), 881.6 cm^{-1} (C-N bend), 1149.7 cm^{-1} (C-H bend), 1461.4-483.1 cm^{-1} (N-H bend), 1584.6. cm^{-1} (C=C ring stretching; C=O stretch and N-H bending),1613.5-1625.1 cm^{-1} (C=C aromatic ring stretch and C=O ring symmetrical stretching) 1704.9 cm^{-1} (C = O ring symmetrical stretch) all assigned to C.I. Vat Blue 1 (Pagnacco et al., 2022; Volkov et al., 2020). C.I. Vat Blue 1 ($C_{16}H_{10}N_2O_2$) is a “vat dye” blue pigment consisting of a C=C double bond connecting two heterocyclic indole ring systems (Ricci et al., 2018). C.I. Vat Blue 1 can be synthesised from natural products such as *Indigofera tinctoria* or synthetic raw materials from the petrochemical industry. As one of the oldest dyes in the world, it has been extensively used in the textile industry as a vat dye for more than 5000 years. However, its low solubility in solvents and limited colour diversity limit its application as a vat dye and pigment (Fleischmann et al., 2015).

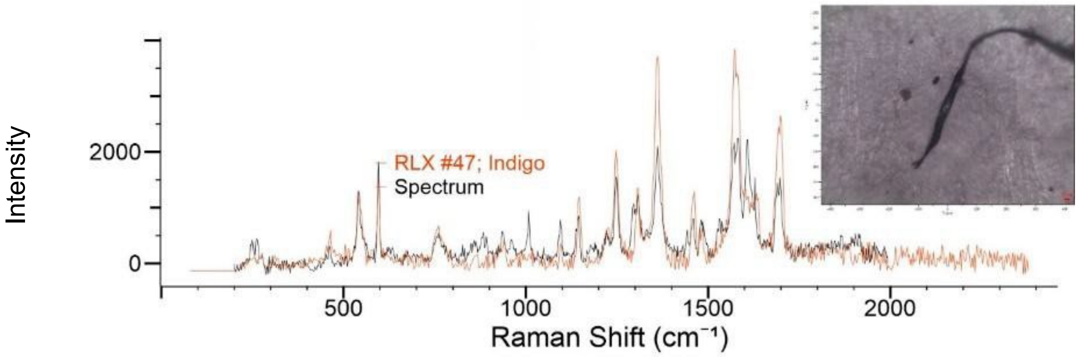

Figure 5-8: Raman micrograph, sample, and reference Raman spectra of C.I. Vat Blue 1.

5.3.5.3 C.I. Pigment Blue 15

The blue fibre shown in Figure 5-9 has a superimposable sample and reference spectra of Copper phthalocyanine/C.I. Pigment Blue 15. The spectra shared main characteristic peaks at 596.1 cm^{-1} (C=C stretch), 683.0–700.4 cm^{-1} (Benzene ring C-C stretch), 832.3 cm^{-1} (C-C stretch and CH_3 rocking), 1339.6 cm^{-1} (N=N stretch), 1452.7 cm^{-1} (CH_2 bending) and 1528.9 cm^{-1} (C=C aromatic ring stretch) all assigned to C.I. Pigment Blue 15 (Anghelone et al., 2015; Ragusa et al., 2021). Phthalocyanines are the most used polycyclic synthetic organic pigments in the world. These dyes are made up of macrocycles formed by four isoindole units that can coordinate different metal atoms. However, there are metal-free phthalocyanines (C.I. Pigment Blue 16) used as pigments. Phthalocyanines are available in reddish-blue and green-blue shades and are used as colourants in plastics such as PVC, LDPE, HDPE, PP, and PET (Anghelone et al., 2015; Christie, 1994; Ragusa et al., 2021). Phthalocyanine pigments have been identified in MPs from sediments (Imhof et al., 2016; Van Cauwenberghe et al., 2015), salt (Karami et al., 2016), cultured bivalves (Van Cauwenberghe & Janssen, 2014), seawater (Frère et al., 2016), bottled mineral water (Oßmann et al., 2018), and the placenta (Ragusa et al., 2021).

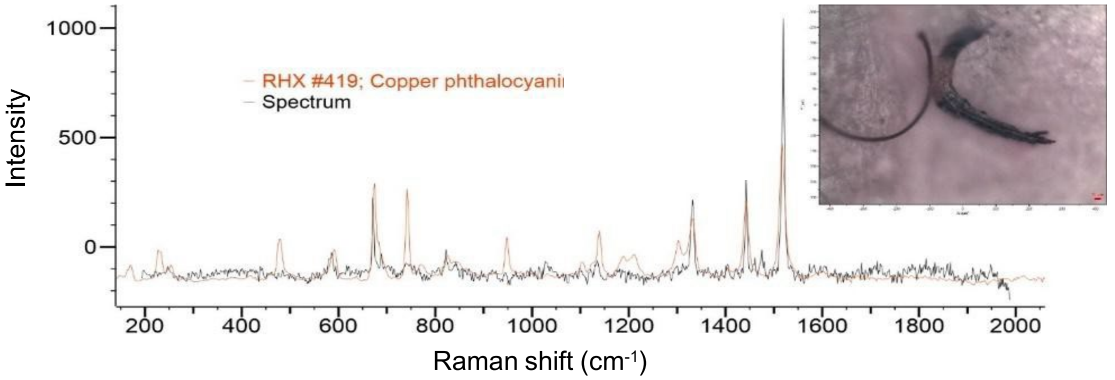

Figure 5-9: Raman micrograph, sample, and reference Raman spectra of C.I. Pigment Blue 15.

5.3.5.4 4-(4-Nitrophenylazo)resorcinol)

The red fibre in Figure 5-10 has sample spectra which were superimposable to the reference spectra of 4-(4-Nitrophenylazo)resorcinol. The spectra shared main peaks at 820.0 cm^{-1} (C-C bending), 858.4 cm^{-1} (C-H out-of-plane bending and C-C breathing mode of the benzene ring), 890.3 cm^{-1} (C-N bend), 1126.6 cm^{-1} (C=C stretch), 1339.8 cm^{-1} (N=N stretch), and 1580.6-1615.9 cm^{-1} (C=C aromatic ring stretch) all assigned to 4-(4-Nitrophenylazo)resorcinol) (Furukawa et al., 2006).

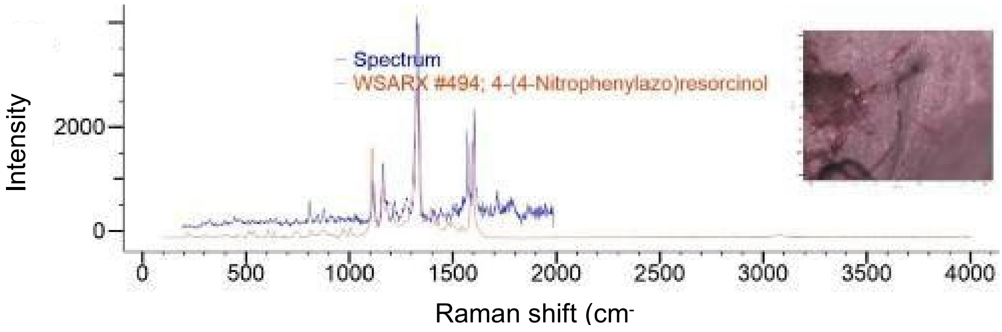

Figure 5-10: Raman micrograph, sample, and reference Raman spectra of 4-(4-Nitrophenylazo)resorcinol).

5.3.5.5 C.I Pigment Red 1

The black fibre shown in Figure 5-11 had a superimposable sample and reference spectra of C.I Pigment Red 1 which shared main peaks at 1142.5 cm^{-1} (Naphthalene C-H bend), 1339.6 cm^{-1} (N=N stretch), 1570. cm^{-1} (N-H bending and C-N stretch) and 1615.0 cm^{-1} (Naphthalene ring C=C stretch) are all assigned to C.I Pigment Red 1 (Barnes et al., 1985; Shinohara et al., 1998).

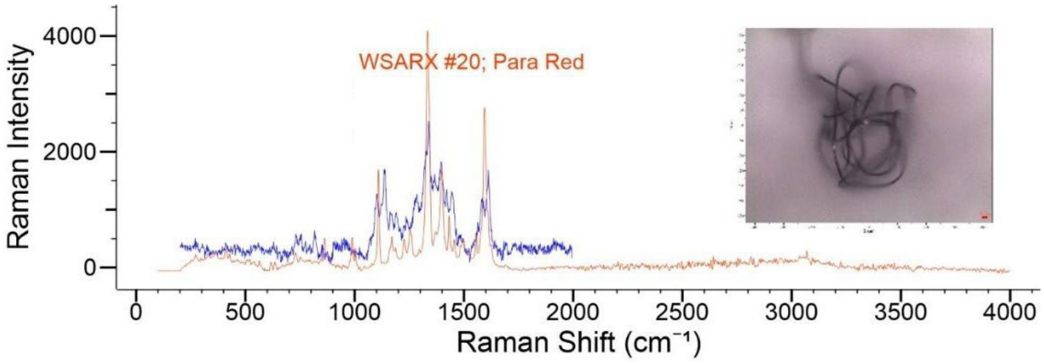

Figure 5-11: Raman micrograph, sample, and reference Raman spectra of C.I. Pigment Red 1.

5.3.5.6 C.I. Direct Yellow

The red fibre shown in Figure 5-12 had a superimposable sample and reference spectra of C.I. Direct Yellow which shared main peaks at 1146.59–1190.95 cm^{-1} (C-H bend), 1311.48 cm^{-1} (C-N stretch), 1395.37–1464.80 cm^{-1} (CH$_2$ bending and N=N stretch), and 1587.27–1623.71 cm^{-1} (N-H bending, C-N stretch, and C=C aromatic ring stretch) all assigned to C.I.Direct Yellow 12 (Barnes et al., 1985). Azo dyes account for about half of the dyes listed in the Colour Index. Azo dyes are present in various shades of colour and are used in textiles, paper, leather, rubber and foodstuffs (Fleischmann et al., 2015). Azo dyes consist of a diazotized amine coupled with an amine or a phenol and one or more azo bonds (– N═N–). The azo dyes 4-(4-Nitrophenylazo) resorcinol (C$_{12}$H$_9$N$_3$O$_4$) or Magneson I have various applications due to their stability and solubility in most solvents. Its versatility has led to its applications in textiles, printing, paper, plastics, and cosmetics.

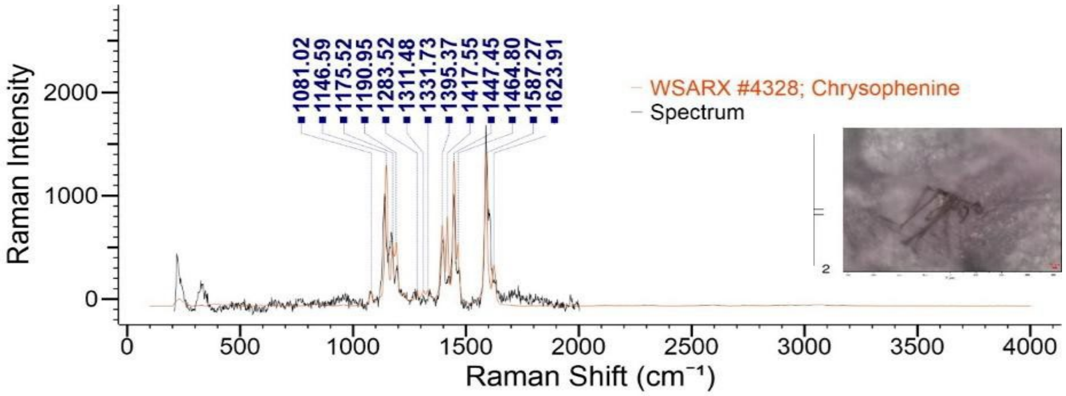

Figure 5-12: Raman micrograph, sample, and reference Raman spectra of C.I.Direct Yellow 12.

In the plastics industry, it is used as a colourant in toys, household, and packaging materials. C.I.Direct Yellow 12 is used as a colourant for textiles, plastic, and paints. It is used as a colourant for polyester, polyamide, and polyvinyl alcohol plastics. On the other hand, C.I. Pigment Red 1 is the first azo dye ever discovered and is synthesised through the diazotisation of *para*-nitroaniline followed by coupling with β-naphthol. C.I. Pigment Red 1 finds its applications as a colourant in rubber and polyethylene plastic products. It is also used in printing ink, wax, leather, and floor polishes (Singh et al., 2015; Xu et al., 2010).

5.3.6 Ecotoxicity of chemical constituents

Human exposure to PET MPs has been reported in infant meconium and adult faeces samples from New York State (Zhang et al., 2021a). Thus, we may be exposed to PET and its associated pollutants from birth and throughout the rest of our lives. C.I. Direct Yellow 12, 4-(4-Nitrophenylazo) resorcinol), and C.I. Pigment Red 1 are synthetic azo dyes which are capable of being metabolised into toxic and carcinogenic aromatic amines (e.g., 2-naphthylamine, 1-amino-2-naphthol, and 4-nitroaniline) when ingested from groundwater. Enzymatic cleavage of azo compounds to toxic amines occurs in the liver and extra-hepatic tissue via cytosolic and microsomal enzymes. Aromatic amines may be metabolically activated to DNA-binding intermediates that cause mutations and cancer. C.I. Pigment Red 1 was reported to have the potential to reduce the metabolism and cell viability of human intestinal bacteria (*Clostridium perfringens, Clostridium ramosum,* and *Clostridium indolis*) (Pan et al., 2012; Singh et al., 2015; H. Xu et al., 2010). Hence, some azo dyes are listed in Group III A1 and Group III A2 as probable human and animal carcinogens, respectively (Wakelyn, 2007; Ziarani et al., 2018). Most colourants are added to increase photostability in addition to the primary function of imparting colour. However, polymer degradation and prolonged exposure to sunlight lead to the generation of reactive oxygen species, which result in the degradation of the polymer matrix. This leads to an increased abundance of micro- and nanoplastics in groundwater aquifers (Allen, 1994; Kemp & McIntyre, 2001).

5.3.7 Comparison to similar studies

As shown in Table 5-2, the earliest report of MP contamination in groundwater was by Panno et al. (2019). The authors reported MP concentration in the 0.86–15.2 particles·ℓ$^{-1}$ range. MPs detected from Dawanshan Island's Yanshanian granite aquifer ranged from 38–64 particles·ℓ$^{-1}$ (mean: 47.5 particles·ℓ$^{-1}$) (Gong et al., 2019). Selvam et al. (2021) and Manikanda et al. (2021) investigated MPs in groundwater in the coastal areas of Tamil Nadu State, India. MPs ranged from 0.0– 4.3 particles·ℓ$^{-1}$ and 2–80 particles·ℓ$^{-1}$, respectively. Esfandiari et al. (2022) detected MPs from an unconfined alluvial aquifer in the range 0.1–1.3 particles·ℓ$^{-1}$ (mean: 0.48 particles·ℓ$^{-1}$), with sizes ≤ 500 µm. Samandra et al. (2022) investigated MPs in groundwater from an unconfined alluvial aquifer in the Bacchus Marsh in the range of 16.0–97.0 particles·ℓ$^{-1}$ (mean: 38 ± 8 particles·ℓ$^{-1}$). MPs in groundwater from the Jiaodong Peninsula, China, were in the range of 87–6832 (mean: 2103 particles·ℓ$^{-1}$) (Mu et al., 2022). Wan et al. (2022) reported MP concentrations in the range of 11–17 particles·ℓ$^{-1}$ in groundwater in an informal landfill.

In more recent studies, MP concentrations in the range of 10–34 particles·ℓ$^{-1}$ from a shallow coastal aquifer in a Northwest Mexico Coastal city. The authors reported MPs in the range of 63–1002 µm with a mean concentration of 18.3 particles·ℓ$^{-1}$ (Alvarado-Zambrano et al., 2023). Patterson et al. (2023) detected MP concentrations in the range of 9–39 particles·ℓ$^{-1}$ from a chalk and sandstone aquifer. A volcanic rock aquifer on Jeju Island, Korea, had MP concentrations in the range of 0.006–0.192 particles·ℓ$^{-1}$ with a size range of 20–100 µm (Kim et al., 2023). Ledieu et al. (2023) recorded MP concentrations in the range of 10.3–106.7 particles·ℓ$^{-1}$ (mean: 36.7 ± 43.5 particles·ℓ$^{-1}$) in Nantes, France. Gong et al. (2023) recorded concentrations of 10.3–106.7 particles·ℓ$^{-1}$ (mean: 36.7 ± 43.5 particles·ℓ$^{-1}$). Cha et al. (2024) analysed MPs during two seasons in groundwater from a Jurassic granite and alluvial aquifer in Seoul, South Korea. MP concentrations in the wet season ranged from 0.04–17.77 particles·ℓ$^{-1}$ and 0.0-0.56 particles·ℓ$^{-1}$ in the dry season. In the present study, MPs were detected in karst aquifers in the North-West and Gauteng Provinces. Microplastic concentrations ranged from 3.7 –30 particles·ℓ$^{-1}$, (mean:11.1 ± 6.9 particles·ℓ$^{-1}$). Microplastics ranged from 20–5000 µm. As can be observed from the studies cited, the majority of them have been from Asia (i.e., India, China, Iran, and South Korea). However, there were no studies found for MPs in African groundwater, which underpins the need for increased research in recording the physical-chemical properties of MPs in groundwater.

Table 5-2: Comparison of characteristics of non-alcoholic beverages.

Location	Aquifer type	Number of samples (Volume in ℓ)	Mean and median* concentration (particles·ℓ^{-1})	Concentration range (particles·ℓ^{-1})	Mean size and size range (µm)	Polymers	Shapes	Colours	Chemical parameters	Reference
Illinois, USA	Open karst aquifer	17 (2.2–2.4)	6.4*	0.00-15.2	<1500	PE	Fibre	Blue and/or clear, red & grey	Temperature, pH, SpC, DO, & ORP	(Panno et al., 2019)
Chennai, Tamil Nadu State, India	Shallow coastal aquifer	20 (1)	34 & 12	2-80	>500	Nylon, PVC, & PE	Pellets, foam, fragments, & fibres	white, black, green, red, blue, & yellow	pH and TDS	(Manikanda et al., 2021)
Tamil Nadu State, India		24 (3.13–3.78)	4.2*	0-10.1	600 ± 1400 1100–12500	PA & PE	Fibre, foam, pellet, film, fragment, & etc	Blue, White, yellow, grey, & transparent	N/A	(Selvam et al., 2021)
Shiraz, Iran	unconfined alluvial aquifer	10 (20)	0.48 0.43*	0.1-1.3	≤500	PS, PE, Nylon, PET, PP, PES, Silicon rubber, & PAMS	Fibres, fragments and films	White-transparent, blue-green, red- yellow & black-grey	N/A	(Esfandiari et al., 2022)
Victoria, Australia	Unconfined alluvial aquifer	21 (1)	38 ± 8	16.0–97.0	89 ± 55 µm, 18-491	PE, PP, PS, PA, PET, PC, PMMA, and PVC	Fragments & fibres	N/A	pH and EC	(Samandra et al., 2022)

Jiaodong Peninsula, China	N/A	5 (0.1–0.3)	2103	87–6832	44 20-471	PET, PU, PP, PC, Acrylates, PMMA Polysulfones, PAT, Alkyd Vanish, Si, PTFE, PEVA, PE, & PVA	N/A	N/A	N/A	(Mu et al., 2022)
Anshun, Guizhou Province, China	Karst aquifer	15 (2)	4.50	2.33-9.50	1–5000	PE, PS, PET, PP, PA, PVC, & etc	Film, fibre, foam, fragment, and pellet	Multicolour transparent, dark, & white	pH, TDS, EC. temperature, WV, TOC, & SP	(An et al., 2022)
Sinaloa State, Mexico	shallow unconfined coastal aquifer	18 (1)	18.3	10–34	160.5, 63–1002	PP, HEC, PVC, & LDPE	Fibres, fragments, & foams	Blue, black, transparent, & white	temperature, pH, DO, EC, TDS, & turbidity	(Alvarado-Zambrano et al., 2023)
Tuticorin, Tamil Nadu State, India	Shallow confined phreatic aquifer	15 (1)	29.7 ± 3.27	9-39	500–5000	PE, PP, PA, PS, PEU, PTFE, PES, & CP	Fibres, & fragments	Red, white, black, blue, green, white, yellow & brown	EC, pH, TDS, alkalinity, etc.	(Patterson et al., 2023)
Nantes, France	Alluvial & Landfill groundwater	8.8–10.2	36.7 ± 43.5	10.3–106.7	104, 32–2758	PE, PP, PET, PA, PS, PVC, ABS, Acr, vinyl copolymer, alkyd & PU	N/A	N/A	Temperature, EC, & pH	(Ledieu et al., 2023)

Dawanshan Island, Guangdong Province, China	Yanshanian granite	8 (2)	38–64	47.5/44.5*	500–5000	PES, PP, PET, PE, Olefin, PS, Rayon, Acr	Fibre & Film	Blue, black, transparent, white & others	pH, TDS, DO, & WV	(X. Gong et al., 2023)
Haean Basin, Seoul, South Korea	alluvial groundwater aquifer	30 (100–500)	NA	0.0–17.77	20–5000	PP, PE, PS, PET, PVC, PA, PMMA, & ABS	Fibre & fragment	N/A	temperature, ORP, TDS, EC, pH, and turbidity	(Cha et al., 2024)
Bangladesh	Groundwater wells	54 (0.5)	24.63 ± 16.13	4–75	500–5000	LDPE, HDPE, EVA, & PETE	Fibres, films, fragments, pellets	Transparent, pink, violet, blue, red, & green	NA	(Paray et al., 2024)
North-West & Gauteng Provinces, South Africa	**Unconfined & semi-confined karst aquifer**	**20 (3)**	**11.1 ± 6.9** **9.5***	**3.67–30.3**	**570 ± 570** **20-5000**	**PU, PET, & PBT**	**Fibre, fragment, pellet, & film**	**Black, blue, transparent, green, white, & others**	**pH, ORP, EC, resistivity, TDS, and salinity**	**This study**

N/A = Not available; ETC = other materials/polymers/parameters; PVC = polyvinyl chloride; PEVA = polyethylene vinyl acetate; Acr = acrylic; PA= = polyamide; PET = Poly(ethylene terephthalate); ABS = Acrylonitrile butadiene styrene; Si = Silicone; PBT = Polybutylene terephthalate; PES = polyester; PAMS = Poly(α-methyl styrene), Polytetrafluoroethylene (PTFE), polyether urethane (PEU), polyethylene chlorinated (PEC), polyacetal (PAT), polymethyl methacrylate (PMMA), acrylonitrile butadiene styrene (ABS), Polyvinyl alcohol (PVA), polyester (PES), cellophane (CP), low-density polyethylene (LDPE), hydroxyethyl cellulose (HEC), Polycarbonate (PC), PU = Polyurethane, EC= Electrical conductivity, TOC = Total organic carbon, SP = Suspended particles in water, SpC = specific conductance; WV = Water velocity, ORP = Oxidation-Reduction potential; ICC = Inorganic chemical composition, TDS = Total dissolved solids

5.4 PRINCIPAL COMPONENTS ANALYSIS AND PEARSON CORRELATION COEFFICIENT MATRIX

The first principal component (PC1) and second principal component (PC2) represented 62.57% of the total variance (Figure 5-13a). As shown in the PCA biplot, the majority of groundwater samples from each province were correlated to each other in PC1, with GP samples dominated by high negative scores and NWP samples having high positive scores. Fibres were correlated to transparent and blue colours (Pearson correlation coefficient: r = 0.91 and r = 0.93). Fibres had very high positive correlations to the 0.1–0.5 mm and 0.5–1 mm size ranges. The positive correlation between pellets and the 0.02–0.1 mm size range is consistent with their applications in cosmetic products (Figure 5-13b).

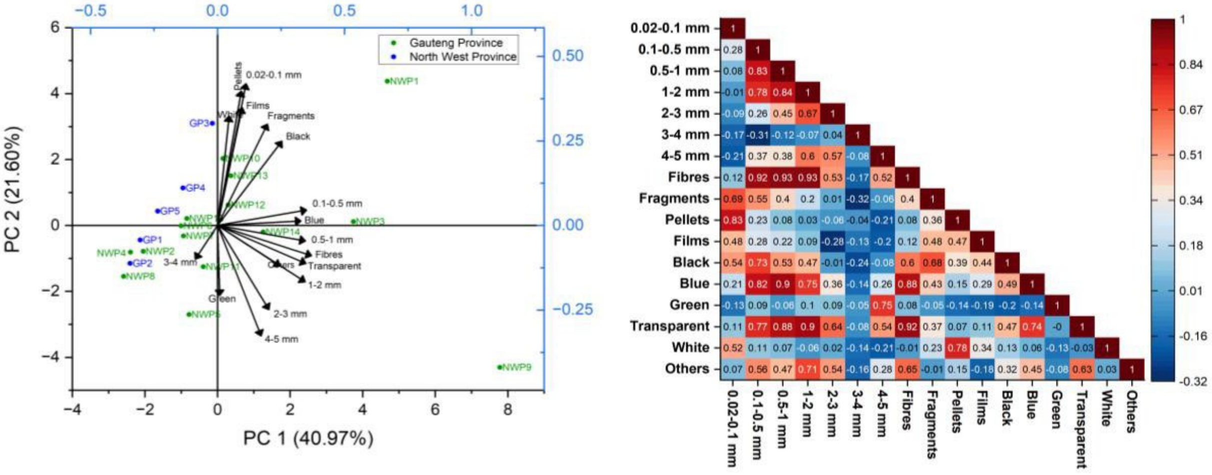

a)

b)

	0.02-0.1 mm	0.1-0.5 mm	0.5-1 mm	1-2 mm	2-3 mm	3-4 mm	4-5 mm	Fibres	Fragments	Pellets	Films	Black	Blue	Green	Transparent	White	Others
0.02-0.1 mm	1																
0.1-0.5 mm	0.28	1															
0.5-1 mm	0.08	0.83	1														
1-2 mm	-0.01	0.78	0.84	1													
2-3 mm	-0.09	0.26	0.45	0.67	1												
3-4 mm	-0.17	-0.31	-0.12	-0.07	0.04	1											
4-5 mm	-0.21	0.37	0.38	0.6	0.57	-0.08	1										
Fibres	0.12	0.92	0.93	0.93	0.53	-0.17	0.52	1									
Fragments	0.69	0.55	0.4	0.2	0.01	-0.32	-0.06	0.4	1								
Pellets	0.83	0.23	0.08	0.03	-0.06	-0.04	-0.21	0.08	0.36	1							
Films	0.48	0.28	0.22	0.09	-0.28	-0.13	-0.2	0.12	0.48	0.47	1						
Black	0.54	0.73	0.53	0.47	-0.01	-0.24	-0.08	0.6	0.68	0.39	0.44	1					
Blue	0.21	0.82	0.9	0.75	0.36	-0.14	0.26	0.88	0.43	0.15	0.29	0.49	1				
Green	-0.13	0.09	-0.06	0.1	0.09	-0.05	0.75	0.08	-0.05	-0.14	-0.19	-0.2	-0.14	1			
Transparent	0.11	0.77	0.88	0.9	0.64	-0.08	0.54	0.92	0.37	0.07	0.11	0.47	0.74	-0	1		
White	0.52	0.11	0.07	-0.06	0.02	-0.14	-0.21	-0.01	0.23	0.78	0.34	0.13	0.06	-0.13	-0.03	1	
Others	0.07	0.56	0.47	0.71	0.54	-0.16	0.28	0.65	-0.01	0.15	-0.18	0.32	0.45	-0.08	0.63	0.03	1

Figure 5-13: a) Principal component analysis biplot and b) Pearson correlation coefficient matrix.

5.5 SUMMARY

Microplastics were detected in all groundwater samples from an unconfined and semi-confined karst aquifer in the North West and Gauteng Provinces. Correlation analysis showed a low to moderate negative relationship between microplastic concentration and groundwater parameters: pH, TDS, and electrical conductivity. While previous studies have suggested high TDS may promote MP aggregation, this study observed the opposite, consistent with findings from other karst aquifer systems. Fibres were the dominant shape (78.6%), followed by fragments (11.5%), films (7.9%), and pellets (1.95%). Most particles were less than 1 mm in size, with an average size of 0.57 ± 0.57 mm. The predominant colours were black, blue, and transparent. Fibre sizes ranged from 0.05 to 4.52 mm, while other forms were generally smaller. Polymer analysis identified six types, including PET, PU, and PBT, using micro-Raman spectroscopy. Six colourants (C.I. Pigment Red 1, C.I Pigment White 6, C.I. Vat Blue 1, 4-(4- Nitrophenylazo)resorcinol, C.I.Direct Yellow 12, and C.I. Pigment Blue 15) were identified via Raman analysis in groundwater. Estimated Daily Intakes (EDIs) suggest that children ingest more MPs from groundwater than adults, especially in rural areas where untreated groundwater is consumed. All samples showed high contamination levels (MPCF > 6; MPLI > 30), indicating danger level 4 exposure risk.

6 MICROPLASTICS IN MUNICIPAL TREATED DRINKING (TAP) WATER

6.1 INTRODUCTION

This chapter provides and examines the findings on the characterisation of MPs in municipal treated drinking (tap) water.

For tap water, samples were collected between March and July 2023 from conventional taps in the Gauteng Province. Samples were collected from Tembisa and Braamfontein in Johannesburg and Silver Lakes in Pretoria. Before collection, tap water was allowed to run for one minute, followed by collection into 3ℓ pre-washed glass jars, stored in cooler boxes and taken to the laboratory for further processing (Chu et al., 2022). The pH of all tap water samples was determined using an InsMark M-log pH meter (InsMark lab instrument supplier, Shanghai, China). Their values were found to meet the minimum specifications set by SANS 241 of $5 \leq \text{pH} \leq 9.7$.

6.2 MICROPLASTICS IN TAP (MUNICIPAL TREATED DRINKING) WATER

6.2.1 MP concentrations in tap water

All tap water samples from Braamfontein, Tembisa, and Silver Lakes contained MP particles (Figure 6-1a). In total, 1236 MPs were detected with concentrations in the range of 4.7 to 31 particles·ℓ^{-1} (mean: 14 ± 5.6 particles·ℓ^{-1}). The highest concentration (range: 9.0 to 31 particles·ℓ^{-1}, mean: 18 ± 6.2 particles·ℓ^{-1}) was observed in Braamfontein samples, followed by Tembisa samples, in which 391 MPs were detected, with concentrations in the range 4.0 to 20 particles·ℓ^{-1} (mean: 13 ± 4.9 particles·ℓ^{-1}). The lowest concentrations were detected in Silver Lakes samples, ranging from 4.7 to 16 particles·ℓ^{-1} (mean: 11 ± 4.0 particles·ℓ^{-1}).

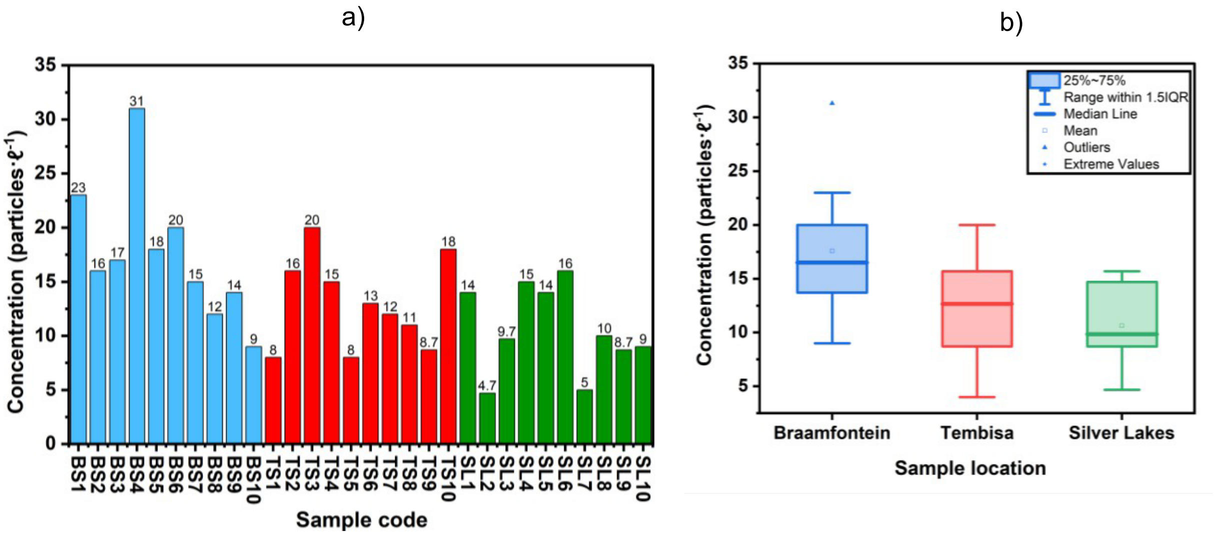
a)
b)

Figure 6-1: a) Bar graph and b) box plots showing variation in MP concentration in tap water samples.

According to the Shapiro-Wilk test for normality and Levene's test for homogeneity of variances, MP concentration data satisfied the requirements for parametric tests with $p > 0.05$ for both tests. MP concentrations in all tap water samples were normally distributed according to the Shapiro-Wilk normality test.

The One-Way ANOVA test revealed statistically significant differences between MP concentrations for the three areas Tembisa (F (2,27) = 4.827, $p < 0.05$). The Tukey post-hoc test was used for bivariant comparison. However, this increased the chance of committing a Type One error (i.e., the rejection of the null hypothesis when it is true). Hence, the Bonferroni correction was applied, and the adjusted p-value for statistical significance was set to $p = 0.016$ (Lam et al., 2020; Weideman et al., 2020). The Tukey post-hoc test revealed that concentrations of MPs in Braamfontein samples were significantly higher than those for Silver Lakes samples ($p < 0.016$). On the other hand, there was no significant difference in concentrations between the Tembisa and Braamfontein samples ($p > 0.016$) and the Tembisa and Silver Lakes samples ($p > 0.016$) (Figure 6-1b).

The findings of this study were compared to those of seventeen other studies that reported mean concentrations of MPs in tap water samples. The concentrations were found to be the tenth highest (Figure 6-2). The highest was reported in Chinese tap water, ranging from 0-1247 particles·ℓ^{-1} (mean: 440 ± 275 particles·ℓ^{-1}) (Tong et al., 2020). Mean concentrations of over 29 particles·ℓ^{-1} were reported in tap water from Brazil (Brasilia), Japan, Finland (Helsinki), Germany (Munich), and France (Paris) (Mukotaka et al., 2021; Pratesi et al., 2021). Lower MP concentrations were reported in Danish tap water (Feld et al., 2021). The first occurrence of MPs in South African tap water was reported by Bouwman et al. (2018). The authors reported MP concentrations ranging from 0.189-1.800 particles·ℓ^{-1} in Tshwane (Pretoria) and Johannesburg. A recent study by Swanepoel et al. (2023), reported MP concentrations (0.26-0.88 particles·ℓ^{-1}) in samples collected from drinking water distribution networks in Johannesburg, Mabopane, Ga-Rankuwa, and Pelindaba (Swanepoel et al., 2023). These values are much lower than those reported in this study. However, it should be emphasised that different sampling, extraction, and characterisation methods were used in these studies, which may limit the accuracy of this comparison.

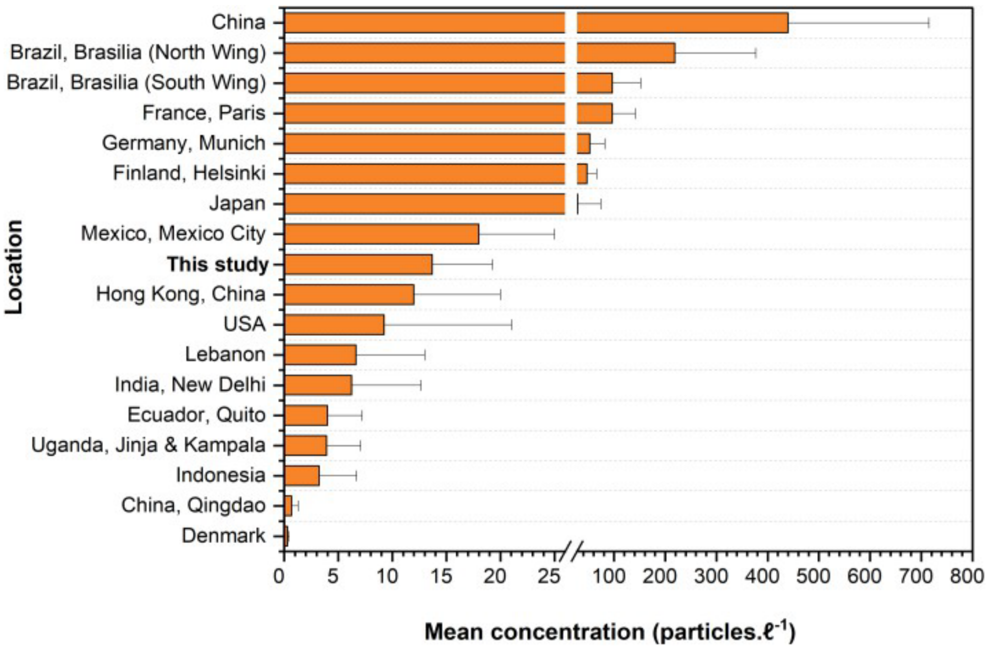

Figure 6-2: Microplastic concentrations in tap water samples from different studies. Data from: (Diaz-Basantes et al., 2020; Feld et al., 2021; Kosuth et al., 2018; Lam et al., 2020; Mukotaka et al., 2021; Pratesi et al., 2021; Shruti et al., 2020; Tong et al., 2020; Zhang et al., 2020).

6.2.2 Physical characteristics of MPs in tap water – surface morphology

Surface morphology of MPs was conducted using SEM, and the most frequently detected shapes are shown in Figure 6-3(a-d). The images showed that the surfaces of MPs were rough, cracked and porous, with some containing smaller particles pitted on the surfaces. Microplastics may be exposed to different weathering and degradation processes, which increase the surface area of MPs, resulting in increased adsorption capacity. This enhances their potential to act as vectors for chemicals and microorganisms (Amaral-Zettler et al., 2020; Liu et al., 2022b). Degraded MPs have a higher adsorption capacity and, as such, portray affinity towards pollutants. For instance, degradation introduces oxygen-containing functional groups, which increase their polarity and affinity towards hydrophilic pollutants.

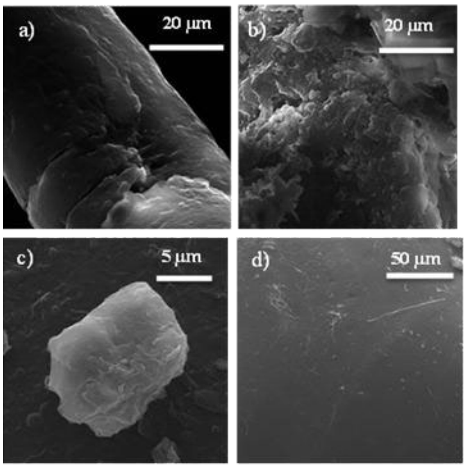

Figure 6-3: SEM images of a (a) fibre, (b) fragment, (c) pellet, and (d) film.

6.2.2.1 Braamfontein

Fibres were the most abundant shape in Braamfontein samples (86.0%, n = 453), accounting for at least 77% in each sample (Figure 6-4a). The majority of fibres were black (37.5%, n = 170), green (33.1%, n = 150), and blue (15%, n = 68). Other colours including red, brown, transparent, grey, and yellow were detected in minor proportions (14.3%, n = 65). Fifty-one fragments were detected (9.68%) in blue (43.1%, n = 22), green (19.6%, n = 10), white (13.7%, n = 7), and black (11.8%, n = 6). The remaining were a combination of transparent, red, and grey. A few pellets 13 (2.47%) were detected in blue (46.2%, n = 6), black (23.1%, n = 3), yellow (15.4%, n = 4), and green (15.4%, n = 2). Only 10 films were detected (1.9%), which showed an equal distribution of green, transparent, and white (90%, n = 3 each,), and one black film (10%, n = 1). Microplastics in Braamfontein samples were detected in five size categories, all smaller than 3 mm with a mean size of 0.49 ± 0.42 mm (Figure 6-4b). The distribution of sizes per shape showed that fibres (0.02–2.41 mm, mean of 0.55 ± 0.42 mm) > films (0.13–0.33 mm, mean of 0.24 ± 0.09 mm) > fragments (0.07–0.28, mean of 0.09 ± 0.06 mm) > pellets (0.02-0.15 mm, mean of 0.06 ± 0.03 mm). At least 80% of the particles in all samples were less than 1 mm. On the other hand, the distribution of shapes per size showed the following: 0.02-0.1 mm (12.0%) with n = 63 (33 fragments, 11 pellets, and 19 fibres). Most of the MPs (53.3%) were in the 0.1-0.5 mm size range with n = 280 (250 fibres, 18 fragments, 2 pellets, and 10 films). All 184 particles in the ranges 0.5-1 mm (24.1%, n = 127), 1-2 mm (10.3%, n = 54), and 2-3 mm (0.57%, n = 3) were fibres (Figure 6-4c).

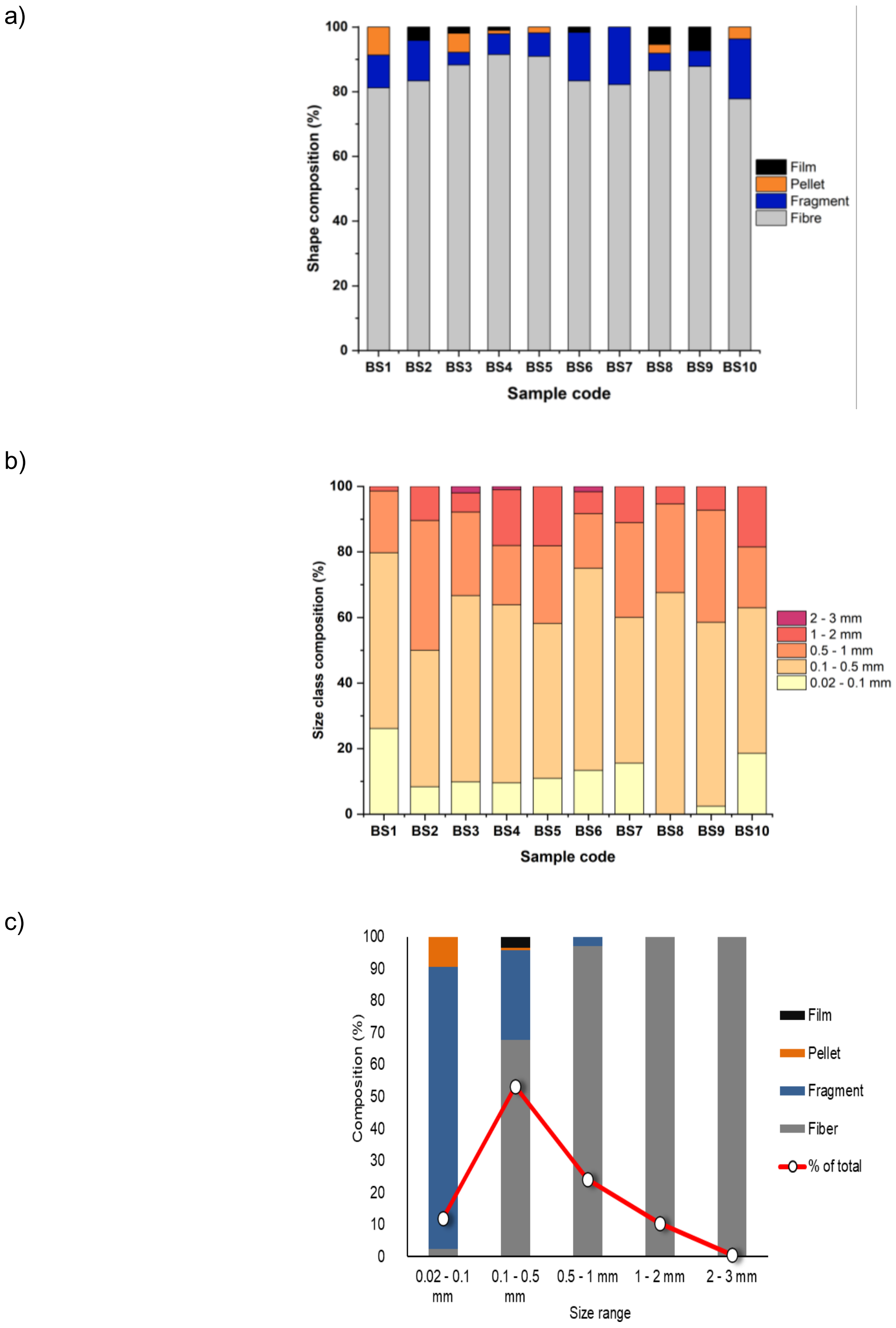

Figure 6-4: Composition of MP a) shapes and b) sizes c) shapes per size class in Braamfontein samples.

6.2.2.2 *Tembisa*

The most abundant shapes in Tembisa samples were fibres (83.6%, n = 327) and fragments (13.8%, n = 54). Films (1.5%, n = 6) and pellets (1.0%, n = 4) were present in smaller quantities. Similar to findings in Braamfontein samples, fibres represented at least 77% of all shapes in each sample (Figure 6-5a). The majority of fibres were black (33.6%, n = 110), green (28.1%, n = 92), and blue (24.5%, n = 80).

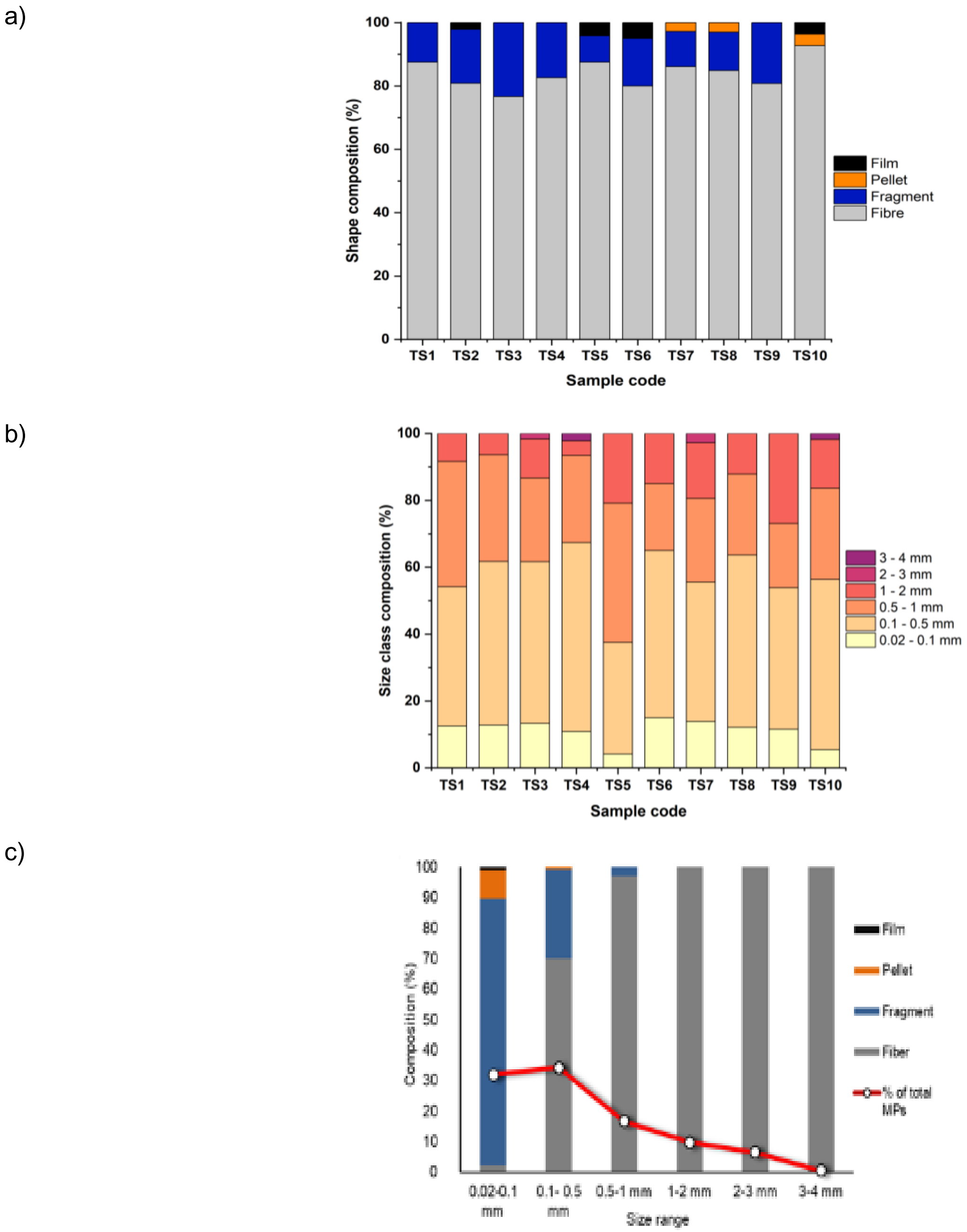

Figure 6-5: Composition of MP a) shapes and b) sizes c) shapes per size class in Tembisa samples.

Fibres of other colours (red, brown, transparent, grey, orange, yellow, purple, and white) were present in minor proportions, representing 13.7% (n = 45) altogether. A higher number of blue (33.3%, n = 18), red (31.5%, n = 17), and green (20.4%, n = 11) fragments were detected. Other colours (white, yellow, and black) only accounted for 13.0% (n = 7). Only one (1.9%) transparent fragment was detected. There was an equal distribution of green, transparent, and white films (33.3% each, n = 2). Black and blue pellets accounted for 25% (n = 2) each, and the remaining 50% (n = 2) were red pellets. Microplastics in Tembisa samples were detected in six of the seven size categories and ranged in size from 0.02-3.33 mm, with a mean of 0.55 ± 0.49 mm (Figure 6-5b). The mean size of fibres, fragments, pellets, and films were 0.62 ± 0.49 mm, 0.12 ± 0.10 mm, 0.1 ± 0.08 mm, and 0.61 ± 0.61 mm, respectively. This is similar to the distribution of sizes per shape observed in Braamfontein samples. Forty-four particles were smaller than 0.1 mm (30 fragments, 12 fibres, and 2 pellets). Almost 48% of MPs were observed in the size range of 0.1-0.5 mm (159 fibres, 23 fragments, 2 pellets, and 3 films). About 27% of MPs were detected in the range of 0.5-1 mm, accounting for 103 fibres, 1 fragment, and 2 pellets. Fifty particles were detected in the range of 1-2 mm (49 fibres and one film). Only fibres were detected in the size ranges 2-3 mm (0.51%, n = 2) and 3–4 mm (0.51%, n = 2) (Figure 6-5c).

6.2.2.3 Silver Lakes

Similar to observations in Tembisa samples, fibres (77.7%, n = 247) and fragments (15.1%, n = 48) were most abundant in samples collected from Silver Lakes, while films (6.6%, n = 21) and pellets (0.63%, n = 2) were observed in smaller quantities. Fibres represented at least 53% of all shapes in each sample (Figure 6-6a).

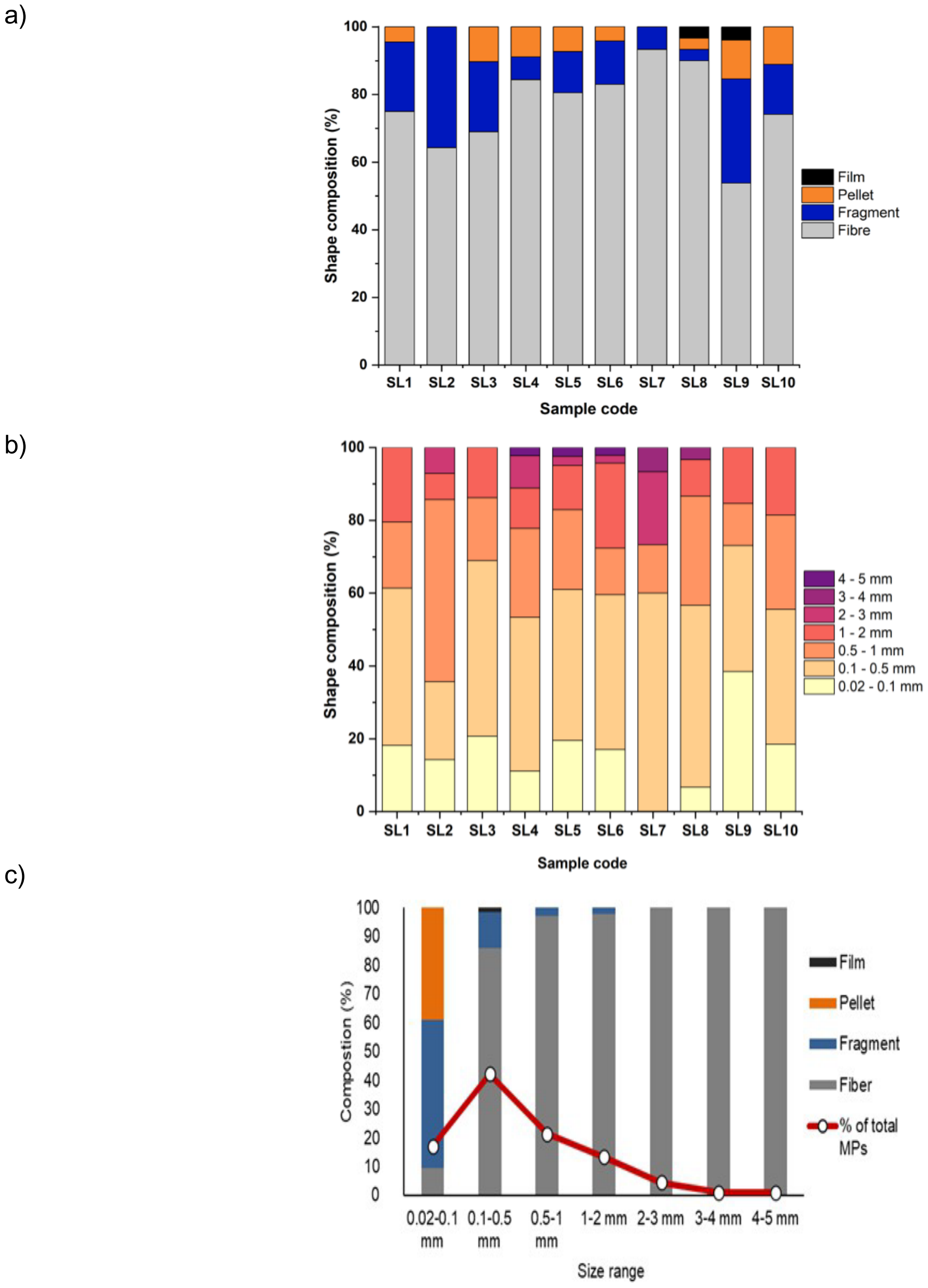

Figure 6-6: Composition of MP a) shapes and b) sizes c) shapes per size class in Silver Lakes samples.

The majority of fibres were blue (30.4%, n = 75), black (26.7%, n = 66), and transparent (17.4%, n = 43) while the rest were green (8.91%, n = 22), red (6.5%, n = 16), and other colours (brown, grey, purple, white, and yellow) that were present in smaller quantities (10.1%, n = 25). Most fragments were red (31.0%, n = 15), blue (25.0%, n = 12), and transparent (14.6%, n = 7). Some fragments were also detected in other colours (red, brown, black, green, yellow, purple, and white), a few each, altogether representing 29.1% (n = 14). Pellets were distributed as follows: blue (57.1%, n = 12), purple (19%, n = 4), transparent (14.3%, n = 3), green and white (9.5%, n = 2). Microplastics in Silver Lakes samples were detected across all seven size categories, with a minimum size of 0.02 and a maximum of 4.44 mm (mean of 0.63 ± 0.79 mm) (Figure 6-6b). Fibres ranged in size from 0.08-4.44 mm, with a mean of 0.78 ± 0.75 mm. Fragments had a mean of 0.13 ± 0.17 mm (range: 0.03-1.02 mm). Pellets ranged from 0.02-0.09 mm, with a mean of 0.05 ± 0.02 mm, and films ranged from 0.07-0.19 mm, with a mean size of 0.77 ± 0.77 mm. At least 72% of the particles in all samples were less than 1 mm. Figure 6-6c shows the distribution of shapes across the different size categories: 16.98% of MPs in the range 0.02-0.1 mm (51.9%, n = 28 fragments; 9.26%, n = 5 fibres; and 38.9%, n = 21 pellets), 134 particles in the range of 0.1-0.5 mm (42.1%). Of these, 115 (85.8%) were fibres, 17 (12.7%) fragments, and 2 (1.50%) films. There were 68 particles in the range of 0.5-1 mm (21.4%), with 66 (97.1%) fibres and 2 (2.94%) fragments. There were 42 particles in the range of 1-2 mm (13.2%) with 41 (97.6%) fibres and 1 (2.38%) fragment. Only fibres were detected in the size range 2-3 mm (4.4%, n = 14), 3-4 mm (0.94%, n = 3), and 4-5 mm (0.94%, n = 3).

6.2.3 Statistical analysis of physical characteristics of MPs

The Pearson Chi-square (χ^2) test was used to determine if the physical properties of MPs (i.e., size range, colour, and shape) differed for the three study areas. The test showed that there is a statistically significant association (i.e., similarity) amongst MP shapes, size ranges, and colours for the three areas: $\chi^2 = 28.392$, $p < 0.05$ (Braamfontein); $\chi^2 = 39.558$, $p < 0.05$ (Tembisa); and $\chi^2 = 211.383$, $p < 0.05$ (Silver Lakes). The association indicates a similarity in sources of MP pollution. To further determine correlations between sample PCA and Pearson correlation matrix were used (Figure 6-7(a-b)). PC 1 and PC 2 accounted for 51.79% of the total variance of their corresponding data set. High positive correlations (Pearson correlation coefficient: r = 0.96) were found between fibres and the 0.1–0.5 mm. Microplastics in Silver Lakes samples were more similar to Tembisa than Braamfontein since 70% of their data points were found in the same PCs.

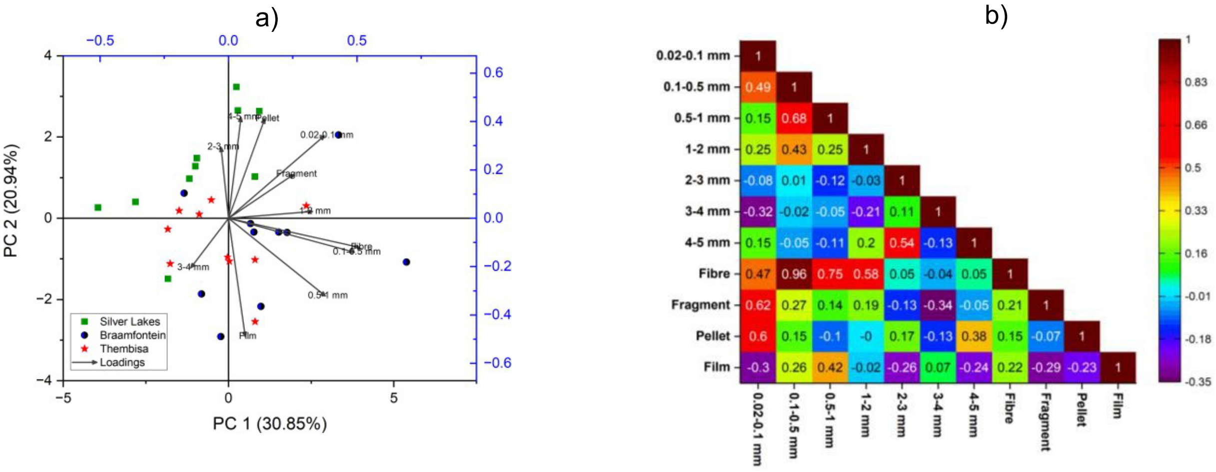

	0.02-0.1 mm	0.1-0.5 mm	0.5-1 mm	1-2 mm	2-3 mm	3-4 mm	4-5 mm	Fibre	Fragment	Pellet	Film
0.02-0.1 mm	1										
0.1-0.5 mm	0.49	1									
0.5-1 mm	0.15	0.68	1								
1-2 mm	0.25	0.43	0.25	1							
2-3 mm	-0.08	0.01	-0.12	-0.03	1						
3-4 mm	-0.32	-0.02	-0.05	-0.21	0.11	1					
4-5 mm	0.15	-0.05	-0.11	0.2	0.54	-0.13	1				
Fibre	0.47	0.96	0.75	0.58	0.05	-0.04	0.05	1			
Fragment	0.62	0.27	0.14	0.19	-0.13	-0.34	-0.05	0.21	1		
Pellet	0.6	0.15	-0.1	-0	0.17	-0.13	0.38	0.15	-0.07	1	
Film	-0.3	0.26	0.42	-0.02	-0.26	0.07	-0.24	0.22	-0.29	-0.23	1

Figure 6-7: a) PCA biplot and b) Pearson correlation coefficient matrix of MPs in tap water samples

6.2.4 Chemical characteristics – polymer types

Five polymers were identified, namely: high-density polyethylene (HDPE), polyurethane (PU), polyethylene terephthalate (PET), poly(hexamethylene terephtalamide) (PA6T), and poly(acrylamide-co-acrylic acid) (Poly(AM-co-AA) (Figure 6-8).

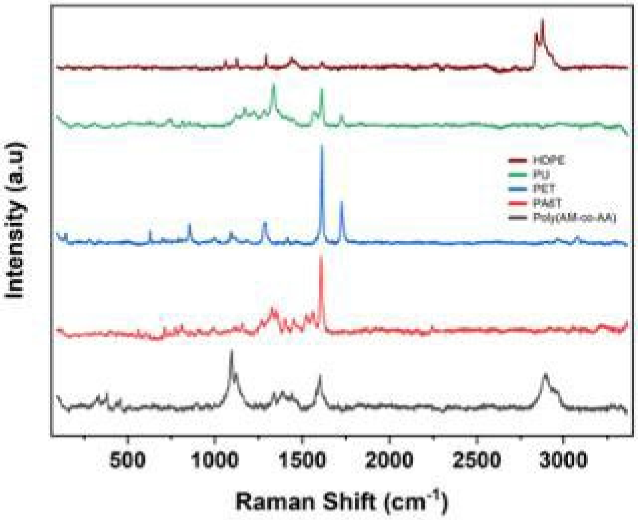

Figure 6-8: Raman spectra of detected polymers (HDPE, PU, PET, PA6T, and Poly(AM-co-AA)).

HDPE is one of the most widely produced polymers, and its applications include large containers, drums, fuel tanks, bottles, pipes, crates, and wrapping film. PET has an extraordinary blend of physical-chemical, thermal, and electrical properties, leading to its extensive use in various industries. About two-thirds of PET polymers are manufactured for the textiles industry and a quarter for the bottled water industry. The rest are used for films, geotextiles, roof insulation, and automotive parts. Other studies reported the release of PET monomers from PET polymers (Aigotti et al., 2022; Bach et al., 2013; Novotna et al., 2019).

Human exposure to PET MPs was reported in New York State infant meconium and adult faecal samples. Thus, exposure to PET and its associated additives may begin at birth. PUs are used in flexible and rigid foams, catheters, adhesives, coatings, and sealants (De Souza et al., 2021; Matías, 2022; Zhang et al., 2021a). PA6T is part of a class of high-performance engineering polyamide polymers used for automotive parts, electronics, and applications requiring high strength (such as cable ties and plastic gears). A study by Song et al. (2024) used human and murine organoids to determine the effect of PET and Nylon fibres on alveolar airways. The authors discovered that nylon inhibited the growth of developing organoids more than developed organoids in both sample types, compared to PET. Thus, inhalation of Nylon by harmful ramifications for infants (Carlsten, 2024; Song et al., 2024). Poly(AM-co-AA) and its sodium salts are extensively used in primary sewage and municipal and industrial wastewater treatment (CROW polymerdatabase, 2022). DWTPs are not designed to remove MPs, which explains the presence of these polymers in tap water. However, the presence of poly(AM-co-AA) suggests that DWTPs may also be a potential source of MPs in tap water.

6.2.5 Chemical characteristics – polymer additives

From micro-Raman spectroscopy analysis, four colourants, *viz*: C.I. Pigment Red 1, C.I. Solvent Yellow 4, potassium indigotetrasulphonate, and C.I. Pigment Black 7 were identified (Figures 6-9). These colourants have extensive applications in the synthetic polymer industry. C.I. Pigment Red 1 and C.I. Solvent Yellow 4 are azo dyes and form part of the largest group of organic dyes, which are used as colourants in polyamides, polyethylenes and antioxidants in rubber (Singh et al., 2015; Xu et al., 2010). Potassium indigotetrasulphonate

(PITS) is an aromatic dye that is chemically stable and has high heat and light stability. C.I. Pigment Black 7 is a reinforcing agent in polymers and polymer blends and is used widely by the plastic industry, ranking it second in this regard to C.I. Pigment White 6. It is stable in polymers and not considered a toxicant (Camargo et al., 2014; Chaudhuri et al., 2018; Lenz et al., 2015).

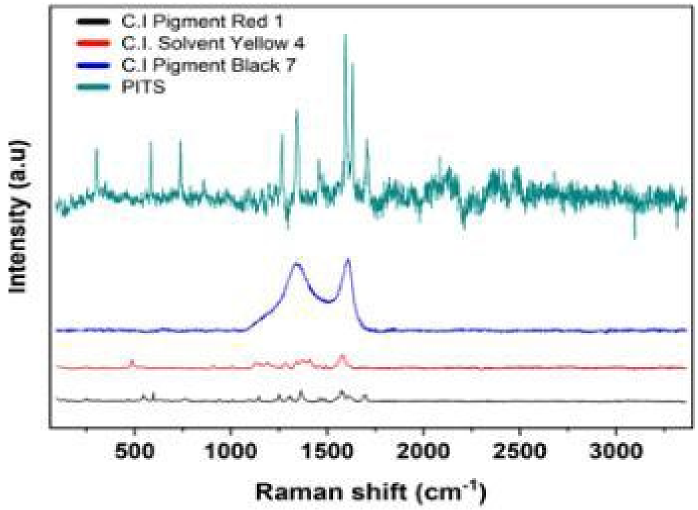

Figure 6-9: Raman spectra of detected additives (C.I Pigment Red 1, C.I. Solvent Yellow 4, C.I Pigment Black 7, and PITS).

C.I. Solvent Yellow 4 and C.I. Pigment Red 1 in the human body may be metabolised into toxic and carcinogenic aromatic amines (2-naphthylamine, 1-amino-2-naphthol, and 4-nitroaniline). Enzymatic cleavage of azo compounds to amines occurs in the liver and extra-hepatic tissue *via* cytosolic and microsomal enzymes. Aromatic amines may be metabolically activated to DNA-binding intermediates that cause mutations and cancer. C.I. Pigment Red 1 was reported to have the potential to reduce the metabolism and cell viability of human intestinal bacteria (*Clostridium perfringens, Clostridium ramosum,* and *Clostridium indolis*) (International Agency for Research on Cancer, 2010; Pan et al., 2012; Xu et al., 2010).

The presence of dyes in tap water implies they are likely to be present in wastewater, and they may cause deterioration of the quality of the treated water as they alter pH and water hardness. Additionally, non-soluble salts can cause partial or complete blockage of tubes, which may force the temporary closure of WWTPs (Camargo et al., 2014; Nunes Costa et al., 2020). Generally, most colourants are added polymers to increase photostability in addition to the primary function of imparting colour. However, polymer degradation and prolonged exposure to sunlight lead to the generation of reactive oxygen species, which degrades the polymer matrix. This leads to an increased abundance of micro-and nanoplastics in consumable liquids (Allen, 1994; Kemp & McIntyre, 2001).

6.2.6 Potential risks associated with drinking water contaminated with MPs

The EDIs of MPs from tap water in children, men, and women were found to be 1.2, 0.71, and 0.50 particles/(kg.day), respectively. These were higher than the EDIs reported by Zhou et al. (2021) for Chinese adults (0.27 particles/kg.day) and children (0.60 particles/(kg.day)). According to these estimates, South African children consume more MPs compared to women and men. Although ingestion of tap water is a source of MPs in humans, a review of the literature suggests that inhalation of airborne MPs could be a greater source of MPs. A systematic review of nano-and MPs in indoor and outdoor settings revealed an average of 5.73×10^{16} particles/(kg.day) (range: 2.73×10^{4} to 6.08×10^{17} particles/(kg.day)). Thus, 4.8×10^{18} more MP particles are inhaled from the air than are ingested from tap water.

Unfortunately, human senses cannot detect the small MP particles in tap water, and they can thus be ingested. Various sources of literature have reported MP particles in the placenta (Ragusa et al., 2021), stool (Schwabl et al., 2019), infant meconium and adult faeces (Zhang et al., 2021a), lung tissue (Amato-Lourenço et al., 2021), human blood (Leslie et al., 2022), semen and ovarian fluid (Montano et al., 2023, 2024). Drinking water in South Africa is, therefore, a potential oral exposure source of MPs. Future studies may further assess MPs in air and food samples from Gauteng and compare their intake to that of tap water.

A high number of fibres were present in tap water, a finding that is consistent with studies by Ramaremisa et al. (2022), Saad et al. (2022), and Weideman et al. (2020). In the preceding studies, high concentrations of MP fibres were reported in surface water, sediment, and fish of the Vaal River (Gauteng Province). Furthermore, Ramaremisa et al. (2022) also observed a high prevalence of green (22.3%), black (19.1%), and blue (18.3%) MPs. This is similar to the findings of this study, in which a high concentration of black (29.3%), green (23.8%), and blue (23.8%) MPs was obtained. Thus, similarities exist between MPs in tap water and surface water from the Vaal River, which forms part of the IVRS, the primary source of potable water in Gauteng. Fibrous particles were reported to be retained longer and have higher acute toxicity and mortality rates in freshwater organisms than other shapes (Eberhard et al., 2024; Gray & Weinstein, 2017; Qiao et al., 2019). Evidence suggests that fibrous MPs behave the same way in humans. Ibrahim et al. (2021) detected up to 96% of MP particles in colectomy samples from adults as fibrous. The longer retention of fibrous MPs may cause more harm as a result of additives and unreacted residual polymers leaching from them. In species with longer gut retention, like humans and fish, the leaching of chemicals might be enhanced (Eberhard et al., 2024; Ibrahim et al., 2021; Wright & Kelly, 2017).

6.3 SUMMARY

Microplastics were detected in all tap water samples from Tembisa, Braamfontein, and Silver Lakes with an average size of 0.55 ± 0.49 mm, 0.49 ± 0.42 mm, and 0.63 ± 0.79 mm, respectively. There was a high abundance of fibrous MPs, with over 77% identified in all three sampling areas, 391 particles were identified as MPs in Tembisa tap water, with an average of 39.1 ± 4.92 particles per sample. Microplastic abundances ranged from 4.00 to 20.0 particles$\cdot\ell^{-1}$, with an average abundance of 12.6 ± 4.92 particles$\cdot\ell^{-1}$. A total of 527 particles in Braamfontein tap water were identified as MPs, with an average of 52.7 ± 18.7 particles per sample. The MP abundances in Braamfontein tap water samples ranged from 9.00 to 31.3 particles$\cdot\ell^{-1}$, with a mean abundance of 17.6 ± 6.24 particles$\cdot\ell^{-1}$. A total of 318 particles were detected in Silver Lakes tap water samples, with an average of 31.8 ± 12.0 particles/sample. Silver Lakes tap water MP abundances ranged from 4.70 to 15.7 particles$\cdot\ell^{-1}$ with an average of 10.6 ± 4.02 particles$\cdot\ell^{-1}$.

In this study, small, coloured MPs were most abundant (<1 mm). This is particularly concerning because coloured MPs may contain toxic chemicals, and MPs <1 mm can pose various threats to organisms (Saad & Alamin, 2024). For instance, the desorption of toxic additives has been reported to increase with a decrease in the size of MPs and may be more pronounced in MPs less than 1 mm (Liu et al., 2020a; Luo et al., 2020). Liu et al. (2020a) reported higher leaching of cadmium-based pigment in MPs less than 0.85 mm compared to those with sizes above 0.85 mm. Consequently, the majority of MPs detected in tap water in this study have the potential to act as micro-vectors and enhance the bioavailability of plastic-derived toxicants. MPs have been reported to be retained in the digestive systems of various freshwater organisms (Saad et al., 2022; Saad & Alamin, 2024; Wright & Kelly, 2017), there is a possibility of translocation to various tissues, and organs (i.e., liver, testicles, brain, lungs, ovaries, and muscle), circulatory and lymphatic systems (Daniel et al., 2020; Eberhard et al., 2024; Montano et al., 2023, 2024).

7 MICROPLASTICS IN PACKAGED COMMERCIAL BEVERAGES

7.1 INTRODUCTION

In South Africa, in the context of the Foodstuffs, Cosmetics and Disinfectants Act, 1972 (Act No. 54 of 1972), which regulates food safety, commercially packaged beverages refer to, any non-alcoholic or alcoholic liquid intended for human consumption that is processed, packaged, sealed, and labelled for sale or distribution. In this study, samples of assorted brands of teas, bottled water (still, sparkling, and flavoured), alcoholic and non-alcoholic beverages were purchased between May and September 2023 from supermarkets in South Africa. The brands' names will be omitted for ethical reasons.

7.2 MICROPLASTICS IN PACKAGED (BOTTLED) WATER

7.2.1 Microplastic concentrations in bottled water

There was a 100% prevalence of MPs in bottled water samples; 373 particles were detected with a mean of 24.9 ± 17.0 particles/sample. Microplastic concentrations in bottled water ranged from 6.00 to 18.0 particles$\cdot\ell^{-1}$ (mean: 10.4 ± 3.76 particles$\cdot\ell^{-1}$) (Table 7-1). To understand the effects of photodegradation, assess consumer exposure risk, guide safe packaging, and inform public health regulations, microplastic concentrations in light-exposed bottled water were also assessed, and the results are shown in Table 7-2. Accordingly, MP particles were detected in all light-exposed bottled water samples, with 90 particles detected with an average of 18.0 ± 6.82 particles/sample. MP concentrations ranged from 7.33 to 18.7 particles$\cdot\ell^{-1}$ (mean: 11.5 ± 5.04 particles$\cdot\ell^{-1}$).

Table 7-1: Characteristics of bottled water samples.

Sample code	Sample type	No. of particles	Volume (ℓ)	pH	Concentration (particles$\cdot\ell^{-1}$)	Packaging
BW1	Sparkling	9	1.5	3.55	6.00	PET
BW2	Sparkling	12	1.5	3.72	8.00	Glass
BW3	Sparkling	21	1.5	2.93	14.0	PET
BW4	Still	23	1.5	6.19	15.3	Glass
BW5	Sparkling	27	1.5	4.36	18.0	PET
BW6	Still	33	5	5.6	6.60	PET
BW7	Still	46	5	5.39	9.20	PET
BW8	Still	68	5	5.17	13.6	PET
BW9	Sparkling	19	1.5	3.02	12.7	PET
BW10	Still	47	5	10.4	9.4	PET
BW11	Sparkling	16	2	2.90	8.00	PET
BW12	Sparkling	14	1.5	3.97	9.30	PET
BW13	Still	19	1.5	7.32	12.7	PET
BW14	Still	9	1.5	6.34	6.00	PET
BW15	Sparkling	10	1.5	4.28	6.70	PET

Table 7-2: The characteristics of light-exposed bottled water samples.

Sample code	Sample	No. of particles	Volume (ℓ)	pH	Concentration (particles·ℓ^{-1})	Packaging
LE1	Sparkling	12	1.5	2.97	8.00	PET
LE2	Sparkling	22	3.0	3.92	7.33	PET
LE3	Sparkling	13	1.5	3.98	8.67	PET
LE4	Sparkling	15	1.0	4.63	15.0	PET
LE5	still	28	1.5	6.58	18.7	PET

7.2.2 Variations in MP concentrations

Since there were two distinct types of bottled water (still and sparkling), statistical analysis was performed to determine whether they had distinct differences in MP concentrations. Microplastic concentrations for sparkling and still water samples were normally distributed (Shapiro-Wilk normality test, sparkling water: W = 0.845, p = 0.110 > 0.05, still water, W = 0.933, p = 0.580 > 0.05). Levene's test for homogeneity of variances failed to reject the null hypothesis of equality of variances within still and sparkling water samples (F = 0.186, *p* = 0.674 > 0.05). The parametric Independent Samples T-Test was used for bivariate comparison between sparkling and still water samples. According to the Independent Samples T-Test, there was no statistically significant difference (t_{12} = 0.187, *p* = 0.854 > 0.05) in MP concentrations between sparkling and still water samples.

Microplastic concentrations in similar brands of bottled water stored at room temperature and those exposed to sunlight for four weeks were normally distributed (Shapiro-Wilk normality test; Light-exposed bottled water: W = 0.840, p = 0.166 > 0.05, room temperature stored bottled water: W = 0.842, p = 0.170 > 0.05) (Figure 7-1). Levene's test for homogeneity of variances failed to reject the null hypothesis equality of variances within tap water samples (F = 0.184, p = 0.679 > 0.05). Therefore, the parametric Independent Samples T-test was used to test for differences in MP concentrations. Although the average concentration of light-exposed bottled water (11.5 ± 5.04) was higher than that of room-temperature stored (10.8 ± 5.49) bottled water, the Independent Sample T-Test did not prove that the differences were statistically significant (t_8 = 1.963, p = 0.825 > 0.05).

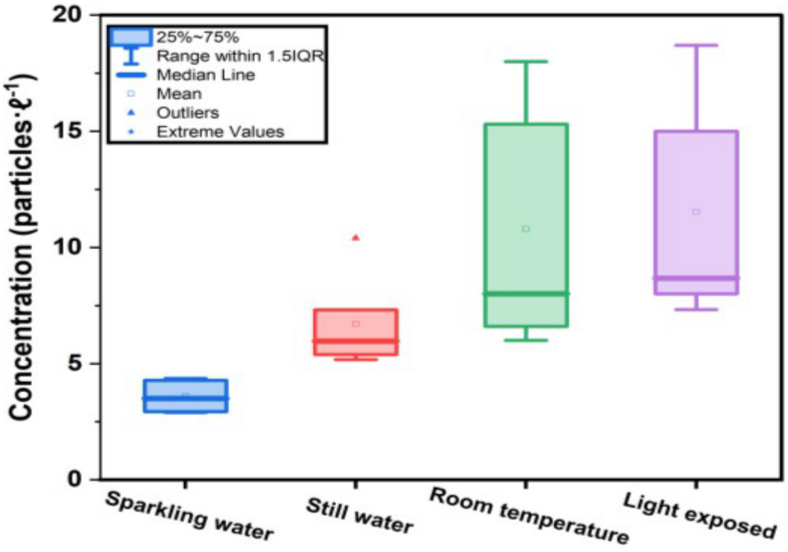

Figure 7-1: Microplastic concentration in different bottled water samples.

7.2.3 Comparison of MP concentrations to similar studies

Microplastic contamination in bottled water has been reported in several studies around the world, as shown in Figure 7-2. This study had the second lowest levels of contamination, with an average of 10.4 ± 3.76 particles·ℓ$^{-1}$ from 15 (Glass and PET) bottled water samples, with a high abundance of fibres (83.3%). MP contamination was highest (140 ± 19.0 particles·ℓ$^{-1}$) in bottled water stored in PET bottles from 10 popular brands collected from Bangkok, Thailand. However, lower levels of MPs (52 ± 4.00 particles·ℓ$^{-1}$) were reported from 3 brands of glass bottled water from the same city. Bottled water from Thailand was mostly contaminated by fibrous MPs (62.8%) (Kankanige & Babel, 2020). A study by Makhdoumi et al. (2021) reported the lowest levels (8.50 ± 10.2 particles·ℓ$^{-1}$) of MPs in 9 out of 11 brands of bottled water from Kermanshah, Iran. (Makhdoumi et al., 2021). Unlike bottled water from South Africa and Thailand, fragments (93.0%) were more abundant than fibres.

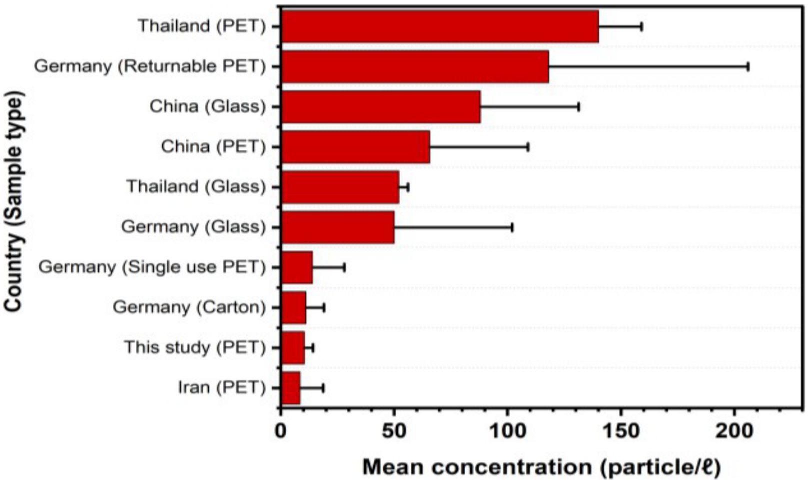

Figure 7-2: Microplastic concentration in bottled water around the world. Data from: (Kankanige & Babel, 2020; Li et al., 2023; Makhdoumi et al., 2021; Schymanski et al., 2018).

7.2.4 Polymers in bottled water samples

Three polymers were identified in bottled water samples, namely polyethylene (PE), polyethylene terephthalate (PET), and polypropylene (PP) (Figure 4.20). The presence of PET, PP, and PE is consistent with their extensive application in the South African FMCG industry, accounting for over 90% of all polymers used.

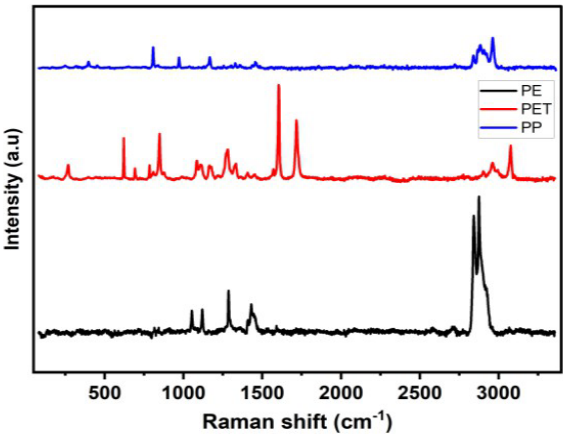

Figure 7-3: Raman spectra of polymers in bottled water samples.

7.3 MICROPLASTICS IN TEA BEVERAGES

7.3.1 Microplastic concentrations in tea

Microplastics were detected in all tea (*Camellia Sinensis* and *Aspalathus linearis*) samples;156 particles were detected with an average of 15.6 ± 5.83 particles per sample. Microplastic concentrations in tea samples ranged from 4.39 to 10.5 particles·g^{-1} (mean: 6.16 ± 2.00 particles·g^{-1}) (Table 7-3). The mean concentration for black and rooibos tea samples was 6.54 ± 2.56 and 5.78 ± 1.44 particles·g^{-1}, respectively.

Table 7-3: Characteristics of tea samples.

Sample code	Type	Count	Volume (ℓ)	Mass (g)	Concentration (particle·g^{-1})	Concentration (particles·ℓ$^{-1}$)
TB1	Rooibos	13	0.2	2.55	5.1	65
TB2	Black tea	20	0.2	2.61	7.66	100
TB3	Black tea	12	0.2	2.61	4.60	60
TB4	Rooibos	22	0.2	2.64	8.33	110
TB5	Rooibos	14	0.2	2.75	5.09	70
TB6	Black tea	28	0.2	2.67	10.5	140
TB7	Rooibos	12	0.2	2.16	5.56	60
TB8	Black tea	9	0.2	2.05	4.39	45
TB9	Rooibos	13	0.2	2.69	4.83	65
TB10	Black tea	13	0.2	2.33	5.58	65

7.3.2 Physical characteristics

7.3.2.1 Shape and colour composition

Typical MP shapes observed from tea leaves are shown in the microscopic images in Figure 7-4(a–d). As shown in Figure 7-5, the major shapes observed were fibres (58.1%, n = 233), fragments (38.7%, n = 155), and pellets (3.24%, n = 13). The majority of MPs were blue (33.3%, n = 52), black (32.1%, n = 50), and green (14.7%, n = 23). Brown, transparent, red, and white MPs accounted for 19.9% of all MPs detected.

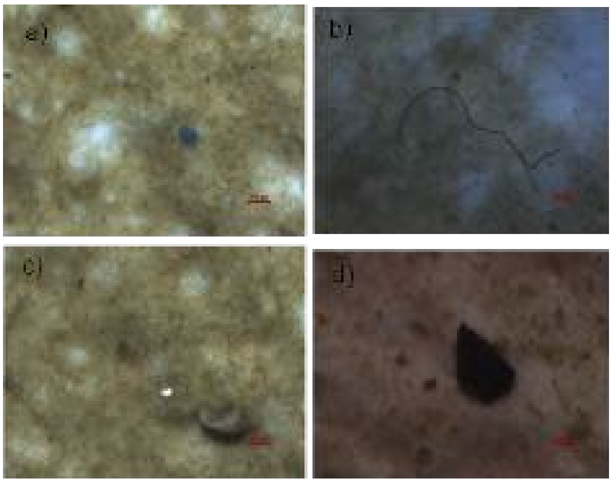

Figure 7-4: Microscopic images of MPs from tea: a) fragment b) fibres c) pellet and d) film.

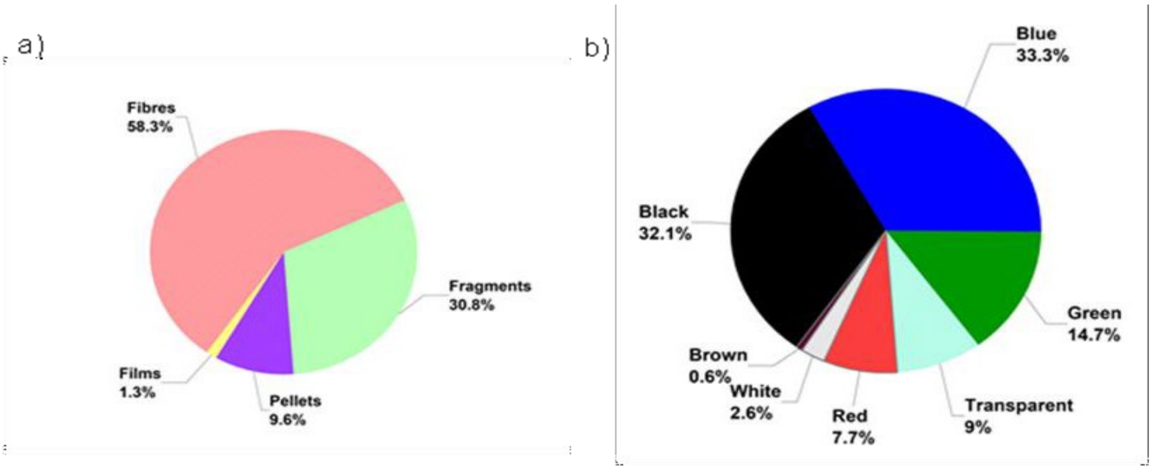

Figure 7-5: Microplastic a) shape and colour b) composition in tea samples

7.3.2.2 *Shape and size composition*

Microplastics in tea samples were distributed as follows: 0.02-0.1 mm (31.9%) with n = 128 (113 fragments, 23 pellets, and 3 fibres), 0.1-0.5 mm (34.2%) with n = 137 (96 fibres, 40 fragments, and 1 pellet), 0.5-1 mm (16.7%) with n = 67 (65 fibres and 2 fragments), 1-2 mm (9.73%, n = 39 fibres), 2-3 mm (6.48%, n = 26 fibres), 3-4 mm (0.5%, n = 2 fibres), and 4-5 mm (0.5%, n = 2 fibres). Microplastic particles in tea samples had the following size trend: 0.1-0.5 mm > 0.02-0.1 mm > 0.5-1 mm > 1-2 mm > 2-3 mm > 3-4 mm (Figure 7-6).

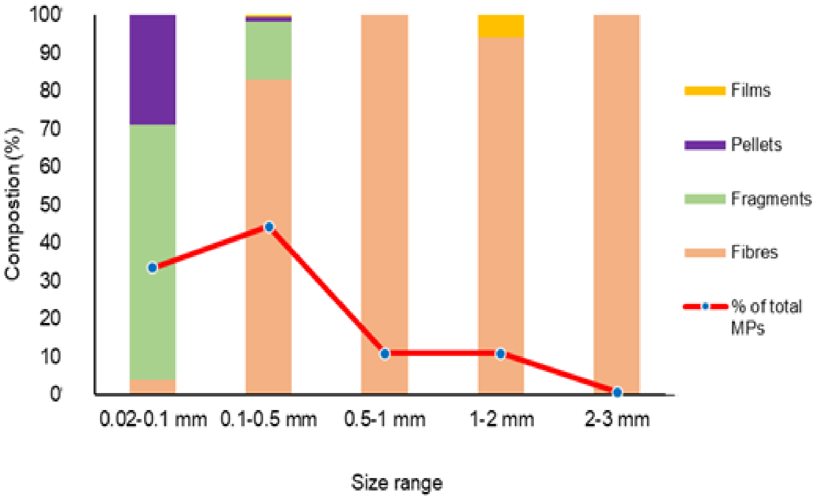

Figure 7-6: Composition of MP shapes within each size and total composition of each size range.

7.3.3 Chemical characteristics - polymers in tea leaves

Four polymers were identified in tea samples, namely polyethylene (PE), polyethylene terephthalate (PET), polypropylene (PP) and polyamide (PA) (Figure 7-7). Potential sources include FCMs used in tea bags, such as nylon, PP, PE, PP copolymers, and PET (Ali et al., 2023; Mochizuki & Matsunaga, 2016; Yurtsever, 2021). Although not detected, it is worth noting that Epichlorohydrin, which is classified as a probable human carcinogen by the United States Environmental Protection Agency (EPA), is used as a sealant in tea bags. Future studies may consider investigating the leaching of Epichlorohydrin from tea bags. Exposure to high brewing temperatures (95–100°C) may cause FCMs to break down and leach potentially toxic oligomers into tea (Ali et al., 2023; Hernandez et al., 2019; Tsochatzis et al., 2020).

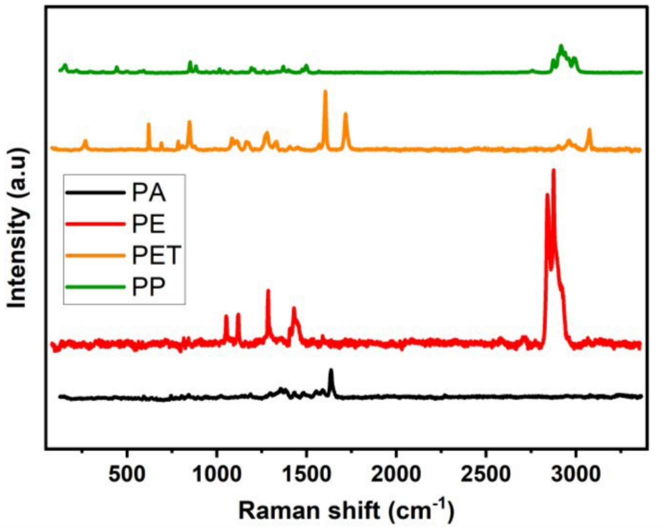

Figure 7-7: Raman spectra of MP polymers in tea leaves.

7.3.4 Comparison to similar studies

Based on the literature review, there are a handful of studies that have been conducted on tea leaves across the world and reported MP concentrations in units consistent with this study (Table 7-4). Li et al. (2022) analysed MPs in tea leaves from four types of tea (i.e., green tea, black tea, dark tea and white tea). The authors reported a median concentration in the range of 200-500 particles·g⁻¹. Xing et al. (2024) reported MP concentrations in tea leaves sampled from different stages of tea production (i.e., planting to processing and brewing) in the range of 0.07 to 3.47 particles·g⁻¹.

Table 7-4: Comparison of findings om MP occurrence in teas around the world.

Country	Tea type	MP concentration (particles·g⁻¹)	Size range (µm)	Shape	Polymer	Colours	Reference
China	Black, white, green & dark	200-500	NA	Fibres & fragments	PE & PET	NA	Li et al. (2022)
China	Oolong	0.07-3.47	<500-5000	Fiber, fragments & films	NA	Blue, transparent, black, red, & others	Xing et al. (2024)
South Africa	Black & Rooibos	4.39-10.5 (6.16 ± 2.00)	20-3000	Fibres, fragments, films, & pellets	PE, PET, PP, & PA	Black, blue, green, brown, transparent, red, & white	This study

NA = Not available; PET = Poly(ethylene terephthalate); PA = Polyamide; PP = Polypropylene; and PU = Polyurethane

The highest MP contamination was found to occur during the production stage (i.e., process rolling and enzyme activation stages). Xing and co-authors reported a high proportion of fibres (94.52%) with films and fragments comprising 4.11% and 1.37%, respectively. Furthermore, the majority of MPs detected were <0.5 mm and accounted for 33.56%. The authors further analysed MPs in the tea plantation soil and detected MPs in each sample in the range of 254–946 particles·kg^{-1}.

In this study, MP concentrations in tea samples ranged from 4.39 to 10.5 particles·g^{-1} (mean: 6.16 ± 2.00 particles·g^{-1}) with a high abundance of fibres (58.3%). Sources of MPs in tea leaves include airborne deposition during growth, withering, shredding, crushing, oxidation, and drying processes. Additional sources include degraded plastic machinery parts, plastics used in mulching, MP-coated fertilisers and compost, and irrigation water (Fard et al., 2025; Li et al., 2022; Xing et al., 2023).

7.3.5 Potential risks associated with the intake of contaminated tea

An empirical approach was also adopted to estimate the risk posed annually by local tea brands. The estimated annual intake (EAI) of MPs was calculated using equation 2, based on the assumption that a person drinks tea twice and at least once a day.

$$EAI = DU \times TP_{RSA} \times M_{avg} \times MP_{tea} \times N \quad (2)$$

Where EAI is the estimated annual intake, DU is the daily usage of teabags; TP_{RSA} is the estimated total population of RSA, which is 60,600, 000 according to Statistics South Africa; MP_{tea} is the average number of MPs in either black or rooibos teabag samples which is 6.54 and 5.78 particles per gram respectively; M_{avg} is the average mass of black and rooibos teabags which is 2.45 and 2.56 g respectively, and N number of days in a year. As shown in Table 7-5, it can be estimated that approximately 40 billion more MPs are ingested annually from drinking black tea than when drinking rooibos tea by the average tea consumer of the South African population. Moreover, a higher number of MPs are ingested by people who drink tea twice per day as opposed to once per day.

Table 7-5: Estimated annual intake from tea.

Daily usage (DU)	EAI Rooibos (particles·individual $^{-1}$ year $^{-1}$)	EAI Black tea (particles·individual $^{-1}$·year $^{-1}$)
1	327,514,590,720	354,655,485,450
2	655,029,181,440	709,310,970,900
1.5	491,271,886,080	531,983,228,175

7.4 MICROPLASTICS IN NON-ALCOHOLIC AND ALCOHOLIC BEVERAGES

7.4.1 Microplastic concentrations

Non-alcoholic and alcoholic beverage brands are abbreviated as NABB and ABB, respectively. Non-alcoholic beverages with PET and Aluminium packaging are referred to as NAB (PET) and NAB (Aluminium). Alcoholic beverages in glass and aluminium packaging are referred to as AB (Glass) and AB (Aluminium). Microplastics were detected in all 20 samples (15 brands) of NAB (PET and aluminium). NAB (PET and Aluminium) had a mean MP concentration of 9.5 ± 8.5 particles·ℓ$^{-1}$ (range: 2.0–38 particles·ℓ$^{-1}$). To assess the influence of different packaging on MP concentrations, 10 samples (5 brands) (NABB1–NABB5) were considered, which were packaged in aluminium and PET bottles. NAB (PET) concentrations ranged from 2.0– 12 particles·ℓ$^{-1}$ (mean: 5.2 ± 4.4 particles·ℓ$^{-1}$). NAB (Aluminium) concentrations ranged from 4.6 to 38 particles·ℓ$^{-1}$ (mean: 16 ± 14 particles·ℓ$^{-}$

^{1}). However, there were no statistically significant differences for the different packaging (Independent Samples T-test, $p > 0.05$). Similar to non-alcoholic beverages, MPs were detected in each of the 23 samples (15 brands) of AB (Aluminium and Glass). MP concentrations ranged from 4.0 to 29 particles·ℓ^{-1} (mean: 15 ± 7.6 particles·ℓ^{-1}). To evaluate the impact of packaging materials and processes (aluminium cans versus glass bottles) on MP concentrations, 16 samples (8 brands) (ABB1–ABB8) were considered. AB (Aluminium) and AB (Glass) had mean concentrations of 14 ± 7.1 particles·ℓ^{-1} (range: 6.1–29 particles·ℓ^{-1}) and 16 ± 7.7 particles·ℓ^{-1} (range: 7.5–29 particles·ℓ^{-1}), respectively (Appendix A). There were no statistically significant differences (Independent Samples T-test, $p > 0.05$) between AB (Aluminium) and AB (Glass).

7.4.2 EDI from beverages

Table 7-6 shows the estimated daily intakes from beverages. Children (EDI = 1.26 particles/kg.day) had higher EDIs than women (mean EDI = 0.45 particles/kg.day) and men (EDI = 0.63 particles/(kg.day)) for NAB. This is consistent with our previous study on tap water, whereby children (1.2 particles/(kg.day)) had higher EDIs than men (0.71 particles/(kg.day)) and women (0.50 particles/(kg.day)) (Ramaremisa et al., 2024). The EDIs from all NAB (men: 0.63 particles/(kg.day)) and women: 0.45 particles/kg.day) were higher than EDIs from all AB (men: 0.09 particles/(kg.day)) and women: 0.04 particles/(kg.day)). Specifically, NAB (Aluminium) had the highest EDIs (women: 0.48 particles/kg.day and men: 0.67 particles/(kg.day)) followed by NAB (PET) (women: 0.15 particles/(kg.day) and men: 0.22 particles/(kg.day)). In alcoholic beverages, AB (Glass) (women: 0.08 particles/(kg.day)) and men: particles/(kg.day)) had higher EDIs than AB (Aluminium) (women: 0.06 particles/(kg.day)) and men: 0.13 particles/kg.day)). Across all sample types, men had higher EDI than women. The EDIs from NAB in this study were higher than those reported for Turkish soft drinks (0.009 particles/(kg.day)), Spanish soft drinks (0.02 particles/kg.day)) and assorted drinks (i.e. energy drinks, Isotonic drinks, and tea) (0.003 particles/(kg.day)) (Altunışık, 2023; Socas-Hernández et al., 2024). Socas-Hernández et al. (2024) reported EDIs of 0.092 and 0.019 particles/(kg.day)) for beer and wine intake, respectively. EDIs were higher than those for South African women but lower than for men. However, socioeconomic dimensions such as lifestyle choices, race, gender, age, religion, and health disorders influence beverage intake (Vorster et al., 2013). Hence, comprehensive studies should be conducted to evaluate the influence of socioeconomic dimensions on MP ingestion through beverages.

Table 7-6: Estimated daily intakes from beverages.

EDI (particles/(kg.day))				
Sample (packaging)	**Mean concentration (particles·ℓ^{-1})**	**Children**	**Women**	**Men**
NAB (PET)	5.2	0.44	0.15	0.22
NAB (Aluminium)	16	1.34	0.48	0.67
NAB (PET and Aluminium)	15	1.26	0.45	0.63
AB (Glass)	16	N/A	0.08	0.16
AB (Aluminium)	14	N/A	0.06	0.13
AB (Glass and aluminium)	9.5	N/A	0.04	0.09

N/A = Not applicable

7.4.3 Determination of MPCF and MPLI

MPCF in non-alcoholic beverages ranged from 0.22–4.31. The contamination in non-alcoholic brands was as follows: NABB1 < NABB4 < NABB5 < NABB2 < NABB3. 70% of all non-alcoholic beverages had low contamination (MPCF<1), and 20% had moderate contamination (MPCF range: 1–3). Alcoholic beverages MPCF values ranged from 1.4–6.4, and the following trend was observed: ABB1 < ABB2 < ABB3 < ABB6 <

ABB5 < ABB8 < ABB7 < ABB4. In alcoholic beverages, 50% of the samples were moderately contaminated (MPCF range: 1–3), 37.5% were considerably contaminated (MPCF range: 3–6), and 12.5% were very highly contaminated (MPCF>6) (Figure 7-8). Non-alcoholic beverages were categorised as risk level 1 (MPLI<10). On the other hand, alcoholic beverages were categorised as danger level 4 (MPLI>30).

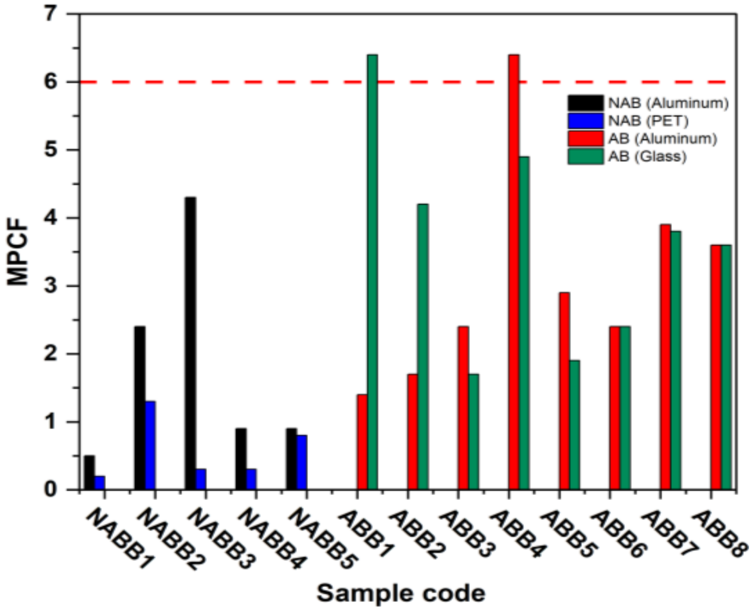

Figure 7-8: MP contamination factors in beverages.

7.4.4 Physical characteristics

Typical shapes of MP particles in beverages are shown in Figure 7-9(a-d) and Figure 7-10 (a-c) shows the composition of microplastic in beverages. Microplastic fibres were the most abundant morphotype in NAB (PET) (85%) and NAB (Aluminium) (83%). NAB (PET), fragments (10%), and pellets (5%) were present in minor proportions, and no films were detected. Fragments, pellets, and films accounted for 12%, 3.4%, and 1.4%, respectively, in NAB (Aluminium) (Figure 7-10a).

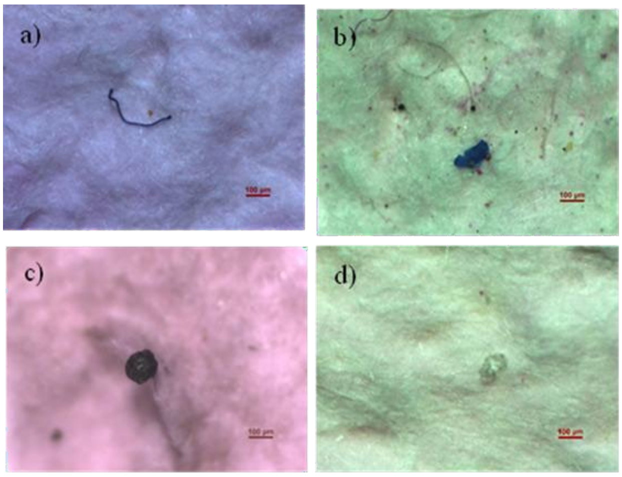

Figure 7-9: Microscopic images of a) blue fibre b) blue fragment c) black pellet, and d) transparent film.

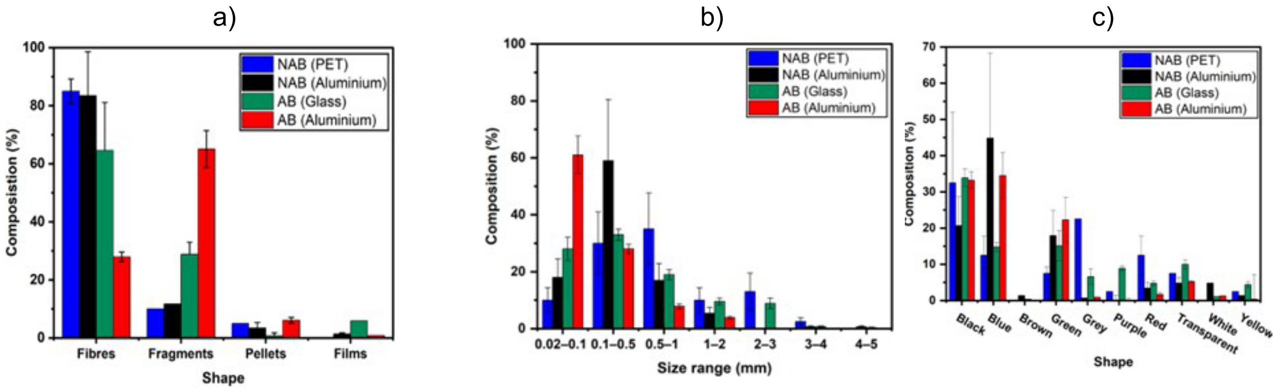

Figure 7-10: Composition of microplastic a) shapes and b) colours c) size ranges.

The majority of MPs in NAB (PET) and NAB (Aluminium) were in the 0.5–1 mm (35%) and 0.1–0.5 mm (59%) size ranges, respectively (Figure 7-10b). NAB (Aluminium) and NAB (PET) had mean sizes of 0.36 ± 0.36 mm and 0.82 ± 0.77 mm. In NAB (PET) samples, fibres, fragments, films, and pellets had mean sizes of 0.94 ± 0.79 mm, 0.09 ± 0.03 mm, and 0.05 ± 0.04 mm, respectively. Thus, MP particles in NAB (PET) had the following trend: fibres> fragments > pellets. On the other hand, fibres, fragments, films, and pellets had mean sizes of 0.41 ± 0.37 mm, 0.10 ± 0.05 mm, 0.13 ± 0.05 mm, and 0.04 ± 0.01 mm, respectively, in NAB (Aluminium). Microplastic particles in NAB (Aluminium) had the following trend: fibres > films > fragments > pellets. There was a high abundance of black (33%), grey (23%), blue (13%), and red (13%) particles in NAB (PET). NAB (Aluminium) samples had a high abundance of blue (45%), black (21%), and green (18%) particles (Figure 7-10c).

Fibres were the most abundant morphotype in AB (Glass) (65%). Fragments (29%), films (5.9%), and pellets (0.74%) were present in minor proportions. However, AB (Aluminium) had more fragments (65%). Fibres (28%), pellets (6.1%), and films (0.87%) were present in minor proportions (Figure 7-10a). The majority of MPs in AB (Glass) and AB (Aluminium) were in the 0.02–0.1 mm (61%) and 0.1–0.5 mm (33) size ranges, respectively (Figure 7-10b). AB (Glass) and AB (Aluminium) had mean sizes of 0.63 ± 0.78 mm and 0.21 ± 0.31 mm, respectively. In AB (Glass), fibres, fragments, films, and pellets had mean sizes of 0.92 ± 0.84 mm, 0.10 ± 0.09 mm, 0.13 ± 0.03 mm, and 0.07 ± 0.06 mm, respectively. In AB (Aluminium) fibres, fragments, films, and pellets had mean sizes of 0.55 ± 0.40 mm, 0.08 ± 0.07 mm, 0.09 ± 0.03 mm, and 0.05 ± 0.04 mm, respectively. Thus, MP particles in alcoholic beverages had the following trend: fibres> films > fragments > pellets. AB (Glass) had a high abundance of black (34%), green (15%), and blue (15%) particles. Similarly, AB (Aluminium) samples had a high abundance of blue (35%), black (33%), and green (22%) particles (Figure 7-10c).

7.4.5 Chemical characterisation

Six different types of polymers were detected in commercially sold beverages, namely polypropylene (PP), polyethylene (PE), polyurethane (PU), polyamide (PA), polyethylene terephthalate (PET), and polybutylene terephthalate (PBT). Polymers detected in NAB (PET) were PP (42%), PET (33%), and PE (25%). In NAB (Aluminium), PET (46%), PP (31%), PE (15%), and PU (7.7%) were detected. In AB (Aluminium) samples, the detected polymers were PP (44%), PET (33%), PA (11%), and PE (11%) while the polymers detected in AB (Glass) were PE (46%), PET (27%), PBT (18%), and PP (9.1%) (Figure 7-11a). Although there were no distinct patterns in polymer composition PP, PE, and PET were the most common polymers throughout the different samples.

a) b)

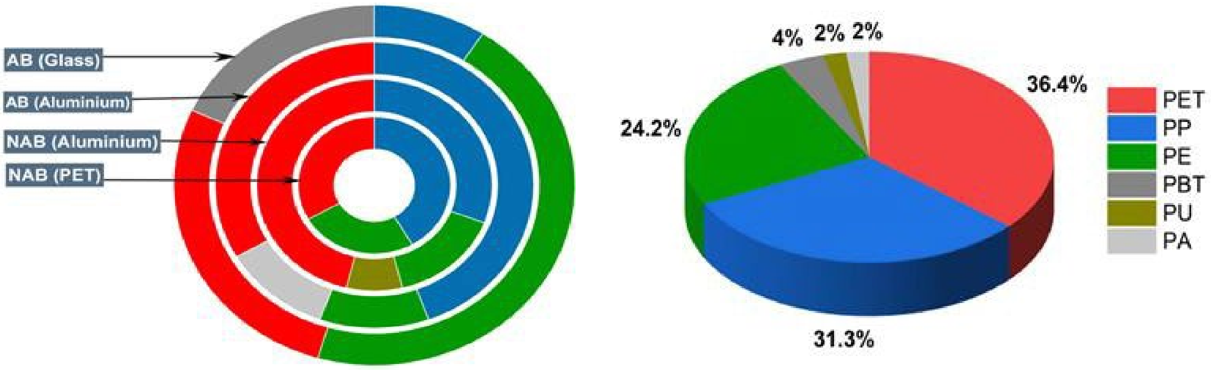

b)

Figure 7-11: a) Polymer composition in a) different sample types and b) all samples.

As shown in Figure 7-11b, there was a high abundance of PET (36.4%), PP (31.3%), and PE (24.2%) in all samples, which is consistent with their extensive application in the South African food and beverage industry accounting for 11%, 45%, and 35%, respectively. PP, PE, and PET were found in different shapes such as fibres, fragments and films. Thus, potential sources include packaging materials (i.e., bottles and caps) and freshwater sources. PBT possesses similar physical-chemical properties to PET and has numerous electrical, electronic, and mechanical applications in the FMCG industry (Sadan & De Kock, 2020; Welz et al., 2022). PU has applications as a sealant, adhesive, coating, insulator, flexible and rigid foams. Potential sources include sealants and adhesives used in packaging materials (Matías, 2022). PA has applications in automotive parts, electronics, plastic gears, and cable ties; thus, potential sources include degraded machinery parts (M. K. Gupta & Bansil, 1981; Tang et al., 2020). However, these polymers have other applications (e.g., textiles, biomedicine, and separation science) not mentioned above, and their MP products have various potential pathways into beverages.

7.4.6 Principal component analysis and Pearson correlation coefficient matrix

PC 1 and PC 2 accounted for 72.02% of the total variance of their corresponding data set (Figure 7-12a). High positive correlations (Pearson correlation coefficient: r = 0.96) were found between fibres and the 0.1–0.5 mm size range in NAB (Aluminium) 2. PC 1 and PC 2 explained 61.49% of the total variance of their corresponding data set (Figure 7-12b). Fibres had high positive correlations with the 1–2 mm and 2–3 mm (Pearson correlation coefficient: r = 0.91 and r = 0.93) size ranges. Correlations were mainly due to fibres in AB (Glass) 1 and AB (Glass) 2. Moreover, fragments had high positive correlations (Pearson correlation, r = 0.96) with 0.02–0.1 mm. Nevertheless, correlations of the physical properties of beverages from the same brand in different packaging could not be ascertained, underlining the variability in their contamination sources.

The level of MP concentration in beverages analysed in this study was as follows: NAB (Aluminium)>AB (Glass)>AB (Aluminium)>NAB (PET). Thus, the source of MPs in beverages could not be linked to specific packaging material. There are numerous possible sources of MPs in drinks, which complicates the task of identifying their origins. MPs in beverages may be introduced during processing, storage, and packaging (Altunışık, 2023; Sewwandi et al., 2023). Potential sources include municipal tap water, rainwater, and groundwater used during production (Jin et al., 2021; Lee et al., 2024). Recent evidence of MPs in South Africa's FMCG water supply chain justifies this assertion and further suggests that water treatment and beverage production facilities are not equipped to extract MPs. Weideman et al. (2020) and Dahms et al. (2022) reported a high abundance of filaments/fibres and green particles from an FMCG industry freshwater source (i.e., the Orange-Vaal River system). Swanepoel et al. (2023) reported the presence of PE, PU, and polyester in South Africa's two main drinking water treatment plants. Bouwman et al. (2018) reported the presence of fibres and fragments in Gauteng tap water samples. Furthermore, studies by Ramaremisa et al. (2022 and 2024) reported a high abundance of fibrous green, black, and blue MPs in surface water and tap water. The mean sizes of MPs were less than 1 mm, and MPs were made up of PE, PP, PU, and PET polymers. Thus, the physical-chemical properties of MPs in beverages are consistent with those from freshwater sources, distribution networks, and tap water.

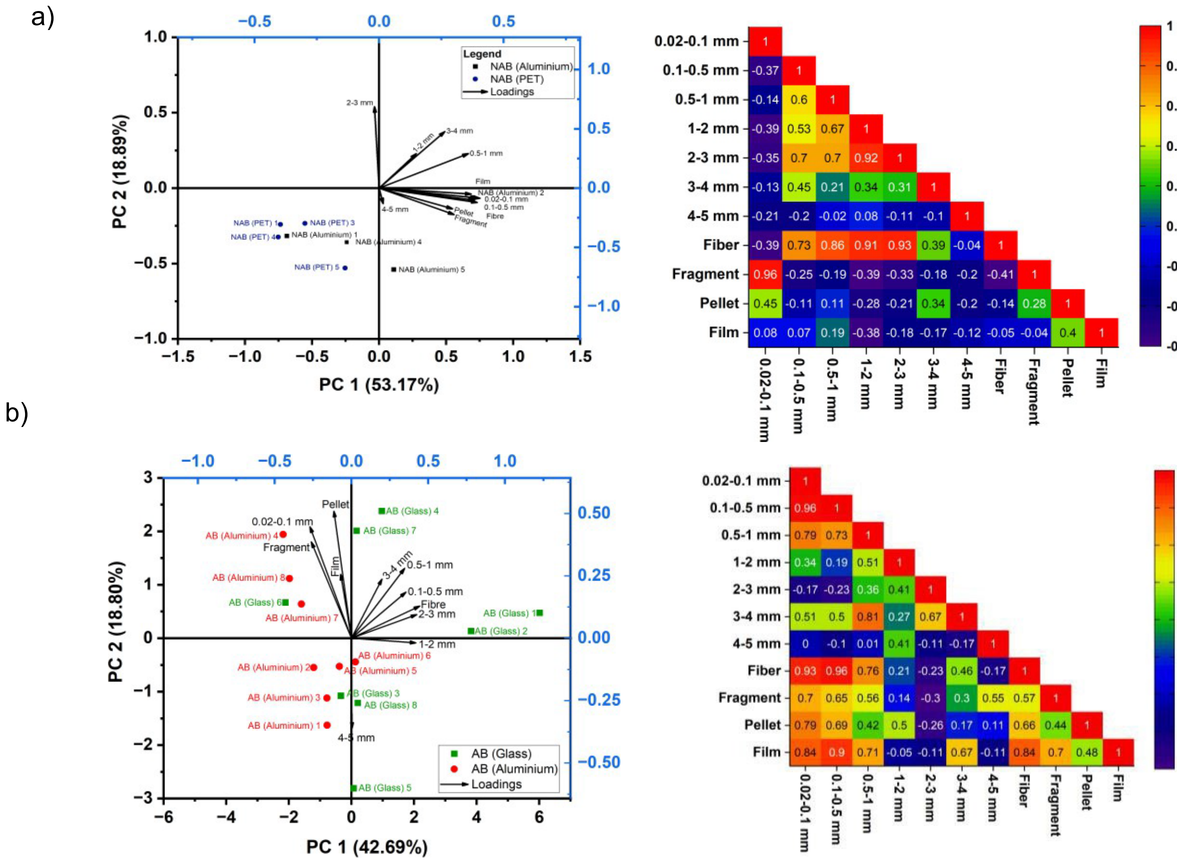

a)

	0.02-0.1 mm	0.1-0.5 mm	0.5-1 mm	1-2 mm	2-3 mm	3-4 mm	4-5 mm	Fiber	Fragment	Pellet	Film
0.02-0.1 mm	1										
0.1-0.5 mm	-0.37	1									
0.5-1 mm	-0.14	0.6	1								
1-2 mm	-0.39	0.53	0.67	1							
2-3 mm	-0.35	0.7	0.7	0.92	1						
3-4 mm	-0.13	0.45	0.21	0.34	0.31	1					
4-5 mm	-0.21	-0.2	-0.02	0.08	-0.11	-0.1	1				
Fiber	-0.39	0.73	0.86	0.91	0.93	0.39	-0.04	1			
Fragment	0.96	-0.25	-0.19	-0.39	-0.33	-0.18	-0.2	-0.41	1		
Pellet	0.45	-0.11	0.11	-0.28	-0.21	0.34	-0.2	-0.14	0.28	1	
Film	0.08	0.07	0.19	-0.38	-0.18	-0.17	-0.12	-0.05	-0.04	0.4	1

b)

	0.02-0.1 mm	0.1-0.5 mm	0.5-1 mm	1-2 mm	2-3 mm	3-4 mm	4-5 mm	Fiber	Fragment	Pellet	Film
0.02-0.1 mm	1										
0.1-0.5 mm	0.96	1									
0.5-1 mm	0.79	0.73	1								
1-2 mm	0.34	0.19	0.51	1							
2-3 mm	-0.17	-0.23	0.36	0.41	1						
3-4 mm	0.51	0.5	0.81	0.27	0.67	1					
4-5 mm	0	-0.1	0.01	0.41	-0.11	-0.17	1				
Fiber	0.93	0.96	0.76	0.21	-0.23	0.46	-0.17	1			
Fragment	0.7	0.65	0.56	0.14	-0.3	0.3	0.55	0.57	1		
Pellet	0.79	0.69	0.42	0.5	-0.26	0.17	0.11	0.66	0.44	1	
Film	0.84	0.9	0.71	-0.05	-0.11	0.67	-0.11	0.84	0.7	0.48	1

Figure 7-12: PCA biplot and Pearson correlation coefficient matrix of MPs in a) non-alcoholic and b) alcoholic beverages.

Ingredients such as grains, fruits, and vegetables used during the production of beverages may uptake MPs from soil and freshwater and release them into beverages (Chen et al., 2023; Lazăr et al., 2024). Other potential sources include MPs from workers' textiles, atmospheric MPs, and degraded plastic machinery parts. Intrinsic and extrinsic factors such as the capping system, copolymers, temperature, pH, and bottle age are also suspected to play a role in the release of MPs and NIAS (Acarer, 2023; Aigotti et al., 2022; Jin et al., 2021; Shruti et al., 2021). PCA revealed no correlations of physical properties in the same brands, which further confirmed the broad spectrum of contaminants. Around the world, there has been an increase in the number of unregulated counterfeit food and beverages (Amankwah-Amoah et al., 2022; Okorie et al., 2019). This significantly exacerbates contamination sources as unregulated beverages flood the market, making source apportionment more challenging.

Given the current global expectation that businesses operate within appropriate environmental, social, and governance (ESG) principles and ethos, the presence of MPs in beverages has significant ramifications for the FMCG sector. Moreover, there is a need to monitor the quality of these CECs in the same way that parameters such as pH, total carbohydrates and proteins, salt and sugar levels, macronutrients and micronutrients are monitored. The general environmental laws and city by-laws are still lagging in terms of the promotion of recycling plastics. This can be addressed by introducing financial penalties or incentives, reducing the extensive use of single-use and non-biodegradable plastics, and eliminating illegal dumping activities (Deme et al., 2022; Vilakati et al., 2021; Welz et al., 2022). Moreover, there should be amendments to South Africa's Foodstuff, Cosmetics and Disinfectants Act (Act 54 of 1972) to address the issue of MPs in FMCG. Alternatively, new laws specifically aimed at addressing MPs in South African food and beverages can be introduced. In the future, the FMCG industry should be mandated to utilise biodegradable plastic alternatives provided that adequate investments are made. This would greatly reduce the perpetual cycle of macro(micro)plastic pollution.

7.4.7 Comparison to similar studies

This study is one of a few that have analysed MPs in non-alcoholic beverages in the world (Table 7-7). The highest mean MP concentration (40.0 ± 24.5 particles·ℓ^{-1}) was reported by Shruti et al. (2020) for 19 soft drinks (PET and glass) from Mexico. The authors reported a high abundance of blue (62.5%), red (25%), and brown (12.5%) fibres. In the same study, the authors also reported a mean concentration of 14.0 ± 5.79 particles·ℓ^{-1} from 8 energy drinks with 93% blue fibres. A recent study from Spain reported mean concentrations of 22.5 ± 18.7 and 24.8 ± 27.3 particles·ℓ^{-1} from soft drinks and other beverages (i.e., energy drinks, isotonic drinks, and tea), respectively. Soft drinks were contaminated with blue (93%) and red (7%) fibres. A mean concentration of 32.0 ± 12.0 particles·ℓ^{-1} was reported by Diaz-Basantes et al. (2020) for 14 soft drinks (PET and Tetra Pak). Altunışık (2023) analysed MPs in the top 10 soft drink brands from Türkiye had a mean concentration of 8.9 particles·ℓ^{-1}. The author reported the presence of fibres (60%), fragments (34%), and films (6%). Pham et al. (2023) reported median concentrations of 29.3 and 2.25 particles·ℓ^{-1} in fruit drinks and soft drinks, respectively. PP and PE were the dominant polymers in fruit juices and soft drinks, respectively. This study had a mean MP concentration of 9.5 ± 8.5 particles·ℓ^{-1} in non-alcoholic beverages (PET and aluminium). The high abundance of fibres and PP, PE, and PET polymers in this study is consistent with the majority of studies considered for comparison.

Table 7-8 shows the characteristics of alcoholic beverages contaminated with MPs. Prata et al. (2020) reported an MP concentration of 183 ± 123 particles·ℓ^{-1} in 26 glass bottles of white wine from Italy. The authors reported the presence of contaminants such as insect parts, fibres, wood fragments, and minerals. Shruti et al. (2020) reported a mean concentration of 152 ± 50.97 particles·ℓ^{-1} with a high abundance of fibres (93.42%) in Mexican alcoholic beverages. Mean concentrations of 56.7 ± 73.5 and 95.2 ± 91.8 particles·ℓ^{-1} were reported in wine and beer samples in Spain, respectively (Socas-Hernández et al., 2024). In Ecuador, Diaz-Basantes et al. (2020) reported mean concentrations of 32 and 47 particles·ℓ^{-1} from glass-packaged craft and industrial beer, respectively. The authors reported the presence of fibres and fragments in various colours (red, green, violet, yellow, and blue). In one of the earliest studies to report on MPs in alcoholic beverages, Liebezeit and Liebezeit. (2014) reported a mean of 22.6 particles·ℓ^{-1} from 24 German beer brands. A median concentration of 9.00 particles·ℓ^{-1} was reported for 18 imported and domestic beer samples (Pham et al., 2023). Kosuth et al. (2018) reported low MP contamination (4.05 ± 1.76 particles·ℓ^{-1}) in 12 American beer brands, with a high abundance of fibres (98.4%). This study had a relatively low mean MP concentration (mean: 15 ± 7.6 particles·ℓ^{-1}) in alcoholic beverages. MPs were classified as fibres, fragments, pellets, and films, with a high number of them being black, blue, and green. Five polymers detected in alcoholic beverages were PP, PE, PA, PET, and PBT.

Table 7-7: Physical-chemical characteristics of MPs in non-alcoholic beverages around the world

Country	Sample & packaging material	No. samples (brands)	Mean (median *) conc. (particles·ℓ^{-1})	Shapes	Size range (µm)	Polymers	Colours	Reference
South Korea	Soft drinks (NA)	3 (1)	2.25*	NA	20–300, >300	PP, PE, PET, etc	NA	Pham et al. (2023)
Türkiye	soft drinks (PET and Tetra Pak)	30 (10)	8.9	Fragment, fibre, and film	10–1000	PA, PET, and PE	Transparent, blue, grey, green, and yellow	Altunışık, (2023)
Italy	Soft drinks (PET)	11 (11)	9.94 ± 0.33	Fibre and fragment	36–2228	NA		Crosta et al. (2023)
Mexico	Energy drinks (PET and Glass)	8 (2)	14 ± 5.79	Fibre	100–3000	PA, PEA, and ABS	Blue and red	Shruti et al. (2020)
Spain	Soft drinks (Can, Glass, and PET	15 (9)	22.5 ±18.7	Fibres, films, foams, and tangles	45–5000	Cellulosic, PES, PE, Acr, PE: Acr and PEVA	Transparent, blue, red, green, orange	Socas-Hernández et al. (2024)
Spain	Assorted drinks (Can, Glass, PET, and Brik)	13 (6)	24.8 ± 27.3	Fibres, films, tangles, and foams	45–5000	Cellulosic, PES, PE, PP, PE: Acr, PVC, POM, and PVL	Transparent, blue, black, red, grey, green	Socas-Hernández et al. (2024)
Ecuador	PET and Tetra Pak	NA	32 ± 12	Fibre and fragment	5.47–2224.25	PP, PE, and PAAm	Red, green, violet, yellow, and blue	Diaz-Basantes et al. (2020)
South Korea	Fruit drinks (NA)	3 (1)	29.3*	NA	20–300, >300	PP, PS, PET, and PA	NA	Pham et al. (2023)
Mexico	Soft drinks (PET and Glass)	19 (10)	40 ± 24.53	Fibre	100–3000	PA and PEA	Blue, red, and brown	Shruti et al. (2020)
South Africa	**Soft drinks (PET and Aluminium)**	**20 (15)**	**9.5 ± 8.5**	**Fibre, fragment, pellet, and film**	**20–5000**	**PP, PE, PU, and PET**	**Black, blue, brown, green, grey, purple, red, White and yellow**	**This study**

NA = Not available; etc = other materials; PVC = polyvinyl chloride; POM = polyacetal; PEVA = polyethylene vinyl acetate; Acr = acrylic; PE: Acr = polyethene-acrylic; PVL = polyvinyl laurate; PA= Polyamide; PET = Poly(ethylene terephthalate); PEA = Poly(ester amide); ABS = Acrylonitrile butadiene styrene; PAAm = Polyacrylamide; PP = Polypropylene; PBT = Polybutylene terephthalate; PES = polyester+ Poly(ethylene terephthalate); and PU = Polyurethane.

Table 7-8: Physical-chemical characteristics of MPs in alcoholic beverages around the world.

Country	Sample type (Packaging material)	No. of samples	Mean conc. (particles·ℓ$^{-1}$)	Shapes	Size range (µm)	Polymer types	Colours	Reference
USA	(Glass and Aluminium can)	12 (12)	4.05 ± 1.76	Fibre and fragment	100–5000	NA	Black, blue, transparent, purple, red/pink, multicolour, and brown	Kosuth et al. (2018)
South Korea	Beer (Aluminium can, Glass, and PET)	18 (NA)	9.00*	NA	20–300, >300	PP, PE, PS, PET, and etc	NA	Pham et al. (2023)
Germany	Beer (NA)	24 (24)	22.6	Fibre, fragment, and granule	36–2228	NA	Whitish, yellow, transparent, blue, black, and green	Liebezeit and Liebezeit (2014)
Ecuador	Craft beer (Glass)	7 (NA)	32	Fibre and fragment	3.505–1740.24	PP, PE, and PAAm	Red, green, violet, yellow, and blue	Diaz-Basantes et al. (2020)
Ecuador	Industrial beer (Glass)	8 (NA)	47	Fibre and fragment	5.47–2224.25	PP, PE, and PAAm	Red, green, violet, yellow, and blue	Diaz-Basantes et al. (2020)
Spain	Wine (Can, Glass, PET, and Brik)	15 (8)	56.7 ± 73.5	Fibres, films, tangles, and foams	45–5000	Cellulosic, PE, and Acr	Colourless, blue, red, black, pink, green	Socas- Hernández et al. (2024)
Spain	Beer (Can and Glass)	15 (11)	95.2 ± 91.8	Fibres, films, foams, and tangles	45–5000, > 5000	Cellulosic, PES, PE, Acr, PE: Acr, and PEVA	Colourless, blue, red, green, orange	Socas-Hernández et al. (2024)
Mexico	Beer	26 (19)	152 ± 50.97	Fibre and fragment	100–3000	PA, PES, and PET	Blue, red, brown, green and black	Shruti et al. (2020)
Italy	White wine (Glass)	26 (6) and 6 not labelled	183 ± 123	NA	7–475	PE	NA	Prata et al. (2020)
China	Spirit (PET)	6 (6)	872	Fibre and fragment	45–5000	Cellulose, PA, PET, PP, PVC, and PE.	NA	Zhou et al. (2023)
South Africa	**Beer (Glass & Aluminium can)**	**23 (15)**	**15 ± 7.6**	**Fibre, fragment, pellet, and film**	**20–5000**	**PP, PE, PA, PET, and PBT**	**Black, blue, brown, green, grey, purple, red, white, and yellow**	**This study**

NA = Not available; etc = other materials; POM = polyacetal; PEVA = polyethylene vinyl acetate; Acr = acrylic; PE:Acr = polyethylene-acrylic; PA= Polyamide; PES = Polyester; PET = Poly(ethylene terephthalate); PAAm = Polyacrylamide; PP = Polypropylene; and PBT = Polybutylene terephthalate

7.4.8 Limitations of this study

Fruit juices were excluded from this assessment due to their tendency to clog filter pores. Including fruit juice samples in the study could offer a more comprehensive view of microplastic contamination. Colourants, fillers, reinforcements, and functional additives can cause high fluorescent background interference, which can overlap polymer spectra (Lenz et al., 2015; Schymanski et al., 2018). Despite the use of countermeasures like photobleaching, some interferences persisted, which could still lead to an underestimation of the polymer composition. Moreover, the use of Rose Bengal dye, which serves to enable the exclusion of natural polymers, can result in further underestimation if natural polymers are still present on MP surfaces after digestion.

7.5 SUMMARY

In bottled water, 373 particles were detected with an average of 24.9 ± 17.0 particles/sample with a mean size of 0.61 ± 0.61 mm. Microplastic abundances in bottled water ranged from 6.00 to 18.0 particles$\cdot\ell^{-1}$ with a mean of 10.4 ± 3.76 particles$\cdot\ell^{-1}$. Similar to tap water samples, there was a high abundance of fibres (83.3%) in bottled water samples. Microplastics were detected in all non-alcoholic and alcoholic beverages. In non-alcoholic beverages, 188 particles were detected with an average of 12.5 particles per sample, and abundances ranged from 2.00 to 13.3 particles$\cdot\ell^{-1}$, with a mean abundance of 7.22 ± 4.45 particles$\cdot\ell^{-1}$. There were 391 in alcoholic beverages with an average of 27.9 ± 15.5 particles/sample, and abundances ranged from 8.60 to 29.3 particles$\cdot\ell^{-1}$, with a mean abundance of 15.9 ± 7.71 particles$\cdot\ell^{-1}$. There was a high abundance of fibrous MPs in non-alcoholic (79.3%) and alcoholic beverages (58.1%). A total of 156 particles were detected from cut tea bags, with an average of 15.6 ± 5.83 particles per tea bag. Microplastic abundances in tea samples ranged from 4.39 to 10.49 particles/g (mean: 6.2 ± 2.0 particles$\cdot g^{-1}$). The mean abundance for black and rooibos tea samples were 6.54 ± 2.56 and 5.78 ± 1.44 particles$\cdot g^{-1}$, respectively. Fibres (58.1%) and fragments (38.7%) were the most abundant morphotypes in tea bags.

The surfaces of MPs were degraded, weathered and contained different smaller materials. Degradation may enhance their potential to act as micro-vectors for other substances in domestic animals and humans. Six different polymers were identified in tap water, bottled water, and alcoholic beverages namely: High-density polyethylene (HDPE), Polyester (PES), Polyurethane (PU), Polyamide (PA), Polyethylene terephthalate (PET), Poly(hexamethylene terephtalamide)/Nylon-6T, and Poly(acrylamide-co-acrylic acid) (Poly(AM-co-AA). Additionally, five additives or colourants, namely: C.I. Pigment Red 1, C.I. Solvent Yellow 4, Potassium indigotetrasulfonate, Perylene, C.I. Direct Yellow 62, and C.I. Pigment Black 7, were identified via Raman analysis in tap water, alcoholic beverages, and non-alcoholic beverages. A review of the literature revealed that these colourants have extensive applications in the synthetic polymer industry and with a variety of potentially toxic activities in the body; some were banned carcinogens and mutagens.

8 MODELLING THE PHYSICAL-CHEMICAL BEHAVIOUR OF MICROPLASTICS

8.1 INTRODUCTION

Modelling the physico-chemical behaviour of microplastics is essential for predicting their environmental dynamics, interactions with pollutants, bioavailability, degradation, and health risks. It provides the scientific basis for management, mitigation, and policy interventions.

8.2 ADSORBENT CHARACTERIZATION

8.2.1 Stereomicroscope

The MP adsorbent had different shapes and sizes; PE and PP had elliptical shapes, PS had a cylindrical appearance, and PVA had a spherical shape (Figure 8-1(a-d)).

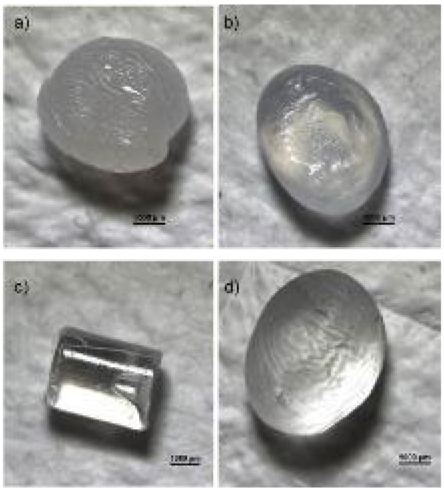

Figure 8-1: Microscopic images of a) PE, b) PP, c) PS, and d) PVA.

8.2.2 FEG-SEM and SEM-EDS

Scanning electron microscope images of the MP particles before the adsorption experiments are displayed in Figures 8-2(a-d). The surfaces of PE and PS appeared relatively smoother compared to PP and PVA. Notably, the surface of PP and PVA exhibited a rough and porous morphology, as evidenced. Conversely, the surface of PE displayed two distinct morphologies, with a smooth inner surface surrounded by a rough outer layer. Furthermore, PS featured a relatively smooth surface with minor cracks and no clear pores. These observations suggest that the rough, cracked, and porous surfaces of MP could potentially provide a high surface area for metal adsorption, as previously reported (Brennecke et al., 2016). Energy-dispersive X-ray spectroscopy (EDS) analysis of adsorbents revealed that they did not contain Pb additives before the adsorption process. Additionally, PE and PVA mainly contained carbon (C), aluminium (Al), and oxygen (O). PP adsorbents contained C, O, Al, and Si. PS had C, O, Al, S, and iron (Fe). Potential sources of these elements may include kaolin (dehydrated aluminium silicates), mica (aluminium silicates), silica (SiO_2), calcite ($CaCO_3$), wollastonite (calcium silicates), gypsum ($CaSO_4 \cdot 2H_2O$), Al_2O_3, alumina trihydrate ($Al(OH)_3$), and Fe_2O_3

compounds find applications in plastic manufacturing as inorganic pigments, electrical retardants, flame retardants, fillers, and photosensitizers. Additives in adsorbents may promote or hinder the adsorption process depending on their quantity (Godoy et al., 2019; Houssa, 2003; Murphy, 2001). Calcite and Kaolin have extensive applications in PP and PE. Wollastonite has been proposed as a healthier alternative to calcined clay and minerals used in thermoplastics and engineered resins (Houssa, 2003; Murphy, 2001).

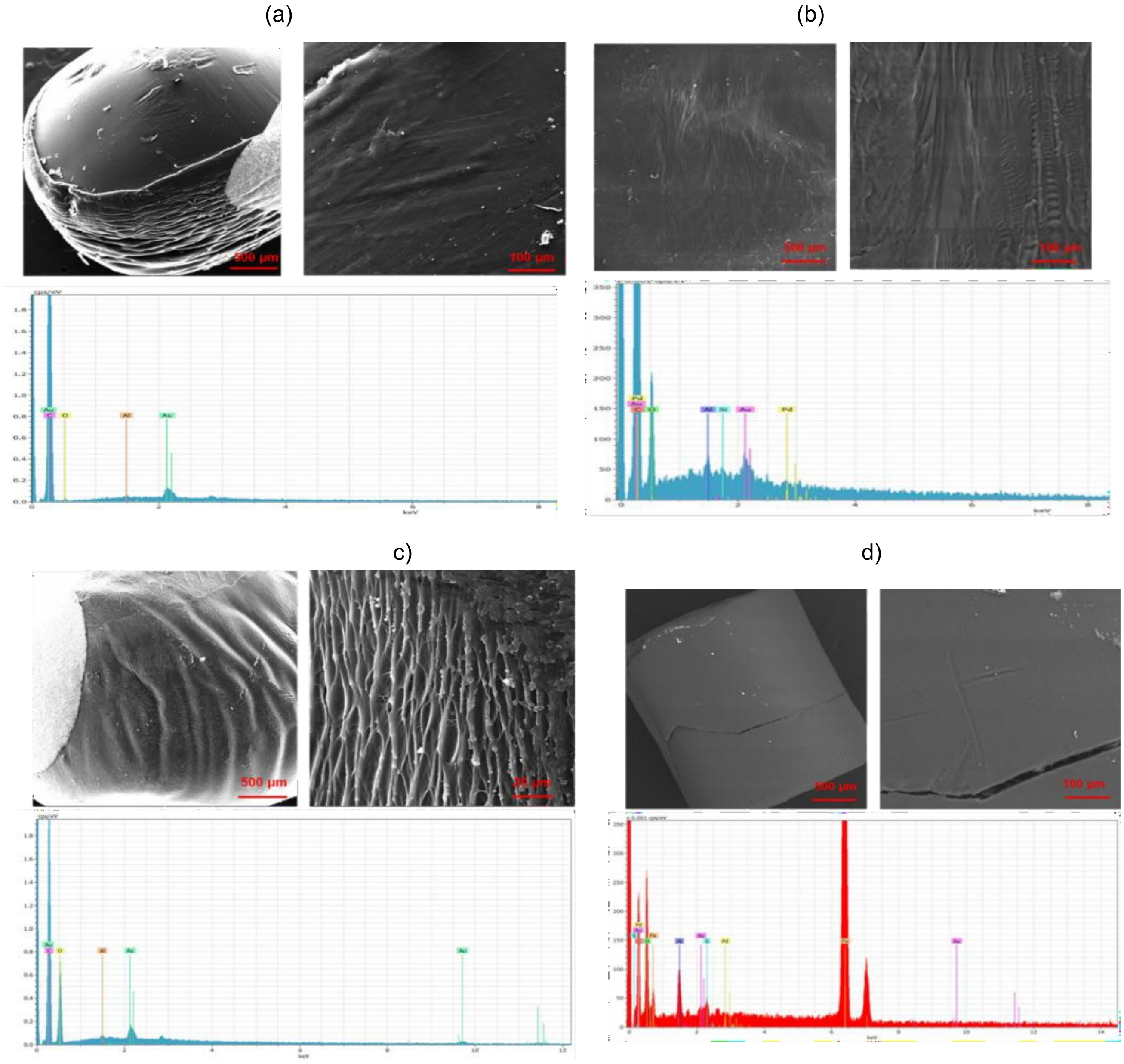

Figure 8-2: SEM images and SEM-EDS spectrum of a) PE b) PP c) PS, and d) PVA.

8.2.3 FTIR

The infrared spectra of the polymeric adsorbents are shown below (Figure 8-3(a-d)). To determine the functional groups, the resulting absorption peaks were compared to those obtained by other authors. The FTIR spectra in Figure 4.45a had characteristic PE peaks at 3396 cm^{-1} (O-H and/or N-H stretching), 3187 cm^{-1} (O-H stretch/N-H), 2915 cm^{-1} (asymmetric CH$_2$ stretching), 2845 cm^{-1} (CH$_2$ asymmetric vibration), 1646 cm^{-1}

(Amide I C=O stretching), 1468 cm^{-1} (CH_2 bending), 718 cm^{-1} (C-H out-of-plane wagging), and 653 cm^{-1} (C–H rocking) (Olayo et al., 2009; Peltzer & Simoneau, 2013; Smith, 2021). The FTIR spectra Figure 4.45b had characteristic PP peaks at 3386 cm^{-1} (O-H stretching), 2976 cm^{-1} (CH_3 asymmetric vibration), 2932 cm^{-1} (asymmetric CH_2 stretching), 2871 cm^{-1} (CH_3 asymmetric vibration), 1608 cm^{-1} (C-C stretching), 1471 cm^{-1} (C-H (-CH_3)) asymmetric deformation), 1402 cm^{-1} (C-H (CH_3)) asymmetric deformation), 1128 cm^{-1} (C-H wagging and CH_3 rocking), 1018 cm^{-1} (CH_3 rocking and C-C stretching), 948 cm^{-1} (C-H out-of-plane vibration), 815 cm^{-1} (C–C stretching), and 663 cm^{-1} (C–H rocking) (Fang et al., 2012). The FTIR spectra in Figure 4.45c had characteristic PS peaks at 3386 cm^{-1} (O-H stretching), 2941 cm^{-1} (asymmetric CH_2 stretching), 2868 cm^{-1} (symmetric CH_2 stretching), 1605 cm^{-1} (C=C aromatic ring stretching), 1492 cm^{-1} (C=C aromatic ring stretching), 1451 cm^{-1} (C=C aromatic ring stretching), 1404 cm^{-1} (CH_2 bending and C=C stretching), 1036 cm^{-1} (C-O stretching), 902 cm^{-1} (C-C stretching), 754 cm^{-1} (C-H aromatic ring out-of-plane bending), 690 cm^{-1} (C-H aromatic ring out-of-plane bending), 539 cm^{-1} (Fe). Peaks at 754 and 690 due to C-H out-of-plane bending vibration indicate the presence of a mono-substituted benzene ring (Al-Kadhemy et al., 2016; Godoy et al., 2019; Peltzer & Simoneau, 2013; Twinkle et al., 2019). The FTIR spectra in Figure 4.45d had characteristic PVA peaks at 3378 cm^{-1} (O-H stretching), 2924 cm^{-1} (asymmetric CH_2 stretching), 2898 cm^{-1} (symmetric CH_2 stretching), 1597 cm^{-1} (asymmetrical vibration of the group O=C-O group), 1405 cm^{-1} (CH_2 bending and asymmetrical vibration of the O=C-O group), 1306 cm^{-1} (O-H stretching), 1097 cm^{-1} (C–C–C and CH_2 vibration), 1024 cm^{-1} (C–O–C stretching), 818 cm^{-1} (C-C stretching) (Estrada-Villegas et al., 2020; Jipa et al., 2012).

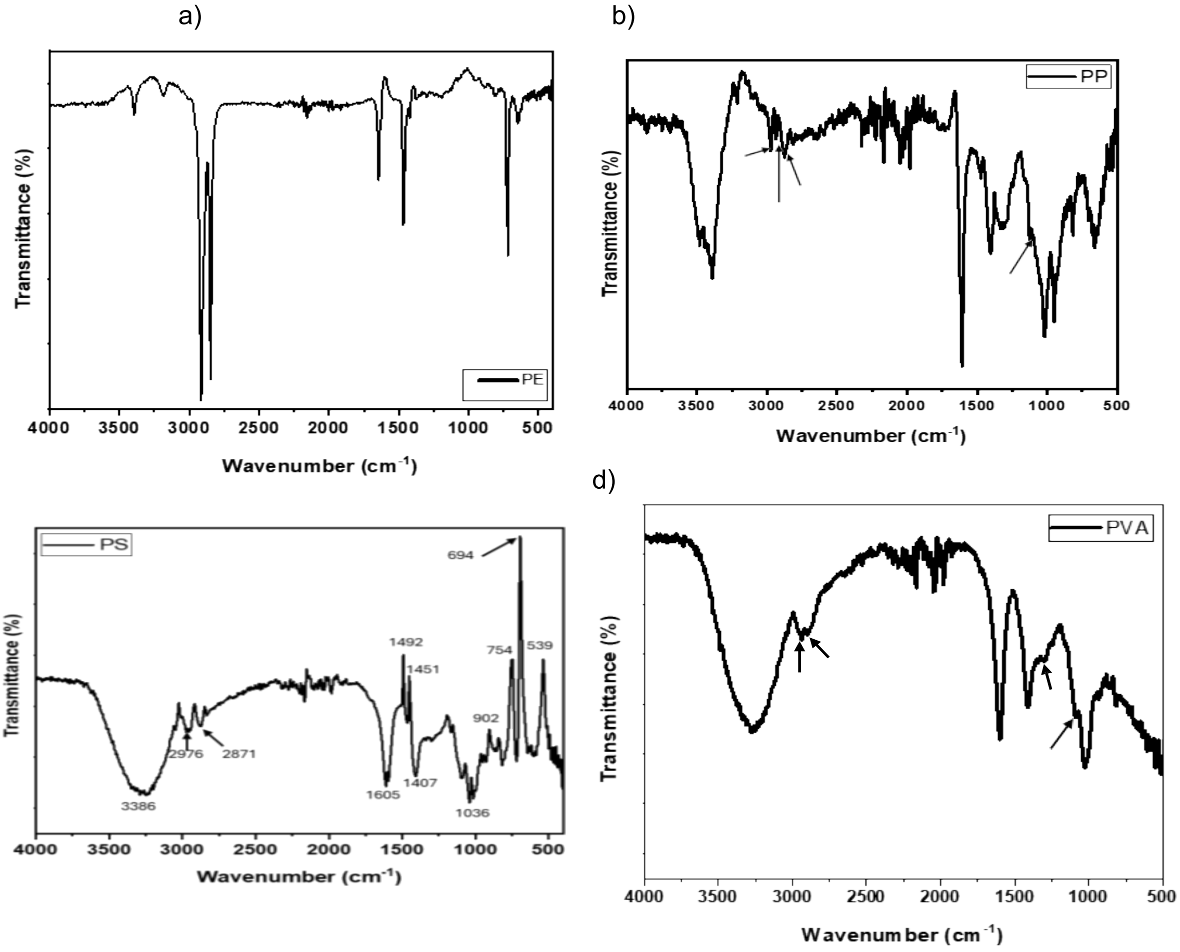

Figure 8-3: FTIR spectra of a) PE b) PP, c) PS, and d) PVA.

8.2.4 Point of zero charge

The point of zero charge (pHpzc) was obtained through titration. Mixtures of 17 $g \cdot \ell^{-1}$ of adsorbent dosage 0.01 $mol \cdot \ell^{-1}$ NaCℓ, were adjusted pH 2 to 9 using 0.01 $mol \cdot \ell^{-1}$ HNO_3 and NaOH. The mixtures were then agitated to achieve equilibrium, and the pHpzc was determined from the graph of ΔpH and initial pH. The pHpzc value represents the point at which the ΔpH vs $pH_{initial}$ curve intersects the line ΔpH = 0 (Adam, 2016; Godoy et al., 2019). As shown in Figure 8-4(a-d), the pHpzc of the different adsorbents was found to be pH_{PZC}(PE) = 4.2, pH_{PZC}(PP) = 6.7, pH_{PZC}(PS) = 2.4, and pH_{PZC}(PVA) = 3.3. Hence, the adsorbents were negatively charged beyond their respective pH_{PZC} and positively charged below their pH_{PZC}.

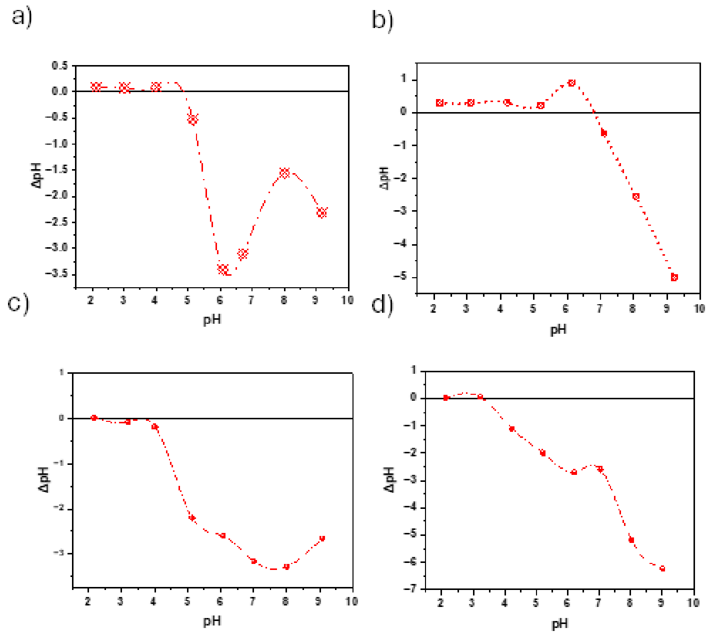

Figure 8-4: ΔpH as a function of pH for a) PE b) PP c) PS and d) PVA.

8.3 INVESTIGATION OF ADSORPTION EFFICIENCY

8.3.1 Effect of pH

The adsorption capacity of adsorbents can depend on the solution's pH, making it important to understand the effect of varying pH on Pb sorption in this instance. To this end, 5 $mg \cdot \ell^{-1}$ of 0.015 ℓ Lead solutions were added to glass containers after adjusting pH (2–9) with 0.01 $mol \cdot \ell^{-1}$ solutions of NaOH and HNO_3. Adsorbent masses of PE = 16.5 $g \cdot \ell^{-1}$, PP = 7.50 $g \cdot \ell^{-1}$, PS = 17.3 $g \cdot \ell^{-1}$, and PVA = 20 $g \cdot \ell^{-1}$ were added and shaken at room temperature at 150 rpm for 48 hours. Two control tests were conducted. One blank was prepared by placing MPs in the MQW (without metals) to check if MPs did not release the metals being studied. The second control was prepared by placing 5 $mg \cdot \ell^{-1}$ of Pb(II) in glass containers without MPs (Godoy et al., 2019; Mosai, 2021). The contents were filtered, and the Pb(II) concentration was analysed with ICP-OES. The adsorption capacity and efficiency were calculated using Equations 17 and 18. As predicted, the solution's initial pH was a significant factor in the adsorption process of Pb onto MPs since the process is primarily mediated by favourable interactions between oppositely charged sorbents and sorbates (Chang et al., 2023; National Academies of Sciences, Engineering, and Medicine, 2017; Oliveira et al., 2019; Zhao et al., 2024). PP and PVA had relatively higher adsorption capacities than PS and PE, which could be in part due to the relatively rough and porous surfaces of the former as opposed to the smooth and slippery surfaces of the latter, as shown in FEG-SEM images. Moreover, PS had an intense Fe peak which may decrease the adsorption capacity of the PS adsorbent (Godoy et al., 2019; Murphy, 2001). Although the highest adsorption efficiencies were observed at pH = 8 and 9 for PE, PP, PS and PVA, these were not considered the optimal pH for adsorption due to the propensity of Pb hydroxide precipitation at pH > 8. Hence, most of the Pb species could be eliminated by precipitation on the adsorbent surface rather than by adsorption. Thus, the optimal pH values for PE, PP, PS, and PVA were 7, 7, 6, and 7, respectively (Figure 8-5(a-d)).

The observed phenomena can be understood from electrostatic and surface complexation interactions between the absorbent and adsorbate. Below their isoelectric points in the acidic region, the surface charge of adsorbents is positively charged. In the acidic region, there are more H^+/H_3O^+ ions surrounding the surface of the MP adsorbents. The H^+/H_3O^+ ions repel Pb, thus, there are fewer Pb(II) ions adsorbed, while at higher pH values, the surface of the adsorbents is negatively charged and electrostatic interactions with Pb increase the number of ions adsorbed. At a pH higher than the pH_{PZC}, the key functional groups would be the acetate (CH_3COO^-) groups (i.e., PVA), especially if the adsorption is driven by the electrostatic attraction and surface complexation with the Pb(II) ions. The surfaces of MP are deprotonated, and there is an increase in negative active sites with increasing pH, which makes it easier for the Pb^{2+} ions to form complexes. Pb sorption by MPs may be primarily influenced by electrostatic adsorption and ionic exchange (Liu et al., 2022a; Tang et al., 2020; Wang et al., 2019a).

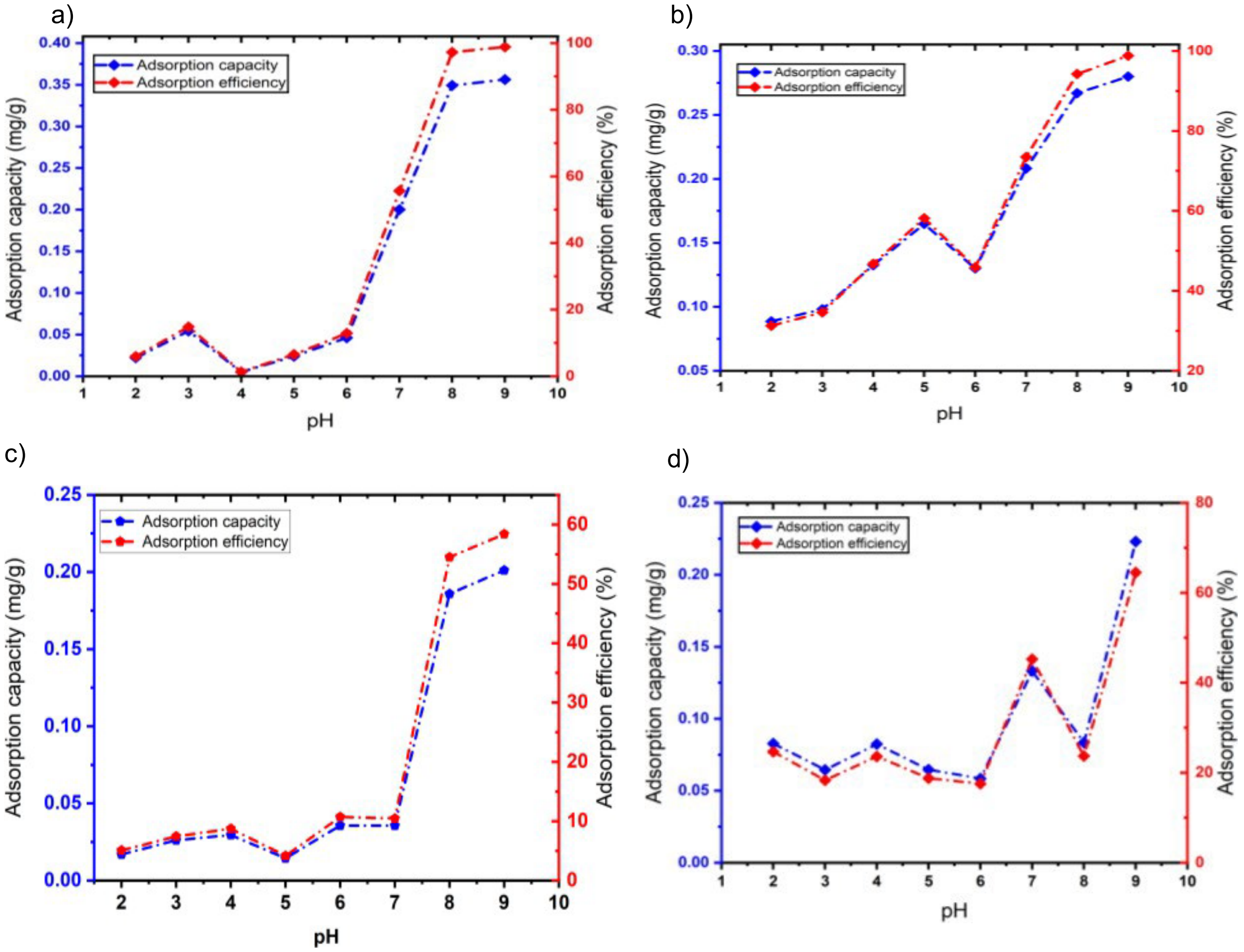

Figure 8-5: Effect of pH on the adsorption of Pb(II) by a) PE b) PP c) PS and d) PVA (concentration = 5 mg·ℓ$^{-1}$, temp = 25°C, volume = 0.015 ℓ, time = 2880 min, n = 3, RSD <10%).

The major species of Pb determined from a PHREEQC simulation of the initial solution (i.e., SOLUTION 1) were Pb^{2+}, $PbOH^{+}$, $PbNO_3^{+}$, $Pb_2(OH)_3^{+}$, $Pb_3(OH)_4^{2+}$, $Pb(OH)_3^{-}$, $Pb(OH)_2$, $Pb(OH)_4^{2+}$, and $Pb_4(OH)_4^{4+}$ (Table 8-1). At pH ≤ 7, Pb^{2+} and $PbOH^{+}$ accounted for more than 90% of the Pb(**II**) concentration in the solution. Adsorbent characterisation data was used to create a PHREEQC input script to get an accurate representation during the modelling. To this end, the polymer’s functional groups, number of moles, and specific surface area were specified (Figure 8-6).

Table 8-1: Molality and activity of major Pb(II) species from PHREEQC model output file.

Species	**Molality (mol·kg^{-1})**	**Activity**
Pb^{2+}	1.924×10^{-5}	1.868×10^{-5}
$PbOH^{+}$	4.765×10^{-6}	4.724×10^{-5}
Pb(OH)2	1.504×10^{-8}	1.504×10^{-8}
$PbNO^{3+}$	8.341×10^{-9}	8.268×10^{-9}
$Pb2OH^{3+}$	1.514×10^{-9}	1.398×10^{-9}
$Pb3(OH)4^{2+}$	8.733×10^{-11}	8.430×10^{-11}
$Pb4(OH)4^{4+}$	1.440×10^{-11}	1.251×10^{-11}
$Pb(OH)^{3-}$	1.528×10^{-12}	1.515×10^{-12}
Pb(NO3)2	4.202×10^{-13}	4.202×10^{-13}
$Pb(OH)4^{2-}$	3.869×10^{-17}	3.735×10^{-17}

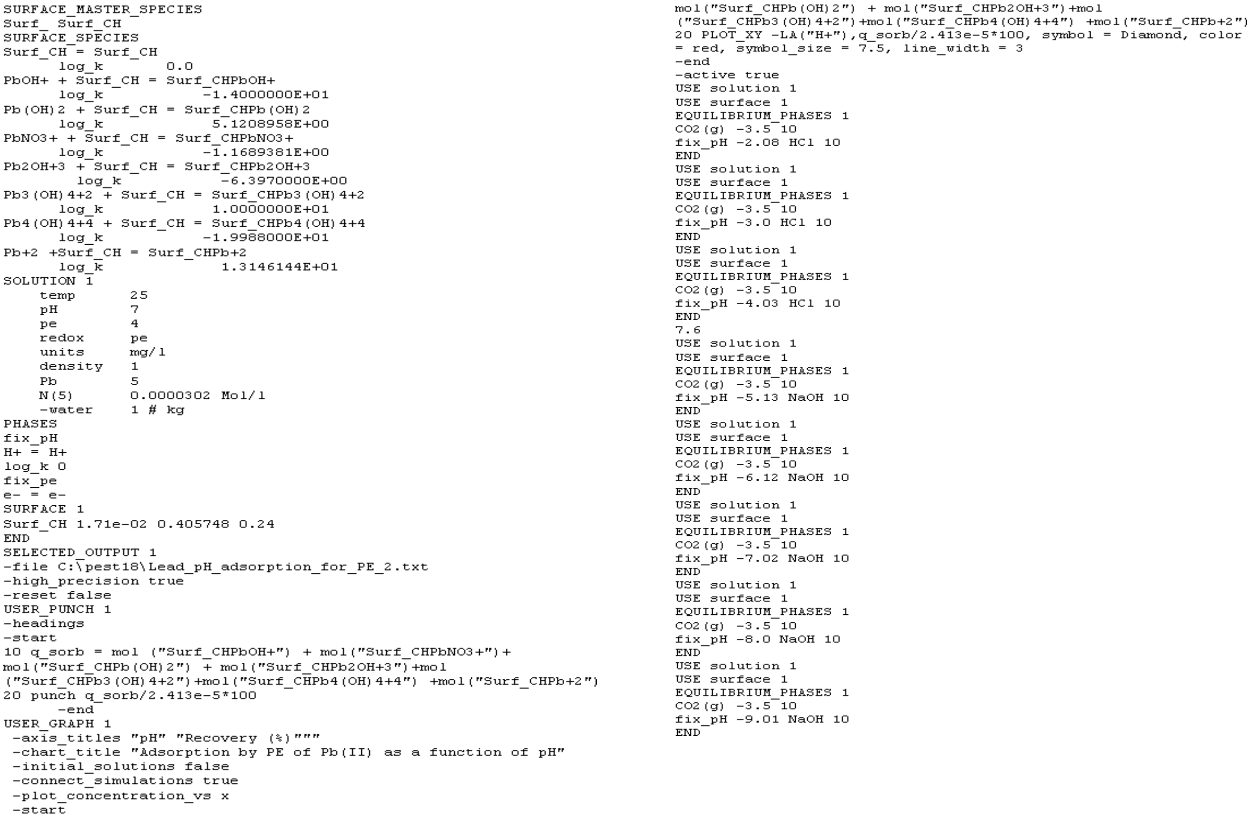

```
SURFACE_MASTER_SPECIES
Surf_ Surf_CH
SURFACE_SPECIES
Surf_CH = Surf_CH
      log_k       0.0
PbOH+ + Surf_CH = Surf_CHPbOH+
      log_k               -1.4000000E+01
Pb(OH)2 + Surf_CH = Surf_CHPb(OH)2
      log_k                5.1208958E+00
PbNO3+ + Surf_CH = Surf_CHPbNO3+
      log_k               -1.1689381E+00
Pb2OH+3 + Surf_CH = Surf_CHPb2OH+3
        log_k              -6.3970000E+00
Pb3(OH)4+2 + Surf_CH = Surf_CHPb3(OH)4+2
      log_k                1.0000000E+01
Pb4(OH)4+4 + Surf_CH = Surf_CHPb4(OH)4+4
      log_k               -1.9988000E+01
Pb+2 +Surf_CH = Surf_CHPb+2
      log_k                 1.3146144E+01
SOLUTION 1
    temp      25
    pH        7
    pe        4
    redox     pe
    units     mg/l
    density   1
    Pb        5
    N(5)      0.0000302 Mol/l
    -water    1 # kg
PHASES
fix_pH
H+ = H+
log_k 0
fix_pe
e- = e-
SURFACE 1
Surf_CH 1.71e-02 0.405748 0.24
END
SELECTED_OUTPUT 1
-file C:\pest18\Lead_pH_adsorption_for_PE_2.txt
-high_precision true
-reset false
USER_PUNCH 1
-headings
-start
10 q_sorb = mol ("Surf_CHPbOH+") + mol("Surf_CHPbNO3+")+
mol("Surf_CHPb(OH)2") + mol("Surf_CHPb2OH+3")+mol
("Surf_CHPb3(OH)4+2")+mol("Surf_CHPb4(OH)4+4") +mol("Surf_CHPb+2")
20 punch q_sorb/2.413e-5*100
     -end
USER_GRAPH 1
 -axis_titles "pH" "Recovery (%)"""
 -chart_title "Adsorption by PE of Pb(II) as a function of pH"
 -initial_solutions false
 -connect_simulations true
 -plot_concentration_vs x
 -start
mol("Surf_CHPb(OH)2") + mol("Surf_CHPb2OH+3")+mol
("Surf_CHPb3(OH)4+2")+mol("Surf_CHPb4(OH)4+4") +mol("Surf_CHPb+2")
20 PLOT_XY -LA("H+"),q_sorb/2.413e-5*100, symbol = Diamond, color
= red, symbol_size = 7.5, line_width = 3
-end
-active true
USE solution 1
USE surface 1
EQUILIBRIUM_PHASES 1
CO2(g) -3.5 10
fix_pH -2.08 HCl 10
END
USE solution 1
USE surface 1
EQUILIBRIUM_PHASES 1
CO2(g) -3.5 10
fix_pH -3.0 HCl 10
END
USE solution 1
USE surface 1
EQUILIBRIUM_PHASES 1
CO2(g) -3.5 10
fix_pH -4.03 HCl 10
END
7.6
USE solution 1
USE surface 1
EQUILIBRIUM_PHASES 1
CO2(g) -3.5 10
fix_pH -5.13 NaOH 10
END
USE solution 1
USE surface 1
EQUILIBRIUM_PHASES 1
CO2(g) -3.5 10
fix_pH -6.12 NaOH 10
END
USE solution 1
USE surface 1
EQUILIBRIUM_PHASES 1
CO2(g) -3.5 10
fix_pH -7.02 NaOH 10
END
USE solution 1
USE surface 1
EQUILIBRIUM_PHASES 1
CO2(g) -3.5 10
fix_pH -8.0 NaOH 10
END
USE solution 1
USE surface 1
EQUILIBRIUM_PHASES 1
CO2(g) -3.5 10
fix_pH -9.01 NaOH 10
END
```

Figure 8-6: PHREEQC input script with adsorbent characteristics, SCM equations of major Pb(II) species, and PEST estimated constants.

Experimental data was used to calibrate the PHREEQC model at pH 2-9 with 5 mg·ℓ^{-1} Pb(II) solution and adsorbent dosages of 16.5, 7.50, 17.3, and 20 g·ℓ^{-1} of PE, PP, PS, and PVA, respectively at 25 °C. The experimental and PHREEQC-PEST-modelled adsorption efficiencies for PE, PP, PS, and PVA are shown in Figure 8-7(a-d). PHREEQC-PEST numerical modelling was conducted in SVD mode for PP and PVA and LSQR mode for PE and PS. The specific surface areas of PE, PP, PS, and PVA were 0.704, 0.406, 2.071, and 0.284 $m^2 \cdot g^{-2}$. For PE, PP, PS generalised surfaces Surf_CH$_3$, Surf_CH, Surf_CH$_2$CH, and Surf_OCOCH$_3$ with concentrations of 2.62×10^{-3}, 1.71×10^{-2}, 2.62×10^{-3}, and 7.00×10^{-3} moles, respectively. To validate the modelled data, the Shapiro-Wilk Test and Levene's Test were conducted using SPSS Statistics version 27. For PE and PS, the Shapiro-Wilk Test and Levene's Test satisfied the requirement for a non-parametric test with $p < 0.05$. Meanwhile, for PP and PVA, Shapiro-Wilk and Levene's tests satisfied the parametric test requirement. The parametric Independent Samples T-Test revealed no statistically significant differences ($p > 0.05$) between the experimental and modelled data for PE and PS. No statistically significant differences existed between the experimental and modelled data for PP and PVA Mann-Whitney U Test, $p > 0.05$. Thus, the PHREEQC was successfully calibrated using PEST and PHREEQC coupled with PEST proved to be an efficient technique for determining sorption constants and accurately representing experimental data.

(a)

(b)

c)

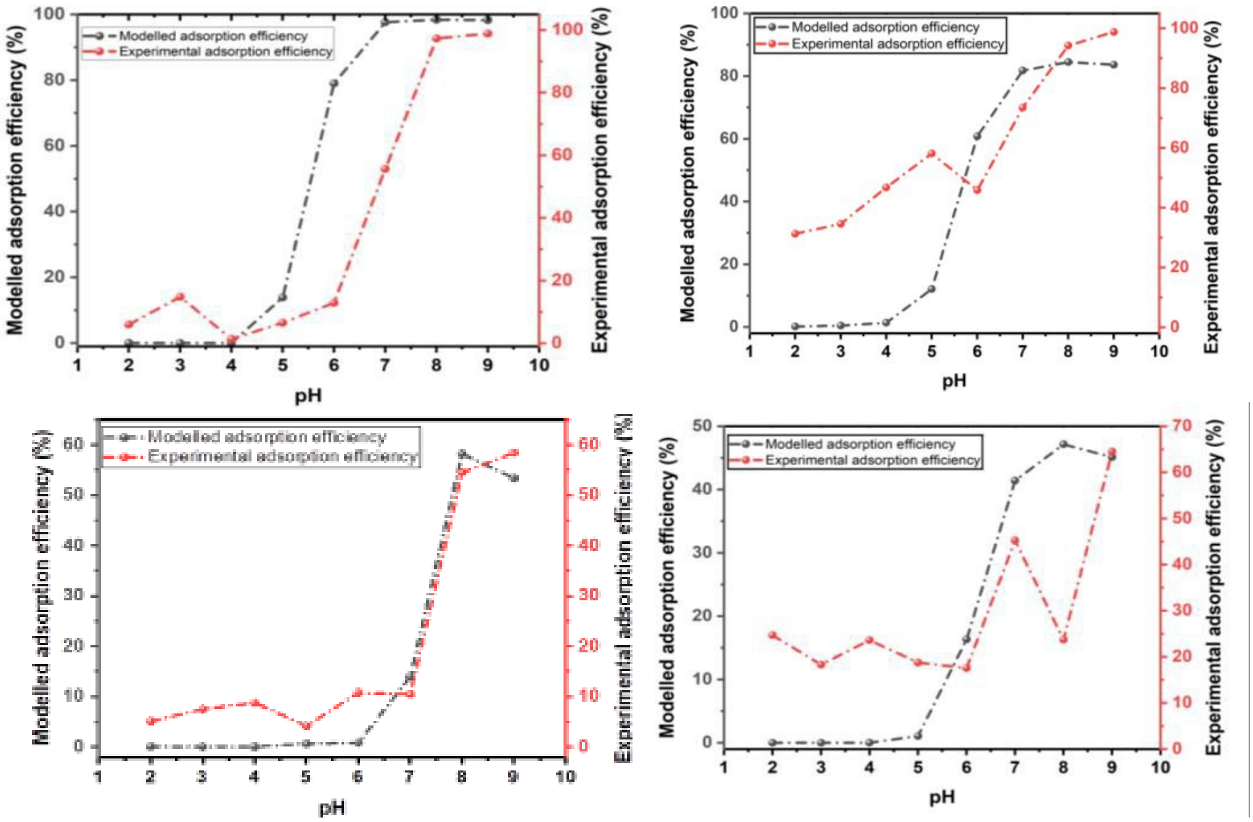

Figure 8-7: Experimental and modelled adsorption efficiencies for Lead by a) PE, b) PP, c) PS, and d) PVA at different pH using estimated sorption constants (Concentration = 5 mg·ℓ^{-1}; adsorbent dosage = 16.5, 7.50, 17.3, and 20 g·ℓ^{-1}; temp = 25°C; volume = 0.015 ℓ; time = 2880 min; n = 3; RSD <10%; Independent Samples T Test and Mann-Whitney U Test, p > 0.05).

8.3.2 Effect of adsorbent dosage

To determine the effect of varying adsorbent masses (1.57-53.5 g·ℓ$^{-1}$) on adsorption efficiency and capacity were added to Pb(II) solutions of fixed pH (PP: pH = 7, PE: pH = 7, PVA: pH = 7, and PS: pH = 6), temperature, and concentration in batch series. As shown in Figure 8-8(a-d), the adsorption capacity of Pb(II) generally increased with increasing adsorbent dosage until 16.5, 7.50, 40.5 and 20.0 g·ℓ$^{-1}$ for PE, PP, PS, and PVA, respectively. The Pb adsorption efficiencies were 55.6%, 88.4%, 27.4% and 45.2% for PE, PP, PS, and PVA, respectively. For PP, the adsorption capacity decreased with the adsorbent dosage, suggesting active sites were still available to adsorb more Pb(II) ions.

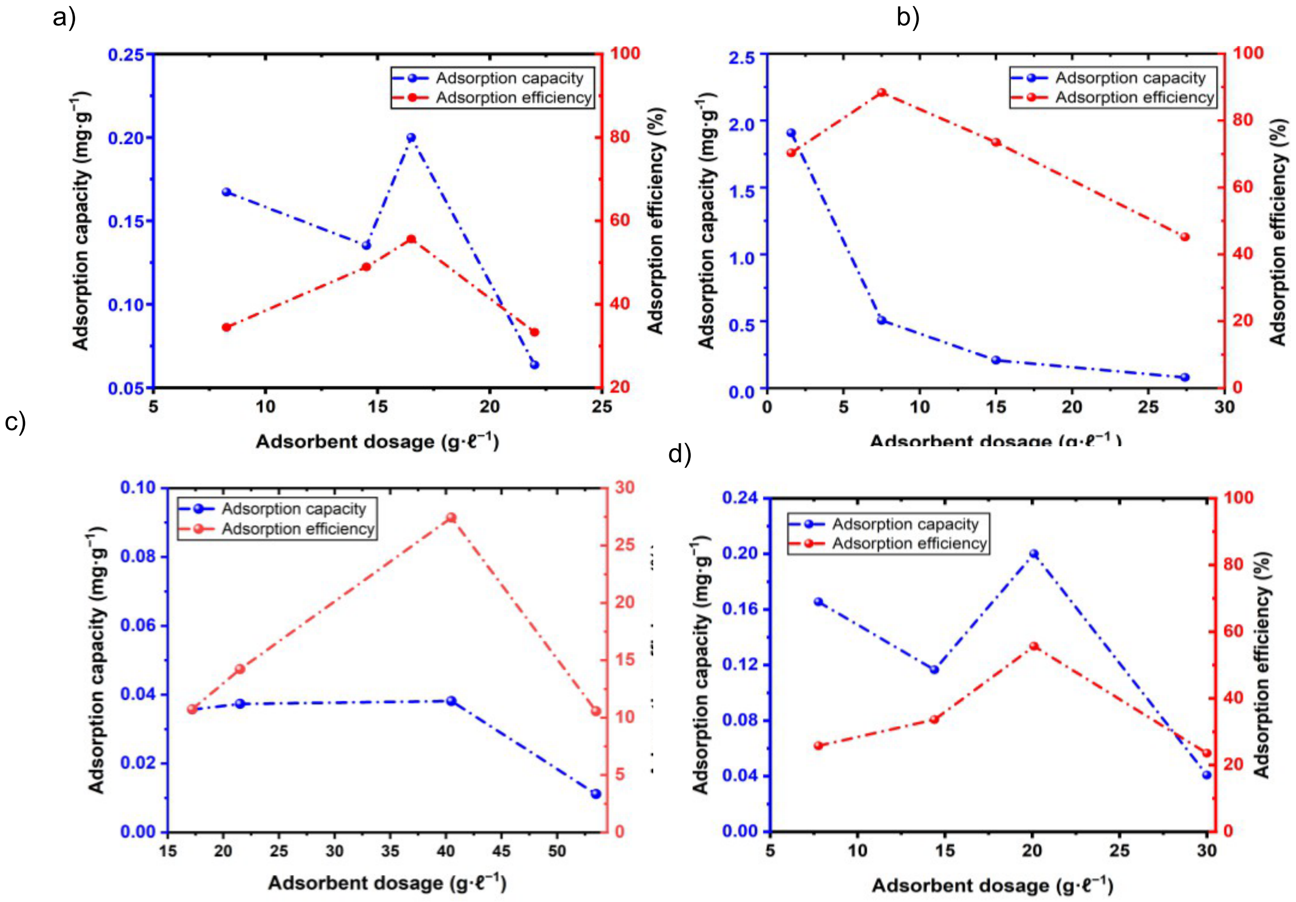

Figure 8-8: Effect of adsorbent dosage on the adsorption of Pb(II) by a) PE b) PP c) PS and d) PVA (concentration = 5 mg·ℓ$^{-1}$, temp = 25°C, volume = 0.015 ℓ, time = 2880 min, n = 3, RSD < 10%).

Since PHREEQC coupled with PEST could be used to model experimental observations reliably, the estimated SCM constants were then used in the PHREEQC input script to model the effect of adsorbent dosage as a function of pH. There were no significant differences in the adsorption efficiencies with an increase in adsorbent dosage, possibly due to the positively charged adsorbent surfaces in the acidic region as previously discussed (Figure 8-9(a-d)). However, the adsorption efficiency generally increased with adsorbent dosage beyond pH = 5. SCM revealed that the PP active since could be saturated when the adsorbent dosage is at least 27.4 g·ℓ$^{-1}$ and there would be a sharp decline in the adsorption efficiency of PVA when at least 30.0 g·ℓ$^{-1}$ of adsorbent is used.

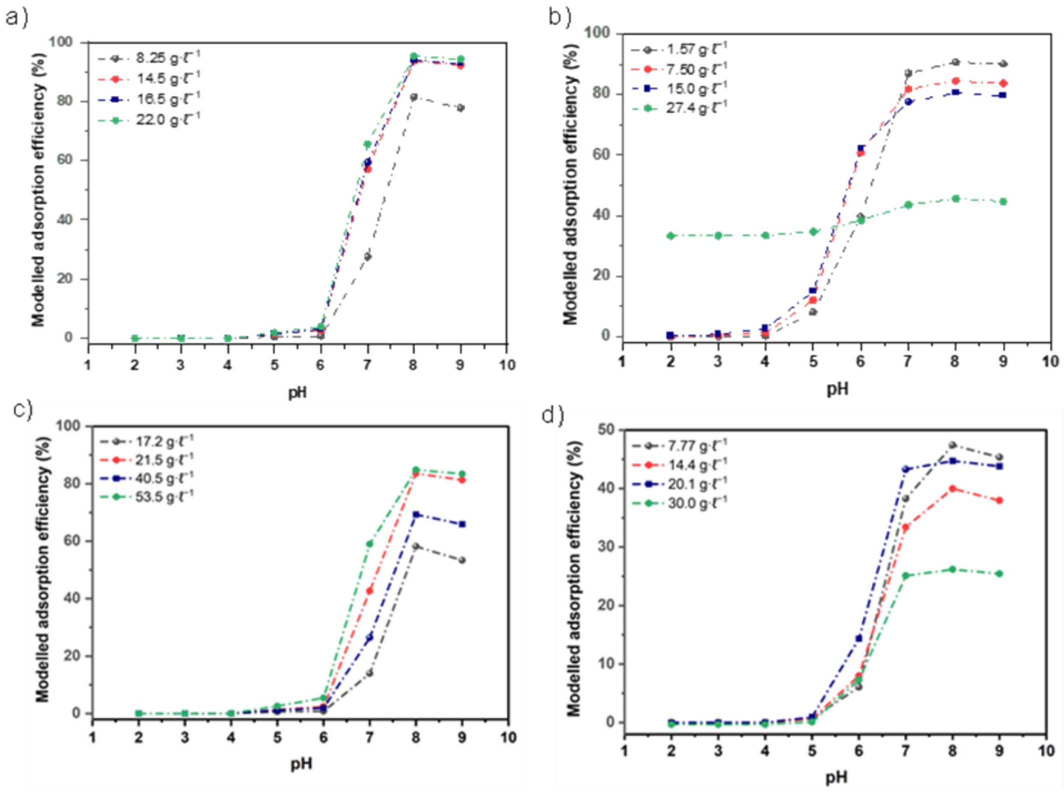

Figure 8-9: PHREEQC-PEST modelled adsorption of Pb(II) by a) PE, b) PP c) PS, and d) PVA as a function of pH at different adsorbent dosages.

4.2.1 Effect of concentration

The effect of initial concentration on the adsorption of Pb(II) by the adsorbent at fixed pH and adsorbent dosage (i.e., 16.5, 7.50, 20.1, and 40.5 g·ℓ$^{-1}$) for PE, PP, PS, and PVA was evaluated in batch series. The quantity of Pb(II) adsorbed increased with concentration due to the availability of active sites up to 15.0, 18.0, 22.0, and 12.0 mg·ℓ$^{-1}$ for PE, PP, PS, and PVA, respectively after which there was saturation of the adsorbent's active sites by the sorbate. The PE, PP, PS, and PVA adsorption capacities were 0.27, 0.64, 0.05, and 0.26 mg·g^{-1} respectively. Thus, the adsorption of Pb(II) had the following trend: PP > PE > PVA > PS (Figure 8-10(a-d)). The relatively low adsorption capacity of PS as compared to PE, and PP is consistent with results obtained by Godoy et al. (2019).

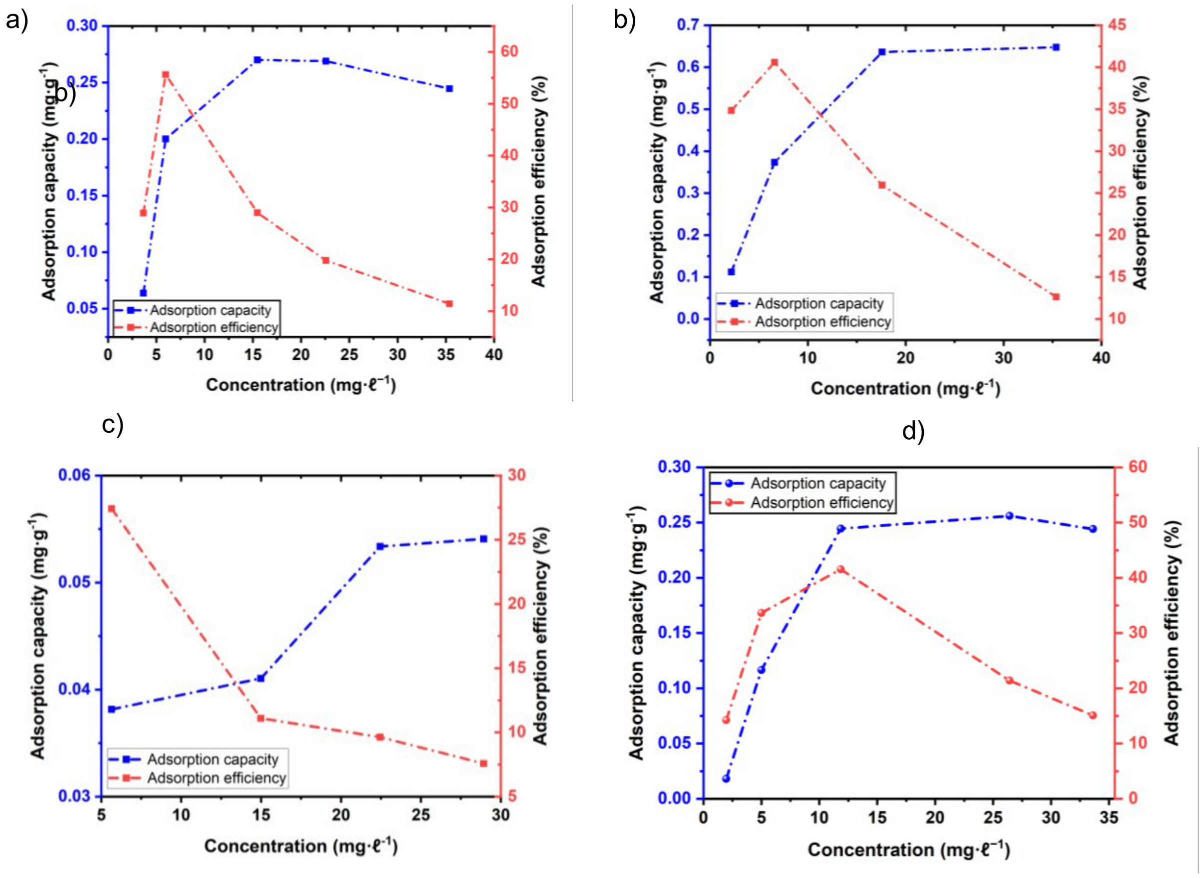

Figure 8-10: Effect of initial concentration on the adsorption of Pb(II) by a) PE b) PP c) PS and d) PVA (temp = 25°C, volume = 0.015 ℓ, time = 2880 min, n = 3, RSD < 10%).

8.3.3 Effect of temperature

The influence of temperature (i.e., 298.1, 303.15, 308.15, and 328.15 K) on Pb(II) adsorption was assessed at constant pH, time, concentration, and adsorbent dosage for PE, PP, and PS. The distribution constant was determined using Equation 20.

$$K_d = \frac{C_{ad}}{C_s} \tag{20}$$

Where C_s denotes the Pb(II) concentration in solution and C_{ad} denotes the Pb(II) quantity adsorbed. A graph of the temperature variation (1/T) in terms of the distribution constant (ln K_d) is shown in Figure 8-11(a-c). As the temperature increased ln K_d, the adsorbent's capacity to absorb Pb(II) diminishes with increasing heat. The Gibbs energy change (ΔG) could be utilised to investigate the spontaneity of Pb(II) adsorption at various temperatures can be calculated using Equation 21.

$$\Delta G = -RT\ln K_d \tag{21}$$

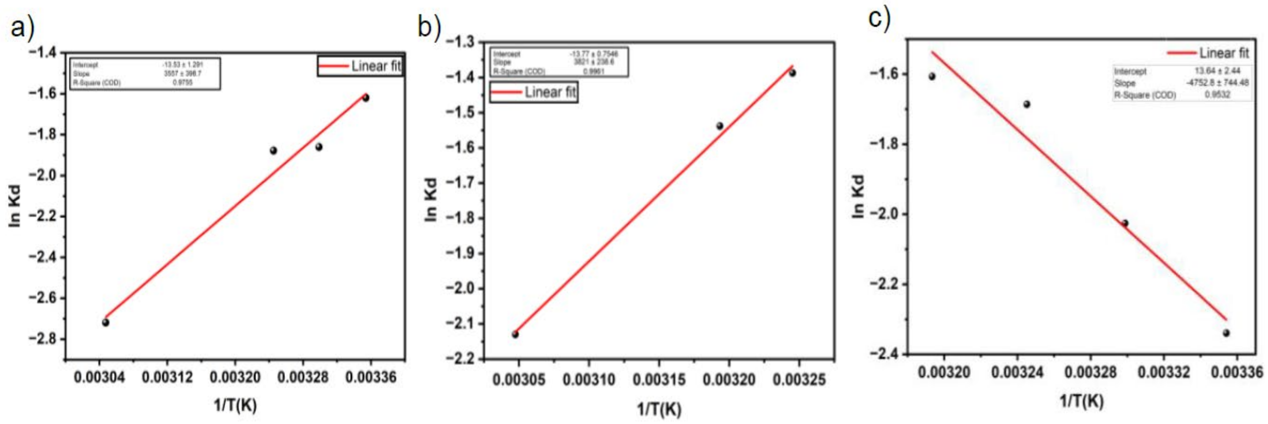

Figure 8-11: Plots of ln Kd as a function of 1/T for adsorption of Pb(II) onto a) PE, b) PP, and c) PS.

Determining the reaction's entropy (ΔS) and enthalpy (ΔH) is essential for better understanding the adsorption process. According to Van't Hoff's equation, the intercept and slope of the plot of 1/T versus $\ln K_d$ can be used to calculate the values of ΔS and ΔH, respectively (Tang et al., 2020).

Van’t Hoff's equation:

$$\ln \mathrm{K_d} = \frac{\Delta S}{R} - \frac{\Delta H}{RT} \qquad (22)$$

For PE, PP, and PS, a positive ΔG indicates that the adsorption of Pb(II) is non-spontaneous. Additionally, the negative ΔS observed for PE and PP suggests a decrease in disorder at the interface between the sorbate and sorbent, indicating that the adsorption process is reversible. Moreover, the negative ΔH values mean that the adsorption process is exothermic, in which the adsorption of Pb(II) decreases with an increase in temperature. However, for PS, positive ΔS and ΔH mean that there is an increase in disorder at the sorbate-sorbent interface, and the adsorption is endothermic with an increase in temperature, leading to an increase in adsorption capacity (Table 8-2).

Table 8-2: PE, PP, and PS thermodynamic parameters Pb(II) adsorption.

Adsorbent	T(K)	ΔG (kJ·mol^{-1})	ΔH (kJ·mol^{-1})	ΔS (J·K^{-1}·mol^{-1})	R^2
PE	298.15	4.017	-29.57	-112.5	0.9755
	303.15	4.688			
	308.15	4.813			
	328.15	7.419			
PP	308.15	3.554	-31.77	-114.5	0.9961
	313.15	4.004			
	328.15	5.811			
PS	298.15	5.800	39.51	113.4	0.9532
	303.15	5.107			
	308.15	4.321			
	313.15	4.184			

9 CONCLUSIONS AND RECOMMENDATIONS

9.1 OVERVIEW

This chapter presents the conclusions of the findings and recommendations on which future research can be based. The theoretical and practical implications of the findings, including potential toxicological aspects have been discussed together with the conclusions. The study explored the quantitative and qualitative distribution of microplastics (MPs) in: environmental aqueous systems (surface water, sediments and groundwater), tap and bottled water, and beverages (non- alcoholic, alcoholic and tea).

9.2 CONCLUSIONS

9.2.1 Surface water and sediments

This study provided new data on the presence and physical-chemical properties of MPs in the surface waters and sediments of the Vaal River. Methods frequently reported in the literature for sampling, digestion, density separation, and filtration were applied and, in some instances, modified. Microplastics were detected in all samples, with a relatively higher abundance of MPs in samples close to urban centres and confluences of the Vaal and its tributaries. Similar observations have been made by other studies around the world. The high abundance of fibres and fragments from this study was consistent with other studies. The high abundance of small-sized MPs, coupled with the dominance of coloured particles, is of particular concern, considering the harmful ecological and toxicological implications that these MPs are reported to have on freshwater biota. These implications may extend to a significant portion of the South African population that depends on the Vaal River for water and food sources. The prevalence of PE and PP is consistent with previous studies in both sample types, which identified these two polymers as the most abundant polymer types.

9.2.2 Groundwater

This study provided new data on the presence and physical-chemical properties of MPs in groundwater. MPs were detected in all samples from the Gauteng and North West Provinces, with a relatively higher average concentration in the North West than in Gauteng. This may be pointing to the Ramotswa Transboundary Aquifer (RTA) as a transboundary aquifer and likely to collect MPs from a wider source recharge. An assessment of the effect of hydrochemical parameters revealed that MP concentration increased with decreasing values of TDS and pH. This could be pointing to the behaviour that MPs adopt under these conditions, e.g., dispersion instead of agglomeration. When compared to similar studies around the world, the concentration of MPs in South African groundwater was relatively low. However, this is not conclusive as there remains a lot of research to be conducted on the occurrence of these contaminants in groundwater in South Africa. Such studies will also point to the contribution of various groundwater compartments (including other transboundary aquifers) as they are likely to be impacted differently. In terms of the physical properties of MPs, fibres dominated the range of 0.1-0.5 mm. The high abundance of small-sized fibrous MPs in all sample types is of great concern, considering their potentially harmful ecotoxicological effects. Three polymers were identified in the groundwater samples, namely, PBT, PUR, and PET. These polymers have relatively high densities, which enhances their propensity to vertically migrate through the soil profile to groundwater aquifers. Additionally, six colourants, namely C.I. Pigment Red 1, C.I Pigment White 6, C.I. Vat Blue 1, 4-(4-Nitrophenylazo)resorcinol, C.I. Direct Yellow 12, and C.I. Pigment Blue 15 were identified in the samples. These colourants are known to have extensive applications in the synthetic polymer industry and have been classified as potential carcinogens and mutagens.

9.2.3 Tap water

This study examined the physical-chemical properties of MPs in tap water in two suburbs and one township in Gauteng Province in South Africa (Tembisa, Braamfontein, and Silver Lakes). The concentrations of MPs were in the ranges of 4 to 20 particles$\cdot\ell^{-1}$(mean: 13 ± 4.9 particles$\cdot\ell^{-1}$), 9.0 to 31 particles$\cdot\ell^{-1}$ (mean: 18 ± 6.2 particles$\cdot\ell^{-1}$), and 4.7 to 16 particles$\cdot\ell^{-1}$ (mean: 11 ± 4.0 particles$\cdot\ell^{-1}$) in Tembisa, Braamfontein, and Silver Lakes, respectively. The most prevalent shape was fibres (83.1%), and the most abundant colours were black, blue, and green. Different polymer types and additives were detected, some of which are potentially toxic, e.g., C. I. Pigment Red 1 and C.I. Solvent Yellow 4. The physical characterisation provided insights into the shape and size of MPs that are more likely to pass through DWTPs. This is essential if future technologies are to be developed for MP removal in DWTPs and faucet systems in household taps. In general, the findings of this study have pointed to the implications of the presence of MPs in tap water on potential exposure to humans, with children showing an elevated likelihood of intake. This offers a benchmark for further work to draw on for the formulation of standards for MP content in drinking water in South Africa.

9.2.4 Bottled water

There were no statistically significant differences between the levels of MPs between still and sparkling water. This suggests that the method of processing various bottled water types does not considerably impact the total MP levels. However, this conclusion must be approached with caution, as additional research is needed to determine the long-term effects of pH variations in still and sparkling bottled water. There is a need for unified and internationally accepted methods of sampling, sample extraction, and characterisation of MPs. This will aid in overcoming limitations encountered in this study and other studies, particularly during MP analysis. Future studies should focus on developing adsorbents, membranes or other removal methods to target MPs in DWTPs. Such studies will usher in a new era whereby the scientific community will start looking for solutions not only to address pharmaceutical or metal pollutants in water but also to consider MPs as water pollutants. The above findings should provide a basis for the physical-chemical properties of the adsorbents to be synthesised. The presence of MPs in bottled water prompts the need for monitoring the quality of FMCG in the same way that other parameters such as pH, sugar levels, cations and anions are monitored. The general environmental laws and city by-laws are still lagging in terms of the promotion of recycling plastics (and reducing extensive use of single-use plastics) and eliminating illegal dumping activities. Industries should also be mandated to produce biodegradable plastic alternatives. This would greatly reduce the perpetuation of the pollution cycle involving MPs. Projects should be put in place and implemented to upgrade drinking water treatment infrastructure, which has undoubtedly exacerbated the problem by its failure to cope with increased domestic effluent as a result of growing populations. Approaches of characterisation of MPs concerning shape and size may be drawn from artificial intelligence tools such as computer vision. The robustness and effectiveness of these tools, based on deep learning and machine learning, would assist in eliminating the disparities mentioned above in terms of consistency in assigning the right shapes for MPs. These tools are already successfully used in remote sensing and medical imagery.

9.2.5 Tea bags

This part of the study provided new data on MPs' presence and physical-chemical properties in commercially sold rooibos and black tea teabags. Microplastics were detected in all tea (*Camellia Sinensis* and *Aspalathus linearis*) samples with concentrations ranging from 4.39 to 10.5 particles$\cdot g^{-1}$ (mean: 6.16 ± 2.00 particles$\cdot g^{-1}$). There were no statistically significant differences in the concentration of MPs in rooibos and black tea. This could suggest that the processing of different types of teas has no significant effect on the overall MP concentration. Fibres and blue-coloured MPs were the most abundant and accounted for 58.1% and 33.3%, respectively. Four polymers were identified in tea samples, namely polyethylene (PE), polyethylene terephthalate (PET), polypropylene (PP) and polyamide (PA).

9.2.6 Beverages

The mean MP concentrations in non-alcoholic beverages (9.5 ±8.5 particles·ℓ^{-1}) and alcoholic beverages (15 ±7.6 particles·ℓ^{-1}) were determined, indicating the extent of occurrence of these contaminants. Statistically, there were no significant differences between alcoholic (glass versus aluminium) and non-alcoholic beverages (PET versus aluminium). Men had a higher potential estimated daily intake of MPs compared to women. Fibres were the most abundant shape in all non-alcoholic beverages and AB (Glass); however, fragments were the most abundant shape in AB (Aluminium). The mean sizes of MPs across all sample types were less than 1 mm, with a high abundance of black, blue, and green MPs. PCA and Pearson correlation coefficient matrix revealed high positive correlations between fibres and various size ranges in alcoholic and non-alcoholic beverages. This highlights their wide distribution across different size ranges. However, correlations between the same brands could not be established. Micro-Raman spectroscopy identified six types of polymers in commercially sold beverages, namely PP, PE, PU, PA, PET, and PBT. A comparison of MP concentration to other studies revealed relatively low levels of MP contamination in South African beverages. This study provides a holistic view of MPs in commercially sold beverages. Moreover, it serves as a framework for a socioeconomic evaluation that considers the commercial, environmental, social, and sustainability repercussions of MP contamination in South Africa. Furthermore, findings can be used in future policy formulation and technology fabrications for MP extraction and control.

9.2.7 Geochemical modelling

This part of the study successfully characterised the physical-chemical properties of PE, PP, PS, and PVA MP particles using a stereomicroscope, FEG-SEM, SEM-EDS, and FTIR. The physical-chemical properties of MPs were then used in the development of generalised surface complexation modelling input scripts. Batch experiments provided the optimal adsorption parameters of Pb(II) onto MPs, and ICP-OES was used to determine the quantity adsorbed. The study was able to provide the first instance whereby model-independent PEST was coupled with PHREEQC to determine surface complexation constants of Pb(II) onto MPs. The estimated parameters were then used to conduct various computational simulations on generalised surface complexation modelling of Pb(II) on PE, PP, PS, and PVA MPs under different conditions that had not been conducted in the laboratory.

The findings pointed to increased adsorption of Pb with the dosage of MPs (adsorbent dosage). This would be expected as active sites increased with dosage. Adsorption was optimal at circum-neutral pH for PE, PS, PP and PVA. Using modelling, the effect of precipitation was delineated from adsorption. This is important as most natural water systems are at this pH regime, suggesting that Pb could remain persistent. Adsorption also increased with an increase in initial Pb(II) concentration. The implications of these findings include the fact that MPs are found as mixtures in the environment owing to their widespread use and disposal. Their exposure to prevailing environmental conditions gives insights into their potential as adsorption sites for other contaminants, such as metals (with Pb studied as a surrogate). This variation in their composition makes them to present challenges in adsorption studies as they tend to have surfaces that are not conventional. It is in such instances that conducting simulations of adsorption processes based on generalised surface complexation on their surfaces becomes important. This approach generalises the surface by using parameter estimations that reduce the need for conducting many experiments to understand the adsorption processes. From the findings, the presence of Fe was observed mainly in PS. The Fe could be from the Fe_2O_3 catalyst used in the synthesis of PS. It should be noted here that Fe could be an important component in adsorption owing to its ability to act as an adsorbent surface, thus playing a synergistic role in the overall adsorption process. However, this would need to be explored in further studies. The study has used Pb as a surrogate for other elements that may be adsorbed onto MP surfaces. This adsorption is not only limited to such elements but could also be extended to include organic contaminants such as pesticides, insecticides, pharmaceutical drugs and their metabolites, and flame-retardant constituents (e.g., polyfluoroalkyl substances (PFAS)). This provides further scope to use modelling approaches to comprehensively understand the adsorption of these contaminants onto MPs. For instance, computational modelling of molecular dynamics can be used to explore the possible trends in adsorption.

9.3 RECOMMENDATIONS

9.3.1 Standardisation and automation of methods for characterisation of MPs

There is a need for unified and internationally accepted methods of sampling, sample extraction, and characterisation of MPs. This will aid in overcoming limitations encountered in this study and other studies, particularly during MP analysis. For instance, there were challenges in the determination of the physical-chemical properties. This was largely due to the lack of automated instruments that can differentiate the shapes, sizes, and colours of MPs, the physical identification of each particle on every filter is often laborious and time-consuming. Additionally, the identification of colours and shapes can be subjective. For example, different analysts may classify different shades of colours differently (lighter shades of red vs pink and darker shades of blue vs green). Manual classification of shapes is also subjective, one analyst may classify pellets and films as fragments while another has a different classification. It is encouraging though to realise that there are ongoing attempts from instrument manufacturers to incorporate artificial intelligence (AI) tools such as computer vision that can make such tasks easier, yielding more accurate results. A lack of standardisation in MP studies affects widespread reporting and forecasting of the wider impact of MP pollution. This causes challenges when comparing results and collaborating with other research communities, government agencies, and other key stakeholders.

9.3.2 Strategies to manage the impact of MPs in surface and groundwater

As pointed out above, there is a need for unified and internationally accepted methods of sampling, sample extraction, and characterisation of MPs in aquatic systems (surface and groundwater). This will aid in evaluating contamination levels, tracking trends, and identifying hotspots through comparison to other studies. Additionally, researchers will be able to overcome limitations encountered during MP analysis. More research should be conducted to understand the fate and transport of MPs in different aquatic systems, including their transformation, accumulation, and potential remediation methods. This can be incorporated into hydrogeological modelling which has largely focused on water volumes, flow rates, flooding, recession, abstraction rates, ingress rates and dispersion aspects. The impact of MPs can be assessed in the context of these metrics and geochemical modelling. The latter offers insights into the behaviour of MPs as vectors of other contaminants such as metals and a host of organic compounds e.g., pharmaceuticals and their metabolites, humic substances, perfluoroalkyl substances, pesticides and herbicides among others.

For transboundary water resources such as the RTA, cooperation by the states through sharing best practices and harmonising policies should be forged. While this has been there, its reach or implementation has been limited to the quantitative usage and abstraction of the resources. Transboundary aquifers such as the RTA have been known to have pollution impacts stemming from the increased use of pit latrines and landfills on the Botswana side, which is upstream. While elevated nitrate concentrations and *Escherichia coli* counts have been reported in the groundwater, no research has been done on the occurrence and extent of the distribution of MPs. This study has provided a benchmark for such follow-up studies.

The challenge still remains the failure of the wastewater treatment facilities that have largely been overwhelmed and fail to remove MPs, resulting in discharge into surface and groundwater systems. This has been a general problem throughout the country, highlighting the infrastructure failures that have plagued most municipalities. Landfill sites have also been identified as major contributors to groundwater pollution. Thus, strategies that are aimed at reducing the impact of these facilities will go a long way in curtailing the footprint and impact of MPs in aqueous systems.

9.3.3 Initiatives for public awareness

The government should increase public education campaigns regarding MPs in general and their potential impacts on water resources such as groundwater. Individual responsibilities and behavioural changes should be underscored. Education on MPs can be introduced into the school curricula, e.g., in Life Orientation books to raise awareness in learners and to promote eco-friendly habits from an early age. Such awareness is being introduced for climate change aspects, for instance, and a lot of activism by youth movements has been centred around this. There should be a consolidation of efforts to reduce plastic pollution by industries, policymakers, NGOs, and community organisations to develop collaborative initiatives and obtain collective commitments. For instance, efforts such as those shown by NGOs such as Save the Vaal Environment and Hennops Revival should be supported and promulgated to assist with a wider cleanup footprint.

9.3.4 Legal enforcement

Policies are not adequately addressed by enforcement through legal provisions. The legal framework, while prescribing that “the polluter pays”, does not seem to have the intended impact as evidenced by the continued disposal of plastic waste into the wastewater systems and landfill sites. Recycling plastic and curbing input from primary waste sources are still major challenges. From the industry side, innovation around the production and use of biodegradable polymers has not had the momentum that it ought to have. There is sufficient scope to reduce pollution in general and to establish regulations and standards to limit the release of MPs into the environment in particular. For instance, there should be a ban on certain products that release primary MPs into the environment, such as face scrubs and cosmetic products. There has also been limited knowledge and information on the extent of contribution by certain industries, e.g., the agricultural sector, where there is extensive use of plastic-based products. Owing to the vast areas under irrigation in most cases, for instance, there is a potentially larger footprint of the spread of MPs through these non-point sources and their subsequent migration to aquifers. Drip or trickle irrigation has been suggested as an alternative system to reduce water volumes, which in turn could result in reduced release of MPs into soil systems.

REFERENCES

Abdelaziz, R., Merkel, B. J., Zambrano-Bigiarini, M., & Nair, S. (2019). Particle swarm optimization for the estimation of surface complexation constants with the geochemical model PHREEQC-3.1.2. Geoscientific Model Development, 12(1), 167–177. https://doi.org/10.5194/gmd-12-167-2019

Abdelnaeim, M. Y., El Sherif, I. Y., Attia, A. A., Fathy, N. A., & El-Shahat, M. F. (2016). Impact of chemical activation on the adsorption performance of common reed towards Cu(II) and Cd(II). International Journal of Mineral Processing, 157, 80–88. https://doi.org/10.1016/j.minpro.2016.09.013

Acarer, S. (2023). Abundance and characteristics of microplastics in drinking water treatment plants, distribution systems, water from refill kiosks, tap waters and bottled waters. Science of The Total Environment, 884, 163866. https://doi.org/10.1016/j.scitotenv.2023.163866

Adam, O. (2016). Removal of Resorcinol from Aqueous Solution by Activated Carbon: Isotherms, Thermodynamics and Kinetics. American Chemical Science Journal, 16(1), 1–13. https://doi.org/10.9734/ACSJ/2016/27637

Adu-Boahene, F., Boakye, P., Agyemang, F. O., Kanjua, J., & Oduro-Kwarteng, S. (2023). Understanding fluoride adsorption from groundwater by alumina modified with alum using PHREEQC surface complexation model. Scientific Reports, 13(1), 12307. https://doi.org/10.1038/s41598-023-38564-1

Aigotti, R., Giannone, N., Asteggiano, A., Mecarelli, E., Dal Bello, F., & Medana, C. (2022). Release of selected non-intentionally added substances (NIAS) from PET food contact materials: A New Online SPE- UHPLC-MS/MS Multiresidue Method.Separations, 9(8), 188. https://doi.org/10.3390/separations9080188

Alarcon, E. I., Poblete, H., Roh, H., Couture, J.-F., Comer, J., & Kochevar, I. E. (2017). Rose Bengal Binding to Collagen and Tissue Photobonding. ACS Omega, 2(10), 6646–6657. https://doi.org/10.1021/acsomega.7b00675

Ali, T., Habib, A., Muskan, F., Mumtaz, S., & Shams, R. (2023). Health risks posed by microplastics in tea bags: Microplastic pollution – a truly global problem. International Journal of Surgery, 109(3), 515–516. https://doi.org/10.1097/JS9.0000000000000055

Al-Kadhemy, M. F. H., Rasheed, Z. S., & Salim, S. R. (2016). Fourier transform infrared spectroscopy for irradiation coumarin doped polystyrene polymer films by alpha ray. Journal of Radiation Research and Applied Sciences, 9(3), 321–331. https://doi.org/10.1016/j.jrras.2016.02.004

Allen, N. S. (1994). Photofading and light stability of dyed and pigmented polymers. Polymer Degradation and Stability, 44(3), 357–374. https://doi.org/10.1016/0141-3910(94)90095-7

Altchenko, Y., Genco, A., Pierce, K., Woolf, R., Nijsten, G.-J., Ansems, N., Magombeyi, M., Ebrahim, G., Lautze, J., Villholth, K. G., Lefore, N., Modisha, R. C. O., Baqa, S., Mcgill, B., & Kenabatho, P. (2017). Resilience in the Limpopo Basin: The potential role of the transboundary Raotswa aquifer—Final draft.

Altunışık, A. (2023). Prevalence of microplastics in commercially sold soft drinks and human risk assessment. Journal of Environmental Management, 336, 117720. https://doi.org/10.1016/j.jenvman.2023.117720

Alvarado-Zambrano, D., Rivera-Hernández, J. R., & Green-Ruiz, C. (2023). First insight into microplastic groundwater pollution in Latin America: The case of a coastal aquifer in Northwest Mexico. Environmental Science and Pollution Research, 30(29), 73600–73611. https://doi.org/10.1007/s11356-023-27461-9

Amankwah-Amoah, J., Boso, N., & Kutsoati, J. K. (2022). Institutionalization of protection for intangible assets: Insights from the counterfeit and pirated goods trade in sub-Saharan Africa. Journal of World Business, 57(2), 101307. https://doi.org/10.1016/j.jwb.2021.101307

Amaral-Zettler, L. A., Zettler, E. R., & Mincer, T. J. (2020). Ecology of the plastisphere. Nature Reviews Microbiology, 18(3), 139–151. https://doi.org/10.1038/s41579-019-0308-0

Amato-Lourenço, L. F., Carvalho-Oliveira, R., Júnior, G. R., Dos Santos Galvão, L., Ando, R. A., & Mauad, T. (2021). Presence of airborne microplastics in human lung tissue. Journal of Hazardous Materials, 416, 126124. https://doi.org/10.1016/j.jhazmat.2021.126124

An, X., Li, W., Lan, J., & Adnan, M. (2022). Preliminary Study on the Distribution, Source, and Ecological Risk of Typical Microplastics in Karst Groundwater in Guizhou Province, China. International Journal of Environmental Research and Public Health, 19(22), 14751. https://doi.org/10.3390/ijerph192214751

Andrady, A. L. (2017). The plastic in microplastics: A review. Marine Pollution Bulletin, 119(1), 12–22. https://doi.org/10.1016/j.marpolbul.2017.01.082

Anghelone, M., Jembrih-Simbürger, D., & Schreiner, M. (2015). Identification of copper phthalocyanine blue polymorphs in unaged and aged paint systems employing micro-Raman spectroscopy and Random Forest. Spectrochimica Acta Part A: Molecular and Biomolecular Spectroscopy, 149, 419–425. https://doi.org/10.1016/j.saa.2015.04.094

Aranovich, G. L. (1992). The theory of polymolecular adsorption. Langmuir, 8(2), 736–739. https://doi.org/10.1021/la00038a071

Areo, O. M., Olowoyo, J. O., Sethoga, L. S., Adebo, O. A., & Njobeh, P. B. (2022). Determination of pesticide residues in rooibos (Aspalathus linearis) teas in South Africa. Toxicology Reports, 9, 852–857. https://doi.org/10.1016/j.toxrep.2022.04.001

Ash, P. (2022). "No end in sight" to Vaal River sewage problem, environmental group says, Timeslive, 4 January. https://www.timeslive.co.za/news/south-africa/2022-01-04-no-end-in-sight-to-vaal-river- sewage-problem-environmental-group-says

Atangana, A., & Noutchie, S. C. O. (2014). A Modified Groundwater Flow Model Using the Space Time Riemann-Liouville Fractional Derivatives Approximation. Abstract and Applied Analysis, 2014, 1–7. https://doi.org/10.1155/2014/498381

Au, S. Y., Bruce, T. F., Bridges, W. C., & Klaine, S. J. (2015). Responses of Hyalella azteca to acute and chronic microplastic exposures. Environmental Toxicology and Chemistry, 34(11), 2564–2572. https://doi.org/10.1002/etc.3093.

Azizi, Z. L., & Daneshjou, S. (2024). Bacterial nano-factories as a tool for the biosynthesis of TiO2 nanoparticles: Characterization and potential application in wastewater treatment. Applied Biochemistry and Biotechnology. https://doi.org/10.1007/s12010-023-04839-6

Bach, C., Dauchy, X., Severin, I., Munoz, J.-F., Etienne, S., & Chagnon, M.-C. (2013). Effect of temperature on the release of intentionally and non-intentionally added substances from polyethylene terephthalate (PET) bottles into water: Chemical analysis and potential toxicity. Food Chemistry, 139(1–4), 672– 680. https://doi.org/10.1016/j.foodchem.2013.01.046

Bachmaf, S., & Merkel, B. J. (2011). Estimating water chemistry parameters from experimental data using PEST with PHREEQC. Uranium Sorption on Clay Minerals: Laboratory Experiments and Surface Complexation Modeling, 123.

Baker, M. J., Hughes, C. S., & Hollywood, K. A. (2016). Biophotonics: Vibrational Spectroscopic Diagnostics: Morgan & Claypool Publishers. https://doi.org/10.1088/978-1-6817-4071-3

Bakir, A., Rowland, S. J., & Thompson, R. C. (2012). Competitive sorption of persistent organic pollutants onto microplastics in the marine environment. Marine Pollution Bulletin, 64(12), 2782–2789. https://doi.org/10.1016/j.marpolbul.2012.09.010

Baldwin, A. K., Corsi, S. R., & Mason, S. A. (2016). Plastic Debris in 29 Great Lakes Tributaries: Relations to Watershed Attributes and Hydrology. Environmental Science & Technology, 50(19), 10377–10385. https://doi.org/10.1021/acs.est.6b02917

Barnes, A. J., Majid, M. A., Stuckey, M. A., Gregory, P., & Stead, C. V. (1985). The resonance Raman spectra of Orange II and Para Red: Molecular structure and vibrational assignment. Spectrochimica Acta Part A: Molecular Spectroscopy, 41(4), 629–635. https://doi.org/10.1016/0584-8539(85)80050-7

Baughman, T. W., Chan, C. D., Winey, K. I., & Wagener, K. B. (2007). Synthesis and Morphology of Well-Defined Poly(ethylene- co -acrylic acid) Copolymers. Macromolecules, 40(18), 6564–6571. https://doi.org/10.1021/ma070841r

Bellasi, A., Binda, G., Pozzi, A., Galafassi, S., Volta, P., & Bettinetti, R. (2020). Microplastic Contamination in Freshwater Environments: A Review, Focusing on Interactions with Sediments and Benthic Organisms. Environments, 7(4), 30. https://doi.org/10.3390/environments7040030

Bidsorkhi, H. C., Soheilmoghaddam, M., Pour, R. H., Adelnia, H., & Mohamad, Z. (2014). Mechanical, thermal and flammability properties of ethylene-vinyl acetate (EVA)/sepiolite nanocomposites. Polymer Testing, 37, 117–122. https://doi.org/10.1016/j.polymertesting.2014.05.007

Bierkens, M. F. P., & Wada, Y. (2019). Non-renewable groundwater use and groundwater depletion: A review. Environmental Research Letters, 14(6), 063002. https://doi.org/10.1088/1748-9326/ab1a5f

Borsig, E., (1999). Polypropylene derivatives. Journal of Macromolecular Science, Part A 36, 1699–1715. https://doi.org/10.1081/MA-100101621

Bott, J., Störmer, A., & Franz, R. (2014). Migration of nanoparticles from plastic packaging materials containing carbon black into foodstuffs. Food Additives & Contaminants: Part A, 31(10), 1769–1782. https://doi.org/10.1080/19440049.2014.952786.

Boucher, J., & Friot, D. (2017). Primary microplastics in the oceans: A global evaluation of sources. IUCN International Union for Conservation of Nature. https://doi.org/10.2305/IUCN.CH.2017.01.en

Bouhlel, Z., Associate, R., Water, I. for, Environment, (UNU-INWEH), H., University, U. N., Smakhtin, V., & Former Director of the Institute for Water. (2023). How the bottled water industry is masking the global water crisis. The Canadian Press, Generic. https://go.exlibris.link/wLhk0vp4

Bouhlel, Z., Köpke, J., Mina, M., & Smakhtin, V. (2023). Global Bottled Water Industry: A Review of Impacts and Trends United Nations, University Institute for Water, Environment and Health, Hamilton, Canada. Bourne, L. T., Harmse, B., & Temple, N. (2007). Water: A neglected nutrient in the young child? A South African perspective. Maternal & Child Nutrition, 3(4), 303–311. https://doi.org/10.1111/j.1740-8709.2007.00114.x

Bouwman, H., Minnaar, K., Bezuidenhout, C., Verster, C., 2018. Microplastics in freshwater environments. WRC Report No. 2610/1/18. Water Research Commission, Pretoria. https://www.wrc.org.za/wp-content/uploads/mdocs/2610-1-18.pdf

Brennecke, D., Duarte, B., Paiva, F., Caçador, I., & Canning-Clode, J. (2016). Microplastics as vector for heavy metal contamination from the marine environment. Estuarine, Coastal and Shelf Science, 178, 189–195. https://doi.org/10.1016/j.ecss.2015.12.003

Brunauer, S., Emmett, P. H., & Teller, E. (1938). Adsorption of Gases in Multimolecular Layers. Journal of the American Chemical Society, 60(2), 309–319. https://doi.org/10.1021/ja01269a023

Bullen, J. C., Landa-Cansigno, O., & Weiss, D. J. (2024). Teaching adsorption chemistry by constructing Surface Complexation Models (SCM) in PHREEQC. Journal of Chemical Education, 101(5), 1914– 1924. https://doi.org/10.1021/acs.jchemed.3c01195

Bumbrah, G. S., & Sharma, R. M. (2016). Raman spectroscopy–Basic principle, instrumentation and selected applications for the characterization of drugs of abuse. Egyptian Journal of Forensic Sciences, 6(3), 209–215. https://doi.org/10.1016/j.ejfs.2015.06.001

Cable, R. N., Beletsky, D., Beletsky, R., Wigginton, K., Locke, B. W., & Duhaime, M. B. (2017). Distribution and Modeled Transport of Plastic Pollution in the Great Lakes, the World's Largest Freshwater Resource. Frontiers in Environmental Science, 5, 45. https://doi.org/10.3389/fenvs.2017.00045

Cai, H., Chen, M., Chen, Q., Du, F., Liu, J., & Shi, H. (2020). Microplastic quantification affected by structure and pore size of filters. Chemosphere, 257, 127198. https://doi.org/10.1016/j.chemosphere.2020.127198

Camargo, V., Ortiz, E., Solis, H., Cortes-Romero, C. M., Loera-Serna, S., & Perez, C. J. (2014). Chemical Degradation of Indigo Potassium Tetrasulfonate Dye by Advanced Oxidation Processes. Journal of Environmental Protection, 05(13), 1342–1351. https://doi.org/10.4236/jep.2014.513128

Carlsten, C. (2024). Inhaled Microplastics and Airway Development: Concerning Evidence from Organoids. American Journal of Respiratory and Critical Care Medicine, 209(4), 355–356. https://doi.org/10.1164/rccm.202311-2131ED.

Carpenter, E. J., & Smith, K. L. (1972). Plastics on the Sargasso sea surface. Science (New York, N.Y.), 175(4027), 1240–1241. https://doi.org/10.1126/science.175.4027.1240

Catarino, A. I., Kramm, J., Völker, C., Henry, T. B., & Everaert, G. (2021). Risk posed by microplastics: Scientific evidence and public perception. Current Opinion in Green and Sustainable Chemistry, 29, 100467. https://doi.org/10.1016/j.cogsc.2021.100467

Cha, J., Lee, J.-Y., & Lee, J. (2024). Effects of groundwater sample volume on identified microplastics in groundwater of an agricultural area in Korea. Science of The Total Environment, 911, 168650. https://doi.org/10.1016/j.scitotenv.2023.168650

Chakraborty, I., Banik, S., Biswas, R., Yamamoto, T., Noothalapati, H., & Mazumder, N. (2022). Raman spectroscopy for microplastic detection in water sources: A systematic review. International Journal of Environmental Science and Technology. https://doi.org/10.1007/s13762-022-04505-0

Chamas, A., Moon, H., Zheng, J., Qiu, Y., Tabassum, T., Jang, J. H., Abu-Omar, M., Scott, S. L., & Suh, S. (2020). Degradation Rates of Plastics in the Environment. ACS Sustainable Chemistry & Engineering, 8(9), 3494–3511. https://doi.org/10.1021/acssuschemeng.9b06635

Chang, E., Zavarin, M., Beverly, L., & Wainwright, H. (2023). A chemistry-informed hybrid machine learning approach to predict metal adsorption onto mineral surfaces. Applied Geochemistry, 155, 105731. https://doi.org/10.1016/j.apgeochem.2023.105731

Chaudhuri, I., Fruijtier-Pölloth, C., Ngiewih, Y., & Levy, L. (2018). Evaluating the evidence on genotoxicity and reproductive toxicity of carbon black: A critical review. Critical Reviews in Toxicology, 48(2), 143–169. https://doi.org/10.1080/10408444.2017.1391746

Chemical Retrieval on the Web (CROW) polymerdatabase. (2022a). https://www.polymerdatabase.com/polymer%20classes/Polyurethane%20type.html

Chemical Retrieval on the Web (CROW) polymerdatabase. (2022b). https://www.polymerdatabase.com/polymer%20classes/Polyamide%20type.html

Chen, J., Zhao, L., & Terry, P. D. (2023, July 21). WHO expert cancer group states that the sweetener aspartame is a possible carcinogen, but evidence is limited–6 questions answered. The Conversation. http://theconversation.com/who-expert-cancer-group-states-that-the-sweetener-aspartame-is-a-possible-carcinogen-but-evidence-is-limited-6-questions-answered-209957.

Cheng, P., & Hu, Y. H. (2016). Dubinin-Astakhov model for acetylene adsorption on metal-organic frameworks. Applied Surface Science, 377, 349–354. https://doi.org/10.1016/j.apsusc.2016.03.124.

Cheung, C. W., Porter, J. F., & McKay, G. (2000). Elovich equation and modified second-order equation for sorption of cadmium ions onto bone char. Journal of Chemical Technology and Biotechnology (1986), 75(11), 963–970. https://doi.org/10.1002/1097-4660(200011)75:11<963::AID-JCTB302>3.0.CO;2-Z.

Christie, R. M. (1994). Pigments, dyes and fluorescent brightening agents for plastics: An overview. Polymer International, 34(4), 351–361. https://doi.org/10.1002/pi.1994.210340401.

Chu, X., Zheng, B., Li, Z., Cai, C., Peng, Z., Zhao, P., & Tian, Y. (2022). Occurrence and distribution of microplastics in water supply systems: In water and pipe scales. Science of The Total Environment, 803, 150004. https://doi.org/10.1016/j.scitotenv.2021.150004

Cobbing, J. (2018). The North West Dolomite Aquifers, South Africa: A stalled opportunity for water security and development. International Water Management Institute (IWMI). https://doi.org/10.5337/2018.223

Coccato, A., Jehlicka, J., Moens, L., & Vandenabeele, P. (2015). Raman spectroscopy for the investigation of carbon-based black pigments: Investigation of carbon-based black pigments. Journal of Raman Spectroscopy, 46(10), 1003–1015. https://doi.org/10.1002/jrs.4715

Crosta, A., Parolini, M., & De Felice, B. (2023). Microplastics contamination in nonalcoholic beverages from the italian market. International Journal of Environmental Research and Public Health, 20(5), 4122. https://doi.org/10.3390/ijerph20054122

Dahms, H. T. J., & Greenfield, R. (2025). Contextualizing microplastic pollution in different river habitats through rapid habitat assessment in South Africa. Aquatic Sciences, *87*(2), 36. https://doi.org/10.1007/s00027-025-01166-2

Dahms, H. T. J., Van Rensburg, G. J., & Greenfield, R. (2020). The microplastic profile of an urban African stream. Science of The Total Environment, 731, 138893. https://doi.org/10.1016/j.scitotenv.2020.138893

Daniel, D. B., Ashraf, P. M., & Thomas, S. N. (2020). Microplastics in the edible and inedible tissues of pelagic fishes sold for human consumption in Kerala, India. Environmental Pollution, 266, 115365. https://doi.org/10.1016/j.envpol.2020.115365

De Souza, F. M., Kahol, P. K., & Gupta, R. K. (2021). Introduction to Polyurethane Chemistry. In R. K. Gupta

& P. K. Kahol (Eds.), ACS Symposium Series, 138, 1–24. American Chemical Society. https://doi.org/10.1021/bk-2021-1380.ch001

Deme, G. G., Ewusi-Mensah, D., Olagbaju, O. A., Okeke, E. S., Okoye, C. O., Odii, E. C., Ejeromedoghene, O., Igun, E., Onyekwere, J. O., Oderinde, O. K., & Sanganyado, E. (2022). Macro problems from microplastics: Toward a sustainable policy framework for managing microplastic waste in Africa. Science of The Total Environment, 804, 150170. https://doi.org/10.1016/j.scitotenv.2021.150170

Diaz-Basantes, M. F., Conesa, J. A., & Fullana, A. (2020). Microplastics in honey, beer, milk and refreshments in Ecuador as emerging contaminants. Sustainability, 12(14), 5514. https://doi.org/10.3390/su12145514

Dikareva, N., & Simon, K. S. (2019). Microplastic pollution in streams spanning an urbanisation gradient. Environmental Pollution, 250, 292–299. https://doi.org/10.1016/j.envpol.2019.03.105

Ding, L., Mao, R. F., Guo, X., Yang, X., Zhang, Q., & Yang, C. (2019). Microplastics in surface waters and sediments of the Wei River, in the northwest of China. Science of The Total Environment, 667, 427–434. https://doi.org/10.1016/j.scitotenv.2019.02.332.

Doherty, J., Brebber, L., & Whyte, P. (1994). PEST: Model-independent parameter estimation. Watermark Computing, Corinda, Australia, 122, 336.

Dris, R., Gasperi, J., Rocher, V., Saad, M., Renault, N., & Tassin, B. (2015). Microplastic contamination in an urban area: A case study in Greater Paris. Environmental Chemistry, 12(5), 592. https://doi.org/10.1071/EN14167

Eberhard, T., Casillas, G., Zarus, G. M., & Barr, D. B. (2024). Systematic review of microplastics and nanoplastics in indoor and outdoor air: Identifying a framework and data needs for quantifying human inhalation exposures. Journal of Exposure Science & Environmental Epidemiology, 34(2), 185–196. https://doi.org/10.1038/s41370-023-00634-x

Egessa, R., Nankabirwa, A., Ocaya, H., & Pabire, W. G. (2020). Microplastic pollution in surface water of Lake Victoria. Science of The Total Environment, 741, 140201. https://doi.org/10.1016/j.scitotenv.2020.140201

Esfandiari, A., Abbasi, S., Peely, A. B., Mowla, D., Ghanbarian, M. A., Oleszczuk, P., & Turner, A. (2022). Distribution and transport of microplastics in groundwater (Shiraz aquifer, southwest Iran). Water Research, 220, 118622. https://doi.org/10.1016/j.watres.2022.118622

Estrada-Villegas, G. M., Morselli, G., Oliveira, M. J. A., González-Pérez, G., & Lugão, A. B. (2020). PVGA/Alginate-AgNPs hydrogel as absorbent biomaterial and its soil biodegradation behaviour. Polymer Bulletin, 77(8), 4147–4166. https://doi.org/10.1007/s00289-019-02966-x

Evans, J. (2021). ‘A story of South Africa’: Emfuleni residents fed up with Vaal River pollution inertia, Daily Maverick, 29 October. https://www.dailymaverick.co.za/article/2021-10-29-a-story-of-south-africa- emfuleni-residents-fed-up-with-vaal-river-pollution-inertia/

Fadare, O. O., Okoffo, E. D., & Olasehinde, E. F. (2021). Microparticles and microplastics contamination in African table salts. Marine Pollution Bulletin, 164, 112006. https://doi.org/10.1016/j.marpolbul.2021.112006

Fang, J., Zhang, L., Sutton, D., Wang, X., & Lin, T. (2012). Needleless melt-electrospinning of polypropylene nanofibres. Journal of Nanomaterials, 2012, 1–9. https://doi.org/10.1155/2012/382639

Fard, N. J. H., Jahedi, F., & Turner, A. (2025). Microplastics and nanoplastics in tea: Sources, characteristics and potential impacts. Food Chemistry, 466, 142111. https://doi.org/10.1016/j.foodchem.2024.142111

Feld, L., Silva, V. H. D., Murphy, F., Hartmann, N. B., & Strand, J. (2021). A Study of Microplastic Particles in Danish Tap Water. Water, 13(15), 2097. https://doi.org/10.3390/w13152097

Feng, S., Lu, H., Yao, T., Liu, Y., Tian, P., & Lu, J. (2021). Microplastic footprints in the Qinghai-Tibet Plateau and their implications to the Yangtze River Basin. Journal of Hazardous Materials, 407, 124776. https://doi.org/10.1016/j.jhazmat.2020.124776

Fiol, N., & Villaescusa, I. (2009). Determination of sorbent point zero charge: Usefulness in sorption studies. Environmental Chemistry Letters, 7(1), 79–84. https://doi.org/10.1007/s10311-008-0139-0.

Fischer, E. K., Paglialonga, L., Czech, E., & Tamminga, M. (2016). Microplastic pollution in lakes and lake shoreline sediments – A case study on Lake Bolsena and Lake Chiusi (central Italy). Environmental Pollution, 213, 648–657. https://doi.org/10.1016/j.envpol.2016.03.012

Fleischmann, C., Lievenbrück, M., & Ritter, H. (2015). Polymers and Dyes: Developments and Applications. Polymers, 7(4), 717–746. https://doi.org/10.3390/polym7040717

Forte, M., Iachetta, G., Tussellino, M., Carotenuto, R., Prisco, M., De Falco, M., Laforgia, V., & Valiante, S. (2016). Polystyrene nanoparticles internalization in human gastric adenocarcinoma cells. Toxicology in Vitro, 31, 126–136. https://doi.org/10.1016/j.tiv.2015.11.006

Fred-Ahmadu, O. H., Bhagwat, G., Oluyoye, I., Benson, N. U., Ayejuyo, O. O., & Palanisami, T. (2020). Interaction of chemical contaminants with microplastics: Principles and perspectives. Science of The Total Environment, 706, 135978. https://doi.org/10.1016/j.scitotenv.2019.135978

Frère, L., Paul-Pont, I., Moreau, J., Soudant, P., Lambert, C., Huvet, A., & Rinnert, E. (2016). A semi-automated Raman micro-spectroscopy method for morphological and chemical characterizations of microplastic litter. Marine Pollution Bulletin, 113(1–2), 461–468. https://doi.org/10.1016/j.marpolbul.2016.10.051

Frias, J., Filgueiras, A., J. Gago, Pedrotti, M. L., Suaria, G., Tirelli, V., Andrade, J., Nash, R., O'Connor, I., Lopes, C., Caetano, M., Raimundo, J., Carretero, O., Viñas, L., Antunes, J. C., Bessa, F., Sobral, P., Goruppi, A., Aliani, S., … Gerdts, G. (2019). Standardised protocol for monitoring microplastics in seawater. https://doi.org/10.13140/RG.2.2.14181.45282

Fu, L., Li, J., Wang, G., Luan, Y., & Dai, W. (2021). Adsorption behaviour of organic pollutants on microplastics. Ecotoxicology and Environmental Safety, 217, 112207. https://doi.org/10.1016/j.ecoenv.2021.112207

Furukawa, T., Sato, H., Kita, Y., Matsukawa, K., Yamaguchi, H., Ochiai, S., Siesler, H. W., & Ozaki, Y. (2006). Molecular structure, crystallinity and morphology of Polyethylene/Polypropylene blends studied by Raman Mapping, Scanning Electron Microscopy, Wide Angle X-Ray Diffraction, and Differential Scanning Calorimetry. PolymerJournal, 38(11), 1127–1136. https://doi.org/10.1295/polymj.PJ2006056

Gaffoor, Z., Gritzman, A., Pietersen, K., Jovanovic, N., Bagula, A., & Kanyerere, T. (2022). An autoregressive machine learning approach to forecast high-resolution groundwater-level anomalies in the Ramotswa/North West/Gauteng dolomite aquifers of Southern Africa. Hydrogeology Journal, 30(2), 575–600. https://doi.org/10.1007/s10040-021-02439-4

Gbogbo, F., Takyi, J. B., Billah, M. K., & Ewool, J. (2020). Analysis of microplastics in wetland samples from coastal Ghana using the Rose Bengal stain. Environmental Monitoring and Assessment, 192(4), 208. https://doi.org/10.1007/s10661-020-8175-8

Gemmell, A., Sterckx, A., Vargas, C. R., Vargas, C. R., Abrahams, E., Flügel, T., Hugman, R., & Mosesane, B. (2021). Consolidation of Data and Application of Big Data Tools to Enhance National and Transboundary Data Sets in Southern Africa that Support Decision-Making for Security of Water Resources (WRC Report No. TT 844/20). Water Research Commission. https://www.umvoto.com/wp-content/uploads/2021/05/WRC-Big-Data-and-Transboundary-Water_One-Pager-v2.pdf

Girão, A. V., Caputo, G., & Ferro, M. C. (2017). Application of Scanning Electron Microscopy–Energy Dispersive X-Ray Spectroscopy (SEM-EDS). Comprehensive Analytical Chemistry (Vol. 75, pp. 153– 168). Elsevier. https://doi.org/10.1016/bs.coac.2016.10.002

Godoy, V., Blázquez, G., Calero, M., Quesada, L., & Martín-Lara, M. A. (2019). The potential of microplastics as carriers of metals. Environmental Pollution, 255, 113363. https://doi.org/10.1016/j.envpol.2019.113363

Gong, J., Kong, T., Li, Y., Li, Q., Li, Z., & Zhang, J. (2018). Biodegradation of Microplastic Derived from Poly(ethylene terephthalate) with Bacterial Whole-Cell Biocatalysts. Polymers, 10(12), 1326. https://doi.org/10.3390/polym10121326

Gong, W., Jiang, M., Han, P., Liang, G., Zhang, T., & Liu, G. (2019). Comparative analysis on the sorption kinetics and isotherms of fipronil on nondegradable and biodegradable microplastics. Environmental Pollution, 254, 112927. https://doi.org/10.1016/j.envpol.2019.07.095

Gong, X., Tian, L., Wang, P., Wang, Z., Zeng, L., & Hu, J. (2023). Microplastic pollution in the groundwater under a bedrock island in the South China Sea. Environmental Research, 239, 117277.

https://doi.org/10.1016/j.envres.2023.117277

Gray, A. D., & Weinstein, J. E. (2017). Size- and shape-dependent effects of microplastic particles on adult daggerblade grass shrimp (*Palaemonetes pugio*). Environmental Toxicology and Chemistry, 36(11), 3074–3080. https://doi.org/10.1002/etc.3881

Grigorescu, Grigore, Iancu, Ghioca, & Ion. (2019). Waste electrical and electronic equipment: A review on the identification methods for polymeric materials. Recycling, 4(3), 32. https://doi.org/10.3390/recycling4030032

Guo, X., Chen, C., & Wang, J. (2019). Sorption of sulfamethoxazole onto six types of microplastics. Chemosphere, 228, 300–308. https://doi.org/10.1016/j.chemosphere.2019.04.155

Guo, X., Liu, Y., & Wang, J. (2019). Sorption of sulfamethazine onto different types of microplastics: A combined experimental and molecular dynamics simulation study. Marine Pollution Bulletin, 145, 547–554. https://doi.org/10.1016/j.marpolbul.2019.06.063

Guo, X., & Wang, J. (2019). The chemical behaviors of microplastics in marine environment: A review. Marine Pollution Bulletin, 142, 1–14. https://doi.org/10.1016/j.marpolbul.2019.03.019

Gupta, M. K., & Bansil, R. (1981). Laser Raman spectroscopy of polyacrylamide. Journal of Polymer Science: Polymer Physics Edition, 19(2), 353–360. https://doi.org/10.1002/pol.1981.180190214

Hahladakis, J. N., Velis, C. A., Weber, R., Iacovidou, E., & Purnell, P. (2018). An overview of chemical additives present in plastics: Migration, release, fate and environmental impact during their use, disposal and recycling. Journal of Hazardous Materials, 344, 179–199. doi.org/10.1016/j.jhazmat.2017.10.014

Hanifpour, A., Bahri-Laleh, N., & Mirmohammadi, S. A. (2019). Silica-grafted poly1-hexene: A new approach to prepare polyethylene/silica nanocomposites. Polymer Composites, 40(3), 1053–1060. https://doi.org/10.1002/pc.24795

Hartmann, N. B., Hüffer, T., Thompson, R. C., Hassellöv, M., Verschoor, A., Daugaard, A. E., Rist, S., Karlsson, T., Brennholt, N., Cole, M., Herrling, M. P., Hess, M. C., Ivleva, N. P., Lusher, A. L., & Wagner, M. (2019). Are We Speaking the Same Language? Recommendations for a Definition and Categorization Framework for Plastic Debris. Environmental Science & Technology, 53(3), 1039–1047. https://doi.org/10.1021/acs.est.8b05297

Hasrod, T., Nuapia, Y. B., & Tutu, H. (2024). The application of transfer machine learning to predict and impute missing sulphate levels in different Acid Mine Drainage treatment plants. Cleaner Water, 2, 100029. https://doi.org/10.1016/j.clwat.2024.100029

Hernandez, L. M., Xu, E. G., Larsson, H. C. E., Tahara, R., Maisuria, V. B., & Tufenkji, N. (2019). Plastic Teabags Release Billions of Microparticles and Nanoparticles into Tea. Environmental Science & Technology, 53(21), 12300–12310. https://doi.org/10.1021/acs.est.9b02540

Ho, Y. S., & McKay, G. (1999). Pseudo-second order model for sorption processes. Process Biochemistry (1991), 34(5), 451–465. https://doi.org/10.1016/S0032-9592(98)00112-5

Hoellein, T., Rojas, M., Pink, A., Gasior, J., & Kelly, J. (2014). Anthropogenic Litter in Urban Freshwater Ecosystems: Distribution and Microbial Interactions. PLoS ONE, 9(6), e98485. https://doi.org/10.1371/journal.pone.0098485

Hou, X., Lv, S., Chen, Z., & Xiao, F. (2018). Applications of Fourier transform infrared spectroscopy technologies on asphalt materials. Measurement, 121, 304–316. https://doi.org/10.1016/j.measurement.2018.03.001

Houssa, C.É. (2003). Minerals in plastics. Bulletin de La Société Royale Des Sciences de Liège, 72(1), 71–80.

Huerta Lwanga, E., Gertsen, H., Gooren, H., Peters, P., Salánki, T., Van Der Ploeg, M., Besseling, E., Koelmans, A. A., & Geissen, V. (2017). Incorporation of microplastics from litter into burrows of Lumbricus terrestris. Environmental Pollution, 220, 523–531. https://doi.org/10.1016/j.envpol.2016.09.096

Hurley, R. R., Lusher, A. L., Olsen, M., & Nizzetto, L. (2018). Validation of a Method for Extracting Microplastics from Complex, Organic-Rich, Environmental Matrices. Environmental Science & Technology, 52(13), 7409–7417. https://doi.org/10.1021/acs.est.8b01517

Ibrahim, Y. S., Tuan Anuar, S., Azmi, A. A., Wan Mohd Khalik, W. M. A., Lehata, S., Hamzah, S. R., Ismail, D., Ma, Z. F., Dzulkarnaen, A., Zakaria, Z., Mustaffa, N., Tuan Sharif, S. E., & Lee, Y. Y. (2021). Detection of microplastics in human colectomy specimens. JGH Open, 5(1), 116–121. https://doi.org/10.1002/jgh3.12457.

Iloms, E., Ololade, O. O., Ogola, H. J. O., & Selvarajan, R. (2020). Investigating Industrial Effluent Impact on Municipal Wastewater Treatment Plant in Vaal, South Africa. International Journal of Environmental Research and Public Health, 17(3), 1096. https://doi.org/10.3390/ijerph17031096

Imhof, H. K., Laforsch, C., Wiesheu, A. C., Schmid, J., Anger, P. M., Niessner, R., & Ivleva, N. P. (2016). Pigments and plastic in limnetic ecosystems: A qualitative and quantitative study on microparticles of different size classes. Water Research, 98, 64–74. https://doi.org/10.1016/j.watres.2016.03.015

Insight Survey. (2021). South African bottled water industry landscape report. https://insightsurvey.co.za/wp-content/uploads/2021/06/South-African-Bottled-Water-Industry-Brochure-2021.pdf

Insight Survey. (2022). South African tea market insights report. https://insightsurvey.co.za/wp-content/uploads/2022/05/SA-Tea-Market-Insights-Report-Brochure-2022-18-May-2022.pdf

International Agency for Research on Cancer (IARC). (2010). Monographs Working Group on the Evaluation of Carcinogenic Risks to Humans. Some aromatic amines, organic dyes, and related exposures. IARC Monogr Eval Carcinog Risks Hum. 2010;99:1-658. PMID: 21528837; PMCID: PMC5046080.

International Water Management Institute (IWMI). (2025). https://conjunctivecooperation.iwmi.org/systems/ramotswa-ngotwane-system/

Islam, S., Apitius, L., Jakob, F., & Schwaneberg, U. (2019). Targeting microplastic particles in the void of diluted suspensions. Environment International, 123, 428–435. doi.org/10.1016/j.envint.2018.12.029

Jéquier, E., & Constant, F. (2010). Water as an essential nutrient: The physiological basis of hydration. European Journal of Clinical Nutrition, 64(2), 115–123. https://doi.org/10.1038/ejcn.2009.111

Jin, M., Wang, X., Ren, T., Wang, J., & Shan, J. (2021). Microplastics contamination in food and beverages: Direct exposure to humans. Journal of Food Science, 86(7), 2816–2837. https://doi.org/10.1111/1750-3841.15802

Jipa, I., Stoica, A., Stroescu, M., Dobre, L.-M., Dobre, T., Jinga, S., & Tardei, C. (2012). Potassium sorbate release from poly(vinyl alcohol)-bacterial cellulose films. Chemical Papers, 66(2). https://doi.org/10.2478/s11696-011-0068-4

Joubert, E., & De Beer, D. (2011). Rooibos (Aspalathus linearis) beyond the farm gate: From herbal tea to potential phytopharmaceutical. South African Journal of Botany, 77(4), 869–886. https://doi.org/10.1016/j.sajb.2011.07.004

Jódar-Reyes, A. B., Ortega-Vinuesa, J. L., & Martín-Rodríguez, A. (2006). Electrokinetic behavior and colloidal stability of polystyrene latex coated with ionic surfactants. Journal of Colloid and Interface Science, 297(1), 170–181. https://doi.org/10.1016/j.jcis.2005.10.033

Kabir, A. H. M. E., Sekine, M., Imai, T., Yamamoto, K., Kanno, A., & Higuchi, T. (2021). Assessing small-scale freshwater microplastics pollution, land-use, source-to-sink conduits, and pollution risks: Perspectives from Japanese rivers polluted with microplastics. Science of The Total Environment, 768, 144655. https://doi.org/10.1016/j.scitotenv.2020.144655.

Kankanige, D., & Babel, S. (2020). Smaller-sized micro-plastics (MPs) contamination in single-use PET-bottled water in Thailand. Science of The Total Environment, 717, 137232. https://doi.org/10.1016/j.scitotenv.2020.137232

Käppler, A., Fischer, D., Oberbeckmann, S., Schernewski, G., Labrenz, M., Eichhorn, K.J., & Voit, B. (2016). Analysis of environmental microplastics by vibrational microspectroscopy: FTIR, Raman or both? Analytical and Bioanalytical Chemistry, 408(29), 8377–8391. https://doi.org/10.1007/s00216-016- 9956-3

Karami, A., Golieskardi, A., Keong Choo, C., Larat, V., Galloway, T. S., & Salamatinia, B. (2017). The presence of microplastics in commercial salts from different countries. Scientific Reports, 7(1), 46173. https://doi.org/10.1038/srep46173

Karami, A., Romano, N., Galloway, T., & Hamzah, H. (2016). Virgin microplastics cause toxicity and modulate the impacts of phenanthrene on biomarker responses in African catfish (*Clarias gariepinus*). Environmental

Research, 151, 58–70. https://doi.org/10.1016/j.envres.2016.07.024

Kemp, T. J., & McIntyre, R. A. (2001). Mechanism of Action of Titanium Dioxide Pigment in the Photodegredation of Poly(Vinyl Chloride) and Other Polymers. Progress in Reaction Kinetics and Mechanism, 26(4), 337–374. https://doi.org/10.3184/007967401103165316

Khan, Md. B., Urmy, S. Y., Setu, S., Kanta, A. H., Gautam, S., Eti, S. A., Rahman, M. M., Sultana, N., Mahmud, S., & Baten, Md. A. (2023). Abundance, distribution and composition of microplastics in sediment and fish species from an Urban River of Bangladesh. Science of The Total Environment, 885, 163876. https://doi.org/10.1016/j.scitotenv.2023.163876

Khan, S. R., Sharma, B., Chawla, P. A., & Bhatia, R. (2022). inductively coupled plasma optical emission spectrometry (ICP-OES): A powerful analytical technique for elemental analysis. Food Analytical Methods, 15(3), 666–688. https://doi.org/10.1007/s12161-021-02148-4

Khumalo, T. (2012). South Africa's tea industry challenges and business strategies: A case study of Ntingwe Tea Estate [University of KwaZulu-Natal]. https://ukzn-dspace.ukzn.ac.za/bitstream/handle/10413/11850/Khumalo_Taurai_2012.pdf?sequence=1&isAllowe d=y

Kim, Y.I., Jeong, E., Lee, J.-Y., Chia, R. W., & Raza, M. (2023). Microplastic contamination in groundwater on a volcanic Jeju Island of Korea. Environmental Research, 226, 115682. https://doi.org/10.1016/j.envres.2023.115682

Koelmans, A. A., Mohamed Nor, N. H., Hermsen, E., Kooi, M., Mintenig, S. M., & De France, J. (2019). Microplastics in freshwaters and drinking water: Critical review and assessment of data quality. Water Research, 155, 410–422. https://doi.org/10.1016/j.watres.2019.02.054

Kosuth, M., Mason, S. A., & Wattenberg, E. V. (2018). Anthropogenic contamination of tap water, beer, and sea salt. PLOS ONE, 13(4), e0194970. https://doi.org/10.1371/journal.pone.0194970.

Kowalski, N., Reichardt, A. M., & Waniek, J. J. (2016). Sinking rates of microplastics and potential implications of their alteration by physical, biological, and chemical factors. Marine Pollution Bulletin, 109(1), 310–319. https://doi.org/10.1016/j.marpolbul.2016.05.064

Kumar, R., Sharma, P., Verma, A., Jha, P. K., Singh, P., Gupta, P. K., Chandra, R., & Prasad, P. V. V. (2021). Effect of physical characteristics and hydrodynamic conditions on transport and deposition of microplastics in riverine ecosystem. Water, 13(19), 2710. https://doi.org/10.3390/w13192710

Kutralam-Muniasamy, G., Pérez-Guevara, F., Elizalde-Martínez, I., & Shruti, V. C. (2020). Branded milks – Are they immune from microplastics contamination? Science of The Total Environment, 714, 136823. https://doi.org/10.1016/j.scitotenv.2020.136823

Lam, T. W. L., Ho, H. T., Ma, A. T. H., & Fok, L. (2020). Microplastic Contamination of Surface Water-Sourced Tap Water in Hong Kong—A Preliminary Study. Applied Sciences, 10(10), 3463. https://doi.org/10.3390/app10103463

Langmuir, I. (1916). The constitution and fundamental properties of solids and liquids. Part i. Solids. Journal of the American Chemical Society, 38(11), 2221–2295. https://doi.org/10.1021/ja02268a002

Latcheman, D. D. S., Richards, H., Madikizela, L. M., Ndungu, K., Newman, B. K., & Chimuka, L. (2024). Occurrence, spatial distribution, and source apportionment of microplastics in Durban Bay, South Africa. Regional Studies in Marine Science, 103496. https://doi.org/10.1016/j.rsma.2024.103496

Lazăr, N.N., Călmuc, M., Milea, Ștefania-A., Georgescu, P.-L., & Iticescu, C. (2024). Micro and nano plastics in fruits and vegetables: A review. Heliyon, 10(6), e28291. https://doi.org/10.1016/j.heliyon.2024.e28291

Lee, J.Y., Cha, J., Ha, K., & Viaroli, S. (2024). Microplastic pollution in groundwater: A systematic review. Environmental Pollutants and Bioavailability, 36(1), 2299545. https://doi.org/10.1080/26395940.2023.2299545

Leketa, K., Abiye, T., Zondi, S., & Butler, M. (2019). Assessing groundwater recharge in crystalline and karstic aquifers of the Upper Crocodile River Basin, Johannesburg, South Africa. Groundwater for Sustainable Development, 8, 31–40. https://doi.org/10.1016/j.gsd.2018.08.002

Lenz, R., Enders, K., Stedmon, C. A., Mackenzie, D. M. A., & Nielsen, T. G. (2015). A critical assessment of visual identification of marine microplastic using Raman spectroscopy for analysis improvement. Marine Pollution Bulletin, 100(1), 82–91. https://doi.org/10.1016/j.marpolbul.2015.09.026.

Lestari, P., Trihadiningrum, Y., Wijaya, B. A., Yunus, K. A., & Firdaus, M. (2020). Distribution of microplastics in Surabaya River, Indonesia. Science of The Total Environment, 726, 138560. https://doi.org/10.1016/j.scitotenv.2020.138560

Li, C., & Zarzycki, P. (2022). A computational pipeline to generate a synthetic dataset of metal ion sorption to oxides for AI/ML exploration. Frontiers in Nuclear Engineering, 1, 977743. https://doi.org/10.3389/fnuen.2022.977743.

Li, Y., Peng, L., Fu, J., Dai, X., & Wang, G. (2022). A microscopic survey on microplastics in beverages: The case of beer, mineral water and tea. The Analyst, 147(6), 1099–1105. https://doi.org/10.1039/D2AN00083K

Li, H., Zhu, L., Ma, M., Wu, H., An, L., & Yang, Z. (2023). Occurrence of microplastics in commercially sold bottled water. Science of The Total Environment, 867, 161553. https://doi.org/10.1016/j.scitotenv.2023.161553

Liebezeit, G., & Liebezeit, E. (2013). Non-pollen particulates in honey and sugar. Food Additives & Contaminants: Part A, 30(12), 2136–2140. https://doi.org/10.1080/19440049.2013.843025

Lim, J.H., Bae, D., & Fong, A. (2018). Titanium Dioxide in Food Products: Quantitative Analysis Using ICP-MS and Raman Spectroscopy. Journal of Agricultural and Food Chemistry, 66(51), 13533–13540. https://doi.org/10.1021/acs.jafc.8b06571

Lin, Z. (2010). Getting Started with PEST. The University of Georgia, Athens, GA.

Liu, H., Liu, K., Fu, H., Ji, R., & Qu, X. (2020a). Sunlight mediated cadmium release from coloured microplastics containing cadmium pigment in aqueous phase. Environmental Pollution, 263,114484. https://doi.org/10.1016/j.envpol.2020.114484

Liu, Y., Zhang, J., Cai, C., He, Y., Chen, L., Xiong, X., Huang, H., Tao, S., & Liu, W. (2020b). Occurrence and characteristics of microplastics in the Haihe River: An investigation of a seagoing river flowing through a megacity in northern China. Environmental Pollution, 262, 114261.

Liu, S., Huang, J., Zhang, W., Shi, L., Yi, K., Zhang, C., Pang, H., Li, J., & Li, S. (2022a). Investigation of the adsorption behavior of Pb(II) onto natural-aged microplastics as affected by salt ions. Journal of Hazardous Materials, 431, 128643. https://doi.org/10.1016/j.jhazmat.2022.128643

Liu, Y., Zhang, K., Xu, S., Yan, M., Tao, D., Chen, L., Wei, Y., Wu, C., Liu, G., & Lam, P. K. S. (2022b). Heavy metals in the “plastisphere” of marine microplastics: Adsorption mechanisms and composite risk. Gondwana Research, 108, 171–180. https://doi.org/10.1016/j.gr.2021.06.017

Lu, P., Zhang, G., Apps, J., & Zhu, C. (2022). Comparison of thermodynamic data files for PHREEQC. Earth-Science Reviews, 225, 103888. https://doi.org/10.1016/j.earscirev.2021.103888

Lu, W., Li, X., Wang, S., Tu, C., Qiu, L., Zhang, H., Zhong, C., Li, S., Liu, Y., Liu, J., & Zhou, Y. (2023). New Evidence of Microplastics in the Lower Respiratory Tract: Inhalation through Smoking. Environmental Science & Technology, 57(23), 8496–8505. https://doi.org/10.1021/acs.est.3c00716

Luo, H., Li, Y., Zhao, Y., Xiang, Y., He, D., & Pan, X. (2020). Effects of accelerated aging on characteristics, leaching, and toxicity of commercial lead chromate pigmented microplastics. Environmental Pollution, 257, 113475. https://doi.org/10.1016/j.envpol.2019.113475

Madikizela, L. M., Nuapia, Y. B., Chimuka, L., Ncube, S., & Etale, A. (2022). Target and Suspect Screening of Pharmaceuticals and their Transformation Products in the Klip River, South Africa, using Ultra-High–Performance Liquid Chromatography–Mass Spectrometry. Environmental Toxicology and Chemistry, 41(2), 437–447. https://doi.org/10.1002/etc.5265.

Mainardi-Remis, J. M., Gutiérrez-Cacciabue, D., Romero, D. S., & Rajal, V. B. (2021). Setting boundaries within a bottled water plant aid to better visualize the water use: An approach through the water footprint indicator. Journal of Water Process Engineering, 43, 102199. https://doi.org/10.1016/j.jwpe.2021.102199

Mak, C. L., Wong, Y. W., & Chan, W. N. (1998). Application of Raman spectroscopy to determine the strain-level in polybutylene terephthalate (PBT). Polymer Testing, 17(6), 451–458. https://doi.org/10.1016/S0142-9418(97)00073-1

Makhdoumi, P., Amin, A. A., Karimi, H., Pirsaheb, M., Kim, H., & Hossini, H. (2021). Occurrence of microplastic particles in the most popular Iranian bottled mineral water brands and an assessment of human exposure. Journal of Water Process Engineering, 39, 101708.

https://doi.org/10.1016/j.jwpe.2020.101708

Manikanda, B. K., Natesan, U., Vaikunth, R., Praveen, K. R., Ruthra, R., & Srinivasalu, S. (2021). Spatial distribution of microplastic concentration around landfill sites and its potential risk on groundwater. Chemosphere, 277, 130263. https://doi.org/10.1016/j.chemosphere.2021.130263

Mao, R., Hu, Y., Zhang, S., Wu, R., & Guo, X. (2020). Microplastics in the surface water of Wuliangsuhai Lake, northern China. Science of The Total Environment, 723, 137820. https://doi.org/10.1016/j.scitotenv.2020.137820

Marine and Environment Research Institute (MERI)., (2015). Guide to microplastic identification. http://static1.squarespace.com/static/55b29de4e4b088f

Martin, N. (2020). Assessing wastewater and sanitation conditions and management in the Ramotswa transboundary aquifer area between South Africa and Botswana.

Masura, J., Baker, J., Foster, G., & Arthur, C. (2015). Laboratory Methods for the Analysis of Microplastics in the Marine Environment: Recommendations for quantifying synthetic particles in waters and sediments.

Mason, S. A., Welch, V. G., & Neratko, J. (2018). Synthetic Polymer Contamination in Bottled Water. Frontiers in Chemistry, 6, 407. https://doi.org/10.3389/fchem.2018.00407

Matías, C. L. (2022). The Role of Polyurethane Chemistry on the Properties of Phenolic Foams Applied in the Thermal Insulation Industry. In S. P.K, S. M.S., & S. Thomas (Eds.), Phenolic Based Foams: Preparation, Characterization, and Applications (pp. 331–357). Springer Nature. https://doi.org/10.1007/978-981-16-5237-0_19

Matlakala, M. E., Kallon, D. V. V., Simelane, S. P., & Mashinini, P. M. (2019). Impact of Design Parameters on the Performance of Centrifugal Pumps. Procedia Manufacturing, 35, 197–206. https://doi.org/10.1016/j.promfg.2019.05.027

McClure, D. J. (2007). POLYESTER (PET) FILM AS A SUBSTRATE: A TUTORIAL.

McGill, B. M., Altchenko, Y., Hamilton, S. K., Kenabatho, P. K., Sylvester, S. R., & Villholth, K. G. (2019). Complex interactions between climate change, sanitation, and groundwater quality: A case study from Ramotswa, Botswana. Hydrogeology Journal, 27(3), 997–1015. https://doi.org/10.1007/s10040-018- 1901-4

Meijer, L. J. J., Van Emmerik, T., Van Der Ent, R., Schmidt, C., & Lebreton, L. (2021). More than 1000 rivers account for 80% of global riverine plastic emissions into the ocean. Science Advances, 7(18), eaaz5803. https://doi.org/10.1126/sciadv.aaz5803

Merga, L. B., Redondo-Hasselerharm, P. E., Van Den Brink, P. J., & Koelmans, A. A. (2020). Distribution of microplastic and small macroplastic particles across four fish species and sediment in an African lake. Science of The Total Environment, 741, 140527. https://doi.org/10.1016/j.scitotenv.2020.140527

Mintenig, S. M., Löder, M. G. J., Primpke, S., & Gerdts, G. (2019). Low numbers of microplastics detected in drinking water from ground water sources. Science of The Total Environment, 648, 631–635. https://doi.org/10.1016/j.scitotenv.2018.08.178

Mochizuki, M., & Matsunaga, N. (2016). Bicomponent polyester fibres for nonwovens. In High-Performance and Specialty Fibres: Concepts, Technology and Modern Applications of Man-Made Fibres for the Future (1–Book, Section, pp. 395–408). https://doi.org/10.1007/978-4-431-55203-1_25

Modisha, R. C. O. (2017). Investigation of the Ramotswa Transboundary Aquifer Area, groundwater flow and pollution [University of the Witwatersrand, Johannesburg]. https://wiredspace.wits.ac.za/server/api/core/bitstreams/216683c5-170a-4085-b10c- d2129cc1ad62/content

Mohammed, A., & Abdullah, A. (2018). Scanning electron microscopy (SEM): A review. 2018, 7–9.

Mokonyama, S., Schalkwyk, M., & Rajagopaul, R. (2017). Guidelines and good practices for water treatment residues handling and reuse in South Africa. 161

Montano, L., Giorgini, E., Notarstefano, V., Notari, T., Ricciardi, M., Piscopo, M., & Motta, O. (2023). Raman Microspectroscopy evidence of microplastics in human semen. Science of The Total Environment, 901, 165922. https://doi.org/10.1016/j.scitotenv.2023.165922

Montano, L., Raimondo, S., Piscopo, M., Ricciardi, M., Guglielmino, A., Chamayou, S., Gentile, R., Gentile, M., Rapisarda, P., Conti, G. O., Ferrante, M., & Motta, O. (2024). First evidence of microplastics in human ovarian follicular fluid: An emerging threat to female fertility. https://doi.org/10.1101/2024.04.04.24305264

Mortensen, N. P., Fennell, T. R., & Johnson, L. M. (2021). Unintended human ingestion of nanoplastics and small microplastics through drinking water, beverages, and food sources. NanoImpact, 21, 100302. https://doi.org/10.1016/j.impact.2021.100302

Mosai, A. K. (2021). Development of functionalised zeolite and bentonite for the recovery of platinum group elements (PGEs) and rare earth elements (REEs) from aqueous systems impacted by mining activities [University of the Witwatersrand, Johannesburg]. https://hdl.handle.net/10539/32393

Mosai, A. K., Johnson, R. H., & Tutu, H. (2024). Recovery of platinum group elements (PGEs) from wastewater: A case for the development of predictive adsorption numerical methods. Minerals Engineering, 217, 108915. https://doi.org/10.1016/j.mineng.2024.108915.

Mu, H., Wang, Y., Zhang, H., Guo, F., Li, A., Zhang, S., Liu, S., & Liu, T. (2022). High abundance of microplastics in groundwater in Jiaodong Peninsula, China. Science of The Total Environment, 839, 156318. https://doi.org/10.1016/j.scitotenv.2022.156318

Mukotaka, A., Kataoka, T., & Nihei, Y. (2021). Rapid analytical method for characterization and quantification of microplastics in tap water using a Fourier-transform infrared microscope. Science of The Total Environment, 790, 148231. https://doi.org/10.1016/j.scitotenv.2021.148231

Muller, M., Schreiner, B., Abri Vermeulen, Taci Reddy, & Maree, G. (2019). Water Security Perspective for the Gauteng City-Region. Securing water for continued growth and well being. https://doi.org/10.13140/RG.2.2.15532.59529

Murphy, J. (2001). Additives for plastics handbook. Elsevier.

National Academies of Sciences, Engineering, and Medicine. (2017). Investigative Strategies for Lead-Source Attribution at Superfund Sites Associated with Mining Activities (p. 24898). National Academies Press. https://doi.org/10.17226/24898

Mutshekwa, T., Munyai, L. F., Mugwedi, L., Cuthbert, R. N., Dondofema, F., & Dalu, T. (2023). Seasonal occurrence of microplastics in sediment of two South African recreational reservoirs. Water Biology and Security, 2(3), 100185. https://doi.org/10.1016/j.watbs.2023.100185

Nel, H. A., Dalu, T., & Wasserman, R. J. (2018). Sinks and sources: Assessing microplastic abundance in river sediment and deposit feeders in an Austral temperate urban river system. Science of The Total Environment, 612, 950–956. https://doi.org/10.1016/j.scitotenv.2017.08.298

Nel, M. (2017). Groundwater: The myths, the truths and the basics. Water Research Commission. https://www.wrc.org.za/wp-content/uploads/mdocs/Groundwater%20book_web.pdf

Novotna, K., Cermakova, L., Pivokonska, L., Cajthaml, T., & Pivokonsky, M. (2019). Microplastics in drinking water treatment – Current knowledge and research needs. Science of The Total Environment, 667, 730–740. https://doi.org/10.1016/j.scitotenv.2019.02.431

Nuelle, M.T., Dekiff, J. H., Remy, D., & Fries, E. (2014). A new analytical approach for monitoring microplastics in marine sediments. Environmental Pollution, 184, 161–169. https://doi.org/10.1016/j.envpol.2013.07.027

Nunes Costa, F., Alex Mayer, D., Valério, A., De Souza Lima, J., De Oliveira, D., & Ulson De Souza, A. A. (2020). Non-isothermal kinetic modelling of potassium indigo-trisulfonate dye discolouration by Horseradish peroxidase. Biocatalysis and Biotransformation, 38(5), 385–391. https://doi.org/10.1080/10242422.2020.1754806

Nyamweya, C., Desjardins, C., Sigurdsson, S., Tomasson, T., Taabu-Munyaho, A., Sitoki, L., & Stefansson, G. (2016). Simulation of Lake Victoria Circulation Patterns Using the Regional Ocean Modeling System (ROMS). PLOS ONE, 11(3), e0151272. https://doi.org/10.1371/journal.pone.0151272.

O'Connor, D., Pan, S., Shen, Z., Song, Y., Jin, Y., Wu, W.-M., & Hou, D. (2019). Microplastics undergo accelerated vertical migration in sand soil due to small size and wet-dry cycles. Environmental Pollution, 249, 527–534. https://doi.org/10.1016/j.envpol.2019.03.092

Okorie, N., Morrison, G., & Enyoh, C. E. (2019). Detecting Counterfeit Beverages using Analytical Techniques related to HPLC/GC/CE. International Journal of Advanced Research in Chemical Science, 6(12), 8–15. https://doi.org/10.20431/2349-0403.0612002

Olayo, M. G., Colín, E., Cruz, G. J., Morales, J., & Olayo, R. (2009). Accelerated nitridation and oxidation by plasma on polyethylene. The European Physical Journal Applied Physics, 48(3), 30501. https://doi.org/10.1051/epjap/2009166

Oliveira, L. C., Botero, W. G., Farias, T. S., Santos, J. C. C., Gabriel, G. V. M., Goveia, D., Cacuro, T. A., & Waldman, W. R. (2019). Application of Natural Organic Residues as Adsorbents to Remove Lead from Waters. Water, Air, & Soil Pollution, 230(8), 191. https://doi.org/10.1007/s11270-019-4240-8

Oni, B. A., Ayeni, A. O., Agboola, O., Oguntade, T., & Obanla, O. (2020). Comparing microplastics contaminants in (dry and raining) seasons for Ox-Bow Lake in Yenagoa, Nigeria. Ecotoxicology and Environmental Safety, 198, 110656. https://doi.org/10.1016/j.ecoenv.2020.110656

Onoja, S., Nel, H. A., Abdallah, M. A.-E., & Harrad, S. (2022). Microplastics in freshwater sediments: Analytical methods, temporal trends, and risk of associated organophosphate esters as exemplar plastics additives. Environmental Research, 203, 111830. https://doi.org/10.1016/j.envres.2021.111830

Oßmann, B. E., Sarau, G., Holtmannspötter, H., Pischetsrieder, M., Christiansen, S. H., & Dicke, W. (2018). Small-sized microplastics and pigmented particles in bottled mineral water. Water Research, 141, 307–316. https://doi.org/10.1016/j.watres.2018.05.027

Pagnacco, M. C., Maksimović, J. P., Nikolić, N. T., Bajuk Bogdanović, D. V., Kragović, M. M., Stojmenović, M. D., Blagojević, S. N., & Senćanski, J. V. (2022). Indigo Carmine in a Food Dye: Spectroscopic Characterization and Determining Its Micro-Concentration through the Clock Reaction. Molecules, 27(15), 4853. https://doi.org/10.3390/molecules27154853

Paige, C. C., & Saunders, M. A. (1982). LSQR: An algorithm for sparse linear equations and sparse least squares. ACM Transactions on Mathematical Software, 8(1), 43–71. https://doi.org/10.1145/355984.355989

Pan, H., Feng, J., He, G.-X., Cerniglia, C. E., & Chen, H. (2012). Evaluation of impact of exposure of Sudan azo dyes and their metabolites on human intestinal bacteria. Anaerobe, 18(4), 445–453. https://doi.org/10.1016/j.anaerobe.2012.05.002

Panno, S. V., Kelly, W. R., Scott, J., Zheng, W., McNeish, R. E., Holm, N., Hoellein, T. J., & Baranski, E. L. (2019). Microplastic contamination in karst groundwater systems. Groundwater, 57(2), 189–196. https://doi.org/10.1111/gwat.12862

Paray, B. A., Yu, J., Sultana, S., Banik, P., Nur, A.-A. U., Haque, Md. R., Rahman, Md. M., Arai, T., Yan, L., & Hossain, M. B. (2024). Contamination, morphological and chemical characterization, and hazard risk analyses of microplastics in drinking water sourced from groundwater in a developing nation. Frontiers in Environmental Science, 12, 1379311. https://doi.org/10.3389/fenvs.2024.1379311

Park, H., & Park, B. (2021). Review of Microplastic Distribution, Toxicity, Analysis Methods, and Removal Technologies. Water, 13(19), 2736. https://doi.org/10.3390/w13192736

Park, S., Yim, C., Lee, B. H., & Choe, S. (2005). Properties of the blends of ethylene-vinyl acetate and ethylene-α-olefins copolymers. Macromolecular Research, 13(3), 243–252. https://doi.org/10.1007/BF03219059

Park, T.J., Lee, S.-H., Lee, M.-S., Lee, J.-K., Lee, S.-H., & Zoh, K.-D. (2020). Occurrence of microplastics in the Han River and riverine fish in South Korea. Science of The Total Environment, 708, 134535. https://doi.org/10.1016/j.scitotenv.2019.134535

Parkhurst, D. K., & Appelo, C. A. J. (2013). Description of input and examples for PHREEQC Version 3—A Computer Program for Speciation, Batch-Reaction, One-Dimensional Transport, and Inverse Geochemical Calculations. In U.S. Geological Survey Techniques and Methods (p. 497). http://pubs.usgs.gov/tm/06/a43/

Parnell, S., Min, K., & Cakmak, M. (2003). Kinetic studies of polyurethane polymerization with Raman spectroscopy. Polymer, 44(18), 5137–5144. https://doi.org/10.1016/S0032-3861(03)00468-3

Patterson, J., Laju, R. L., Jeyasanta, K. I., Shelciya, S., Esmeralda, V. G., Asir, N. G. G., Narmatha, M., & Booth, A. M. (2023). Hydrochemical quality and microplastic levels of the groundwaters of Tuticorin, southeast coast of India. Hydrogeology Journal, 31(1), 167–184. https://doi.org/10.1007/s10040-022- 02582-6

Peltzer, M. A., & Simoneau, C. (2013). Report of an inter-laboratory comparison from the European Reference Laboratory for Food Contact Materials: ILC 002 2013 : identification of polymeric materials. Publications Office. https://data.europa.eu/doi/10.2788/6233

Peñalver, R., Zapata, F., Arroyo-Manzanares, N., López-García, I., & Viñas, P. (2023). Raman spectroscopic strategy for the discrimination of recycled polyethylene terephthalate in water bottles. Journal of Raman Spectroscopy, 54(1), 107–112. https://doi.org/10.1002/jrs.6457

Pham, D. T., Kim, J., Lee, S.-H., Kim, J., Kim, D., Hong, S., Jung, J., & Kwon, J.-H. (2023). Analysis of microplastics in various foods and assessment of aggregate human exposure via food consumption in Korea. Environmental Pollution, 322, 121153. https://doi.org/10.1016/j.envpol.2023.121153

Pivokonsky, M., Cermakova, L., Novotna, K., Peer, P., Cajthaml, T., & Janda, V. (2018). Occurrence of microplastics in raw and treated drinking water. Science of The Total Environment, 643, 1644–1651. https://doi.org/10.1016/j.scitotenv.2018.08.102

PlasticsEurope., (2021). Plastics-the Facts 2021 An analysis of European plastics production, demand and waste data. https://plasticseurope.org/wp-content/uploads/2021/12/Plastics-the-Facts-2021-web- final.pdf

Popkin, B. M., D’Anci, K. E., & Rosenberg, I. H. (2010). Water, hydration, and health. Nutrition Reviews, 68(8), 439–458. https://doi.org/10.1111/j.1753-4887.2010.00304.x.

Powell, K. J., Brown, P. L., Byrne, R. H., Gajda, T., Hefter, G., Leuz, A.-K., Sjöberg, S., & Wanner, H. (2009). Chemical speciation of environmentally significant metals with inorganic ligands. Part 3: The Pb2+ + $OH^{–}$, $Cl^{–}$, $CO_3^{2–}$, SO_4^{2-}, and PO_4^{2-} systems (IUPAC Technical Report). Pure and Applied Chemistry, 81(12), 2425–2476. https://doi.org/10.1351/PAC-REP-09-03-05

Prata, J. C., Paço, A., Reis, V., Da Costa, J. P., Fernandes, A. J. S., Da Costa, F. M., Duarte, A. C., & Rocha-Santos, T. (2020). Identification of microplastics in white wines capped with polyethylene stoppers using micro-Raman spectroscopy. Food Chemistry, 331, 127323. https://doi.org/10.1016/j.foodchem.2020.127323

Pratesi, C. B., A. L. Santos Almeida, M. A., Cutrim Paz, G. S., Ramos Teotonio, M. H., Gandolfi, L., Pratesi, R., Hecht, M., & Zandonadi, R. P. (2021). Presence and quantification of microplastic in urban tap water: A pre-screening in Brasilia, Brazil. Sustainability, 13(11), 6404. https://doi.org/10.3390/su13116404

Puchowicz, D., & Cieslak, M. (2022). Raman Spectroscopy in the Analysis of Textile Structures. In C. Shakher Pathak & S. Kumar (Eds.), Recent Developments in Atomic Force Microscopy and Raman Spectroscopy for Materials Characterization. IntechOpen. https://doi.org/10.5772/intechopen.99731

Qi, K., Lu, N., Zhang, S., Wang, W., Wang, Z., & Guan, J. (2021). Uptake of Pb(II) onto microplastic-associated biofilms in freshwater: Adsorption and combined toxicity in comparison to natural solid substrates. Journal of Hazardous Materials, 411, 125115. https://doi.org/10.1016/j.jhazmat.2021.125115

Qiao, R., Deng, Y., Zhang, S., Wolosker, M. B., Zhu, Q., Ren, H., & Zhang, Y. (2019). Accumulation of different shapes of microplastics initiates intestinal injury and gut microbiota dysbiosis in the gut of zebrafish. Chemosphere, 236, 124334. https://doi.org/10.1016/j.chemosphere.2019.07.065

Qiu, Q., Peng, J., Yu, X., Chen, F., Wang, J., & Dong, F. (2015). Occurrence of microplastics in the coastal marine environment: First observation on sediment of China. Marine Pollution Bulletin, 98(1–2), 274–280. https://doi.org/10.1016/j.marpolbul.2015.07.028

Qiu, Q., Tan, Z., Wang, J., Peng, J., Li, M., & Zhan, Z. (2016). Extraction, enumeration and identification methods for monitoring microplastics in the environment. Estuarine, Coastal and Shelf Science, 176, 102–109. https://doi.org/10.1016/j.ecss.2016.04.012

Quintero Balbas, D., Lanterna, G., Cirrincione, C., Ricci, M., Becucci, M., Fontana, R., & Striova, J. (2022). Noninvasive identification of turmeric and saffron dyes in proteinaceous textile fibres using Raman spectroscopy and multivariate analysis. Journal of Raman Spectroscopy, 53(3), 593–607. https://doi.org/10.1002/jrs.6175

Ragusa, A., Svelato, A., Santacroce, C., Catalano, P., Notarstefano, V., Carnevali, O., Papa, F., Rongioletti, M. C. A., Baiocco, F., Draghi, S., D’Amore, E., Rinaldo, D., Matta, M., & Giorgini, E. (2021). Plasticenta: First evidence of microplastics in human placenta. Environment International, 146, 106274. https://doi.org/10.1016/j.envint.2020.106274

Rajendran, S., Veerasimman, A., Vairavan, M., Shanmugam, V., & Rajendran, D. J. J. (2020). Mechanical Performance Studies on Composites Using Polyethylene Terephthalate Char Derived from

Polyethylene terephthalate waste bottle–reinforced polyester composites. materials performance and characterization, 9(1), 726–738. https://doi.org/10.1520/MPC20190066

Rand Water. (2022). Integrated Annual Report 2022. https://www.randwater.co.za/media/comm_pdf/INTEGRATED%20ANNUAL%20REPORT%202022.p df

Ramaremisa, G., Ndlovu, M., & Saad, D. (2022). Comparative Assessment of Microplastics in Surface Waters and Sediments of the Vaal River, South Africa: Abundance, Composition, and Sources. Environmental Toxicology and Chemistry, 41(12), 3029–3040. https://doi.org/10.1002/etc.5482

Ramaremisa, G., Tutu, H., & Saad, D. (2024). Detection and characterisation of microplastics in tap water from Gauteng, South Africa. Chemosphere, 356, 141903. https://doi.org/10.1016/j.chemosphere.2024.141903

Ramos-Corella, K. J., Sotelo-Lerma, M., Gil-Salido, A. A., Rubio-Pino, J. L., Auciello, O., & Quevedo-López, M. A. (2019). Controlling crystalline phase of TiO_2 thin films to evaluate its biocompatibility. Materials Technology, 34(8), 455–462. https://doi.org/10.1080/10667857.2019.1576821

Re, V. (2019). Shedding light on the invisible: Addressing the potential for groundwater contamination by plastic microfibres. Hydrogeology Journal, 27(7), 2719–2727. https://doi.org/10.1007/s10040-019- 01998-x

Ricci, M., Lofrumento, C., Becucci, M., & Castellucci, E. M. (2018). The Raman and SERS spectra of indigo and indigo-Ag2 complex: DFT calculation and comparison with experiment. Spectrochimica Acta Part A: Molecular and Biomolecular Spectroscopy, 188, 141–148. https://doi.org/10.1016/j.saa.2017.06.036

Richard, H., Carpenter, E. J., Komada, T., Palmer, P. T., & Rochman, C. M. (2019). Biofilm facilitates metal accumulation onto microplastics in estuarine waters. Science of The Total Environment, 683, 600– 608. https://doi.org/10.1016/j.scitotenv.2019.04.331

Rodrigues, M. O., Gonçalves, A. M. M., Gonçalves, F. J. M., Nogueira, H., Marques, J. C., & Abrantes, N. (2018). Effectiveness of a methodology of microplastics isolation for environmental monitoring in freshwater systems. Ecological Indicators, 89, 488–495. https://doi.org/10.1016/j.ecolind.2018.02.038

Saad, D., & Alamin, H. (2024). The first evidence of microplastic presence in the River Nile in Khartoum, Sudan: Using Nile Tilapia fish as a bio-indicator. Heliyon, 10(1), e23393. https://doi.org/10.1016/j.heliyon 2023.e23393

Saad, D., Chauke, P., Cukrowska, E., Richards, H., Nikiema, J., Chimuka, L., & Tutu, H. (2022). First biomonitoring of microplastic pollution in the Vaal river using Carp fish (Cyprinus carpio) “as a bio- indicator”. Science of The Total Environment, 836, 155623. https://doi.org/10.1016/j.scitotenv.2022.155623

Saad, D., Ramaremisa, G., Ndlovu, M., Chauke, P., Nikiema, J., & Chimuka, L. (2024). Microplastic Abundance and Sources in Surface Water Samples of the Vaal River, South Africa. Bulletin of Environmental Contamination and Toxicology, 112(1), 23. https://doi.org/10.1007/s00128-023- 03845-y

Samandra, S., Johnston, J. M., Jaeger, J. E., Symons, B., Xie, S., Currell, M., Ellis, A. V., & Clarke, B. O. (2022). Microplastic contamination of an unconfined groundwater aquifer in Victoria, Australia. Science of The Total Environment, 802, 149727. https://doi.org/10.1016/j.scitotenv.2021.149727

Sangkham, S., Aminul Islam, Md., Adhikari, S., Kumar, R., Sharma, P., Sakunkoo, P., Bhattacharya, P., & Tiwari, A. (2023). Evidence of microplastics in groundwater: A growing risk for human health. Groundwater for Sustainable Development, 23, 100981. https://doi.org/10.1016/j.gsd.2023.100981

Scherrer, N. C., Stefan, Z., Francoise, D., Annette, F., & Renate, K. (2009). Synthetic organic pigments of the 20th and 21st century relevant to artist’s paints: Raman spectra reference collection. Spectrochimica Acta Part A: Molecular and Biomolecular Spectroscopy, 73(3), 505–524. https://doi.org/10.1016/j.saa.2008.11.029

Schwabl, P., Köppel, S., Königshofer, P., Bucsics, T., Trauner, M., Reiberger, T., & Liebmann, B. (2019). Detection of Various Microplastics in Human Stool: A Prospective Case Series. Annals of Internal Medicine, 171(7), 453–457. https://doi.org/10.7326/M19-0618

Schymanski, D., Goldbeck, C., Humpf, H.-U., & Fürst, P. (2018). Analysis of microplastics in water by micro-Raman spectroscopy: Release of plastic particles from different packaging into mineral water. Water Research, 129, 154–162. https://doi.org/10.1016/j.watres.2017.11.011.

Sadan, Z., & De Kock, L. (2020). Plastics: Facts and Futures: Moving beyond pollution management towards a circular plastics economy in South Africa. World Wide Fund for Nature, Cape Town, South Africa. https://wwfafrica.awsassets.panda.org/downloads/wwf_plastics_report_final_2nov2020.pdf

Sekudewicz, I., Dąbrowska, A. M., & Syczewski, M. D. (2021). Microplastic pollution in surface water and sediments in the urban section of the Vistula River (Poland). Science of The Total Environment, 762, 143111. https://doi.org/10.1016/j.scitotenv.2020.143111

Selvam, S., Jesuraja, K., Venkatramanan, S., Roy, P. D., & Jeyanthi Kumari, V. (2021). Hazardous microplastic characteristics and its role as a vector of heavy metal in groundwater and surface water of coastal south India. Journal of Hazardous Materials, 402, 123786. https://doi.org/10.1016/j.jhazmat.2020.123786

Sewwandi, M., Wijesekara, H., Rajapaksha, A. U., Soysa, S., & Vithanage, M. (2023). Microplastics and plastics-associated contaminants in food and beverages; Global trends, concentrations, and human exposure. Environmental Pollution, 317, 120747. https://doi.org/10.1016/j.envpol.2022.120747

Sharma, S., & Chatterjee, S. (2017). Microplastic pollution, a threat to marine ecosystem and human health: A short review. Environmental Science and Pollution Research, 24(27), 21530–21547. https://doi.org/10.1007/s11356-017-9910-8.

Shehu, Z., Nyakairu, G. W. A., Tebandeke, E., & Odume, O. N. (2022). Overview of African water resources contamination by contaminants of emerging concern. Science of The Total Environment, 852, 158303. https://doi.org/10.1016/j.scitotenv.2022.158303

Shinohara, H., Yamakita, Y., & Ohno, K. (1998). Raman spectra of polycyclic aromatic hydrocarbons. Comparison of calculated Raman intensity distributions with observed spectra for naphthalene, anthracene, pyrene, and perylene. Journal of Molecular Structure, 442(1–3), 221–234. https://doi.org/10.1016/S0022-2860(97)00335-9

Shruti, V. C., Pérez-Guevara, F., Elizalde-Martínez, I., & Kutralam-Muniasamy, G. (2020). First study of its kind on the microplastic contamination of soft drinks, cold tea and energy drinks—Future research and environmental considerations. Science of The Total Environment, 726, 138580. https://doi.org/10.1016/j.scitotenv.2020.138580

Shruti, V. C., Pérez-Guevara, F., Elizalde-Martínez, I., & Kutralam-Muniasamy, G. (2021). Toward a unified framework for investigating micro(nano)plastics in packaged beverages intended for human consumption. Environmental Pollution, 268, 115811. https://doi.org/10.1016/j.envpol.2020.115811

Shruti, V. C., Pérez-Guevara, F., & Kutralam-Muniasamy, G. (2020). Metro station free drinking water fountain- A potential "microplastics hotspot" for human consumption. Environmental Pollution, 261, 114227. https://doi.org/10.1016/j.envpol.2020.114227

Singh, R. L., Singh, P. K., & Singh, R. P. (2015). Enzymatic decolorization and degradation of azo dyes – A review. International Biodeterioration & Biodegradation, 104, 21–31. https://doi.org/10.1016/j.ibiod.2015.04.027

Smith, B. C. (2021). The Infrared Spectra of Polymers III: Hydrocarbon Polymers. Spectroscopy, 36(11), 22–25. https://doi.org/10.56530/spectroscopy.mh7872q7

Sneddon, J., & Vincent, M. D. (2008). ICP-OES and ICP-MS for the Determination of Metals: Application to Oysters. Analytical Letters, 41(8), 1291–1303. https://doi.org/10.1080/00032710802013991

Socas-Hernández, C., Miralles, P., González-Sálamo, J., Hernández-Borges, J., & Coscollà, C. (2024). Assessment of anthropogenic particles content in commercial beverages. Food Chemistry, 447, 139002. https://doi.org/10.1016/j.foodchem.2024.139002

Song, Y. K., Hong, S. H., Jang, M., Han, G. M., Rani, M., Lee, J., & Shim, W. J. (2015). A comparison of microscopic and spectroscopic identification methods for analysis of microplastics in environmental samples. Marine Pollution Bulletin, 93(1–2), 202–209. https://doi.org/10.1016/j.marpolbul.2015.01.015

Song, S., Van Dijk, F., Vasse, G. F., Liu, Q., Gosselink, I. F., Weltjens, E., Remels, A. H. V., De Jager, M. H., Bos, S., Li, C., Stoeger, T., Rehberg, M., Kutschke, D., Van Eck, G. W. A., Wu, X., Willems, S. H., Boom, D. H. A., Kooter, I. M., Spierings, D., … Melgert, B. N. (2024). Inhalable Textile Microplastic Fibres Impair Airway Epithelial Differentiation. American Journal of Respiratory and Critical Care Medicine, 209(4), 427–443. https://doi.org/10.1164/rccm.202211-2099OC

South African Human Rights Commission [SAHRC], (2021). Final Report of the Gauteng Provincial Inquiry into the Sewage Problem of the Vaal River.

South African Rooibos Council, (2023). Industry statistics https://sarooibos.co.za/industry-statistics/

South African National Bottled Water Association (SANBWA). (2021). The SANBWA standard. https://www.sanbwa.org.za/wp-content/uploads/2021/07/The-SANBWA-Standard.pdf

South African National Bottled Water Association (SANBWA). (2023). What is bottled water, and what is not? https://www.sanbwa.org.za/categories-of-bottled-water.html

South African Breweries (SAB). (2020).https://www.sab.co.za/brands/local

Statistics South Africa (StatsSA). (2023).Statistical release P0141: Consumer Price Index. https://www.statssa.gov.za/publications/P0141/P0141May2023.pdf

Su, L., Xue, Y., Li, L., Yang, D., Kolandhasamy, P., Li, D., & Shi, H. (2016). Microplastics in Taihu Lake, China. Environmental Pollution, 216, 711–719. https://doi.org/10.1016/j.envpol.2016.06.036

Swanepoel, A., Preez, H. du, & Bouwman, H. (2023). A baseline study on the prevalence of microplastics in South African drinking water: From source to distribution. Water SA, 49(4 October), Article 4 October. https://doi.org/10.17159/wsa/2023.v49.i4.3998

Tagg, A. S., Sapp, M., Harrison, J. P., & Ojeda, J. J. (2015). Identification and Quantification of Microplastics in Wastewater Using Focal Plane Array-Based Reflectance Micro-FT-IR Imaging. Analytical Chemistry, 87(12), 6032–6040. https://doi.org/10.1021/acs.analchem.5b00495

Tan, X., Yu, X., Cai, L., Wang, J., & Peng, J. (2019). Microplastics and associated PAHs in surface water from the Feilaixia Reservoir in the Beijiang River, China. Chemosphere, 221, 834–840. https://doi.org/10.1016/j.chemosphere.2019.01.022

Tang, S., Lin, L., Wang, X., Feng, A., & Yu, A. (2020). Pb(II) uptake onto nylon microplastics: Interaction mechanism and adsorption performance. Journal of Hazardous Materials, 386, 121960. https://doi.org/10.1016/j.jhazmat.2019.121960

Tempelhoff, J., Munik, V., & Viljoen, M. (2007). The Vaal River Barrage, South Africa’s hardest working water way: An historical contemplation·. The Journal for Transdisciplinary Research in Southern Africa, 3(1). https://doi.org/10.4102/td.v3i1.322

Tham, D. Q., Tuan, V. M., Thanh, D. T. M., Chinh, N. T., Giang, N. V., Trang, N. T. T., Hang, T. T. X., Huong, H. T., Dung, N. T. K., & Hoang, T. (2015). Preparation and properties of ethylene vinyl acetate copolymer/silica nanocomposites in presence of EVA-g-Acrylic acid. Journal of Nanoscience and Nanotechnology, 15(4), 2777–2784. https://doi.org/10.1166/jnn.2015.9209

Tintor, Đ., Ninković, K., Milošević, J., & Polović, N. Đ. (2024). Gaining insight into protein structure via ATR-FTIR spectroscopy. Vibrational Spectroscopy, 134, 103726. https://doi.org/10.1016/j.vibspec.2024.103726

Tomasini, E. P., Halac, E. B., Reinoso, M., Di Liscia, E. J., & Maier, M. S. (2012). Micro-Raman spectroscopy of carbon-based black pigments. Journal of Raman Spectroscopy, 43(11), 1671–1675. https://doi.org/10.1002/jrs.4159

Tong, H., Jiang, Q., Hu, X., & Zhong, X. (2020). Occurrence and identification of microplastics in tap water from China. Chemosphere, 252, 126493. https://doi.org/10.1016/j.chemosphere.2020.126493.

Tourinho, P. S., Kočí, V., Loureiro, S., & Van Gestel, C. A. M. (2019). Partitioning of chemical contaminants to microplastics: Sorption mechanisms, environmental distribution and effects on toxicity and bioaccumulation. Environmental Pollution, 252, 1246–1256. https://doi.org/10.1016/j.envpol.2019.06.030

Tsochatzis, E. D., Alberto Lopes, J., Kappenstein, O., Tietz, T., & Hoekstra, E. J. (2020). Quantification of PET cyclic and linear oligomers in teabags by a validated LC-MS method – In silico toxicity assessment and consumer’s exposure. Food Chemistry, 317, 126427. https://doi.org/10.1016/j.foodchem.2020.126427

Turner, A., & Holmes, L. A. (2015). Adsorption of trace metals by microplastic pellets in fresh water. Environmental Chemistry, 12(5), 600. https://doi.org/10.1071/EN14143

Twinkle, Singh, K., Bansal, S. A., & Kumar, S. (2019). Graphene oxide (GO)/Copper doped Hematite (α - Fe_2O_3) nanoparticles for organic pollutants degradation applications at room temperature and neutral pH. Materials Research Express, 6(11), 115026. https://doi.org/10.1088/2053-1591/ab4459

Vakros, J., Kordulis, C., & Lycourghiotis, A. (2002). Potentiometric mass titrations: A quick scan for determining the point of zero charge. Chemical Communications, 17, 1980–1981. https://doi.org/10.1039/b205398e

Van Cauwenberghe, L., Devriese, L., Galgani, F., Robbens, J., & Janssen, C. R. (2015). Microplastics in sediments: A review of techniques, occurrence and effects. Marine Environmental Research, 111, 5–17. https://doi.org/10.1016/j.marenvres.2015.06.007

Van Cauwenberghe, L., & Janssen, C. R. (2014). Microplastics in bivalves cultured for human consumption. Environmental Pollution, 193, 65–70. https://doi.org/10.1016/j.envpol.2014.06.010

Vega-Garcia, P., Schwerd, R., Schwitalla, C., Johann, S., Scherer, C., & Helmreich, B. (2021). Leaching prediction for vertical test panels coated with plaster and mortars exposed under real conditions by a PHREEQC leaching model. Chemosphere, 280, 130657. https://doi.org/10.1016/j.chemosphere.2021.130657

Verlag W. Sachon (2020). A portrait of the South African beer industry. https://blog.drinktec.com/beer/south-african-beer-industry/

Velzeboer, I., Kwadijk, C. J. A. F., & Koelmans, A. A. (2014). Strong Sorption of PCBs to Nanoplastics, Microplastics, Carbon Nanotubes, and Fullerenes. Environmental Science & Technology, 48(9), 4869–4876. https://doi.org/10.1021/es405721v

Vernon-Parry, K. D. (2000). Scanning electron microscopy: An introduction. III-Vs Review, 13(4), 40–44. https://doi.org/10.1016/S0961-1290(00)80006-X

Verster, C., & Bouwman, H. (2020). Land-based sources and pathways of marine plastics in a South African context. South African Journal of Science, 116(5/6). https://doi.org/10.17159/sajs.2020/7700

Vethaak, A. D., & Leslie, H. A. (2016). Plastic Debris Is a Human Health Issue. Environmental Science & Technology, 50(13), 6825–6826. https://doi.org/10.1021/acs.est.6b02569.

Vilakati, B., Sivasankar, V., Nyoni, H., Mamba, B. B., Omine, K., & Msagati, T. A. M. (2021). The Py – GC-TOF-MS analysis and characterization of microplastics (MPs) in a wastewater treatment plant in Gauteng Province, South Africa. Ecotoxicology and Environmental Safety, 222, 112478. https://doi.org/10.1016/j.ecoenv.2021.112478

Völker, C., Kramm, J., & Wagner, M. (2020). On the Creation of Risk: Framing of Microplastics Risks in Science and Media. Global Challenges, 4(6), 1900010. https://doi.org/10.1002/gch2.201900010

Volkov, V. V., Chelli, R., Righini, R., & Perry, C. C. (2020). Indigo chromophores and pigments: Structure and dynamics. Dyes and Pigments, 172, 107761. https://doi.org/10.1016/j.dyepig.2019.107761

Volmer, M. (1925). Thermodynamische Folgerungen ans der Zustandsgleichung für adsorbierte Stoffe. Zeitschrift für Physikalische Chemie, 115U(1), 253–260. https://doi.org/10.1515/zpch-1925-11519 Vorster, H., Badham, J., Venter, C., (2013). An introduction to the revised food-based dietary guidelines for South Africa. S. Afr. J. Clin. Nutr. 26(S), S5-S12. http://sajcn.co.za/index.php/SAJCN/article/view/740 Wakelyn, P. J. (2007). 14—Health and safety issues in cotton production and processing. S. Gordon & Y.-L. Hsieh (Eds.), Cotton (pp. 460–483). Woodhead Publishing. https://doi.org/10.1533/9781845692483.3.460

Walker, T. R. (2021). (Micro)plastics and the UN Sustainable Development Goals. Current opinion in green and sustainable chemistry, 30, 100497. https://doi.org/10.1016/j.cogsc.2021.100497

Wan, Y., Chen, X., Liu, Q., Hu, H., Wu, C., & Xue, Q. (2022). Informal landfill contributes to the pollution of microplastics in the surrounding environment. Environmental Pollution, 293, 118586. https://doi.org/10.1016/j.envpol.2021.118586

Wang, F., Yang, W., Cheng, P., Zhang, S., Zhang, S., Jiao, W., & Sun, Y. (2019). Adsorption characteristics of cadmium onto microplastics from aqueous solutions. Chemosphere, 235, 1073–1080. https://doi.org/10.1016/j.chemosphere.2019.06.196

Wang, J., & Guo, X. (2020). Adsorption isotherm models: Classification, physical meaning, application and solving method. Chemosphere, 258, 127279. https://doi.org/10.1016/j.chemosphere.2020.127279

Wang, K., & Deng, Q. (2019). The Thermal and Mechanical Properties of Poly(ethylene-co-vinyl acetate) Random Copolymers (PEVA) and its Covalently Crosslinked Analogues (cPEVA). Polymers, 11(6), 1055. https://doi.org/10.3390/polym11061055.

Wang, L., Wu, W.-M., Bolan, N. S., Tsang, D. C. W., Li, Y., Qin, M., & Hou, D. (2021). Environmental fate, toxicity and risk management strategies of nanoplastics in the environment: Current status and future perspectives. Journal of Hazardous Materials, 401, 123415. https://doi.org/10.1016/j.jhazmat.2020.123415

Wang, W., Ndungu, A. W., Li, Z., & Wang, J. (2017). Microplastics pollution in inland freshwaters of China: A case study in urban surface waters of Wuhan, China. Science of The Total Environment, 575, 1369– 1374. https://doi.org/10.1016/j.scitotenv.2016.09.213.

Weakley, A. T., Warwick, P. C. T., Bitterwolf, T. E., & Aston, D. E. (2012). Multivariate Analysis of Micro-Raman Spectra of Thermoplastic Polyurethane Blends Using Principal Component Analysis and Principal Component Regression. Applied Spectroscopy, 66(11), 1269–1278. https://doi.org/10.1366/12-06588

Weideman, E. A., Perold, V., & Ryan, P. G. (2019). Little evidence that dams in the Orange–Vaal River system trap floating microplastics or microfibres. Marine Pollution Bulletin, 149, 110664. https://doi.org/10.1016/j.marpolbul.2019.110664

Weideman, E. A., Perold, V., & Ryan, P. G. (2020). Limited long-distance transport of plastic pollution by the Orange-Vaal River system, South Africa. Science of The Total Environment, 727, 138653. https://doi.org/10.1016/j.scitotenv.2020.138653

Weisser, J., Beer, I., Hufnagl, B., Hofmann, T., Lohninger, H., Ivleva, N. P., & Glas, K. (2021). From the Well to the Bottle: Identifying Sources of Microplastics in Mineral Water. Water, 13(6), 841. https://doi.org/10.3390/w13060841

Welz, P. J., Linganiso, L. Z., Murray, P., Kumari, S., Arthur, G. D., Ranjan, A., Collins, C., & Bakare, B. F. (2022). Status quo and sector readiness for (bio)plastic food and beverage packaging in the 4IR. South African Journal of Science, 118(7/8). https://doi.org/10.17159/sajs.2022/9748

Wenhold, F., & Faber, M. (2009). Water in nutritional health of individuals and households: An overview. Water SA, 35(1). http://www.wrc.org.za.

Wepener, V., Van Dyk, C., Bervoets, L., O'Brien, G., Covaci, A., & Cloete, Y. (2011). An assessment of the influence of multiple stressors on the Vaal River, South Africa. Physics and Chemistry of the Earth, Parts A/B/C, 36(14–15), 949–962. https://doi.org/10.1016/j.pce.2011.07.075

Wiggins, K. M., & Bielawski, C. W. (2013). Synthesis of poly(ethylene-co-acrylic acid) via a tandem hydrocarboxylation/hydrogenation of poly(butadiene). Polym. Chem., 4(7), 2239–2245. https://doi.org/10.1039/C2PY20855E

Wijesekara, H., Bolan, N. S., Bradney, L., Obadamudalige, N., Seshadri, B., Kunhikrishnan, A., Dharmarajan, R., Ok, Y. S., Rinklebe, J., Kirkham, M. B., & Vithanage, M. (2018). Trace element dynamics of biosolids-derived microbeads. Chemosphere, 199, 331–339. https://doi.org/10.1016/j.chemosphere.2018.01.166

World Health Organization (WHO). (2022). Guidelines for drinking-water quality: fourth edition incorporating the first and second addenda. Geneva. https://iris.who.int/bitstream/handle/10665/352532/9789240045064-eng.pdf?sequence=1

Wright, S. L., & Kelly, F. J. (2017). Plastic and Human Health: A Micro Issue? Environmental Science & Technology, 51(12), 6634–6647. https://doi.org/10.1021/acs.est.7b00423

Wu, P., Huang, J., Zheng, Y., Yang, Y., Zhang, Y., He, F., Chen, H., Quan, G., Yan, J., Li, T., & Gao, B. (2019). Environmental occurrences, fate, and impacts of microplastics. Ecotoxicology and Environmental Safety, 184, 109612. https://doi.org/10.1016/j.ecoenv.2019.109612.

Xiong, X., Zhang, K., Chen, X., Shi, H., Luo, Z., & Wu, C. (2018). Sources and distribution of microplastics in China's largest inland lake – Qinghai Lake. Environmental Pollution, 235, 899–906. https://doi.org/10.1016/j.envpol.2017.12.081

Xu, H., Heinze, T. M., Paine, D. D., Cerniglia, C. E., & Chen, H. (2010). Sudan azo dyes and Para Red degradation by prevalent bacteria of the human gastrointestinal tract. Anaerobe, 16(2), 114–119. https://doi.org/10.1016/j.anaerobe.2009.06.007

Xu, J.L., Lin, X., Hugelier, S., Herrero-Langreo, A., & Gowen, A. A. (2021). Spectral imaging for characterization and detection of plastic substances in branded teabags. Journal of Hazardous Materials, 418, 126328. https://doi.org/10.1016/j.jhazmat.2021.126328

Yurtsever, M. (2021). Are nonwoven fabrics used in foods made of cellulose or plastic? Cellulose/plastic separation by using Schweizer's reagent and analysis based on a sample of tea bags. Process Safety and Environmental Protection, 151, 188–194. https://doi.org/10.1016/j.psep.2021.05.016

Zavarin, M., Chang, E., Wainwright, H., Parham, N., Kaukuntla, R., Zouabe, J., Deinhart, A., Genetti, V., Shipman, S., Bok, F., & Brendler, V. (2022). Community Data Mining Approach for Surface Complexation Database Development. Environmental Science & Technology, 56(4), 2827–2838. https://doi.org/10.1021/acs.est.1c07109

Zhang, H., Wang, J., Zhou, B., Zhou, Y., Dai, Z., Zhou, Q., Chriestie, P., & Luo, Y. (2018). Enhanced adsorption of oxytetracycline to weathered microplastic polystyrene: Kinetics, isotherms and influencing factors. Environmental Pollution, 243, 1550–1557. https://doi.org/10.1016/j.envpol.2018.09.122

Zhang, J., Wang, L., Trasande, L., & Kannan, K. (2021a). Occurrence of Polyethylene Terephthalate and Polycarbonate Microplastics in Infant and Adult Feces. Environmental Science & Technology Letters, 8(11), 989–994. https://doi.org/10.1021/acs.estlett.1c00559

Zhang, K., Gong, W., Lv, J., Xiong, X., & Wu, C. (2015). Accumulation of floating microplastics behind the Three Gorges Dam. Environmental Pollution, 204, 117–123. https://doi.org/10.1016/j.envpol.2015.04.023

Zhang, M., Li, J., Ding, H., Ding, J., Jiang, F., Ding, N. X., & Sun, C. (2020). Distribution Characteristics and Influencing Factors of Microplastics in Urban Tap Water and Water Sources in Qingdao, China. Analytical Letters, 53(8), 1312–1327. https://doi.org/10.1080/00032719.2019.1705476

Zhang, L., Xie, Y., Zhong, S., Liu, J., Qin, Y., & Gao, P. (2021b). Microplastics in freshwater and wild fishes from Lijiang River in Guangxi, Southwest China. Science of The Total Environment, 755, 142428. https://doi.org/10.1016/j.scitotenv.2020.142428

Zhang, Q., Liu, T., Liu, L., Fan, Y., Rao, W., Zheng, J., & Qian, X. (2021c). Distribution and sedimentation of microplastics in Taihu Lake. Science of The Total Environment, 795, 148745. https://doi.org/10.1016/j.scitotenv.2021.148745

Zhao, W., Huang, W., Yin, M., Huang, P., Ding, Y., Ni, X., Xia, H., Liu, H., Wang, G., Zheng, H., & Cai, M. (2020). Tributary inflows enhance the microplastic load in the estuary: A case from the Qiantang River. Marine Pollution Bulletin, 156, 111152. https://doi.org/10.1016/j.marpolbul.2020.111152.

Zhao, Y.-H., Xia, R.-Z., Liang, B., Gao, Z.-W., Song, Z.-Y., Yang, M., Chen, S.-H., Li, P.-H., Xiao, X., & Huang, X.-J. (2024). Highly Accurate Determination of the Total Amount of Pb 2+ and Pb(OH) + in a Natural Water Environment Revealed by Dynamic Simulation and DFT Calculation: Benefit from the Electron Inverse Effect of Pt Nanoclusters over Defective g-C 3 N 4. Analytical Chemistry, 96(13), 5232–5241. https://doi.org/10.1021/acs.analchem.3c05707

Zhou, X., Wang, J., Li, H., Zhang, H., Hua-Jiang, & Zhang, D. L. (2021). Microplastic pollution of bottled water in China. Journal of Water Process Engineering, 40, 101884. https://doi.org/10.1016/j.jwpe.2020.101884

Ziajahromi, S., Neale, P. A., Rintoul, L., & Leusch, F. D. L. (2017). Wastewater treatment plants as a pathway for microplastics: Development of a new approach to sample wastewater-based microplastics. Water Research, 112, 93–99. https://doi.org/10.1016/j.watres.2017.01.042

Ziarani, G. M., Moradi, R., Lashgari, N., & Kruger, H. G. (2018). Chapter 4—Azo Dyes. In G. M. Ziarani, R. Moradi, N. Lashgari, & H. G. Kruger (Eds.), Metal-Free Synthetic Organic Dyes (pp. 47–93). Elsevier. https://doi.org/10.1016/B978-0-12-815647-6.00004-2

Xing, D., Hu, Y., Sun, B., Song, F., Pan, Y., Liu, S., & Zheng, P. (2023). Behavior, Characteristics and Sources of Microplastics in Tea. Horticulturae, 9(2), 174. https://doi.org/10.3390/horticulturae9020174

Zohuri, G., 2012. Polymer science: a comprehensive reference, Elsevier.

Zubris, K. A. V., & Richards, B. K. (2005). Synthetic fibres as an indicator of land application of sludge. Environmental Pollution, 138(2), 201–211. https://doi.org/10.1016/j.envpol.2005.04.013

Zuccarello, P., Ferrante, M., Cristaldi, A., Copat, C., Grasso, A., Sangregorio, D., Fiore, M., & Oliveri Conti, G. (2019). Exposure to microplastics (<10 μm) associated to plastic bottles mineral water consumption: The first quantitative study. Water Research, 157, 365–371. https://doi.org/10.1016/j.watres.2019.03.091

APPENDIX – DATA AND CHARACTERISTICS OF BEVERAGE SAMPLES

Sample code	Brand number	Beverage type	Number of particles	Sample volume (ℓ)	Concentration (particles·$ℓ^{-1}$)
AB (Aluminium) 1	ABB1	lager	12	1.98	6.1
AB (Aluminium) 2	ABB2	Lager	15	2.00	7.5
AB (Aluminium) 3	ABB3	Lager	19	1.80	11
AB (Aluminium) 4	ABB4	Cider	57	2.00	29
AB (Aluminium) 5	ABB5	Pilsener	23	1.80	13
AB (Aluminium) 6	ABB6	Lager	28	2.64	11
AB (Aluminium) 7	ABB7	Cider	46	2.64	17
AB (Aluminium) 8	ABB8	Cider	29	1.80	16
AB (Glass) 1	ABB1	lager	58	1.98	29
AB (Glass) 2	ABB2	lager	38	1.98	19
AB (Glass) 3	ABB3	lager	15	2.00	7.5
AB (Glass) 4	ABB4	Cider	43	1.98	22
AB (Glass) 5	ABB5	Pilsener	17	1.98	8.6
AB (Glass) 6	ABB6	lager	40	1.98	20
AB (Glass) 7	ABB7	Cider	42	2.64	16
AB (Glass) 8	ABB8	Cider	18	1.98	9.1
AB (Glass) 9	ABB9	Spitzer	29	1.65	18
AB (Glass) 10	ABB10	Lager	32	1.98	16
AB (Glass) 11	ABB11	White wine	12	0.75	16
AB (Glass) 12	ABB12	Red wine	21	0.75	28
AB (Glass) 13	ABB13	Lager	10	1.98	5.1
AB (Glass) 14	ABB14	Vodka	10	1.65	6.1
AB (Glass) 15	ABB15	Cider	8.0	1.98	4.0
NAB (Aluminium) 1	NABB1	Carbonated	9.0	2.00	4.5
NAB (Aluminium) 2	NABB2	Carbonated	38	1.80	21
NAB (Aluminium) 3	NABB3	Carbonated	69	1.80	38
NAB (Aluminium) 4	NABB4	Carbonated	15	1.80	8.3
NAB (Aluminium) 5	NABB5	Carbonated	14	1.80	7.8
NAB (PET) 1	NABB1	Carbonated	3.0	1.50	2.0
NAB (PET) 2	NABB2	Carbonated	18	1.50	12
NAB (PET) 3	NABB3	Carbonated	69	1.50	46
NAB (PET) 4	NABB4	Carbonated	15	1.50	10
NAB (PET) 5	NABB5	Carbonated	11	1.50	7.3
NAB (PET) 6	NABB6	Carbonated	12	2.00	6.0
NAB (PET) 7	NABB7	Carbonated	5.0	1.50	3.3
NAB (PET) 8	NABB8	Carbonated	17	1.50	11
NAB (PET) 9	NABB9	Soft drink	15	1.30	12
NAB (PET) 10	NABB10	Iced tea	38	3.00	13
NAB (PET) 11	NABB11	Carbonated	12	2.00	6.0
NAB (PET) 12	NABB12	Carbonated	5.0	2.00	2.5
NAB (PET) 13	NABB13	Carbonated	5.0	2.00	2.5
NAB (PET) 14	NABB14	Carbonated	20	1.50	13
NAB (PET) 15	NABB15	Carbonated	19	1.50	13